INSIGHTS ON THE FATES OF DIARYLAMINE RADICAL-TRAPPING ANTIOXIDANTS DURING INHIBITED AUTOXIDATIONS USING ISOTOPICALLY-ENRICHED COMPOUNDS

by

Neill Penner

A thesis submitted in partial fulfillment of the requirements for the

degree of Master of Science in Chemistry

Department of Chemistry and Biomolecular Sciences

Faculty of Science

University of Ottawa

Abstract

The oxidative degradation of organic materials typically operates through a radical-mediated chain mechanism known as autoxidation; a process that has severe consequences in both biological settings (i.e. accumulation of lipid peroxides) and non-living substrates (i.e. breakdown of petroleum-derived materials, such as lubricants/oils, plastics, polymers, rubbers, etc.). However, autoxidation can be retarded by radical-trapping antioxidants (RTAs); chemical species that capture chain-carrying radicals to break the chain of oxidation. A particular class of RTA, diarylamines, have proven especially effective at elevated temperatures due to a purported catalytic mechanism of inhibiting autoxidation, and thus, have found significant use as protective agents in engine lubricant oils. However, the current diarylamine technology struggles to manage the increased oxidative stress placed on it by modern internal combustion engines (ICEs), which burn fuel at higher temperatures in order to meet emission standards. Designing superior diarylamines is not straightforward, however, as the mechanisms by which they are forced from their catalytic cycle are not well understood.

Herein, we report our investigations into the fate of an industrially-representative, isotopically-enriched diarylamine during hydrocarbon autoxidation at elevated temperatures using a novel 2D $^{1}H - ^{15}N$ heteronuclear multiple bond correlation (HMBC) spectroscopic technique. Synthesis of a small scope of oxidation products allowed for the identification of a previously unreported product of diarylamine autoxidation. Additionally, a consistent pattern of diarylamine speciation under varying conditions was observed spectroscopically. Use of the HMBC technique also confirmed previous reports of the regenerative ability of the diarylamine and the intermediates of its purported catalytic cycle. Quantification studies using ultra performance liquid chromatography (UPLC) during the early stages of autoxidation provided insight into the formation of initial diarylaminic intermediates.

Additionally, we examined the fate of the diarylamine during autoxidations in the presence of nitrogen oxides (NO_x), which are found in the blow-by gas of ICEs and have been shown to exacerbate hydrocarbon autoxidation. The performance of diarylamine was drastically reduced under such conditions, and HMBC spectroscopy illustrated its rapid conversion to a number of intermediates. The most prominent two

intermediates were identified as *mono*- and *di*-nitrated analogues of the original diarylamine, and were demonstrated to possess no RTA activity; regardless of temperature or substrate. HMBC spectroscopy also illustrated the differences in product distribution under each set of conditions.

Statement of Originality

I hereby certify that the work reported in this thesis is the original work of the author, with the exception of work performed by collaborators or fellow researchers, noted in the preface of the corresponding chapter. Any published or unpublished work, ideas, or results of others is fully acknowledged in the references.

Neill Penner

Acknowledgements

Firstly, I wish to thank my supervisor Derek Pratt for his guidance and teaching throughout this experience. Derek encouraged scientific thought, invited invigorating discussions, welcomed questions, and instilled a desire for greater understanding. His dedication, passion, and knowledge are truly inspiring.

Secondly, I would like to express my gratitude to the fantastic group of people that I have had the pleasure of working with over the past few years. I consider it a privilege to have shared this time with a group of such intelligent, ambitious, humorous, and down-to-earth individuals. I first want to thank Kareem Harrison for his amazing mentorship when I started in the laboratory and for our lighter conversations. I also want to thank Ron Shah for his scientific insight, inspiring work ethic, and our great discussions. I am grateful to Mark Raycroft for his keen scientific mind, eagerness to help and teach, and for our conversations. I also want to express my thanks to Luke Farmer for his knowledge, helpfulness, and sense of humour, J-P Chauvin for his positive attitude, the laughs, and great advice, Emily Schaefer for being the most kind and caring teammate one could ask for, Spencer Short for his companionship, all the laughs, and our conversations, and Melodie Mallais for being a great researcher, teammate, and friend. I would also like to thank Jia-Fei Poon, Zijun Wu, Zosia Zielinski, Omkar Zilka, Katie Shirley, Dmitry Saraev, Anas Abou-Zaid, and Evan Haidasz for all your help and for being great colleagues. I am also very grateful to Glenn Facey for his expertise and assistance during my undergraduate and graduate studies.

Most importantly, I want to express my deepest gratitude to my friends and family who have provided the necessary support that allowed me to achieve my aspirations. My brothers, Cameron and Andrew, for their continued friendship and for giving me constant reasons to smile and laugh. Also, to my wonderful parents; John and Carmyn, for their love and support during all my endeavours and for giving me every opportunity to pursue my aspirations. And I especially want to thank Alli, the best person I have ever known, for her unwavering patience, encouragement, and understanding, and for providing levity and comfort during our academic pursuits; I could not have done this without you.

Table of Contents

List of Figures

Chapter 1: Background and Significance

Chapter 2: Determining Oxidation Products of Diarylamine RTAs During Hydrocarbon Autoxidation at Elevated Temperatures

List of Schemes

Chapter 1: Background and Significance

Chapter 2: On the Fate of Diarylaminic RTAs During Hydrocarbon Autoxidation at Elevated Temperatures

Chapter 3: Effects of NO_x on Diarylaminic RTAs During Hydrocarbon Autoxidation at Elevated Temperatures

List of Tables

Chapter 3: Effects of NO_x on Diarylaminic RTAs During Hydrocarbon Autoxidation at Elevated Temperatures

List of Abbreviations

AIBN	azobisisobutryonitrile
APCI	atmospheric pressure chemical ionization
α-TOH	*alpha*-tocopherol
BDE	bond dissociation enthalpy
BHT	butylated hydroxytoluene
BOB	base oil blend
BODIPY	boron-dipyrromethene
cP	centipoise
DMAP	4-dimethylaminopyridine
DMP	Dess-Martin periodinane
DPPH	2,2-diphenyl-1-picrylhydrazine
DTBP	di-*tert*-butyl peroxide
DTBN	di-*tert*-butyl hyponitrite
EDG	electron-donating group
EI	electron impact
EPR	electron paramagnetic resonance
ESI	electrospray ionization
EWG	electron-withdrawing group
FID	flame ionization detector
GC	gas chromatography
HAT	hydrogen atom transfer
HMBC	heteronuclear multiple bond correlation (spectroscopy)
HOMO	highest occupied molecular orbital

HPLC	high performance liquid chromatography
ICE	internal combustion engine
mCPBA	*meta*-chloroperoxybenzoic acid
MS	mass spectrometry
NBS	N-bromosuccinimide
NMR	nuclear magnetic resonance (spectroscopy)
NO_x	nitrogen oxides
PBD	phenyl butadienyl
PDA	photodiode array
PeT	photoinduced electron transfer
PETX	pentaerythritol tetrahexanoate\
PNX	phenoxazine
PTZ	phenothiazine
PUFA	poly-unsaturated fatty acid
RCE	retro-carbonyl-ene
RP	reverse phase
RTA	radical-trapping antioxidant
SET	single electron transfer
SOMO	singly occupied molecular orbital
STY	styrenyl
TEMPO	(2,2,6,6-tetramethylpiperidin-1-yl)oxyl
TLC	thin-layer chromatography
UPLC	ultra performance liquid chromatography
YB4	yubase-4

Master Legend

Chapter 1: Background and Significance


(**1**)


(**2**)


(**3**)


(**4**)

R = alkyl

Ar = 

Chapter 2: On the Fate of Diarylaminic RTAs During Hydrocarbon Autoxidation at Elevated Temperatures


(**1**)


(**2**)


(**3**)


(**4**)

R = alkyl

Ar = 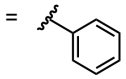

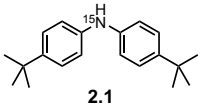
2.1

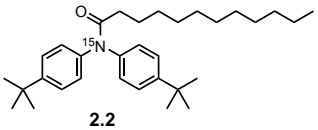
2.2

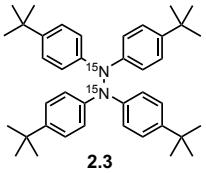
2.3

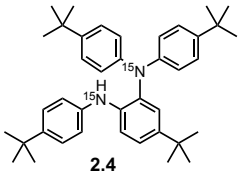
2.4

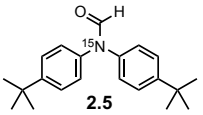
2.5

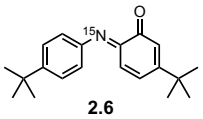
2.6

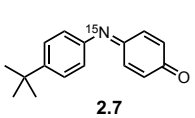
2.7

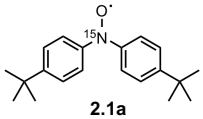
2.1a

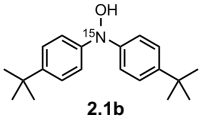
2.1b

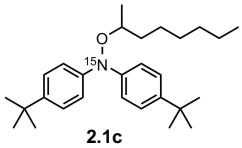
2.1c

Chapter 3: Effects of NO_x on Diarylaminic RTAs During Hydrocarbon Autoxidation at Elevated Temperatures

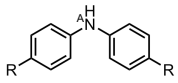
3.1

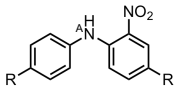
3.2

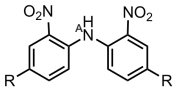
3.3

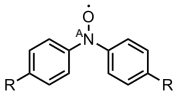
3.4

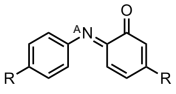
3.5

A = 14, 15

R = 

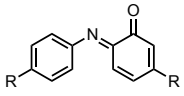
'Product A'

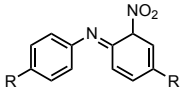
'Product B'

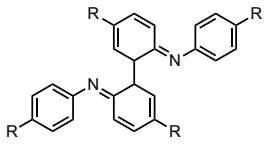
'Product 1'

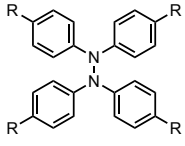
'Product 2'

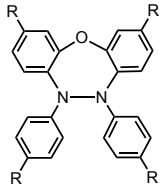
'Product 3'

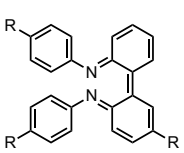
'Product 4'

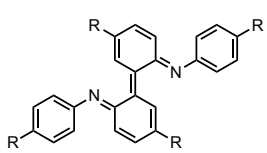
'Product 5'

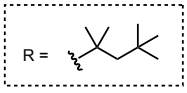

Chapter 1: Background and Significance

Molecular oxygen (O_2), also referred to as dioxygen, is the second-most abundant gas in the earth's atmosphere and takes part in countless chemical reactions and metabolic processes; allowing for life to exist in its current manner.[1,2] However, oxygen is the subject of a cruel paradox: it slowly destroys organic materials over time by oxidizing them; a process known as autoxidation, which will be further discussed later.[3-5] To put simply, oxygen giveth and oxygen taketh away.

Triplet oxygen ($^3O_2$) is the most stable form of oxygen, and consequently it comprises the majority of the different allotropes of molecular oxygen, which include singlet oxygen, ozone, etc.[5] Triplet oxygen possesses two unpaired, spin-parallel electrons that occupy separate, anti-bonding π-orbitals.[5] Although often mischaracterized and drawn as singlet oxygen, most molecular oxygen is a paramagnetic, di-radical. In fact, triplet oxygen is approximately 23 kcal/mol lower in energy than singlet oxygen.[6]

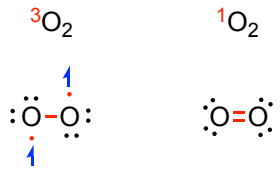

Figure 1.1 Lewis structures of triplet oxygen (left) and singlet oxygen (right)

The distinction between the two forms of molecular oxygen is important, as the di-radical character of triplet oxygen underlies its participation in radical chain reactions. To satisfy Pauli's exclusion principle, triplet oxygen is forced to react through one-electron (free radical) processes; its mode of reacting with, and subsequently destroying, organic materials. This insidious process, named autoxidation, has an immeasurable impact on the world: it causes food to spoil, breaks down rubbers, plastics, and polymers over time, causes discolouration of materials, and perhaps most importantly, is implicated in numerous disease states as well as the overall ageing process.[7-9] Effective chemical solutions to combat autoxidation provide massive economic relief

in commercial and industrial sectors, and demonstrate potential as therapeutic and/or preventative agents in modern medicine.

1.1 Autoxidation of Hydrocarbons

Hydrocarbon autoxidation is a spontaneous process by which atmospheric oxygen is incorporated into organic substrates. It occurs through a radical chain mechanism, similar to a slow, flameless combustion reaction. Autoxidation occurs in three distinct steps: initiation, propagation, and termination; all of which are comprised of multiple reactions (Figure 1.2).[3,4] Initiation by thermal or photochemical processes produces radical species which can abstract a hydrogen atom from the substrate. The resulting alkyl radicals react with molecular oxygen to form peroxyl radicals; the primary culprit of oxidative degradation. Peroxyl radicals continue to propagate the chain reaction by reacting with more equivalents of substrate. Alternatively, they can react with one another or a radical-trapping antioxidant (RTA) to form non-radical products.[4,10] Both pathways terminate the individual chain reactions, but generate different products and consequently, provide different outcomes.

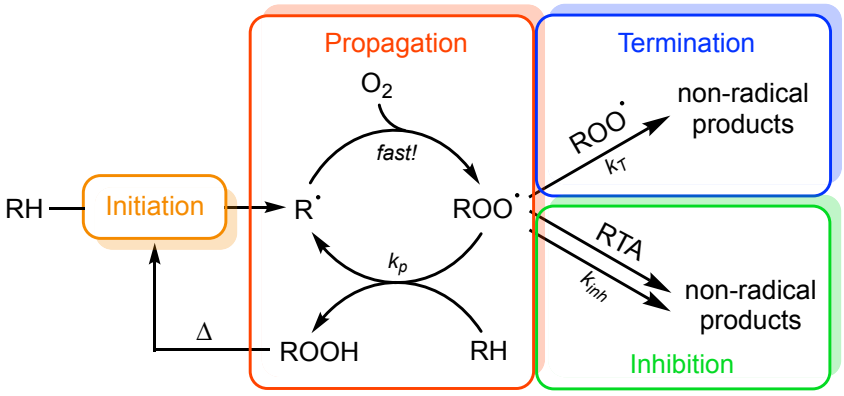

Figure 1.2 Radical chain mechanism of hydrocarbon autoxidation.

1.1.1 Initiation

The primary step in the process of autoxidation is initiation, which kickstarts the formation of radicals through input of thermal or photochemical energy (Figure 1.3).[3,4] Compounds with chemical bonds that are easily homolyzed, such as peroxides (O-O BDE ≈ 35-50 kcal/mol), promote autoxidation unlike inert species such as saturated hydrocarbons (C-C BDE ≈ 85-90).[3,11] Peroxides and azo-derivatives such as azobisisobutyronitrile (AIBN) are used as initiators of free-radical chain processes in organic synthesis and polymerization, in addition to autoxidation research (as discussed later).[7,11]

It is impractical to remove trace impurities present in hydrocarbons during their bulk-preparation/purification, therefore organic peroxides exist in hydrocarbons at low concentrations, acting as initiating species upon excitation with heat or light energy. Upon homolysis of a peroxide initiator, the resulting oxygen-centred radical will abstract an H-atom from the hydrocarbon substrate forming a carbon-centred, or alkyl, radical (Eq. 1.1, 1.2).[3,4]

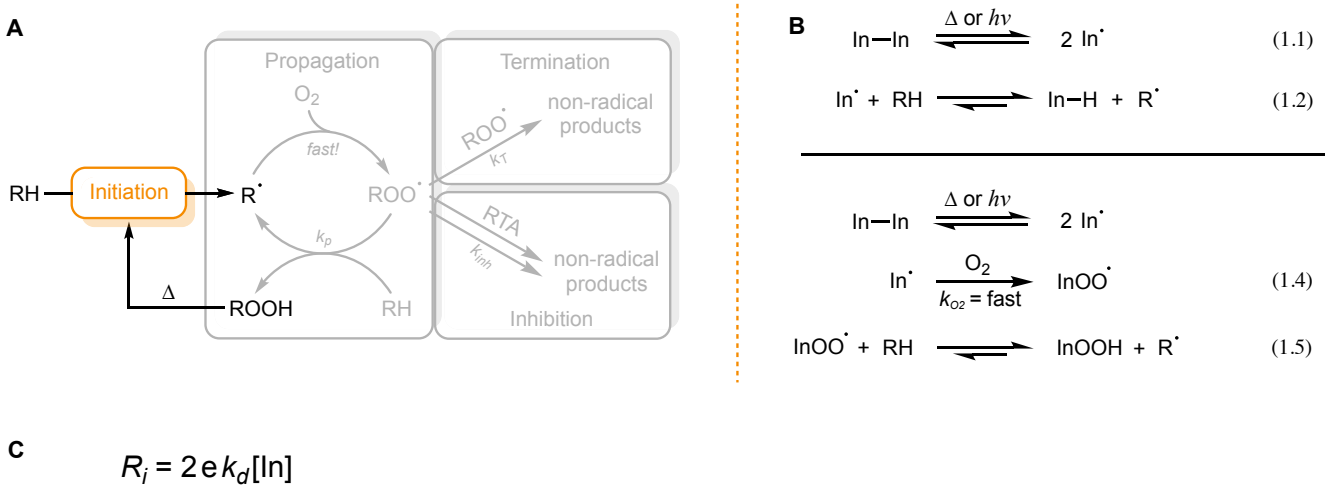

Figure 1.3 (**A**) Initiation step in overall autoxidation scheme. (**B**) Initiation of hydrocarbon autoxidation by decomposition of general initiating species, In_2. (**C**) Equation that describes the rate of initiation.[3,4]

Alternatively, initiators that form alkyl radicals upon homolysis will first react with atmospheric oxygen at rates approaching the diffusion limit ($k \approx 10^9$ M^{-1} s^{-1})[12] to form peroxyl radicals (Eq. 1.4) before abstracting an H-atom from substrate, generating a hydroperoxide and alkyl radical (Eq. 1.5).[3,4]

The rate of initiation (R_i) is an important characteristic of autoxidation, governed by the concentration of initiating species, their rate constant of dissociation (k_d), and the efficiency of cage escape (e).[3] As the name suggests, e represents how many radicals escape combination or disproportionation reactions occurring within the solvent cage, or alternatively, the average number of radicals produced following a homolysis event. In the absence of initiators, however, certain organic substrates are still be susceptible to initiation depending on their bond-dissociation enthalpies (BDEs) and chemical structure. Saturated hydrocarbons are better suited to withstand initiation due to the strength of their C-C/C-H bonds and lack of conjugation, whereas chromophores such as aldehydes can undergo photo-oxidation to produce transient radicals capable of prompting autoxidation.[3,13-16] As a result, the primary mode of initiation in saturated hydrocarbons is generally considered to be via the decomposition of trace amounts of peroxides present in the substrate. Moreover, the hydroperoxide products formed from initiation steps (Eq. 1.5) can decompose into corresponding alkoxyl and hydroxyl radicals, capable of initiating new chains by H-atom abstraction of substrate C-H bonds.[3] The decomposition of hydroperoxides is increasingly problematic when chains are permitted to propagate unchecked, leading to autoinitiation (when initiating radicals are derived from chain reaction products).[17]

1.1.2 Propagation

Once a substrate-derived alkyl radical is formed, it rapidly combines with molecular oxygen to yield a peroxyl radical (Eq. 1.7). The peroxyl radical can abstract a hydrogen atom from another equivalent of substrate producing a hydroperoxide and another alky radical, capable of continuing the chain reaction (Eq. 1.8).[3,4] The alkyl and peroxyl radicals are hence dubbed the chain-carrying radicals (Figure 1.4).

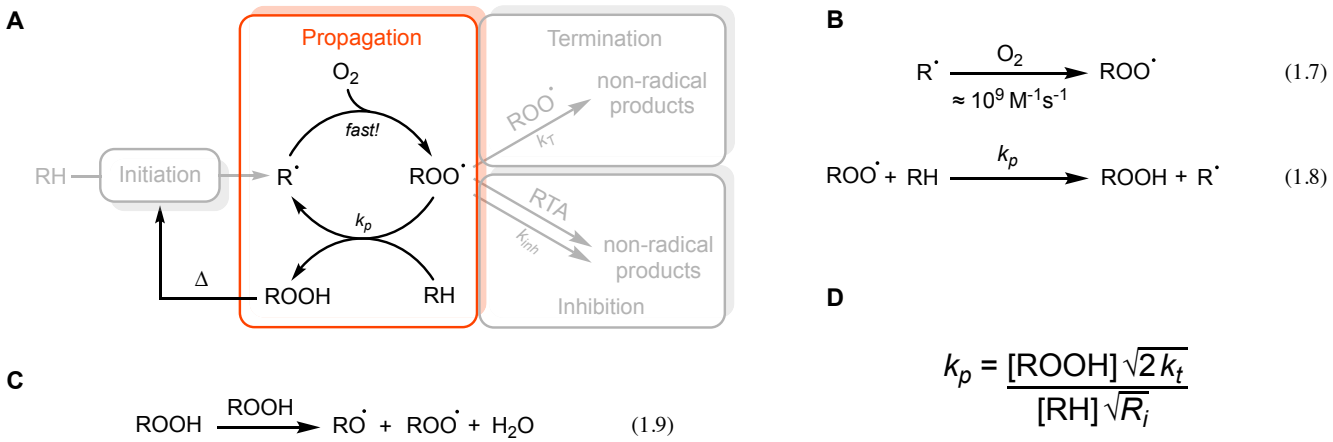

Figure 1.4 (**A**) Propagation step(s) in overall autoxidation scheme. (**B**) Discrete propagation reactions of hydrocarbon autoxidation. (**C**) Decomposition of hydroperoxides yields two initiating species. (**D**) Equation that describes the rate constant of propagation.[3,4]

Oxygen addition to alkyl radicals is extremely fast ($k_{O2} = 3 \times 10^9$ M^{-1} s^{-1})[12], while H-atom abstraction of hydrocarbons by peroxyl radicals is comparatively slow (k values range from <1 to 1×10^2 M^{-1} s^{-1} at ambient temperatures).[18] Consequently, (Eq. 1.8) serves as the rate-limiting step of propagation, characterized by the second-order rate constant, k_p. The physical manifestation of this characteristic is demonstrated by the relative steady-state concentrations of the chain-carrying species: during propagation, the concentration of peroxyl radicals in solution is much greater than that of alkyl radicals, which are highly transient under these conditions.

The rate constant of propagation (k_p) varies considerably between substrates, but can be determined if both the rate of initiation (R_i) and rate constant of termination (k_t) are known. The value is tied closely to stability of the alkyl radical formed upon HAT from the substrate (Eq. 1.8); k_p generally increases as the stability of the alkyl radical increases. As such, relative BDEs can be useful measures for 'autoxadizability' when considering a narrow, structurally-homogeneous group of substrates. This is demonstrated by polyunsaturated fatty acids (PUFAs): k_p values are strongly correlated to BDE of C-H site and to number of bis-allylic positions (Figure 1.5 A).[18-20] However, BDE is not the sole factor in predicting or explaining the ease of which a hydrogen atom is abstracted from a given hydrocarbon.

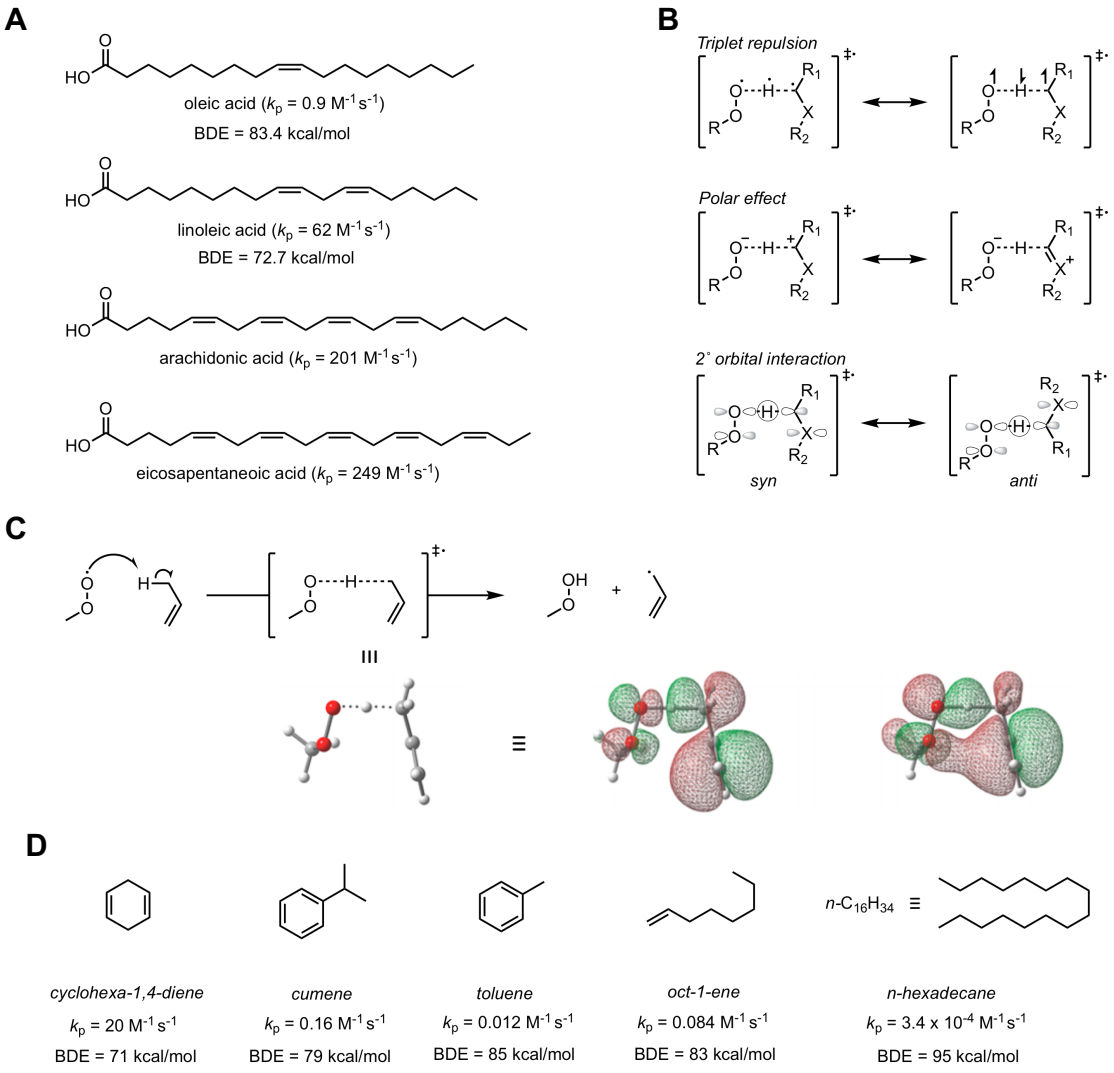

Figure 1.5 (**A**) Propagation rate constants of PUFAs increase with decreasing C-H BDE and with increasing number of bis-allylic positions. (**B**) Triplet repulsion, polar effects, and secondary orbital interactions influence the rate of hydrogen atom abstraction via stabilization of the transition-state activated-complex. (**C**) H-atom abstraction of propene by methylperoxyl radical is stabilized by a *syn* transition state. (**D**) Chemical structures, propagation rate constants, and bond dissociation enthalpies of various hydrocarbons at ambient temperatures.[21] (Adapted with permission from Zielinski, Z.; Pratt. D. A. *J. Org. Chem.* **2017**, *82,* 2817-2825, © 2020 American Chemical Society)

Triplet repulsion, which suggests that the electronegativity of the two non-hydrogen atoms involved in the HAT transition state dictate the barrier, is often used to explain deviations from BDE-k_p correlations as it describes why H-atom abstraction from heteroatoms (i.e. X-H, where X = O, N, S) by oxygen proceeds over lower barriers than with C-H bonds (Figure 1.5 B).[22,23] Per Pauli's exclusion principle, the spin-parallel electrons

in the activated complex repel one another; therefore repulsion is greater for those of lower electronegativity (i.e. carbon) than those of higher electronegativity. Yet triplet repulsion fails to fully explain cases where H-atoms are abstracted *alpha* to heteroatoms, which can be rationalized by polar effects.[24-26] The electronegativities of involved atoms or distal substituents can be invoked to explain stabilization of the dipole in the HAT transition state (Fig. 1.5 B) Recent computational work indicates that secondary orbital interactions play a significant role as well, which furthers understanding of how transition states are stabilized during HAT. Peroxyl radicals *syn* to substituents of the substrate during the transition state benefit from positive orbital interactions, as demonstrated in the HAT between propene and methylperoxyl radical, which proceeds through a *syn* transition state that is 1.1 kcal/mol lower in enthalpy than the *anti* due to favourable interactions between the π highest occupied molecular orbital (HOMO) of propene and π* singly-occupied molecular orbital (SOMO) of methylperoxyl radical (Figure 1.5 C).[19,27,28] It is important to note that k_p is not a direct measure of substrate 'oxidizability'; the rate constant of propagation needs to be compared with the rate constant of termination (k_t) to determine how susceptible it is to autoxidation. Conjugated hydrocarbons, such as styrene and some sterols, are susceptible to propagation via addition pathways as well as through HAT reactions. Autoxidation of styrene leads to a co-polymer of styrene and oxygen, which occurs through a similar mechanism to desired polymerization reactions of styrene.[18]

Propagation to yield substrate-derived hydroperoxides is problematic in two ways: the obvious issue being change of the chemical, and eventually physical, properties of the original organic material. Secondly, the substrate-derived hydroperoxides that are formed can serve as initiators, which is exceedingly detrimental at higher temperatures.[18,29] Thermal decomposition of hydroperoxides initially yields alkoxyl and hydroxyl radicals that can each initiate new chains via H-atom abstraction of substrate.[18] Conversely, hydroperoxides can reportedly react with each other to yield an alkoxyl radical, peroxyl radical, and water (Eq. 1.9, Figure 1.4 C), yet such transformations are likely the exception rather than the rule.[30] At elevated temperatures (>120˚C), hydroperoxide decomposition results in autoinitiation of the autoxidation: each chain propagation produces multiple equivalents of hydroperoxide, each of which can initiate more chains, quickly resulting in an

uncontrollable reaction.[17] In kinetic terms, this translates to a variable rate of initiation (R_i) that increases over the course of the process as more hydroperoxide is produced.

1.1.3 Termination

Propagating chains are terminated when chain-carrying radicals encounter one another and react to form non-radical products (Figure 1.6). Theoretically, there are three possible termination reactions: those between two peroxyls, between two alkyl radicals, or between an alkyl and peroxyl radical (Eq. 1.10-1.12, Figure 1.6 B). Due to the low steady-state concentrations of alkyl radicals, scenarios (Eq. 1.10) and (Eq. 1.11), which are typically diffusion-controlled, are largely irrelevant to the overall rate of termination. Instead, the rate is governed by the relatively slower peroxyl-peroxyl addition (Eq. 1.12), characterized by the second-order termination rate constant, k_T (Figure 1.6 C).[3,4] Combination of two secondary alkylperoxyl radicals results in the formation of the products seen in (Eq. 1.12);[31,32] however, this pathway is impossible for tertiary alkylperoxyl radicals due to their lack of hydrogen atoms on the *alpha*-carbon. Instead, they react to yield oxygen and a peroxide.[33]

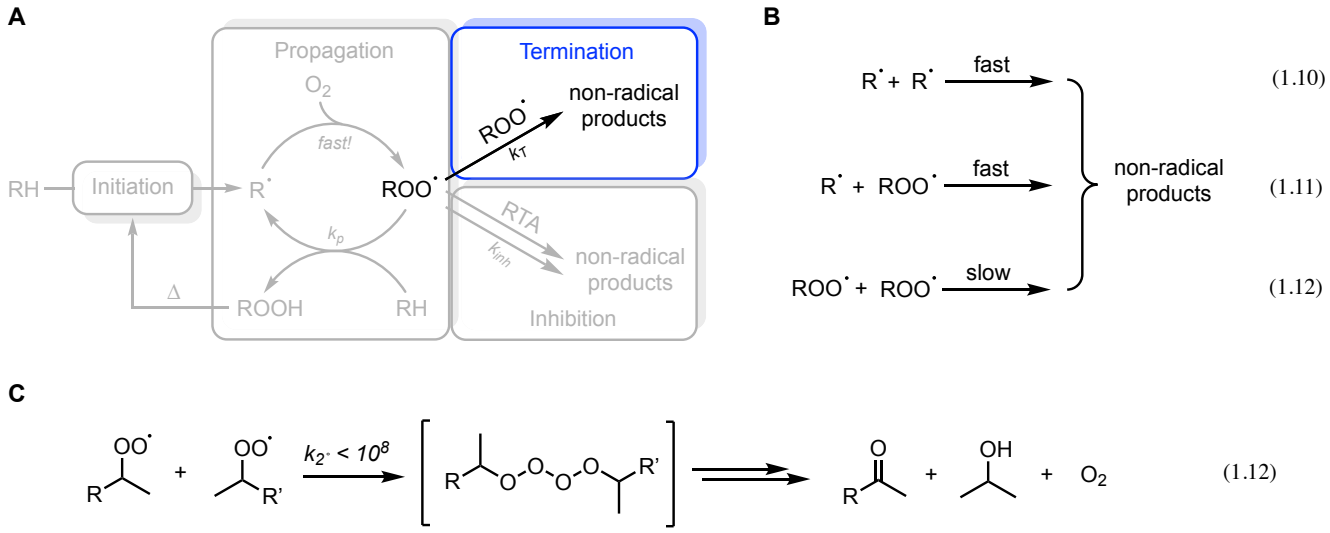

Figure 1.6 (**A**) Termination step in overall autoxidation scheme. (**B**) Termination reactions of hydrocarbon autoxidation. (**C**) The most likely termination event, peroxyl-peroxyl termination, yields a ketone, alcohol, and molecular oxygen in the case of secondary peroxyl radicals.[3,4,31,32]

Although individual termination reactions are beneficial, termination overall is not necessarily a protective failsafe due to the requirement that peroxyl concentrations be elevated for them to occur to a significant degree. At the beginning of autoxidation, the steady-state concentration of peroxyl radicals is low, translating to a low rate of termination. Once a sufficiently high concentration of peroxyl radicals has accumulated such that the rate of termination is competitive with the rate of propagation, countless chains will have been formed and the substrate will have already experienced significant damage.

1.1.4 Products of Hydrocarbon Autoxidation at Elevated Temperatures

The primary products of autoxidation are substrate-derived hydroperoxides which are unstable at elevated temperatures and prone to thermal decomposition.[3] Consequently, these species do not accumulate indefinitely; their concentration generally plateaus due to increased homolysis once an apparent steady-state concentration is reached. Additionally, peroxyl-peroxyl terminations occur more readily during later stages of the process, giving rise to ketones, alcohols, and peroxides.[3,34-36] Traditionally, hydroperoxide concentrations in autoxidation samples have been quantified using iodometric titrations or via HPLC/GC following reduction with triphenylphosphine (PPh_3); laborious methods our group sought to circumvent by development of a pro-fluorescent phosphine probe assay (discussed in detail later).[36]

Under conditions that emulate harshly oxidative environments, such as engines or turbines, substrates are functionalized to a variety of oxygenated products, of which carboxylic acids are prominent.[34-36] Formation of carboxylic acids from *n*-alkanes can be rationalized by intramolecular reactions between substrate-derived peroxyls (Scheme 1.1). Cleavage products alter the carefully-designed viscosity of lubricating oils and the resulting acids cause corrosion of metallic components of engines and the like. Carboxylic acid formation is sufficiently consistent to serve as a useful marker for autoxidation progress, with its accumulation generally lagging slightly behind hydroperoxides. As such, our group has developed a dual, fluorescent-probe method for

monitoring the increase in both species, discussed in detail later.[36] Conventionally, acid production has been tracked and quantified during autoxidation through acid-base titrations.

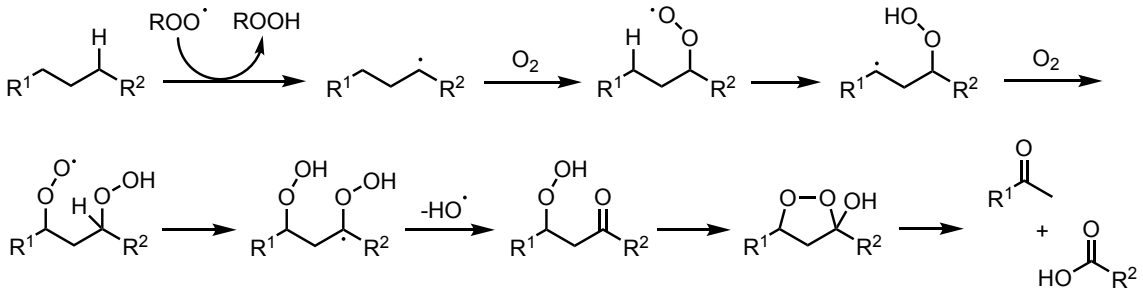

Scheme 1.1 Proposed mechanism of carboxylic acid formation in linear, saturated hydrocarbons during autoxidation.[34,35]

Ketones are also quite prevalent in the product distribution due to their formation from peroxyl-peroxyl termination in addition to the same intramolecular reactions that yield carboxylic acids.[34-36] Although not as reactive or damaging as carboxylic acids, suppressing the conversion of the intended substrate into the corresponding ketone derivatives is desired for similar reasons. The production of carbonyl moieties during autoxidation make IR spectroscopy a common technique for monitoring autoxidation progress, and the typical method for observing ketone formation during experiments.

1.1.5 Effects of Nitrogen Oxides on Autoxidation

Although molecular oxygen, through formation of peroxyl radicals, is the chief perpetrator of autoxidative damage, nitrogen oxides (NO_x) are also known contributors to oxidative degradation of fuel lubricants used in internal combustion engines.[37,38] Nitrogen oxide is the generic term for nitric oxide (NO) and nitrogen dioxide (NO_2), which are the two nitrogen oxide species (of many) most culpable for air pollution; typically produced during combustion of hydrocarbons (Figure 1.7 A). Both species are free radicals: they each possess an unpaired electron on their respective nitrogen atoms and exist in a temperature-dependent equilibrium, where NO is the predominant component to form at extremely high temperatures (>1500˚C) and NO_2 is predominant at lower temperatures (Eq. 1.17).[38] The unpaired electrons allow NO_x to participate in the

one-electron processes that constitute autoxidation. Consequently, NO_x have been demonstrated to cause sludge formation and oil thickening, resulting in the development of multiple engine tests in industry that evaluate oil degradation under conditions with high levels of NO_x present.[37] Past research has reported the effects of NO_x on the autoxidation of saturated hydrocarbons, indicating gas containing higher levels of NO_x is detrimental to such substrates due to the initiation reactions they undergo. Nitrogen dioxide initiates the radical chain via HAT of the substrate to form an alkyl radical and nitrous acid, the latter of which decomposes at high temperatures to yield two more free-radical species: a hydroxyl radical and nitric oxide (Eq. 1.13, 1.14).[37,39]

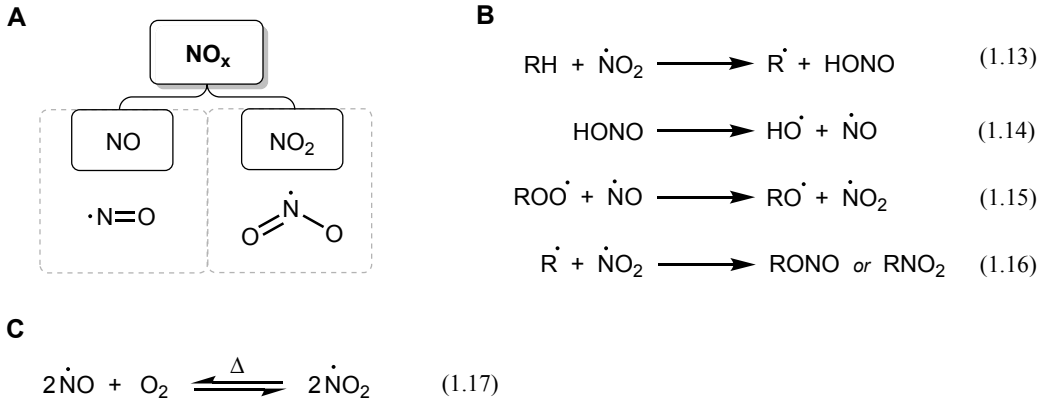

Figure 1.7 (**A**) The two individual components of NO_x: NO and NO_2. (**B**) Observed initiation and termination reaction(s) of NO_x during autoxidation. (**C**) Thermal equilibrium of NO_x under aerobic conditions.[37,39-41]

Nitric oxide itself is not a prominent player in initiation, but readily reacts with peroxyl radicals to form alkoxyl radicals and nitrogen dioxide (Eq. 1.15).[40] In the absence of oxygen, nitrogen dioxide is consumed by reaction with alkyl radicals to nitro-alkyl derivatives (Eq. 1.16).[41]

NO_x is observed to have little influence on autoxidation beyond its propensity to spur initiation; no increased degradation of hydrocarbon is observed once a high steady-state concentration of peroxyl radicals arise.[37] This observation can partially be explained by reactions between NO_x and the primary intermediates of autoxidation. NO does not directly initiate the process, instead reacting with molecular oxygen or peroxyl radicals, present at increasing concentrations throughout the process, producing NO_2.[38,40] NO_2 reacts with peroxyl and alkoxyl radicals at rates typical of radical-radical reactions, forming nitrates and peroxy nitrates,

respectively (Eq. 1.18, 1.19).[40,41] Furthermore, NO_2 exists in equilibrium with nitrogen tetroxide (N_2O_4), which has been demonstrated to form both radical and non-radical products by reaction with hydroperoxide, governed by the rate constant k_{dec}; determined to be approximately 10^4 $M^{-1}s^{-1}$ at ambient temperatures (Eq. 1.20, 1.21).[42] NO_x species also undergo radical-radical combination with alkyl radicals to form non-radical products, but such transformations are largely irrelevant under oxygenated conditions where the concentration of alkyl radicals is very low.

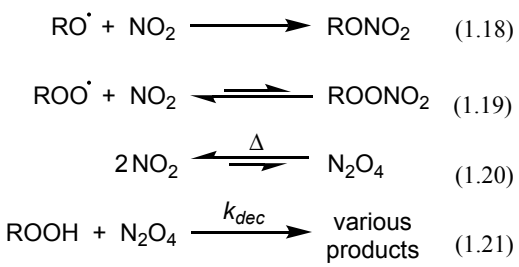

Scheme 1.2 Non-initiating reactions between NO_2 and autoxidation intermediates/products.[38-42]

Concomitant to the aforementioned reactions, NO_x likely become irrelevant to autoxidation once hydroperoxide concentrations have climbed significantly, or rather, once hydroperoxide decomposition via autoinitiation functions as the main driver of the process.[37]

1.2 Antioxidants

Antioxidants are chemical compounds that serve as protective agents against the deleterious effects of hydrocarbon autoxidation.[4] These compounds generally inhibit autoxidation by reacting with peroxyl radicals or initiating species to retard substrate degradation.[3,4] In living organisms, endogenous and dietary antioxidants are essential for managing such species, which contribute to oxidative stress experienced on a cellular level. Antioxidants are of similar importance in non-living substrates, such as petroleum-derived materials, which possess no inherent ability to combat the process.

However, the general term “antioxidant” has been sensationalized in recent years, and ignores the functions encapsulated by the oversimplified designation. There are two distinct classes of antioxidant:

preventative antioxidants and *radical-trapping antioxidants* (RTAs), which possess different mechanisms of action towards inhibiting autoxidation.[4] Preventative (or secondary) antioxidants, slow the rate of initiation of autoxidaton (R_i, *vide supra*). They react with initiating species, such as hydroperoxides, to prevent them from starting new chains; a crucial function in slowing the overall process.[3,4] Organosulfur and organophosphorus are recognized as secondary antioxidants for their ability to decompose hydroperoxides into alcohols and catalyze decomposition of hydroperoxides when oxidized to their corresponding oxyacids (Scheme 1.3).[43,44]

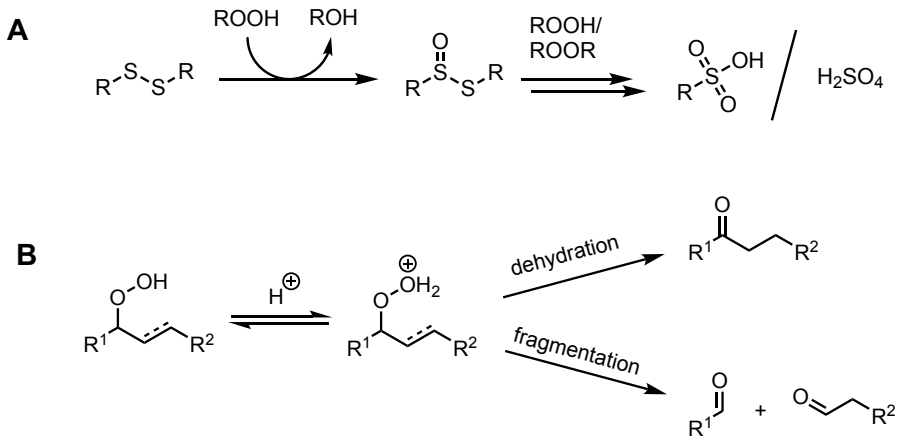

Scheme 1.3 (A) Decomposition of hydroperoxide/peroxide by alkyl disulfide. (**B**) Acid-catalyzed decomposition of hydroperoxide.[43,44]

Resultingly, polysulfides and phosphines have found industrial use in-tandem with RTAs, which complement preventative protection by directly breaking the propagating chains to slow autoxidation.[4]

1.2.1 Radical-Trapping Antioxidants

Radical-trapping antioxidants (RTAs) 'break' chain reactions by intercepting chain-carrying radical species to form non-radical products (Figure 1.8 A).[3,4] Although exceptions exist, RTAs generally possess two distinct characteristics that contribute to their efficacy towards inhibiting propagation: (*i*) they easily give up a hydrogen atom, and (*ii*), they form persistent and/or stable radicals upon doing so. Rather than reacting with oxygen or substrate, the RTA-derived radical ideally combines with another peroxyl radical to yield non-radical

products (Eq. 1.22, 1.23).[3,4] In this scenario, the RTA has a stoichiometric number (n) of two: it consumes two peroxyl radicals per equivalent of RTA.

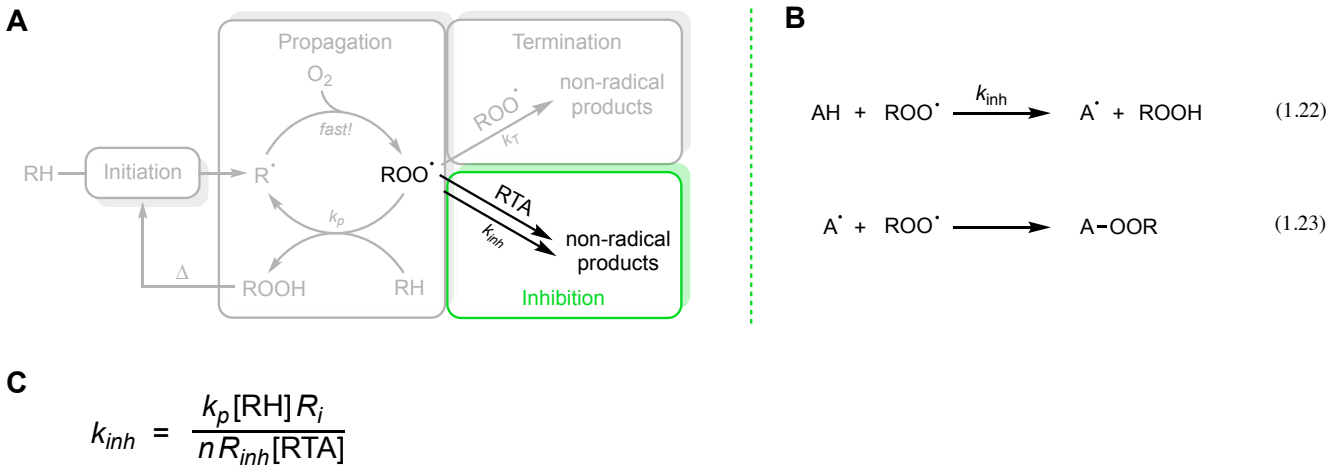

Figure 1.8 (**A**) Inhibition step in overall autoxidation scheme by a general RTA. (**B**) Inhibition reactions between generic RTA and chain-carrying radicals.[1,2] (**C**) Equation that describes the inhibition rate constant.

Theoretically, RTAs are capable of consuming alkyl radicals in a similar manner, provided the RTA is sufficiently reactive and that partial pressure of O_2 is sufficiently low for alkyl radicals to have the necessary lifetime.[45] Nitroxide radicals, such as TEMPO, have demonstrated trapping of alkyl radicals at rates as high as 10^8 M^{-1} s^{-1}, but need to be present in incredibly high concentrations to be competitive with alkyl radical consumption by atmospheric oxygen.[46-49] But this unfortunate reality highlights why RTAs are effective at consuming peroxyl radicals at such low loadings: RTAs are much better at providing peroxyl radicals a hydrogen atom than substrate; an observation reflected in their corresponding rate constants (Figure 1.9).

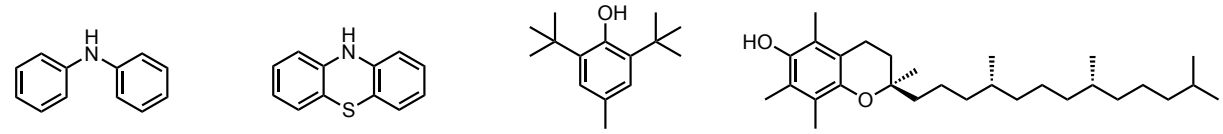

Figure 1.9 Chemical structures and inhibition rate constants of common RTAs measured at 37°C.[4,50]

The inhibition rate constant (k_{inh}) for an effective RTA greatly exceeds the rate constant of propagation (k_p).[10] This can be attributed to a number of physical properties that RTAs possess. Generally, the X-H bond dissociation enthalpy (BDE) of an RTA is relatively low (X = O, N, S), providing facile HAT/PCET to peroxyl radicals;[51,52] RTAs ideally undergo exergonic HAT reactions with peroxyl radicals.[10] However, thermodynamics (i.e. BDEs) are not the sole predictor of RTA activity, similarly to how k_p values can deviate from such trends, therefore simply minimizing the BDE of an RTA is not desirable for a number of reasons (discussed in more detail later). The reactivity of RTAs rely largely on favourable kinetics; not just thermodynamics. Stabilization of transition states via polar effects, triplet repulsion, and secondary orbital interactions are key factors in reactivity. As such, HAT reactions between oxygen (ie. peroxyl radicals) and heteroatoms (of RTAs) are more favourable than HAT between oxygen and carbon atoms; peroxyls prefer to react with RTA from a kinetic standpoint, regardless of BDE.[10,52] This preference is obvious when examining the structure of RTAs that inhibit peroxyls via HAT: they possess labile hydrogen atoms that are bonded to heteroatoms.

One of the most common and effective classes of RTA is phenolic RTAs. At ambient temperatures, phenols possess a stoichiometric number (n) of two: they typically trap two peroxyl radicals (Scheme 1.4).[4,10] Butylated hydroxytoluene (BHT), is a phenolic RTA used to slow autoxidation in countless commercial products including foods, cosmetics, rubber, and are similarly useful for high-temperature applications in transformer and hydraulic fluids, lubricants, and gasoline (Figure 1.9)[53]. Phenolic RTAs are also abundant in nature, the most heralded being *alpha*-tocopherol (α-TOH); the active form of vitamin E preferentially absorbed by humans (Figure 1.9). This essential micronutrient is nature's best RTA, crucial for managing oxidative stress in human cells and often used as the benchmark compound when assessing RTA performance in biological settings.[54-56]

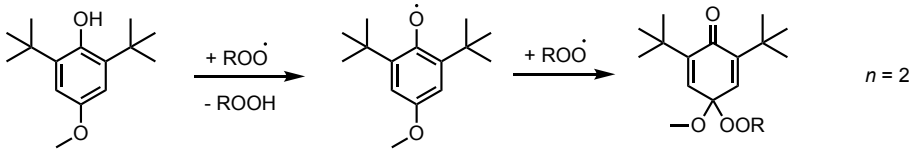

Scheme 1.4 Mechanism of inhibition of butylated hydroxyanisole (BHA) at ambient temperatures. Each equivalent of BHA traps two peroxyls, providing a stoichiometry of 2.

1.2.2 Diarylaminic RTAs

Diarylamines are another prominent class of RTA, often used for high-temperature applications in petroleum-derived products, such as lubricating oils for engines. These additives are produced and consumed on a massive scale; one percent (by mass) of all oil added to an internal combustion engine is composed of diarylamine(s). Diarylamines have proven to be moderately useful at ambient temperatures, at which they react similarly to phenolic RTAs: they trap a peroxyl radical with their N-H bond and then subsequently trap an additional peroxyl by combination with the resulting diarylaminyl radical (Scheme 1.4).[4,57-58] However, these compounds are uniquely useful for applications under elevated temperatures at which autoxidation is particularly harmful.[4,10]

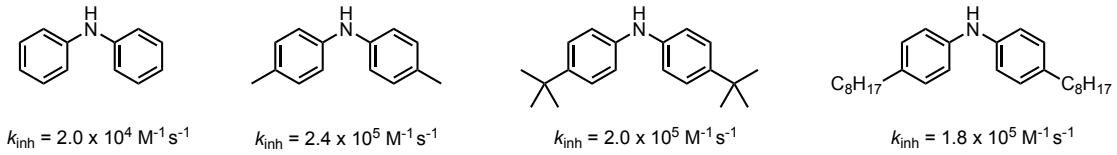

Figure 1.10 Chemical structures and inhibition rate constants of some simple diarylamines. Inhibition rate constants measured at ambient temperatures (37˚C).[4,59]

Diarylamines' increased efficacy at higher temperatures has been observed for many years; they have been a staple additive in lubricants since the mid-point of the twentieth century.[4,] Estimates for the stoichiometric number of the compound have ranged from dozens to hundreds,[60] but precise quantification is difficult due to the continually-increasing rate of initiation at high temperatures. In the late twentieth-century, Korcek and his colleagues at the Ford Motor Company observed its high stoichiometric numbers of inhibition along with regenerative capabilities.[61] They demonstrated that *bis*(4-octylphenyl)amine (**1**) could be regenerated in 70% yield during autoxidation of hexadecane at 160˚C when experiments were commenced with the corresponding nitroxide radical (**3**) (Scheme 1.5 A). Additionally, the corresponding alkoxyamine (**4**) was converted to the amine (**1**) in 64% yield via thermal decomposition. Consequently, they proposed a catalytic mechanism for the diarylamine that accounted for the requirement of elevated temperatures to explain the observed stoichiometry of

inhibition. Computational and mechanistic studies by Haidasz et al. corroborated the proposed 'Korcek cycle' and helped elucidate the mechanism of diarylamine regeneration from diarylalkoxy-amine (Scheme 1.5 B).[62]

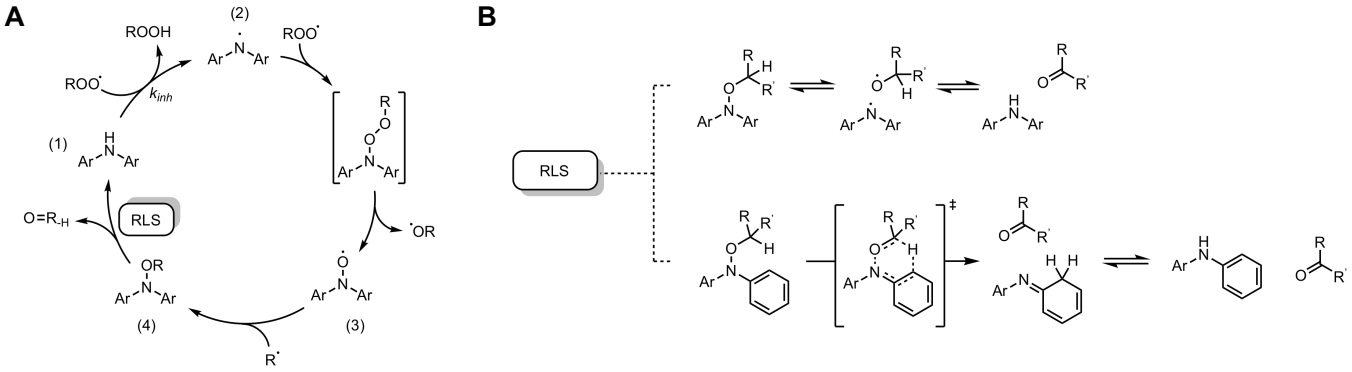

Scheme 1.5 (**A**) Proposed mechanism of catalytic activity of diarylamine RTAs at high temperatures. (**B**) Distinct pathways of diarylamine regeneration from diarylalkoxyamine: N-O homolysis and disproportionation (in saturated substrates) and retro-carbonyl-ene reaction (in unsaturated substrates).[61,62] (Adapted with permission from Haidasz, E. A.; Shah, R.; Pratt, D. A. *J. Am. Chem. Soc.* **2014**, *136*, 47, 16643-1665, © 2020 American Chemical Society)

At the beginning of the cycle, diarylamine (**1**) consumes a peroxyl radical, forming the diarylaminyl radical (**2**) and ejecting an equivalent of hydroperoxide. Another peroxyl radical can be trapped by (**2**), forming a short-lived intermediate that rapidly decomposes to form the diarylnitroxide radical (**3**) and an alkoxyl radical. An alkyl radical not yet attacked by oxygen can rapidly combine with (**3**) to form the diarylalkoxyamine (**4**). The starting material, (**1**), is regenerated via homolysis and disproportionation of (**4**) or by a pericylic retro-carbonyl-ene (RCE) reaction.[61,62] The diarylamine consumes a net two chain-carrying radicals per cycle, and can perform multiple cycles at high temperatures to break numerous chains. Although the conversion of (**1**) to (**2**) by consumption of a peroxyl radical is the rate-limiting step of inhibition (with the rate constant k_{inh}), the rate-limiting step of the catalytic cycle is the final transformation: conversion of the alkoxyamine to the diarylamine.[62] The substrate is effectively used as the stoichiometric reductant in this step, providing the diarylamine with abundant material to encourage regeneration and subsequent turnover.

The ability of diarylamine to form diarylnitroxide *in situ* also lends it inhibitory reactivity in unsaturated substrates, an observation recently reported by Harrison et al.[58] At lower rates of radical generation – conditions more representative of 'real world' applications – diarylnitroxides were demonstrated to be far better inhibitors across a range of temperatures than their parent diarylamines, owing such reactivity to their ability of cross-dismutation of hydroperoxyl and alkylperoxyl radicals. Hydroperoxyl radicals are proposed to form under such conditions via tunneling-assisted, intramolecular 1,4-HAT. (Scheme 1.6 A). Through a regenerative cycle involving diarylnitroxide and the corresponding diarylhydroxylamine, chain-carrying hydroperoxyl and peroxyl radicals are converted to oxygen and hydroperoxide (Scheme 1.6 B). Diarylamines that generate a sufficient concentration of diarylnitroxide also demonstrate the ability to retard autoxidation under said conditions, albeit to a much lesser degree.

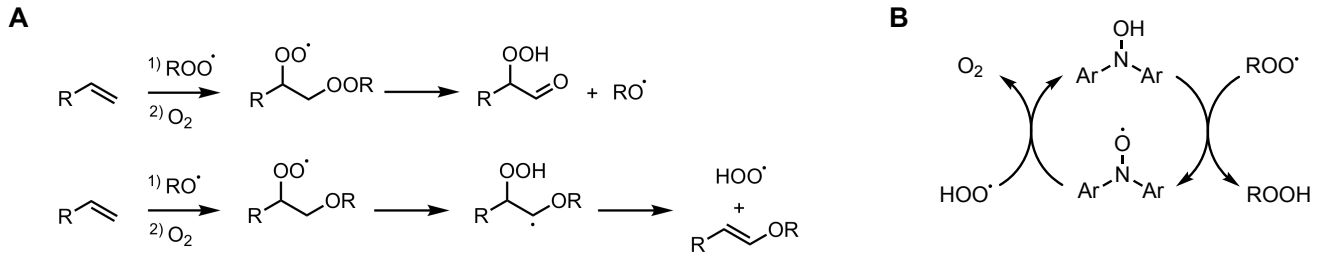

Scheme 1.6 (**A**) Formation of hydroperoxyl radical via intramolecular 1,4-HAT. (**B**) Proposed mechanism of nitroxide-catalyzed dismutation of hydroperoxyl and alkylperoxyl radicals.[58]

Diarylamines can be functionalized to maximize the efficiency of these individual reactions. For example, substituents at the *para*-positions of the aryl rings prevent unwanted side reactions, such as HAT or peroxyl addition.[62] Industrial diarylamines are alkylated in this manner with by-products from cracking and distillation processes, which also provide the benefit of increased solubility and reduced volatility. However, the electron-donating ability of substituents also plays a role in RTA reactivity, as previously mentioned. EDGs increase k_{inh} for diarylamines by weakening the N-H bond, via stabilization of (**2**).[4,10,62-64] The N-O bond of (**4**) is similarly weakened, providing faster regeneration of (**1**) from (**4**); the rate-limiting step of the process.[62]

Diarylamines, however, are not immune to the aforementioned side-effects this functionalization: reduced oxidation potential. Diarylaminic RTAs that are *too* electron rich can have greatly reduced oxidation potentials, exposing them to side-reactions in oxygen-rich environments; especially at high temperatures. Single-electron transfer (SET) between diarylamine and oxidants, including oxygen or hydroperoxides, can generate initiating species that lead to further autoxidation of the substrate, rather than inhibition (Scheme 1.7).[52,65]

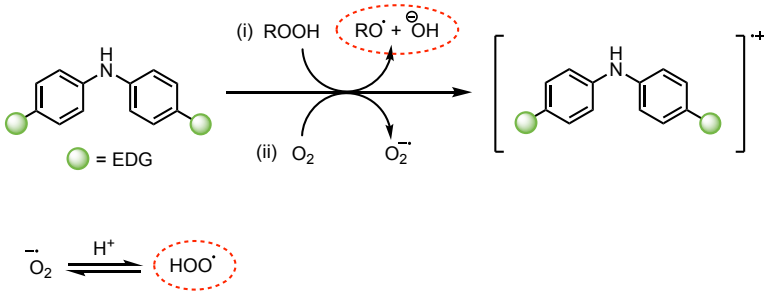

Scheme 1.7. Pro-oxidant activity of electron-rich diarylamine via SET to generate initiating species: (i) alkoxyl and hydroxyl radicals and (ii) hydroperoxyl radicals via protonation of superoxide.[52,65]

Although increasingly electron-rich RTAs can be prone to undesired reactivity, efforts towards their optimization have resulted in the development of some of the most reactive RTAs ever reported.[10,63,64] Studies have illustrated that the incorporation of nitrogen heteroatoms into the aryl substituents of the diaryl-amines increase the k_{inh} without drastically reducing the oxidation potential, and diarylamines built upon this heterocyclic scaffold have demonstrated the longest inhibition periods in model systems reported to date.[64]

In comparison to 4,4-dialkyldiphenylamine, a model of the industrial standard, heterocyclic diarylamines outstrip its reactivity by up to two orders of magnitude (Figure 1.11).[64] However, incorporation of pyrimidinyl and pyridinyl aryl substituents alters the RTAs ability to inhibit autoxidation in the presence of acids. The heteroaromatic rings can be protonated, reducing their electron-donating ability and effectively nullifying any benefit they normally provide. As acids are a major product of autoxidation at high temperatures, this proves detrimental to the diarylamine's performance unless mitigated by the addition of base to the reaction mixture.

Fortunately, this does not misrepresent high-temperature applications such as fuel lubricants, which generally have base and detergent additives that counteract accumulation of acids.

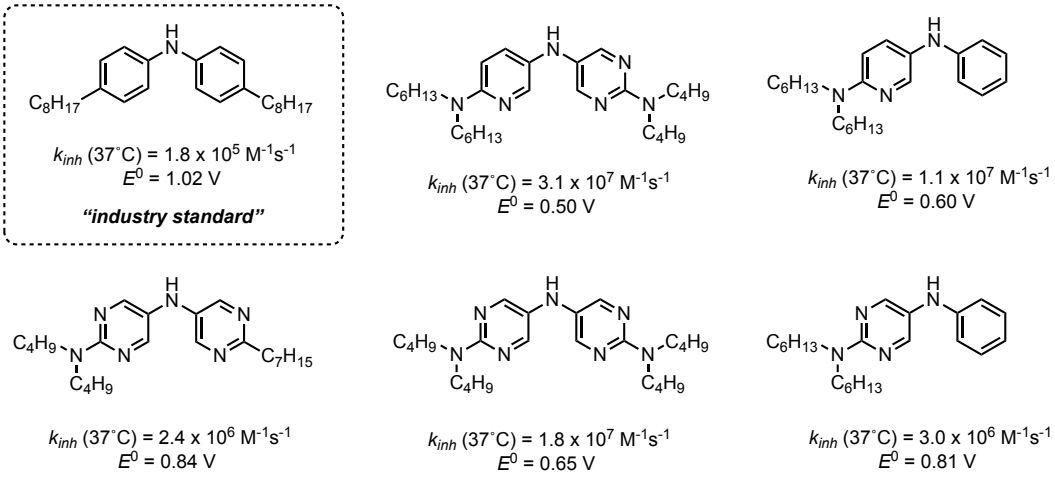

Figure 1.11 Chemical structures, rate constants of inhibition, and oxidation potentials of pyrimidinyl and pyridinyl diarylamines alongside a diarylamine similar to those used widely in industry.[52,63,64]

Phenoxazine and phenothiazine, compounds with a diarylamine scaffold that possess a bridging chalcogen between the aryl substituents, also show increased reactivity from incorporation of nitrogen into aryl substituents. As the basic scaffolds yield inhibition rate constants that far exceed that of diphenylamine, the diazaphenoxazines and diazaphenothiazines provide some of the fastest k_{inh} values ever recorded (Figure 1.12).[10,66]

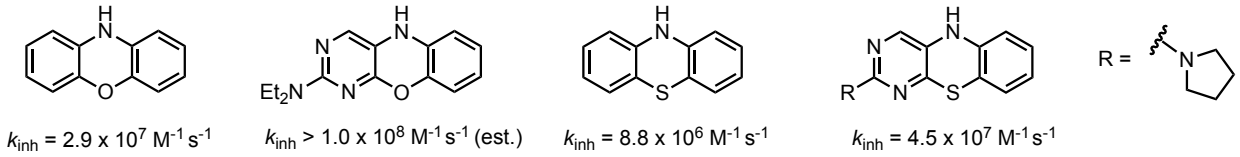

Figure 1.12 Chemical structures and inhibition rate constants of phenoxazine, phenothiazine, and their corresponding di-*aza* derivatives.[50,66]

Additionally, isolating the products of diarylamine oxidation is of interest in order to better understand the mechanisms of their eventual decomposition, and thus, how to produce more robust compounds. Previous endeavours have resorted to performing autoxidations on large scale with high loadings of diarylamine in order

to isolate their oxidation products from the reaction mixture using chromatography.[67] Although some efforts have been partially successful, they involved the use of long-chain polyester substrates which require base-hydrolysis to be separated from products, likely altering the structure of some of the oxidation products. Furthermore, higher temperatures (200˚C) and RTA loadings of 20 weight percent were employed in these autoxidations, likely encouraging the formation of RTA dimers and oligomers that were found to be major products.

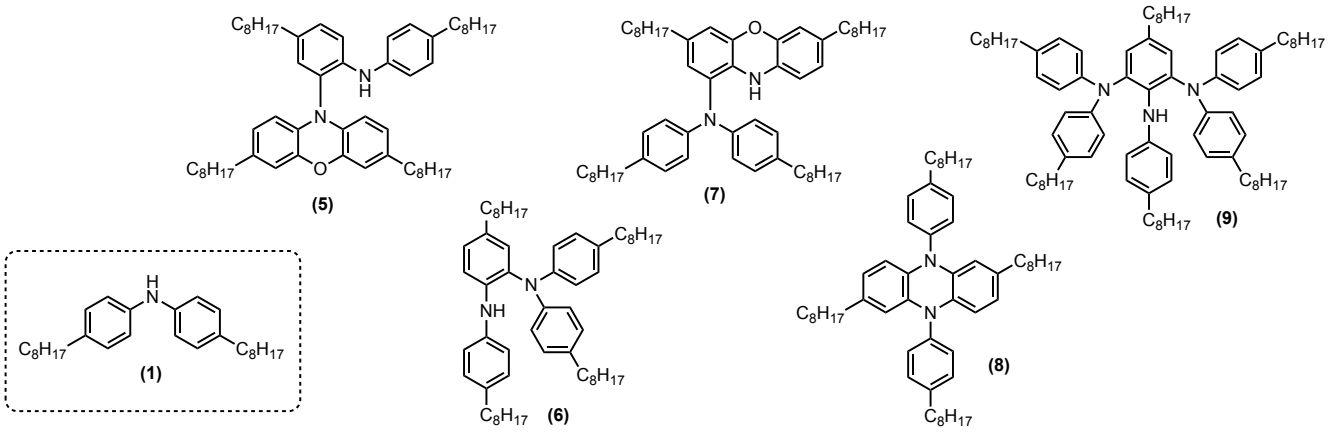

Figure 1.13 Diarylamine-derived dimeric and oligomeric products (**5**-**9**) observed and isolated upon high-temperature autoxidation inhibited by (**1**).[67]

In addition to experimental pitfalls, autoxidations were monitored by TLC, and diarylamine-derived products isolated by prep-TLC; no real-time characterization was performed, potentially skewing results towards silica-stable products or altering products further. Overall, such experiments have provided little information regarding the changes that occur to the diarylamine *in situ* during autoxidation, at what point during autoxidation changes occur, and whether or not key intermediates accumulate before forming end-products.

1.3 Measurements of RTA Activity

Although physicochemical properties of RTAs such as X-H BDE and oxidation potential can be useful predictors of activity, numerous techniques exist to determine an antioxidant's efficacy; some more reliable than others. The most accurate way to determine a compound's efficacy is through inhibited autoxidation

experiments, yet many researchers favour simpler, fluorescent or colorimetric assays based on redox activity.[68] Monitoring the reactions between putative RTAs and the major chain-carrying species, substrate-derived peroxyl radicals, is the most representative method to measure the efficacy.[69] Such experiments yield results that translate to non-research applications and provide useful kinetic data that cannot be obtained from many other assays.

1.3.1 Redox-based Assays

Redox-based assays are common methods of RTA assessment that have increased in popularity drastically in recent years due to their simplicity of use, which can be credited to the simple premise that they are based upon: absorbance or fluorescence change of a probe caused by reaction with a proposed RTA.[70] These experiments involve *in-situ* incubation of a fluorescent or colourimetric probe and a compound proposed to possess radical-trapping activity for an indiscriminate period of time. Reaction between the probe and suggested RTA is monitored by an accompanied change in colour or fluorescence; used to quantify its radical-trapping ability.

The quintessential redox-based assay is the DPPH assay; a colourimetric method that involves the reduction (or lack thereof) of 2,2-diphenyl-1-picrylhydrazyl (DPPH) by a putative RTA.[71] Among a myriad of issues, this assay fails to report on the kinetic properties of the RTA and instead simply measure the position of the redox equilibrium. In this regard, redox assays neglect to provide relevant information about the RTA; information that can only be properly acquired via inhibited autoxidation experiments.

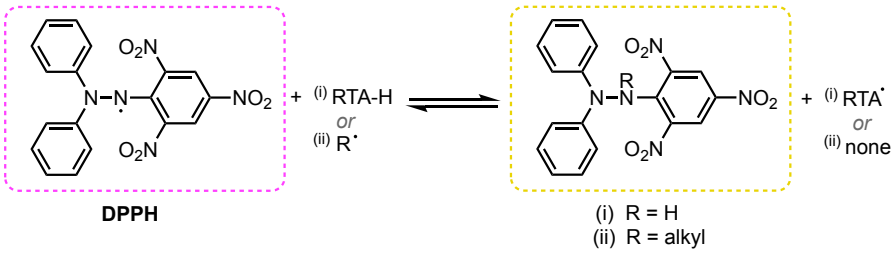

Scheme 1.8 Equilibrium between DPPH and reducing species: (i) radical-trapping antioxidant, or (ii) free radical.

1.3.2 Inhibited Autoxidations

Inhibited autoxidations mimic the conditions that RTAs encounter in real-world applications, whether it be suppression of autoxidation in lubricating oils at elevated temperatures or lipid bilayers under biological conditions. The experimental advantage inhibited autoxidations possess is their assessment of RTA efficacy with respect to the actual perpetrators of autoxidation: peroxyl radicals. They involve subjecting substrate to oxygenated atmosphere and initiating the reaction at well-defined rates, either through heating or via chemical initiation with free-radical initiators, or most often, a combination of both. Although autoxidation will occur spontaneously without prompting, accurate measurements of RTA activity require a definitive beginning to experiments. Additionally, the rates of initiation and propagation at ambient temperature are so low that experiments would be impractically long without kickstarting the process.

Generally, experiments at lower temperatures are primed with known concentrations of initiating species such as peroxides, hyponitrites, or azo-derivatives, to produce a known rate of radical generation (Figure 1.14).

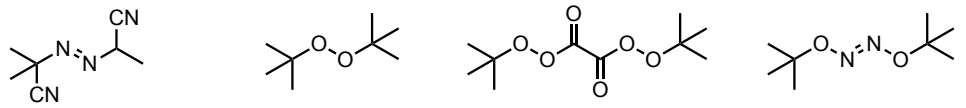

Figure 1.14 Chemical structures of common initiators and their half-life values ($t_{1/2}$) at various temperatures.[11]

These react with substrate to form substrate-derived radicals that quickly react with oxygen, entering the propagation cycle of autoxidation. RTA efficacy is measured by its ability to stifle the exponential accumulation of radical species over time. The kinetic parameters reflective of their performance, rate constant of inhibition (k_{inh}) and stoichiometry (n), are calculated using the observed time of inhibition (t_{inh}) (Figure 1.15 B). Initiators are utilized up to ca. 120˚C, at which point autoinitiation is possible.

Once initiated, the progress of an autoxidation can, in principle, be tracked either by consumption of starting materials or accumulation of products, namely O_2 or hydroperoxides; methods that both have their

respective drawbacks. Monitoring the consumption of oxygen is difficult from a technical aspect: it requires specialized equipment and a closed-system in order to measure the uptake of O_2 by substrate. The pressure of oxygen is monitored relative to a reference reaction that is completely inhibited; one in which no oxygen will be consumed.[3] As decomposition of the initiator is constant over time, the rate of oxygen incorporation into substrate is similarly constant. As reactions are monitored by the decrease of oxygen pressure and its rate, the efficacy of a radical-trapping antioxidant is reflected in the retardation of oxygen uptake. An additional disadvantage of this technique is the requirement for large concentrations of initiator: a sufficiently high R_i is required to produce quantifiable changes in pressure. Additionally, such techniques lose their utility at high temperatures due to oxygen dissolution into hydrocarbon becoming rate-limiting: oxygen therefore needs to be bubbled continuously, which is incompatible with the closed-vessel system required for monitoring its consumption.[34,72]

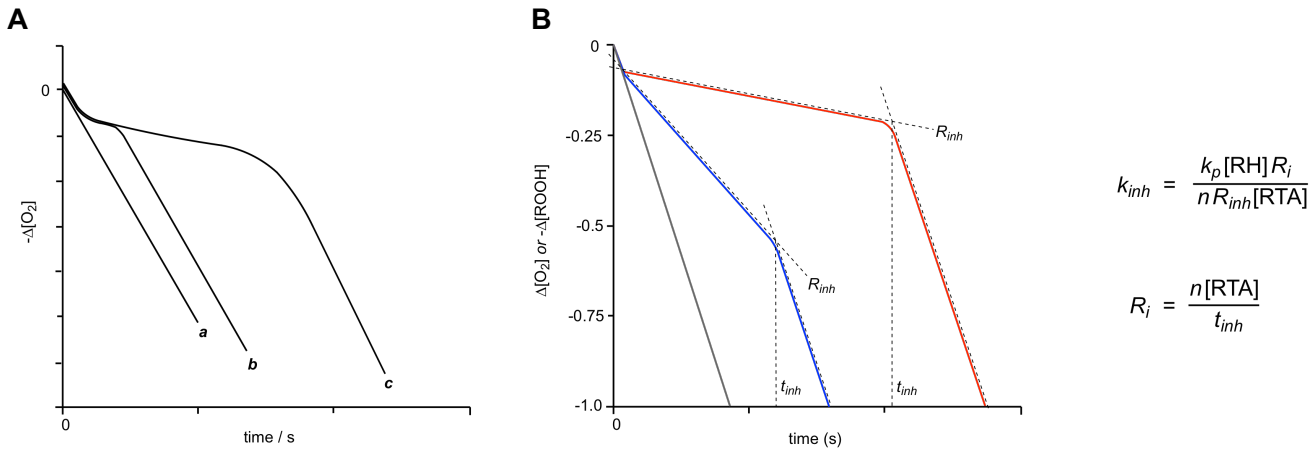

Figure 1.15 (**A**) Representative oxygen consumption trace: [a] Uninhibited, [b] Inhibited by poor RTA, [c] Inhibited by effective RTA.[72] (**B**) Representative uninhibited (•) and inhibited (•,•) autoxidation traces monitored by product formation or starting material consumption that follow well-defined kinetics. Initial rates used for calculations. Kinetic properties k_{inh} and n are obtained using the displayed formulas.

However, tracking autoxidation progress by oxygen consumption provides near-instantaneous information as the acquisition of pressure data is continuous. In contrast, traditional methods for quantifying the concentration *increase* of oxidation products, specifically hydroperoxides, are discontinuous: aliquots of the

reaction mixture obtained at set intervals during the experiment are analyzed by HPLC or GC to determine hydroperoxide concentration. Hydroperoxide products in solution are also first reduced with triphenylphosphine before comparison with authentic standards. Substrates with a variety of potential oxidation products such as long chain, unsaturated hydrocarbons, are therefore more laborious to analyze than those that produce comparatively fewer hydroperoxides, reducing its utility as a tool to monitor autoxidation progress.[20,73]

Iodometric titration can also be used to quantify oxidation products over the course of an autoxidation, yet doesn't require knowledge of the specific hydroperoxide structure(s) formed.[20,74,75] Hydroperoxide present in autoxidation samples oxidize iodide to form iodine and triiodide (I_3^-), which is subsequently titrated with a reducing agent. This method's utility suffers from its arduous, discontinuous nature, in addition to the large volumes of sample required for accuracy and the lack of selectivity for hydroperoxides: the iodide and reducing agent can undergo redox reactions with other species present in the sample.

1.3.3 Novel Methods for Monitoring Inhibited Autoxidations

In recent years, our group has developed methods that circumvent the specific issues that plague the aforementioned analytical techniques for monitoring autoxidations. Primarily, a continuous, visible-light spectrophotometric approach using a boron dipyrromethene (BODIPY)-derived probe was established in order to provide a technique for obtaining kinetic information that is operationally simple as redox assays like the DPPH method, but is quantitative and chemically rigorous as an inhibited autoxidation.[76] The BODIPY core is functionalized with conjugated, autoxidizable substituents such as styrenyl or 1-phenylbutadienyl fragments to yield STY-BODIPY and PBD-BODIPY respectively, which alter the absorbance spectrum of the dye upon deconjugation via reaction with peroxyl radicals. Thus, the BODIPY dyes function as co-substrates, autoxidizing at known rates relative to the substrate, allowing for facile tracking of autoxidations with a UV-VIS spectrophotometer in a manner analogous to the continuous oxygen consumption method (Figure 1.16 A-C). Relevant kinetic data pertaining to antioxidant efficacy (k_{inh}, n) are then easily obtained from the absorbance data. Although autoxidation is monitored indirectly with this method via concentration changes of a proxy, it

provides flexibility in regards to solvents, substrates, concentrations, and temperatures, provided that the dye can be standardized under the desired set of conditions.

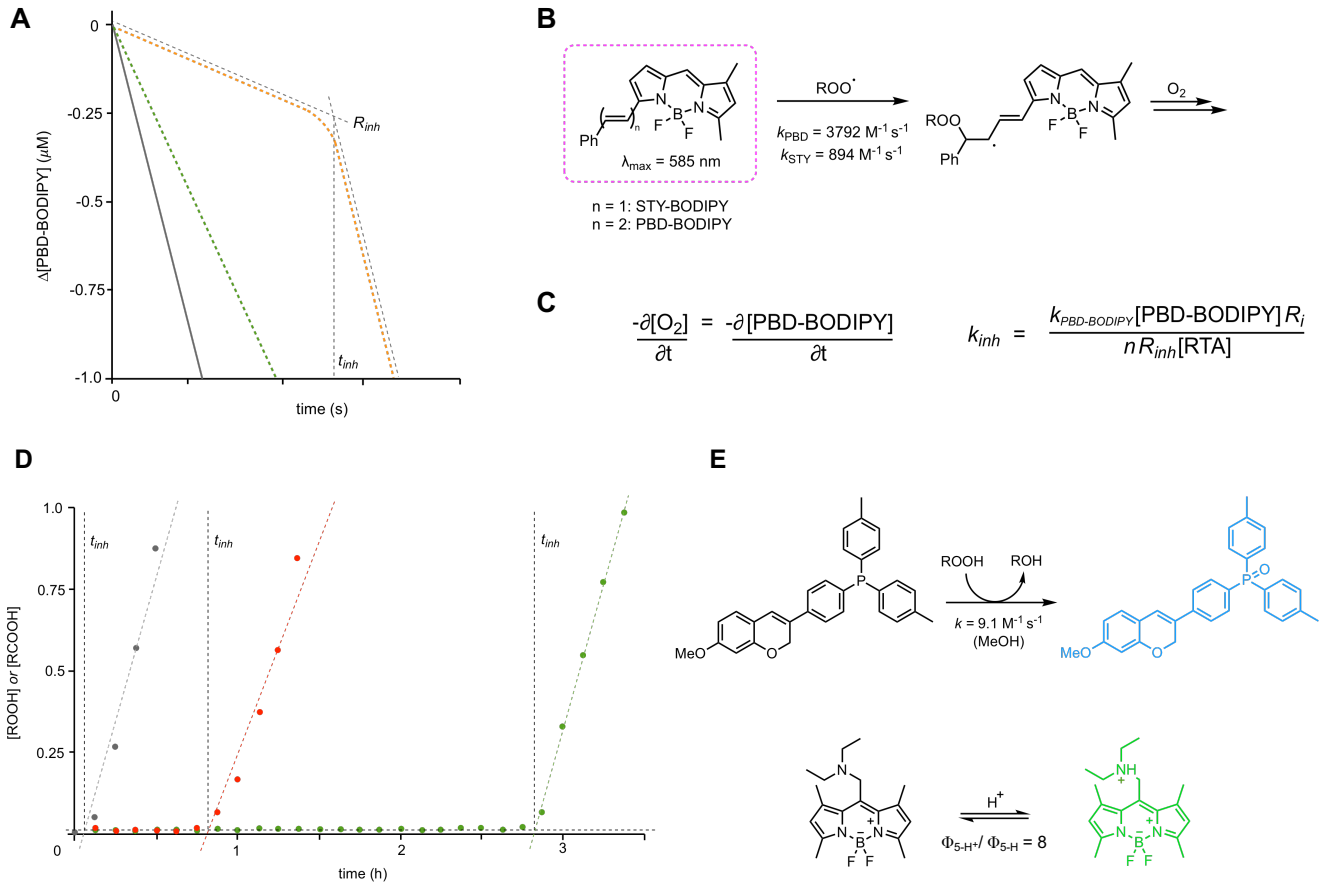

Figure 1.16 (**A**) Representative PBD-BODIPY co-autoxidations of uninhibited (●), inhibited with weakly reactive RTA (●) and inhibited with reactive RTA (●). (**B**) PBD-BODIPY loss of colour via reaction with peroxyl radical and oxygen.[76] (**C**) Equations used to calculate kinetic properties of RTAs when using co-autoxidizable substrate dye, PBD-BODIPY. (**D**) Representative traces of high-temperature autoxidation using hydroperoxide-sensitive coumarin triarylphosphine- or trialkylamine-BODIPY-probe with: no RTA (●), moderate RTA (●), and good RTA (●).[36] (**E**) Reactions of phosphine probe with hydroperoxide and acid-sensitized BODIPY probe with acid to yield fluorescent products. (Adapted with permission from Haidasz, E. A.; Van Kessel, A. T. M.; Pratt, D. A. *J. Org. Chem.* **2016**, *81*, 3, 737-744 and Shah, R.; Pratt, D. A. *J. Org. Chem. 81*, 15, 6649-6656, © 2020 American Chemical Society)

Our group also recently designed a dual-probe method that boasts a simple, albeit discontinuous method of simultaneously quantifying both acid and hydroperoxide concentrations in autoxidation samples in order to avoid employing laborious HPLC/GC analyses or iodometric titrations.[36,77] Pro-fluorescent phosphine probes

have proven useful tools for quantifying hydroperoxides in hydrocarbon substrates and lipid membranes. Harnessing the reactivity of organophosphorus compounds with hydroperoxides – the primary product of autoxidation – allows hydroperoxides to be quantified, indicating the severity of hydrocarbon damage, i.e. the progression of autoxidation. The coumarin-triarylphoshphine probe developed by our group is oxidized by alkylhydroperoxides at the phosphine, precluding it from participating in photoinduced electron transfer (PeT) with the fluorophore, enhancing the fluorescence of the probe (Figure 1.16 E).[77] Measurement of the *pseudo*-first order rate of fluorescence increase via microplate assay allows for rapid and convenient quantification of hydroperoxides in each sample, yielding curves that indicate the inhibition periods (Figure 1.16 D). Combination of the fluorogenic coumarin-triarylphosphine with an acid-sensitive BODIPY probe allows for quantification of the second key product that arises *in-situ* during autoxidation: carboxylic acids. The BODIPY-trialkylamine is protonated by acids in solution resulting in enhanced fluorescence of the neighbouring BODIPY fluorophore, the emission data of which is then used to calculate acid concentration (Figure 1.16 E).[36] This duality is made even more efficient by its application using an automated microplate reader, allowing an enormous number of samples to be easily analyzed with minimal preparation. Also, unlike with HPLC/GS analyses, the fluorogenic phosphine method is not dependent on the structures of the hydroperoxide, enabling quantification in more complex substrates and experiment conditions, specifically at high temperatures. However, reliable kinetic data can rarely be extracted from high temperature autoxidations due to autoinitiation: ever-increasing R_i prohibits accurate calculations of kinetic properties of the RTAs. As a result, high temperature assessment of RTA efficacy generally involves qualitative observations, measurement of simple values such as t_{inh}, and comparison to kinetic properties calculated at ambient temperatures.

1.4 Research Objectives

1.4.1 On the Fate of Diarylaminic RTAs During Hydrocarbon Autoxidation at Elevated Temperatures

Although a major component of lubricant formulations, the mechanism of diarylamine radical-trapping antioxidants at high temperatures is poorly understood, particularly in their off-cycle, unproductive reactions that yield non-RTA products. Due to the difficulty of isolating and analyzing these products, not to mention the issues associated with doing so, little information about the fates of these compounds exists beyond computational experiments. Although there are multiple methods of monitoring high-temperature autoxidations, there are no reported methods for specifically monitoring the speciation of diarylaminic RTAs during such processes. However, recent efforts by our group have led to the development of a spectroscopic method of doing so: solvent-suppressed, $^{1}H–^{15}N$ HMBC of isotopically labelled diarylamines. With the foundation for a characterization method to 'track' diarylamines over the course of autoxidations and ^{15}N enriched compounds at hand, we sought to accomplish a number of related objectives:

- Identify the major diarylamine-derived oxidation products that force an exit from the Korcek cycle
- Determine the regenerative ability of purported 'Korcek intermediates'

1.4.2 Effects of NO_x on Diarylaminic RTAs During Hydrocarbon Autoxidation at Elevated Temperatures

NO_x has been a known contributor to autoxidation in lubricating oils of internal combustion engines via initiation of new radical chains and has been demonstrated to interact with phenolic RTAs. Although phenolic RTAs 'trap' NO_x, they do so in a manner similar to their uncomplicated, stoichiometric trapping of peroxyl radicals.

Diarylamines on the other hand, possess a more complex mechanism of turnover due to their seemingly catalytic activity at high temperatures, which may be complicated by exposure to NO_x and/or NO_x derived oxidation products. However, little research has reported the effects of NO_x on diarylaminic RTAs when inhibiting high-temperature autoxidation past end-product analysis, despite diarylamines ubiquity and

importance as an additive. Reports on the effects of NO_x on diarylaminic RTA during high-temperature autoxidation performed in 'real-time' utilized GC-MS to measure reaction progress and speciation. Thus, research in this area suffers from similar issues as diarylamine speciation studies under normal autoxidation conditions. Our group proposed to investigate in collaboration alongside an industrial partner, with the following objectives guiding our efforts:

- Determine the effect of NO_x on high-temperature, hydrocarbon autoxidation in the presence of industrially-representative, labelled diarylaminic RTAs using our HMBC technique
- Determine if NO_x affect the diarylamine during autoxidation, identifying any unique intermediate and/or decomposition species that result

1.5 References

[1] Valko, M.; Leibfritz, D.; Moncol, J.; Cronin, M. T. D.; Mazur, M.; Telser, J. *Int. J. Biochem. Cell Biol.* **2007**, *39*, 44-84.

[2] Dröge, W. *Physiol. Rev.* **2002**, *82*, 47-95.

[3] Ingold, K. U. *Chem. Rev.* **1961**, *61*, 563-589.

[4] Ingold, K. U.; Pratt, D. A. *Chem. Rev.* **2014**, *114*, 9022-9046.

[5] Borden, W. T.; Hoffman, R.; Stuyver, T.; Chen, B. *J. Am. Chem. Soc.* **2017**, *139,* 9010-9018.

[6] Halliwell, B.; Gutteridge, J. M. C. Free Radical Biology & Medicine. *Free Radic. Biol. Med.* **2015**, *34* (12)

[7] Finkel, T.; Holbrook, N. J. *Nature,* **2000**, *408,* 239-247.

[8] Halliwell, B. *Biochem. J.* **2007**, *401*, 1-11.

[9] Hwang, O. *Exp. Neurobiol.* **2013**, *22*, 11-17.

[10] Poon, J-F; Pratt, D. A. *Acc. Chem. Res.* **2018**, *51*, 1996-2005.

[11] Denisov, E. T.; Denisova, T. G.; Pokidova, T. S. *Handbook of Free Radical Initiators.* Hoboken, NJ. **2003**.

[12] Maillard, B.; Ingold, K. U.; Scaiano, J. C. *J. Am. Che. Soc.* **1983**, *105*, 5095-5099.

[13] Cooper, H. R.; Melville, H. W. *J. Chem. Soc.* **1951,** 1984-1993.

[14] Cooper, H. R.; Melville, H. W. *J. Chem. Soc.* **1951**, 1994-2002.

[15] Ingold, K. U. *J. Inst. Petrol.* **1959**, *45,* 244-251.

[16] Russell, G. A. *J. Am. Chem. Soc.* **1956**, *78*, 1041-1044.

[17] Jensen, R.; Korcek, S.; Zinbo, M.; Johnson, M. *Int. J. Chem. Kinet.* **1990**, *22*, 1095-1107

[18] Howard, J. A.; Ingold, K. U. *Can. J. Chem.* **1967**, *45*, 793-802.

[19] Zielinski, Z.; Pratt, D. A. *J. Org. Chem.* **2017**, *82*, 2817-2825.

[20] Xu, L.; Davis, T. A.; Porter, N. A. *J. Am. Chem. Soc.* **2009**, *131*, 13037-13044.

[21] Zavitsas, A. A. *J. Am. Chem. Soc.* **1972**, *94*, 2779-2789.

[22] Korcek, S.; Chenier, J. H. B.; Howard, J. A.; Ingold, K. U. *Can. J. Chem.* **1972**, *50*, 2285-2297.

[23] Zavitsas, A. A; Chatgilialoglu, C. *J. Am. Chem. Soc.* **1995**, *117*, 10645-10654.

[24] Beckwith, A. L. *Chem. Soc. Rev.* **1993**, *22*, 143-151.

[25] Giese, B. *Angew. Chem. Int. Ed. Engl.* **1983**, *22*, 753-764.

[26] Kaushal, P.; Mok, P. L. H.; Roberts, B. P. *J. Chem. Soc., Perkin Trans. 2* **1990**, 1663.

[27] Isborn, C.; Hovrat, D. A.; Borden, T. W.; Mayer, J. M.; Carpenter, B. K. *J. Am. Chem. Soc.* **2005**, *127*, 5794-5795.

[28] Hu, D.; Pratt, D. *Chem. Commun.* **2010**, *46*, 3711-3713.

[29] Avila, D. V.; Brown, C. E.; Ingold, K. U.; Lusztyk, J. *J. Am. Chem. Soc.* **1993**, *115*, 466-470.

[30] Batten, J. J.; Mulcahy, M. F. R. *J. Chem. Soc.* **1956**, 2949-2959.

[31] Russell, G. A. *J. Am. Chem. Soc.* **1957**, *79*, 3871-3877.

[32] Lee, R.; Gryn'ova, G.; Ingold, K. U.; Coote, M. L. *Phys. Chem. Chem. Phys.* **2016**, *18*, 23673-23679.

[33] Howard, J. A.; Adamic, K.; Ingold, K. U. *Can. J. Chem.* **1969**, *47*, 3793-3795.

[34] Jensen, R. K.; Korcek, S.; Mahoney, L. R.; Zinbo, M. *J. Am. Chem. Soc.* **1979**, *101*, 25, 7574-7584.

[35] Jensen, R. K.; Korcek, S.; Mahoney, L. R.; Zinbo, M. *J. Am. Chem. Soc.* **1981**, *103*, 1742-1749.

[36] Shah, R.; Pratt, D. A. *J. Org. Chem.* **2016**, *81,* 15, 6649-6656.

[37] Johnson, M. D.; Korcek, S. *Lubri. Sci.* **1991**, *3*, 95-118.

[38] Spindt, R. S.; Wolfe, C. L.; Stevens, D. R. *SAE Trans.* **1956**, *64,* 797-804.

[39] Titov, A. I. *Tetrahedron.* **1963**, *19*, 557-580.

[40] Adachi, H.; Basco, N. *Int. J. Chem. Kinet.* **1982**, *14*, 1243.

[41] Atkinson, R.; Aschmann, S. M.; Carter, W. P. L.; Winer, A. M.; Pitts Jr., J. N. P. *J. Phys. Chem.* **1982**, *86*, 4563-4569.

[42] Pryor, W. A.; Castle, L.; Church, D. F. *J. Am. Chem. Soc.* **1985**, *107,* 211-217.

[43] Holdsworth, J. D.; Scott, G.; Williams, D. *J. Chem. Soc.* **1964**, 4692-4699.

[44] Chauvin, J-P. R.; Griesser, M.; Pratt, D. A. *Chem. Sci.* **2019**, *10*, 4999-5010.

[45] Brownlie, I. T.; Ingold, K. U. *Can. J. Chem.* **1967**, *45*, 2427-2432.

[46] Bowry, V. W.; Ingold, K. U. *J. Am. Chem. Soc.* **1992**, *114*, 4992-4996.

[47] Sobek, J.; Martschke, R.; Fischer, H. J. *J. Am. Chem. Soc.* **2001**, *123*, 2849-2857.

[48] Haidasz, E. A.; Meng, D.; Amorati, R.; Baschieri, A.; Ingold, K. U.; Valgimigli, L.; Pratt, D. A. *J. Am. Chem. Soc.* **2016**, *138*, 5290-5298.

[49] Mayer, J. M.; Hovrat, D. A.; Thomas, J. L. Borden, W. T. *J. Am. Chem. Soc.* **2002**, *124*, 11142-11147.

[50] Shah, R.; Margison, K.; Pratt, D. A. *ACS Chem. Biol.* **2017**, *12*, 2538-2545.

[51] DiLabio, G. A.; Johnson, E. R. *J. Am. Chem. Soc.* **2007**, *129,* 6199-6203.

[52] Hanthorn, J. J.; Amorati, R.; Valgimigli, L.; Pratt, D. A. *J. Org. Chem.* **2012**, *77*, 6895-6907.

[53] Yehye, W. A.; Rahman, N. A.; Ariffin, A.; Hamid, S. B. A.; Alhadi, A. A.; Kadir, F. A.; Yaeghoobi, M. *Eur. J. Med. Chem.* **2015**, *101*, 295-312.

[54] Burton, G. W.; Ingold, K. U. *Acc. Chem. Res.* **1986**, *19*, 194-201

[55] Ingold, K. U.; Bowry, V. W.; Stocker, R.; Walling, C. *Proc. Natl. Acad. Sci.* **1993**, *90*, 45-49.

[56] Weenen, H.; Porter, N. A. *J. Am. Chem. Soc.* **1982**, *104*, 5216-5221.

[57] Takahashi, M.; Tsuchiya, J.; Niki, E. *Bull. Chem. Soc. Jpn.* **1989**, *62*, 6, 1880-1884.

[58] Harrison, K.; Haidasz, E. A.; Griesser, M.; Pratt, D. A. *Chem. Sci.* **2018**, *9*, 6068-6079.

[59] Shah, R. *Autoxidation and its Inhibition in Both Industrial and Biological Contexts: New Molecules, Methods, and Mechanisms.* Ph.D. Dissertation, University of Ottawa, Ottawa, CA. **2019**.

[60] Bolsman, T. A. B. M.; Blok, A. P.; Frijns, J. H. G. *Recl. Trav. Chim. Pays-Bas.* **1978**, *97*, 12, 310-312.

[61] Jensen, R. K.; Korcek, S.; Zinbo, M.; Gerlock, J. L. *J. Org. Chem.* **1995**, *60*, 5396-5400.

[62] Haidasz, E. A.; Shah, R.; Pratt, D. A. *J. Am. Chem. Soc.* **2014**, *136*, 47, 16643-16650.

[63] Hanthorn, J. J.; Valgimigli, L.; Pratt, D. A. *J. Am. Chem. Soc.* **2012**, *134*, 8306-8309.

[64] Shah, R.; Haidasz, E. A.; Valgimigli, L.; Pratt, D. A. *J. Am. Chem. Soc.* **2015**, *137*, 7, 2440-2443.

[65] Pratt, D. A.; DiLabio, G. A.; Brigati, G.; Pedulli, G. F.; Valgimigli, L. *J. Am. Chem. Soc.* **2001**, *123*, 4625-4626.

[66] Haidasz, E. A.; Pratt, D. A. *Org. Lett.* **2017**, *19*, 1854-1857.

[67] Zeman, A.; Römer, R.; Von Roenne, V. *Lubr. Sci.* **1986**, *3*, 4, 309-326.

[68] Li, B.; Pratt, D. A. *Free Radic. Biol. Med.* **2015**, *82,* 187-202.

[69] Amorati, R.; Valgimigli, L. *Free Radic. Res.* **2015**, *49*, 633-649.

[70] Shah, R.; Farmer, L. A.; Zilka, O.; Van Kessel, A. T. M.; Pratt, D. A. *Cell Chem. Biol.* **2019**, *26*, 11, 1594-1607.

[71] Kedare, S. B.; Singh, R. P. *J. Food Sci. Technol.* **2011**, *48*, 412-422.

[72] Lucarini, M.; Pedrielli, P.; Pedulli, G. F.; Valgimigli, L.; Gigmes, D.; Tordo, P. *J. Am. Chem. Soc.* **1999**, *121*, 49, 11546-11553.

[73] Igarashi, J.; Jensen, R. K.; Lusztyk, J.; Korcek, S.; Ingold, K. U. *J. Am. Chem. Soc.* **1992**, *114*, 7727-7736.

[74] Howard, J. A.; Ingold, K. U. *Can. J. Chem.* **1966**, *44*, 1119-1130.

[75] Barthel, G.; Grosch, W. *J. Am. Oil. Chem. Soc.* **1974**, *51*, 540-544.

[76] Haidasz, E. A.; Van Kessel, A. T. M.; Pratt, D. A. *J. Org. Chem.* **2016**, *81*, 3, 737-744.

[77] Hanthorn, J. J.; Haidasz, E. A.; Gerbhardt, P.; Pratt, D. A. *Chem. Comm.* **2012**, *48*, 10141-10143.

Chapter 2: On the Fate of Diarylaminic RTAs During Hydrocarbon Autoxidation at Elevated Temperatures

Preface

Preventing or impeding autoxidation is an essential endeavour due to the economic and environmental benefits realized, and constant improvement in this field is a key focus of research and development in the chemical industry. An important strategy for countering autoxidation is the use of radical-trapping antioxidants (RTAs), which react with chain-carrying radicals to inhibit propagation. Of such RTAs, diarylamines are uniquely useful at elevated temperatures due to their ability to break many chains through a catalytic mechanism. As such, they are key additives in lubricant formulations used in internal combustion engines. However, ever-stricter emissions requirements have forced manufacturers to design engines that burn fuel at higher temperatures, resulting in an increased demand from diarylamines, which the current technology cannot effectively meet. Given their catalytic activities, understanding the off-cycle pathways that ultimately lead to their consumption is essential to properly inform efforts of improvement and structural design. Past efforts in this area have suffered from a lack of real-time analysis and difficulty deciphering complex product distributions using analytical tools such as gas chromatography and liquid chromatography. Our group recently developed a ^{1}H ^{15}N heteronuclear multi-bond correlation (HMBC) technique/spectroscopic method to track isotopically-enriched diarylamines throughout autoxidation experiments. Herein, we describe our efforts of employing this technique to assist in the identification of diarylamine oxidation products, and thus propose possible mechanisms of deactivation. Our results also provide support to the regeneration of diarylamine from diarylnitroxide and diarylalkoxyamine intermediates, and probe the effects of altering conditions on diarylamine speciation. The implementation of the ^{1}H ^{15}N HMBC approach was made possible with the very kind assistance of Dr. Glenn A. Facey and calculations were carried out by Dr. Evan A. Haidasz.

2.1 Introduction

Diarylamine RTAs have been staple additives in the chemical industry for decades as a result of their utility as preservatives. Due to their highly-efficient performance in high temperature applications, they are particularly useful for stifling autoxidation in lubricating oils used in internal combustion engines (ICEs). However, in order to meet ever-stricter emissions standards, ICE automobile manufacturers often turn to the simplest solution to increase efficiency: design engines to operate at higher temperatures. Although this maximizes fuel-burning efficiency and reduces incomplete combustion, it places the lubricating oil under greater oxidative stress which is difficult to effectively counter by current diarylamine technology. Therefore, fuel lubricants degrade more quickly under the harsher conditions, requiring more frequent replacement of lubricant and filters (resulting in increased consumption of petrochemical feedstocks) and/or more widespread adoption of expensive synthetic lubricants in order to obtain similar engine performance. As such, improving the current diarylamine scaffold is highly desirable for increasing lubricant oil and engine performance and for slowing the use of non-renewable, fossil fuel resources.

Previous research has suggested that diarylamines (**1**) owe the efficiency with which they suppress autoxidation at high temperatures to a catalytic mechanism that regenerates the starting material while trapping multiple chain-carrying species.[1,2] Stoichiometric numbers of peroxyl consumption by diarylamines (*n*) have been measured as high as 41 during the autoxidation of paraffin oil at 130˚C,[1] but could be even greater; quantification of stoichiometry at higher temperatures becomes problematic due to the variable rate of initiation caused by decomposition of hydroperoxide products formed during inhibition.[3] Upon observation that the diarylnitroxide (**2**) could be regenerated from (**1**) – and vice versa – during autoxidation, Korcek and co-workers proposed a catalytic cycle to explain the reactivity of diarylamines under these conditions (Figure 2.1 A).[2,4] The 'Korcek cycle' involves the consumption of a net two radicals per revolution and involves the regeneration of (**1**) via the diarylalkoxyamine (**4**) through elimination of a carbonyl species. The regeneration of the RTA is presumably limited by off-cycle pathways (Figure 2.1 B). This reduces the concentration of diarylamine

available to inhibit autoxidation and results in more rapid degradation of the substrate. The diarylamine is likely most vulnerable to problematic off-cycle reactions once converted to the diarylaminyl radical (**2**) and diarylnitroxide radical (**3**), due to the extremely rapid rates at which radical-radical reactions occur.[3]

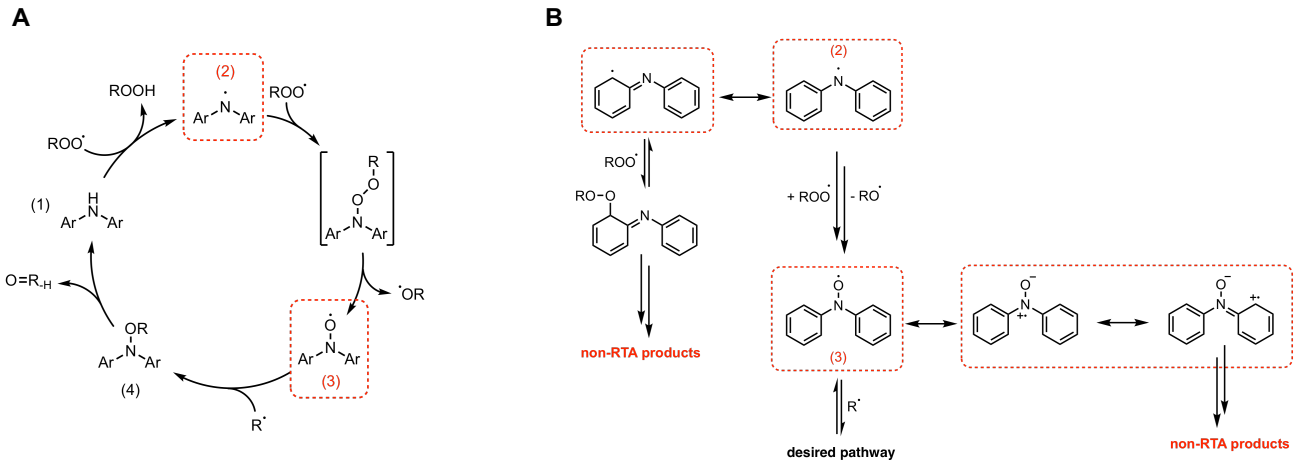

Figure 2.1 (**A**) Species in Korcek cycle vulnerable to off-cycle, competing reactions.[3,4] (**B**) Potential, competing off-cycle reactions between (**2**) or (3) and peroxyl radicals. (Adapted with permission from Haidasz, E. A.; Shah, R.; Pratt, D. A. *J. Am. Chem. Soc.* **2014**, *136*, 47, 16643-1665, © 2020 American Chemical Society)

The diarylaminyl radical (**2**) is stabilized by delocalization of the radical throughout the π-system of the phenyl substituents. The diarylnitroxide radical also benefits from delocalization into the phenyl substituents, but is further stabilized by π-orbital delocalization between the nitrogen and oxygen; the reason many aminoxyl radicals with sufficient steric bulk are bench-stable. Although (**2**) is less stable (more reactive) than (**3**), it is carried forward through the cycle by combination with a peroxyl radical; the more abundant of the two chain-carrying species. Conversely, (**3**) requires an alkyl radical to form (**4**); an unfavourable scenario due to the low, steady-state concentration of alkyl radicals during autoxidation. Due to the relative reactivity of (**2**) and the higher steady-state concentration of (**3**), both species provide potential sources for off-cycle reactions.

Characterization of the products of diarylamine oxidation is difficult: GC-MS and HPLC/UPLC-MS techniques can provide useful information, but deconvoluting diarylaminic products from substrate-derived products complicates the process; especially when performed at the RTA loadings representative of 'real-world' applications. Past efforts have involved carrying out inhibited autoxidations of long-chain ester substrates

followed by base-hydrolyses to separate from diarylaminic products.[5] However, this assumes that the product distribution is not affected by hydrolysis, which seems dubious given that oxidation products are generally electrophilic. Product identification *in situ,* without the need for extraction and/or derivatization would be the ideal approach, and we envisioned this could be achieved using NMR spectroscopy.

Tracking the speciation of diarylamines spectroscopically over the course of an autoxidation presents a unique challenge as RTAs are generally present at extremely low concentrations. Increasing the concentration of RTA would not only result in prohibitively lengthy experiments unless large quantities of initiators are added, but would also not be representative of the loadings used in applications, which are approximately one weight-percent. As such, common NMR spectroscopy employing nuclei such as ^{1}H and ^{13}C are impractical as signals of any diarylamine-derived species will be drowned out by the substrate and its corresponding oxidation products. Incorporation of a ^{19}F atom into the diarylamine is an attractive approach, but would obviously require fluorination of the species in a manner that would not alter its electronics and reactivity. The ideal positions to minimize the impact of changes in electronics would be the *meta* position(s) of the aryl substituents, but this substitution would require *de novo* synthesis of the RTA. Fluorination of any groups too far removed from the aryl rings themselves, such as innocuous fluorination of the *para*-alkyl substituents, would not be guaranteed to provide enough signal variation to resolve the multitude of diarylamine oxidation products that are expected.

The nitrogen atom of diarylamine RTAs enables resolution of its oxidation products to be distinguished from the hydrocarbon mixture by utilization of ^{15}N NMR techniques. In preliminary work, we evaluated the feasibility of a 2D heteronuclear multiple bond correlation (HMBC) NMR experiment to track diarylamine-derived autoxidation products by their characteristic ^{15}N and ^{1}H correlations. Ideally, non-correlative, direct ^{15}N NMR spectroscopy could be used to monitor the speciation of the diarylamine during experiments, but the required experimental conditions and properties of ^{15}N isotopes/nuclei exclude this possibility. Although stable, the ^{15}N isotope has a natural abundance of approximately 0.36% combined with a relatively low gyromagnetic ratio ($\gamma = -27.116 \times 10^{6}$ rad $T^{-1}s^{-1}$) compared to those of ^{1}H or ^{13}C ($\gamma = 267.52 \times 10^{6}$ rad $T^{-1}s^{-1}$ and $\gamma = 67.28 \times 10^{6}$ rad $T^{-1}s^{-1}$, respectively), offering extremely poor sensitivity.[6] To make matters worse, the relaxation time for the

^{15}N nucleus is also relatively long, increasing acquisition times significantly.[7] Due to the low concentrations of RTAs used in autoxidations, a more sensitive method is required even if autoxidations could be performed with ^{15}N-enriched diarylamines.

HMBC techniques exploit the proton channel to provide increased sensitivity and reduce acquisition times normally encountered with direct ^{15}N NMR.[8] Experiments with the diarylamine display long-range coupling between the ^{15}N and the *ortho* and *meta* hydrogen atoms (optimized for J = 10 Hz) and are sensitive enough such that functionalization on the nitrogen or aryl substituents themselves during oxidation alters signals sufficiently for differentiation. We were able to strategically suppress signals of the native substrate by pre-saturating the receiver, enabling quick acquisition of HMBC data with minimal signal interference by *n*-hexadecane and without further diluting sample in deuterated solvent. Although still technically discontinuous since the autoxidations are carried out at elevated temperature in a stirred-flow reactor, this method provides results more rapidly than the aforementioned methods and the need to separate and/or purify the samples before analysis, providing the most accurate characterization of the RTA and its oxidation products *in situ.* Furthermore, it can be used as a method to confirm if purification or separation of a sample alters the structure or functionality of the oxidation products present when used in tandem with other analytical approaches.

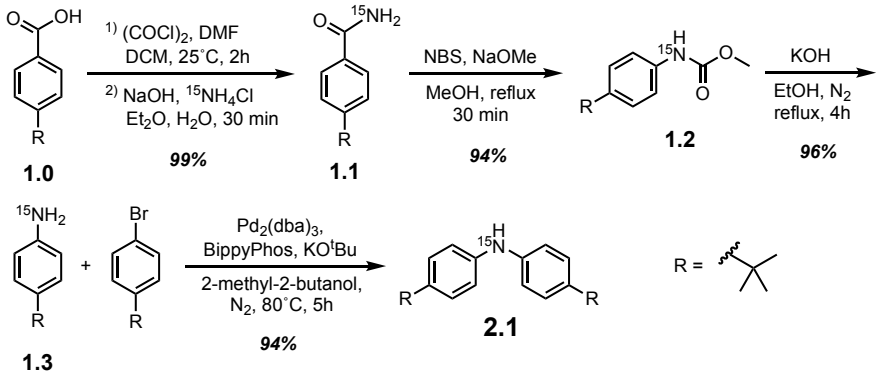

Scheme 2.1 Synthesis of ^{15}N *bis*(4-*tert*-butylphenyl)amine (**2.1)** from 4-*tert*-butylbenzoic acid (**1.0**) and ^{15}N ammonium chloride.

^{15}N-enriched diarylamines can be accessed easily using well-precedented chemistry. For example, diarylamine **2.1**, a truncated analog of the *tert*-alkylated diphenylamines used in engine lubricants, can be obtained in

excellent overall yields from relatively inexpensive starting materials (Scheme 2.1). Our preliminary experiments demonstrated a unique signal for enriched diarylamine **2.1** (Figure 2.2 A) that was easily distinguished from the products it formed during high-temperature autoxidation experiments in *n*-hexadecane (Figure 2.2 B,C), as described in 2.6.1 of the Experimental section.

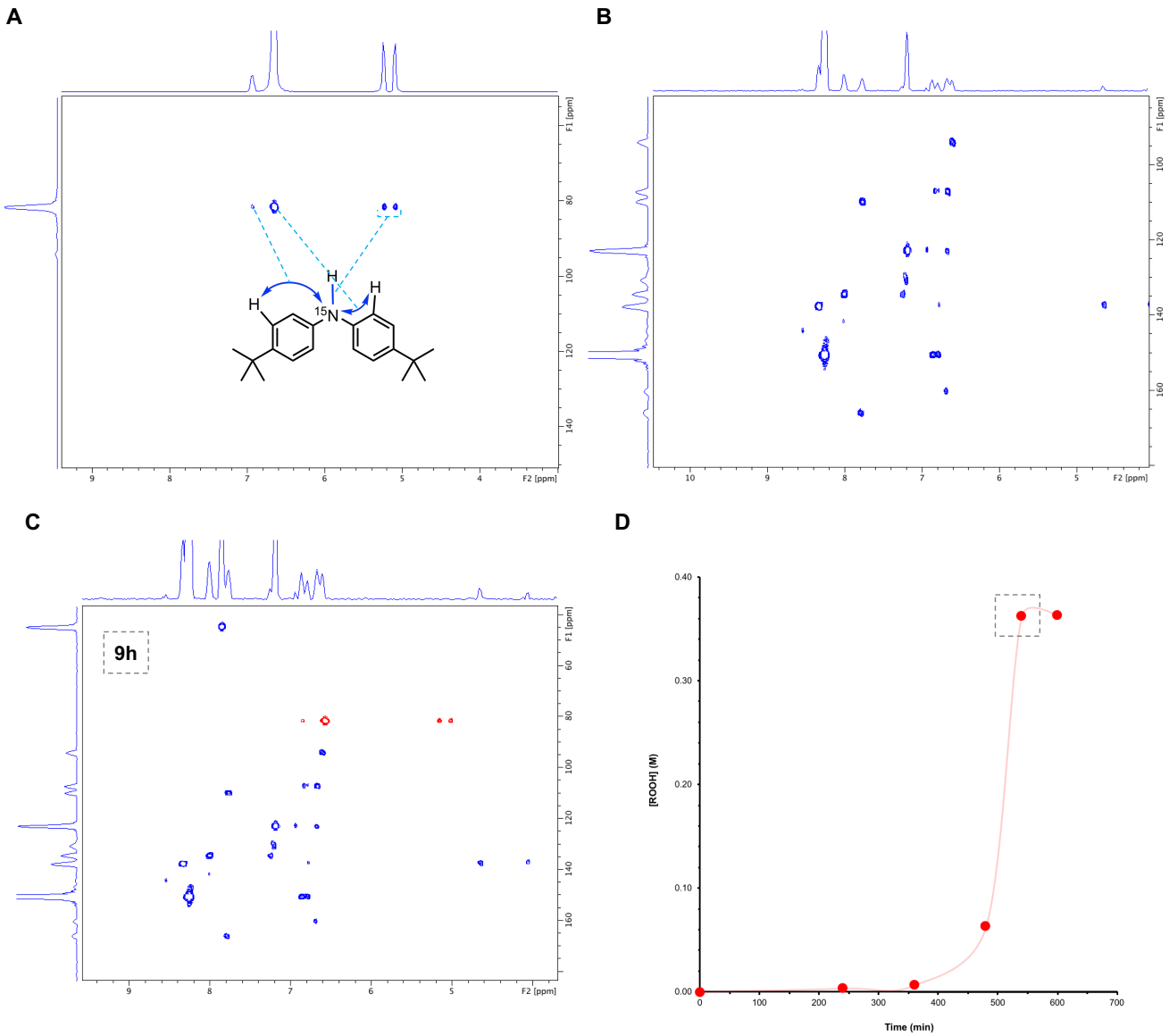

Figure 2.2 Representative HMBC spectra (where *x*-axis = ^{1}H, *y*-axis = ^{15}N) of: (**A**) diarylamine before autoxidation, (**B**) post-inhibition products of diarylamine during high-temperature autoxidation of *n*-hexadecane at 9 hours, and (**C**) overlay of starting diarylamine (red) and oxidation products (blue). (**D**) Corresponding hydroperoxide formation during autoxidation, with 9 hours indicated.

These experiments also correlate well to analysis of hydroperoxide concentration using our hydroperoxide-sensitive phosphine probe assay[9]: the disappearance of the starting diarylamine coincides with the end of the inhibited period, which is associated with the rapid increase of hydroperoxide concentration (Figure 2.2 C,D).

As part of our preliminary efforts, we also carried out the synthesis of ^{15}N-enriched samples of the hydroxylamine and alkoxyamine derivatives of the diarylamine, the latter being the key intermediate of the Korcek cycle (Scheme 2.2). However, they did not correlate with any of the observed oxidation products, suggesting that if they are formed, they are transient intermediates and do not accumulate. The diarylnitroxide (**2.1a**) is a useful standard for electron paramagnetic resonance (EPR) spectroscopy but is not visible by NMR due to the anomalous Zeeman effect.

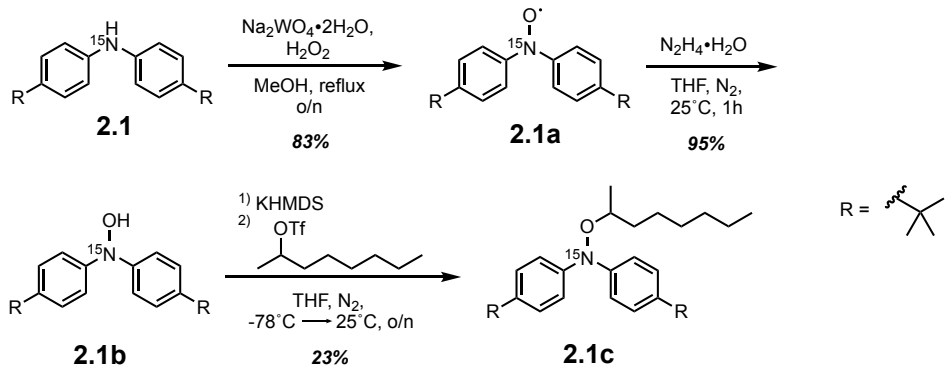

Scheme 2.2 Synthesis of purported intermediates of the Korcek cycle; diarylnitroxide radical (**2.1a**) and the diarylalkoxyamine (**2.1c**), as well as the synthetic intermediate, diarylhydroxylamine (**2.1b**).

Although the HMBC method provides chemical shifts of nitrogen species, the signals do not provide enough information to characterize each compound beyond general functional group chemical shift ranges. Therefore, we sought to synthesize ^{15}N-enriched species that we postulated were likely products of diarylamine autoxidation (Figure 2.3) in order to compare their respective HMBC signals to those of diarylamine speciation. These products included species described in previous reports, implicated by computational work, or plausible based on our current understanding of radical chemistry and autoxidation.

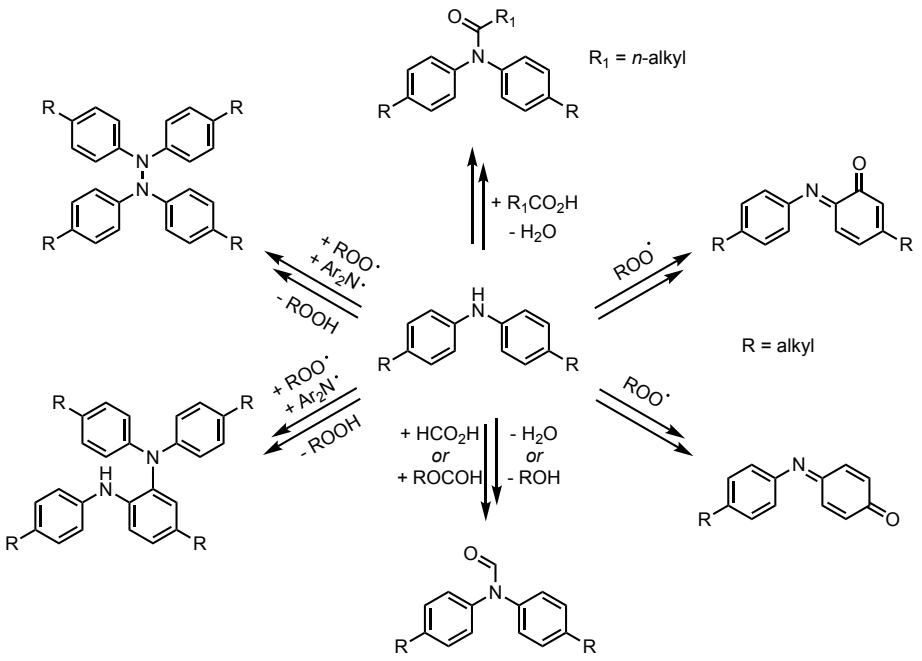

Figure 2.3 Possible non-RTA species derived from diarylamine during high-temperature hydrocarbon autoxidation.

Though a largely exploratory effort, we set out with two explicit objectives; the primary of which being to identify diarylamine oxidation products through synthetic efforts and/or isolation and characterization, if necessary. We also sought to investigate the mechanism of the Korcek cycle by performing autoxidations using its purported intermediates (namely the diarylnitroxide and diarylalkoxyamine), which would provide information on the resultant (oxidation) products and insight into the role of the intermediates themselves. In addition to such aims, we hoped to demonstrate the utility of our technique as a diagnostic tool that could be used in tandem with conventional methods, such as liquid chromatography, to assess the state of an RTA at a given time.

2.2 Results

2.2.1 Synthesis of Potential Diarylamine-Derived Oxidation Products

Autoxidation is known to generate substrate-derived carboxylic acids as a major product,[9-11] therefore we surmised that condensation between acids and **2.1** could yield non-RTA products. The water generated would be quickly driven from the system due to the high temperature (160˚C), allowing for an irreversible reaction to amide products (Figure 2.4 B).

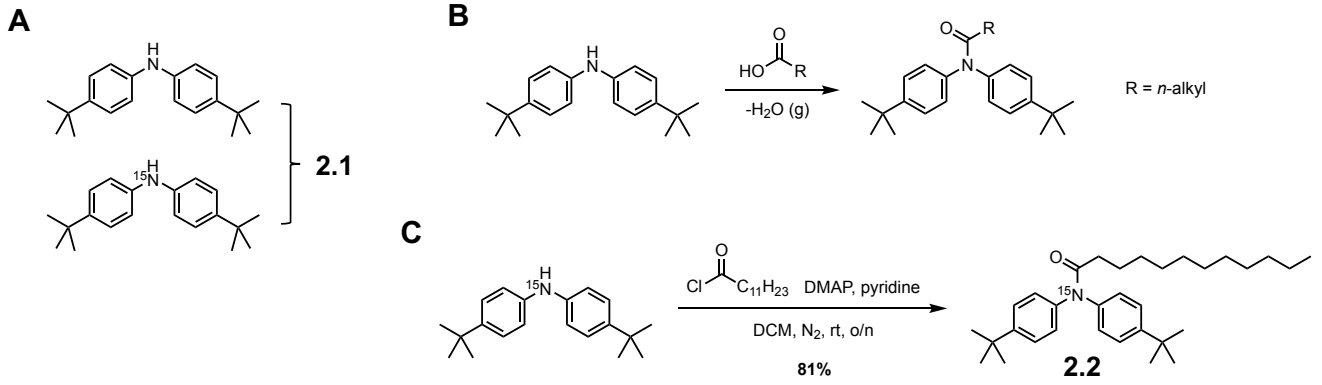

Figure 2.4 (**A**) Chemical structure of **2.1** (**B**) Proposed formation of **2.1**-derived amides via condensation with substrate-derived carboxylic acids. (**C**) Synthesis of ^{15}N labelled authentic standard, *N,N-bis*(4-*tert*-butylphenyl)-laurylamide, **2.2**.

Synthesis of the authentic standard of general, long-chain **2.1**-derived amides was performed via base-catalyzed condensation at room temperature using 4-dimethylaminopyridine (DMAP), pyridine, and lauroyl chloride (Figure 2.4 C). The product, **2.2**, was afforded in 81% isolated yield as a viscous oil.

Next, we considered the possibility that diarylaminyl radicals could undergo radical combination with one another to generate either a N-N linked (hydrazine) dimer (**2.3**) or a C-N linked dimer (**2.4**) that had been identified in previous reports (Figure 2.5 A).[5,12] We anticipated that **2.3** would be less stable at higher temperatures due to reported N-N BDE values (35-42 kcal/mol for similar compounds),[13,14] but that this could lead to accumulation of **2.4** via in-cage isomerization.

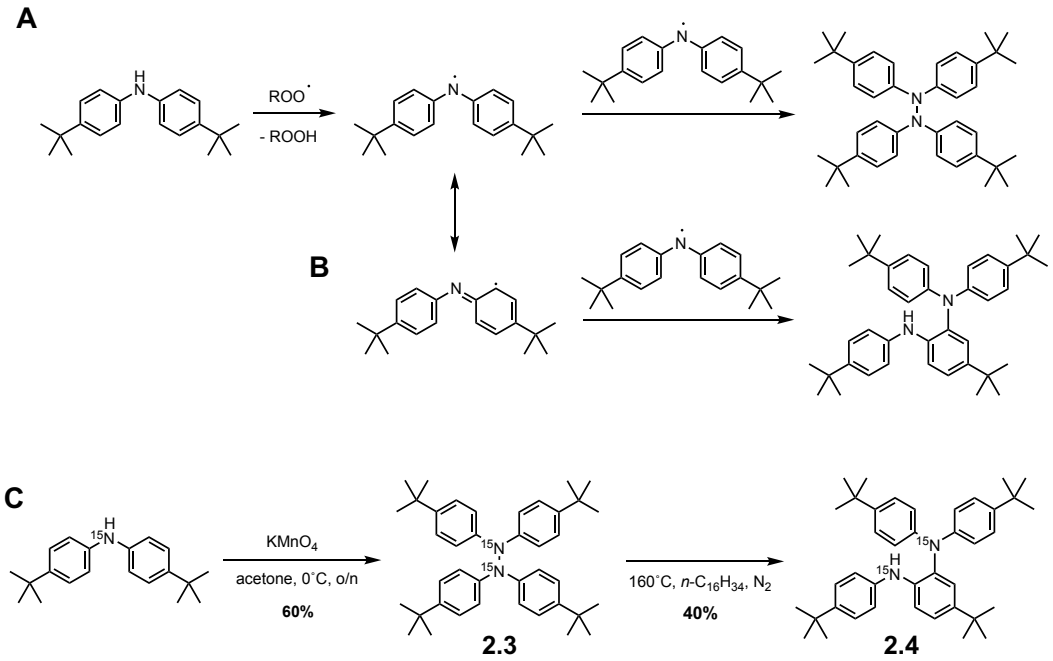

Figure 2.5 (**A**) Proposed formation of **2.3 N-N** aminyl radical combination. (**B**) Proposed formation of **2.4** via C-N radical combination (**C**) Synthesis of ^{15}N labelled **2.3** and **2.4**.

The tetra-arylhydrazine **2.3** was synthesized using potassium permanganate in acetone at room temperature, yielding the N-N coupled product in moderate yield as a white solid. We originally attempted to synthesize the *ortho*-coupled dimer via either a Buchwald-Hartwig amination or an iron(II)-coupling,[15] but neither method proved successful. We then elected to synthesize **2.4** in a manner similar to its expected formation during autoxidation: high temperature radical combination via N-N homolysis of **2.3**. Not only did this provide quantitative conversion of **2.4** from **2.3** (albeit with a low isolated yield), but supported the notion of its formation through such a reaction. We monitored the conversion of **2.3** to **2.4** during the reaction via HMBC and TLC, which both indicated full consumption of **2.3**. However, we had issues isolating **2.4** via flash chromatography, and instead recovered it via precipitation out of reaction solvent via cooling.

Industry collaborators had identified a diarylamine oxidation product that possessed an IR absorption frequency corresponding to an aldehydic carbonyl, along with a mass 29 units higher than the parent compound. We posited that addition of a CHO fragment via N-formylation was the most likely substitution, which could

form via substitutions on substrate-derived formate esters (Figure 2.5 A). Synthesis of the corresponding N,N-*bis*(4-*tert*-butylphenyl)formamide (**2.5**) was performed using formic acid and catalytic iodine under moderate heating, affording the desired compound in 71% yield.

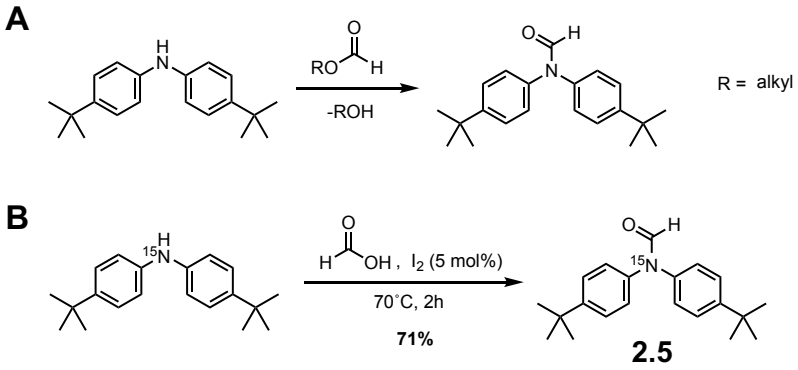

Figure 2.6 (**A**) Proposed formation of **2.5** during high-temperature hydrocarbon autoxidation. (**B**) Synthesis of ^{15}N N,N-*bis*(4-*tert*-butylphenyl)formamide, **2.5**.

In addition, we sought to synthesize an *ortho*-iminoquinone derivative of **2.1**, which we anticipated was a likely oxidation product arising from peroxyl addition to *ortho* positions through the delocalized diarylaminyl radical (Figure 2.7 A) Oxidation of 4-*tert*-butylcatechol provided the corresponding 4-*tert*-butyl-1,2-benzo-quinone, which was reacted with ^{15}N 4-*tert*-butylaniline at room temperature to yield condensation product(s) **2.6** (Figure 2.7 B).

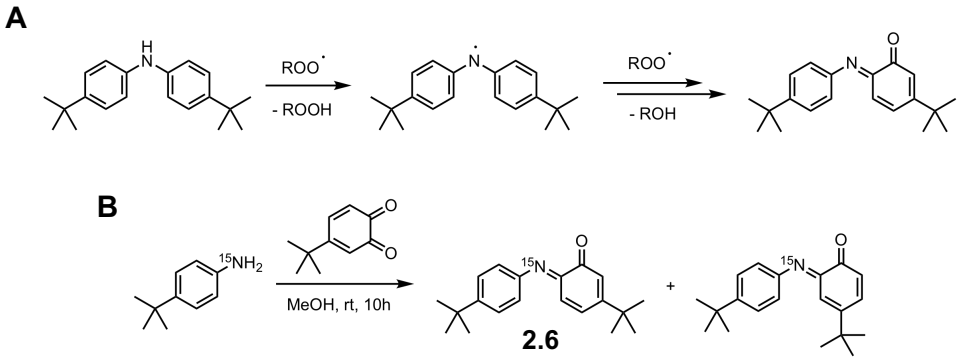

Figure 2.7 (**A**) Proposed formation of **2.6** during high-temperature hydrocarbon autoxidation. (**B**) Attempted synthesis of *ortho*-quinone-imine product, **2.6**.

Due to the lack of regioselectivity, we anticipated the formation of both regioisomers and hoped separation could be achieved via flash chromatography. Unfortunately, we obtained a complex mixture of products that were not easily separated from one another. After unsuccessful purification attempts, we set aside one of the 'cleaner' samples for ^{1}H ^{15}N HMBC analysis (dubbed **2.6***) to determine if any of the products correlated to oxidation species; an indicator for whether to continue isolation attempts and/or consider another synthetic approach. Consultation of the literature provided an alternative method to the desired compounds (**2.6** and **2.7**), reported by Ma et al. via Dess-Martin periodinane (DMP) oxidation of *para*-methoxy aryl substituents to the corresponding iminoquinones (Figure 2.8 A).[16] We expected that the transformation could be applied to **1.6** and **1.7**, which could be accessed via cross-coupling between **1.3** and the appropriate aryl bromide (**1.4** or **1.5**) (Figure 2.8 B).

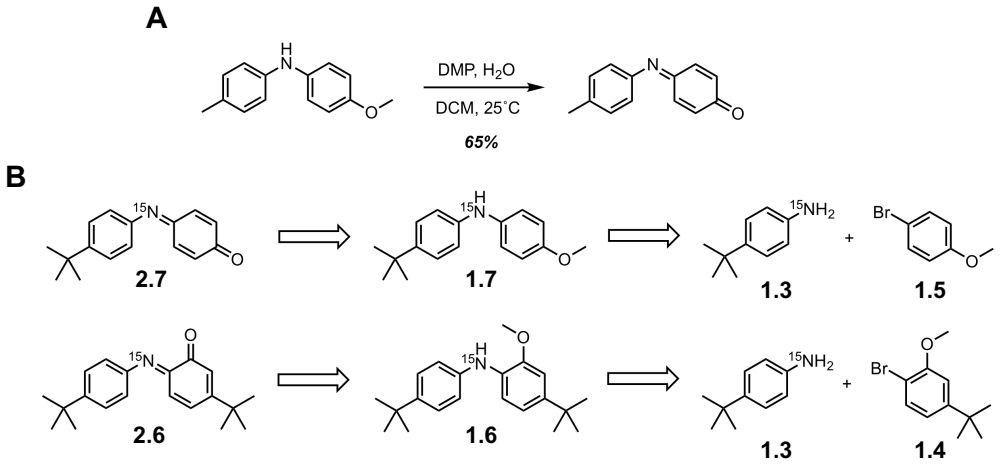

Figure 2.8 (**A**) Reported method for synthesis of iminoquinones from methoxy-bearing diarylamines via DMP-mediated oxidation.[16] (**B**) Retro-synthesis of iminoquinones **2.6** and **2.7** from aniline (**1.3**) and aryl bromides (**1.4**, **1.5**).

Syntheses of precursors **1.6** and **1.7** were achieved in high yields, but the DMP-mediated oxidations were unsuccessful. Although yields in the original report were fairly good with no mention of laborious work-up, we were unable to obtain either of the desired products, let alone in satisfatory yield.

Moving forward, we compared our newly-prepared ^{15}N standards to the oxidation products of **2.1** observed during high-temperature hydrocarbon autoxidation. Overlaying the 2D data of our presumed products **2.2-2.6*** by HMBC illustrated no correlations for compounds **2.2-2.4** and **2.6*** (Figure 2.9), but excitingly, **2.5**

showed identical overlap to one of the most prominent signals observed (Figure 2.9 A). However, we were surprised with this particular result: we expected it more likely that **2.1** would encounter carboxylic acids, leading to formation of **2.2**, than formylated species during autoxidation (more on this in the later). Additionally, we were surprised that **2.4** was not identified as an oxidation product, as it had been isolated from similar experiments previously.[5] The hydrazine-like dimer **2.3** was also not observed among the product distribution, which was unsurprising due to its labile N-N bond that likely homolyses readily at 160˚C. The product mixture **2.6*** did not correlate to any of the oxidation products, so we neglected to continue further purification.

Although synthetic efforts had identified one of the prominent oxidation products of **2.1**, we sought to expedite identification efforts by isolating the observed products rather than continue with synthetic speculation. We reasoned that this would allow us to more easily obtain tricky synthetic targets (i.e. **2.6**) in addition to the remaining species that remained unidentified.

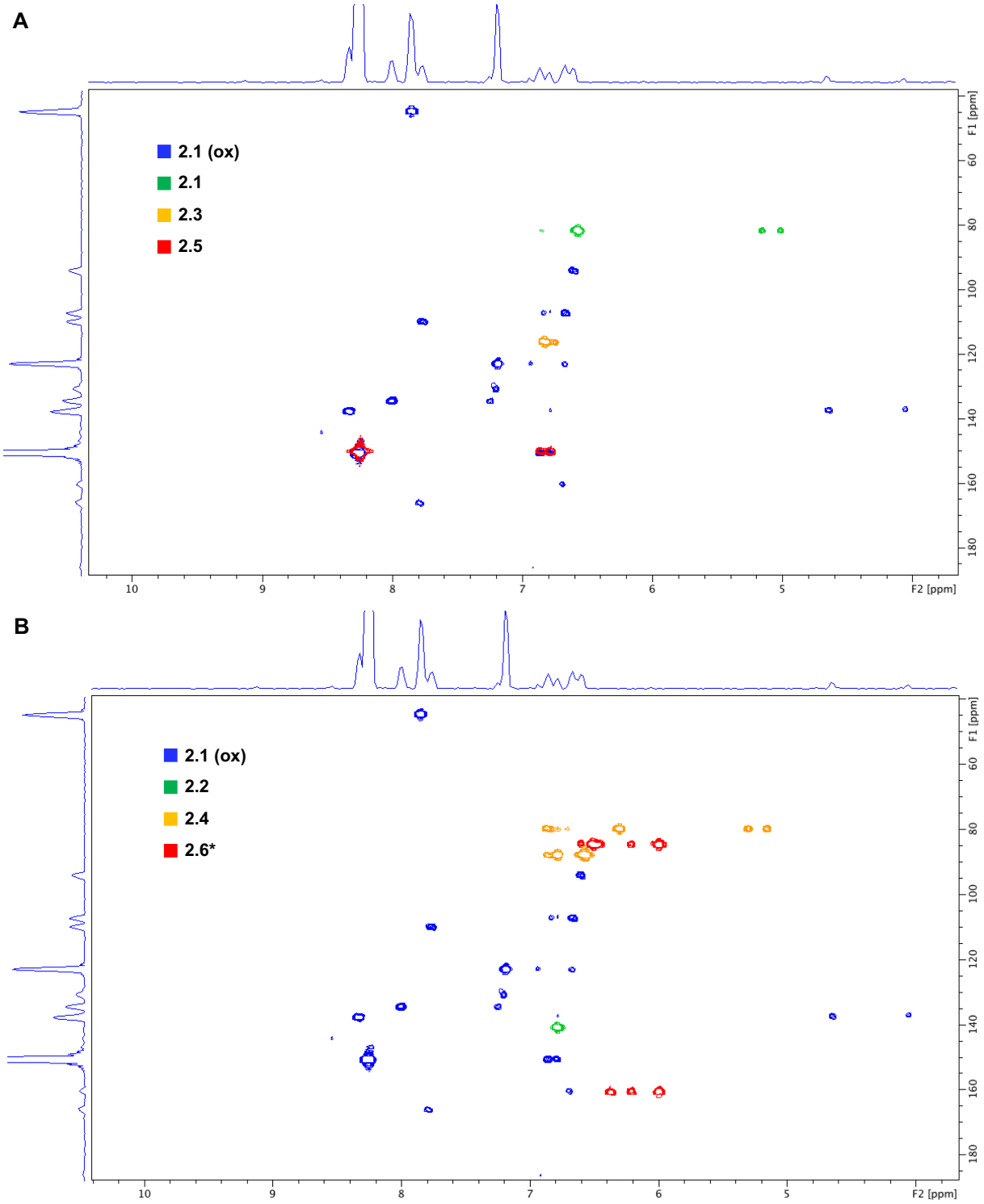

Figure 2.9 Overlay of HMBC spectra with high-temp autoxidation products of **2.1** (blue). (**A**) **2.1** (green), **2.3** (orange), **2.5** (red). (**B**) **2.2** (green), **2.4** (orange), **2.6*** (red).

2.2.2 Attempted Isolation of Diarylamine-Derived Oxidation Products from Large-Scale Autoxidations

In an attempt to expedite the identification of products and circumvent the need to independently synthesize each plausible oxidation product, we sought to isolate diarylamine-derived oxidation products from autoxidations. We surmised that diarylaminic products could be isolated through flash chromatography, extractions, or a combination of the two, if reactions were performed at sufficiently high loadings of **2.1** and on an increased scale.

Thus, we performed autoxidations at 1.0 weight-percent loading of diarylamine; almost three-times the concentration of our previous experiments (27.3 mM vs. 10 mM), and elected to use a larger reaction vessel in order to obtain sufficient quantities of each oxidation product for retrieval from substrate. Consequently, the inhibited period of the experiment was drastically increased, which led to some practical issues, but which afforded spectra of the **2.1**-derived oxidation species that possessed few differences to those of previous experiments (Figure 2.10), and had observed similarly minor differences in autoxidations under the same conditions. Given the harsh reaction conditions, the abundance of radical intermediates, and small discrepancies in sampling time, spectra may appear slightly different for experiments that are equivalent.

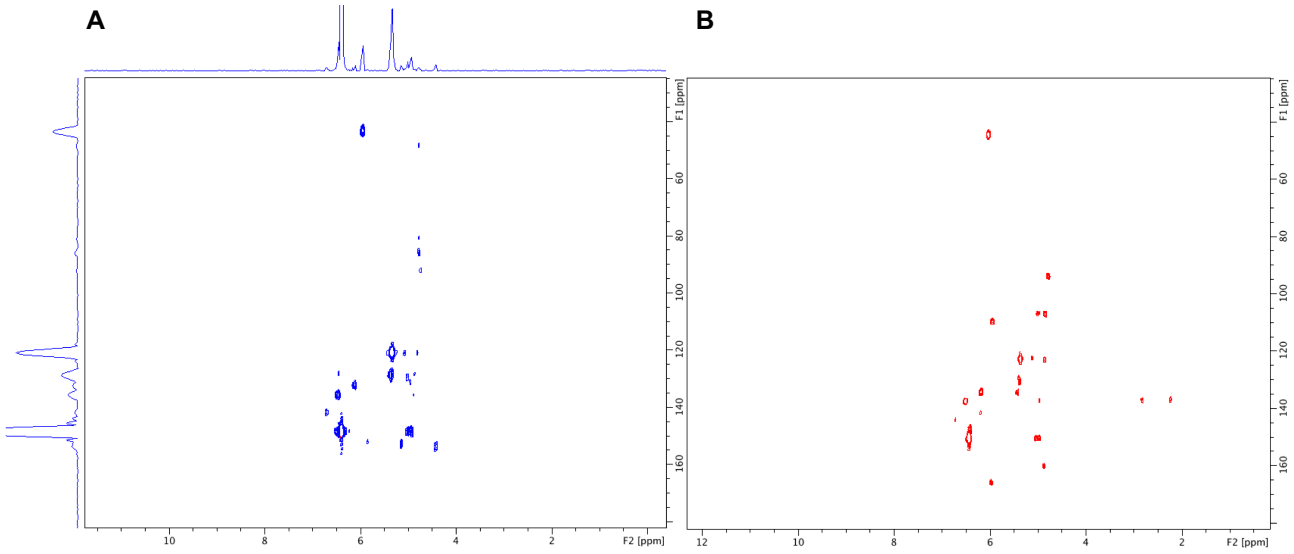

Figure 2.10 ^{1}H ^{15}N HMBC spectra of **2.1**-derived autoxidation products at: (**A**) 1.0 wt% loading (27.3 mM) (blue) (**B**) 10 mM (red).

Flash chromatography using a non-polar mobile phase was able to resolve oxidation products from the bulk of substrate, however a large amount of substrate remained. Attempts to further concentrate the oxidation products using flash methods, regardless of the mobile phase, flow rate, or size of column, failed. As such, we pivoted our approach and attempted to extract the diarylamine-derived products from the substrate. Although numerous solvents were readily immiscible with *n*-hexadecane, only acetonitrile and methanol would separate from the autoxidation sample on a reasonable time scale. Unfortunately, despite being able to remove the substrate, its oxidation products were largely retained in the extracts. Attempts to mitigate this transfer via base washes and centrifugation were unsuccessful and only resulted in transfer losses of the small amount of material present. Preparative thin-layer chromatography of the poorly-extracted autoxidation samples was carried out in an attempt to provide minimal quantities of components of the mixture for characterization, however co-elution of many species resulted in 'fractions' multiple ^{15}N species present. Moreover, despite all the foregoing efforts to remove it, the substrate-derived products remained present, further confounding isolation or characterization.

As attempts to isolate ^{15}N oxidation products from *n*-hexadecane proved fruitless, we decided to explore other autoxidizable substrates that would enable easier separations. Primarily, we synthesized pentaerythritol tetrahexanoate (PETX) that had been used in previously in experiments designed to inform on diarylamine oxidation products at high temperatures. The investigators were able to isolate the diarylamine-derived oxidation products following base-hydrolysis of the substrate followed by aqueous-organic extractions. In addition, we sought to perform the autoxidations in Yubase-4 (YB4), a group III base oil, and a base-oil-blend (BOB) (see the Experimental Section for blend details); substrates more similar to those used in lubricant applications. Although there was no clear indication that isolations from YB4 or BOB would be easier, it nevertheless provided an opportunity to compare the speciation of the RTA in these media to that which we observed in *n*-hexadecane.

Synthesis of PETX was achieved in quantitative yield in a single step by refluxing pentaerythritol in neat hexanoyl chloride, followed by removal of any unreacted acyl chloride by distillation (Figure 2.11 A). Subsequent autoxidation of PETX using ^{15}N labelled **2.1** as the inhibitor yield confusing results: primarily,

HMBC signals of **2.1** did not match those in *n*-hexadecane. Instead of multiple proton-couplings stemming from a single nitrogen chemical shift, we observed multiple mono-coupled ^{15}N nitrogen signals (Figure 2.11 B).

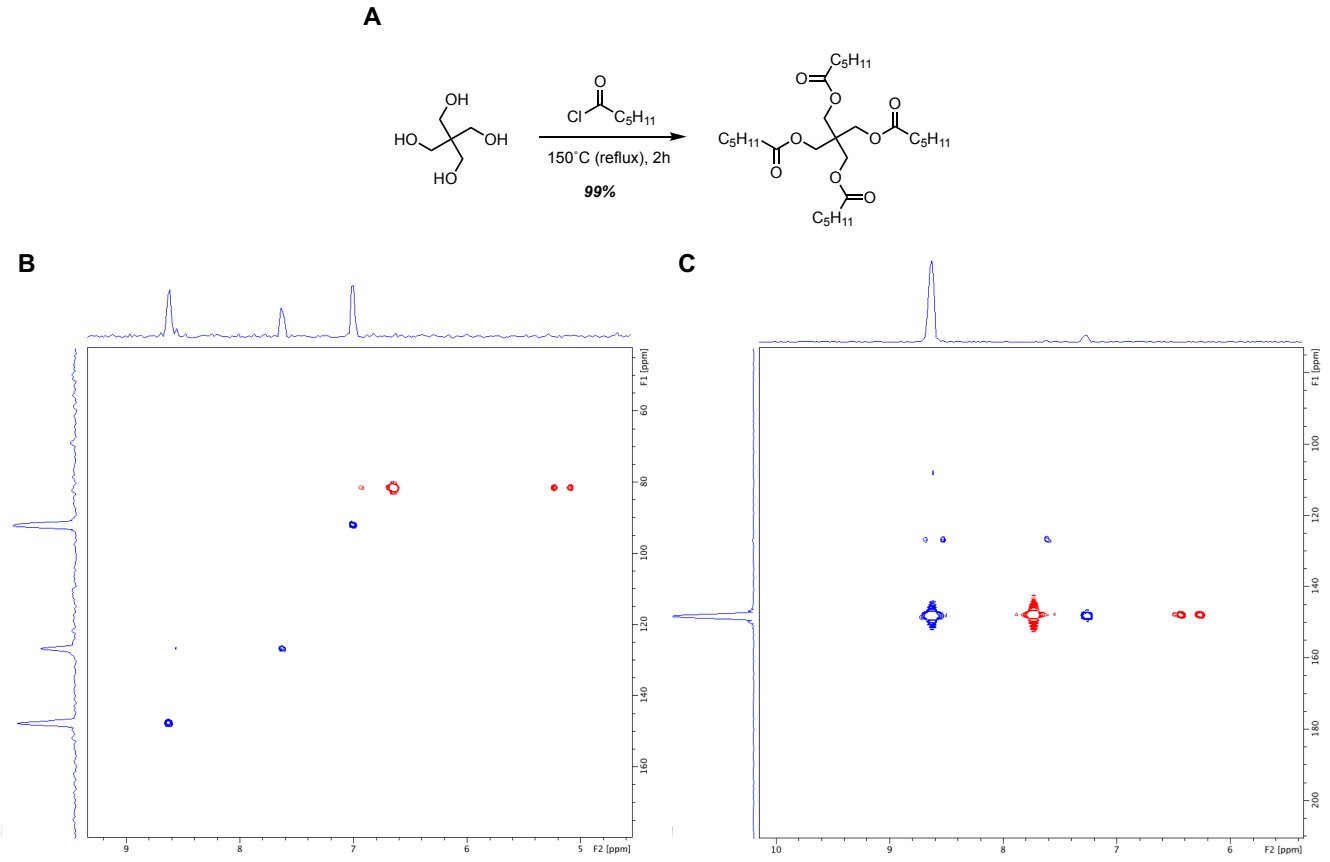

Figure 2.11 (**A**) Synthesis of pentaerythritol tetrahexanoate (PETX). (**B**) HMBC spectra of ^{15}N speciation during PETX autoxidation at 0h (blue) compared to signal of **2.1** at 0h in *n*-hexadecane (red). (**C**) HMBC spectra of ^{15}N speciation during PETX autoxidation at 8h (blue) vs. signal of **2.5** (red).

The signals did not appear to correlate in any way to the starting material. Additionally, the diarylamine showed far worse activity in PETX, providing almost no inhibition (see Figure S.2.1 in Appendix for hydroperoxide data). After seven hours, we observed the formation of a prominent ^{15}N species downfield from the parent compound at 148 ppm that became quite distinct by the eight-hour mark (Figure 2.11 C). This species occupied a similar chemical shift to **2.5**, which was observed as a major product in *n*-hexadecane experiments. Although the nitrogen shifts were similar, the proton shifts were downfield with respect to those of **2.5**, and appeared slightly different. We considered the possibility that the protons were shifted downfield and appeared slightly different

due to PETX, and that the observed species was in fact **2.5**. We carried out a base-hydrolysis of the sample, following the procedure of Zeman et al.,[5] and identified **2.1** as the major product via proton NMR (see Figure S2.2 in the Appendix). We rationalized that **2.1** perhaps formed from **2.5**, or a similar species, under the strongly basic conditions via hydrolysis. However, this hypothesis could not be verified, as the native species could not be obtained from the substrate without subjecting the sample to hydrolytic conditions prior to extraction. This result further highlighted the issues with the methods used in previous reports; we were unable to identify the species *in-situ* without altering its structure and could only speculate on its identity based on chemical shift data acquired in *n*-hexadecane.

Discouraged by the signal differences and worried that we might overcomplicate our efforts by working in substrates that provided dissimilar results, we abandoned our efforts with PETX and moved to the industrial base oils, YB4 and BOB. Before using precious starting material for autoxidations, we compared the extraction efficiency of unoxidized YB4 and BOB using unlabelled **2.1**, finding that YB4 yielded slightly more efficient extractions and separated from methanol and acetonitrile more quickly than BOB. As such, we performed high-temperature autoxidations in YB4 using labelled **2.1** to compare to our results in *n*-hexadecane. Notably, oxidation of **2.1** occurred more quickly in YB4 than in *n*-hexadecane: full consumption was observed 3.5 hours into the autoxidation, whereas this occurred after 9-11 hours in *n*-hexadecane (see Figure S2.3 in the Appendix for hydroperoxide data). Although this indicated that YB4 was more oxidizable, it did not appear to affect the product speciation; minor differences notwithstanding, the product pattern of **2.1** looked analogous to that observed in *n*-hexadecane (Figure 2.12). The parent amine appeared identical in YB4 and *n*-hexadecane, and the 'fingerprint' of oxidation products demonstrated commonality for the most intense signals (Figure 2.12 B).

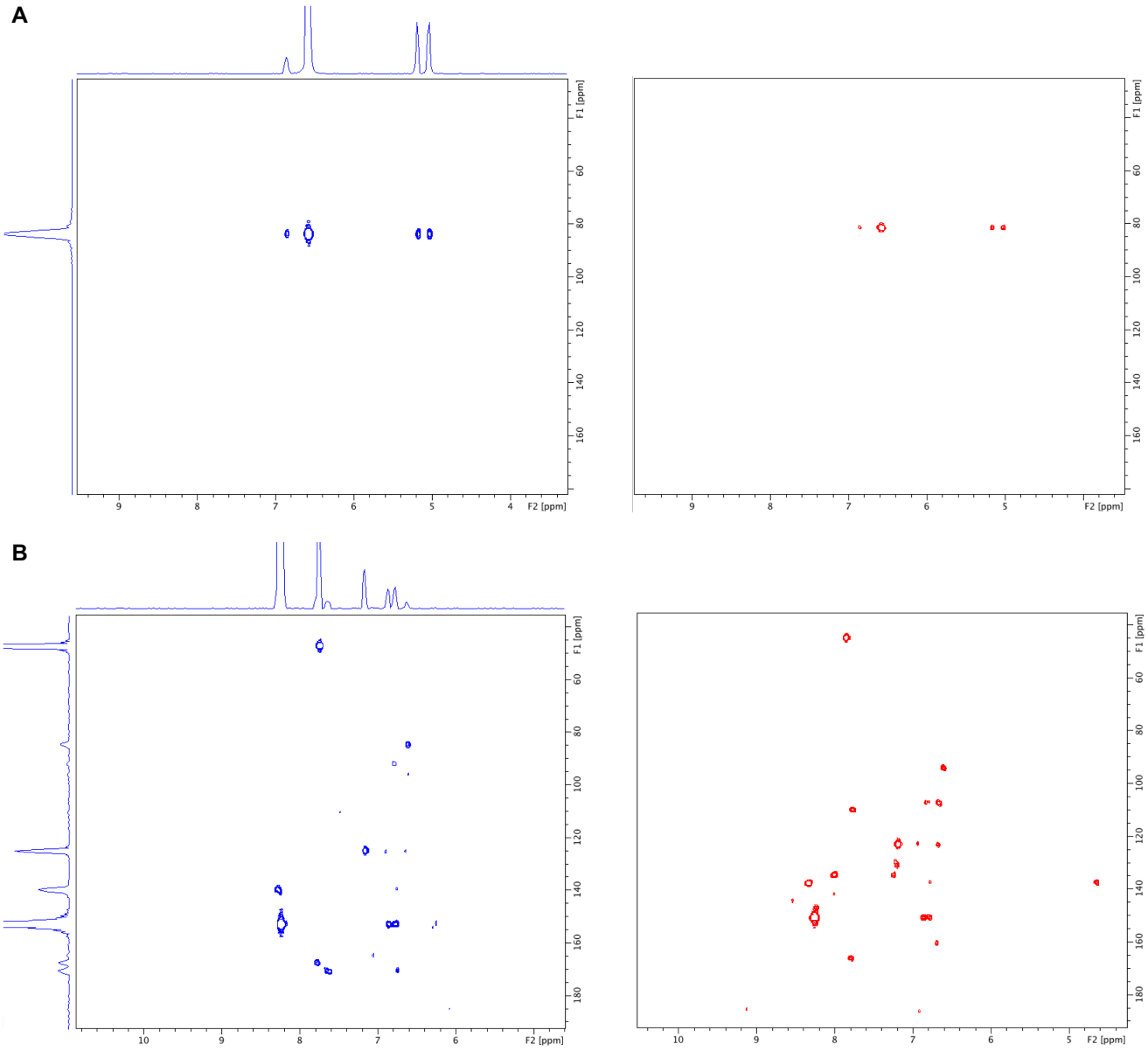

Figure 2.12 (**A**) HMBC spectra of parent compound **2.1** before autoxidation in: YB4 (blue) and *n*-hexadecane (red). (**B**) HMBC spectra of **2.1**-derived oxidation products in: YB4 (blue) and *n*-hexadecane (red).

Pleased with being able to demonstrate the reproducibility of diarylamine speciation in a more industrially-relevant substrate, we sought to isolate the oxidation species from YB4 using the methods discussed earlier. Product isolations out of YB4 were prone to similar issues that stalled efforts using *n*-hexadecane: carry-over of oxidized substrate intro polar phases of extractions (methanol, acetonitrile) and inability to fully remove sufficient amounts of said substrate via flash chromatography techniques (flash columns, preparatory TLC).

2.2.3 Preliminary Attempts at Direct Autoxidation of Diarylamine Using Initiators

Due to our difficulties separating oxidation products from substrate, we wondered if **2.1** could be speciated in a similar manner to high-temperature autoxidations, but without involvement of the substrate, to avoid isolation issues that arise during extractions or flash chromatography. Concomitantly, we sought to simplify the product distribution by performing such experiments at lower temperatures (i.e. 40˚C – 80˚C), and then work up to higher temperature experiments (i.e. 100-120˚C) at which we expected a similar product distribution to autoxidations at 160˚C. Due to the prevalence of alkoxyl and hydroxyl radicals at the latter stage of autoxidation (when diarylamine speciation is observed), we posited that some of the diarylamine-derived oxidation products might derive from interactions with such radicals. By performing 'pseudo-autoxidations' with initiators that form alkoxyl radicals, we sought to promote similar reactions with diarylamine.

We chose to perform the initial reactions with unlabelled **2.1** at 40, 60, and 80˚C in isooctane with di-*tert*-butylperoxide (DTBP) as the initiator, which decomposes to yield a pair of *tert*-butoxyl radicals. Due to the slow rate of radical generation from DTBP at lower temperatures ($t_{1/2}$ = 200h at 100˚C)[17], it was used at in high concentration relative to **2.1** and isooctane. To ensure hydrogen-atom abstraction from **2.1** and not isooctane, we also increased the concentration of diarylamine to 100 mM (Figure 2.13 A).

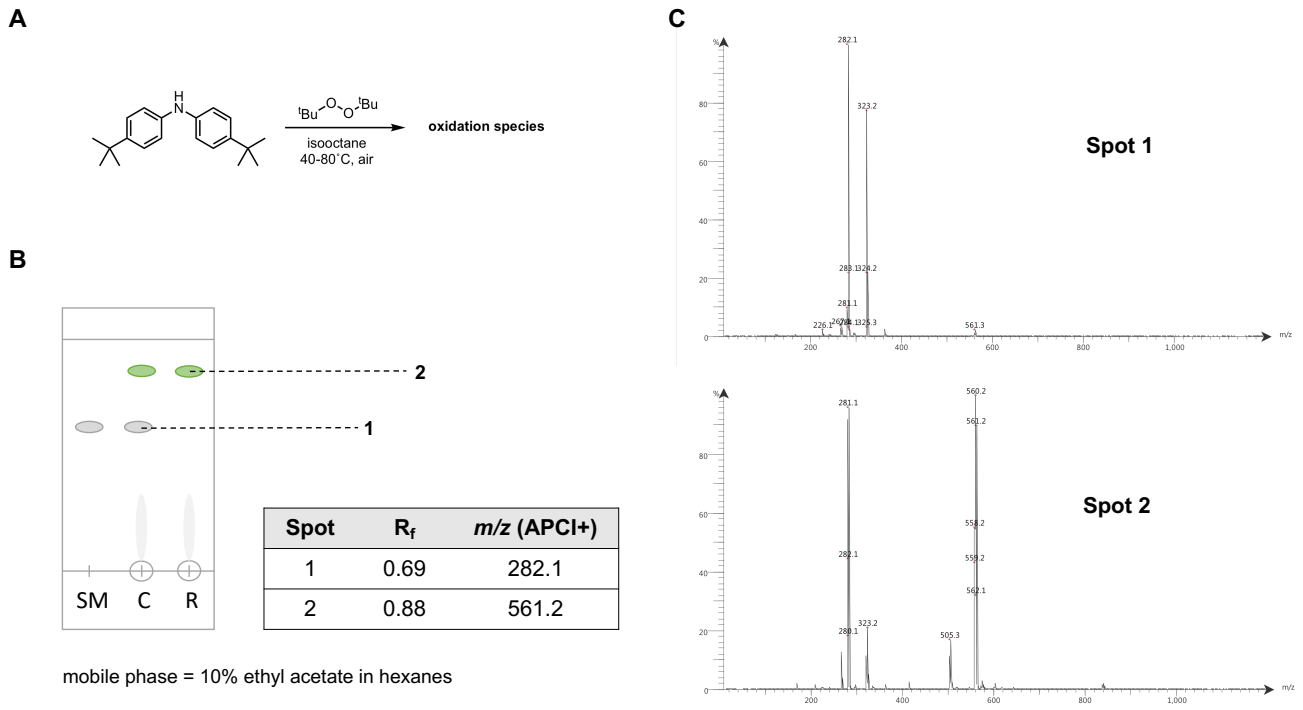

Spot	R_f	*m/z* (APCI+)
1	0.69	282.1
2	0.88	561.2

Figure 2.13 (**A**) Reaction scheme for direct diarylamine oxidation experiments. (**B**) Representative image of TLC at point of reaction completion (SM = starting material, C = co-spot, R = reaction) and data acquired from each spot. (**C**) APCI+ spectra corresponding to TLC-MS analysis of direct autoxidation samples.

Reactions were monitored via consumption of starting material by TLC, followed by TLC-MS of any prominent products observed (Figure 2.13 B). The major product of the reactions (regardless of temperature) appeared further up the TLC plate than **2.1**, correlating to the R_f observed for **2.3** and **2.4**. Subsequent MS analysis of the spots via atmospheric-pressure chemical ionization APCI (+) yielded two *m/z* peaks of high intensity at 561.2 and 282.2, which also indicate formation of a **2.1**-dervived dimeric species; likely **2.3** or **2.4** (Figure 2.13 C). This suggests that the diarylaminyl radical preferentially undergoes radical-radical dimerization in the presence of alkoxyl radicals. Future work is required to assess the product distribution of such reactions at higher temperatures to determine if the reaction conditions are capable of generating the same products observed during high-temperature autoxidations.

2.2.4 Monitoring the Formation of Early Oxidation Species by UPLC

Quantifying the products arising from oxidation of **2.1** would provide insight to the degree that each off-cycle reaction or oxidation pathway is responsible for loss of its RTA activity. Unfortunately, HMBC experiments are not suitable for quantification of signals (see Chapter 2 Introduction for details), therefore such results must be provided from alternative techniques. Recently, our group has had preliminary success identifying and quantifying RTA intermediates during the inhibited period by performing micro-extractions of autoxidation samples and analyzing them via reverse-phase (RP) ultra-performance liquid chromatography (UPLC). We surmised that the most important oxidation products are likely those that are formed during the late stages of the inhibited period and which presumably lead to a loss in the RTA's ability to suppress oxidation. Moreover, at this point, the samples are 'cleaner' and therefore easier to analyze as fewer oxidation products have formed – of both the substrate and the inhibitor. In fact, HMBC analyses had revealed that the 'major' product, **2.5**, accumulated significantly before the usual rapid increase of hydroperoxides (Figure 2.14 B,D).

As such, we sought to employ a UPLC photo-diode array (PDA) detected method to determine the concentration of **2.5** before the end of the inhibited period and to probe for the appearance of chromophores corresponding to other signals observed by HMBC during said timeframe. Primarily, we developed calibration (standard) curves and extraction efficiency curves for both **2.1** and **2.5** to ensure accurate quantification of each species across a realistic concentration range (Figures S2.4 and S2.5 in the Appendix). UPLC analysis of autoxidation samples indicated that **2.5** accounted for approximately 0.4 mM (of the original 10.5 mM) at the eight-hour mark of the experiment, despite nearly full consumption of **2.1** and no presence of the diarylnitroxide (**2.1a**).

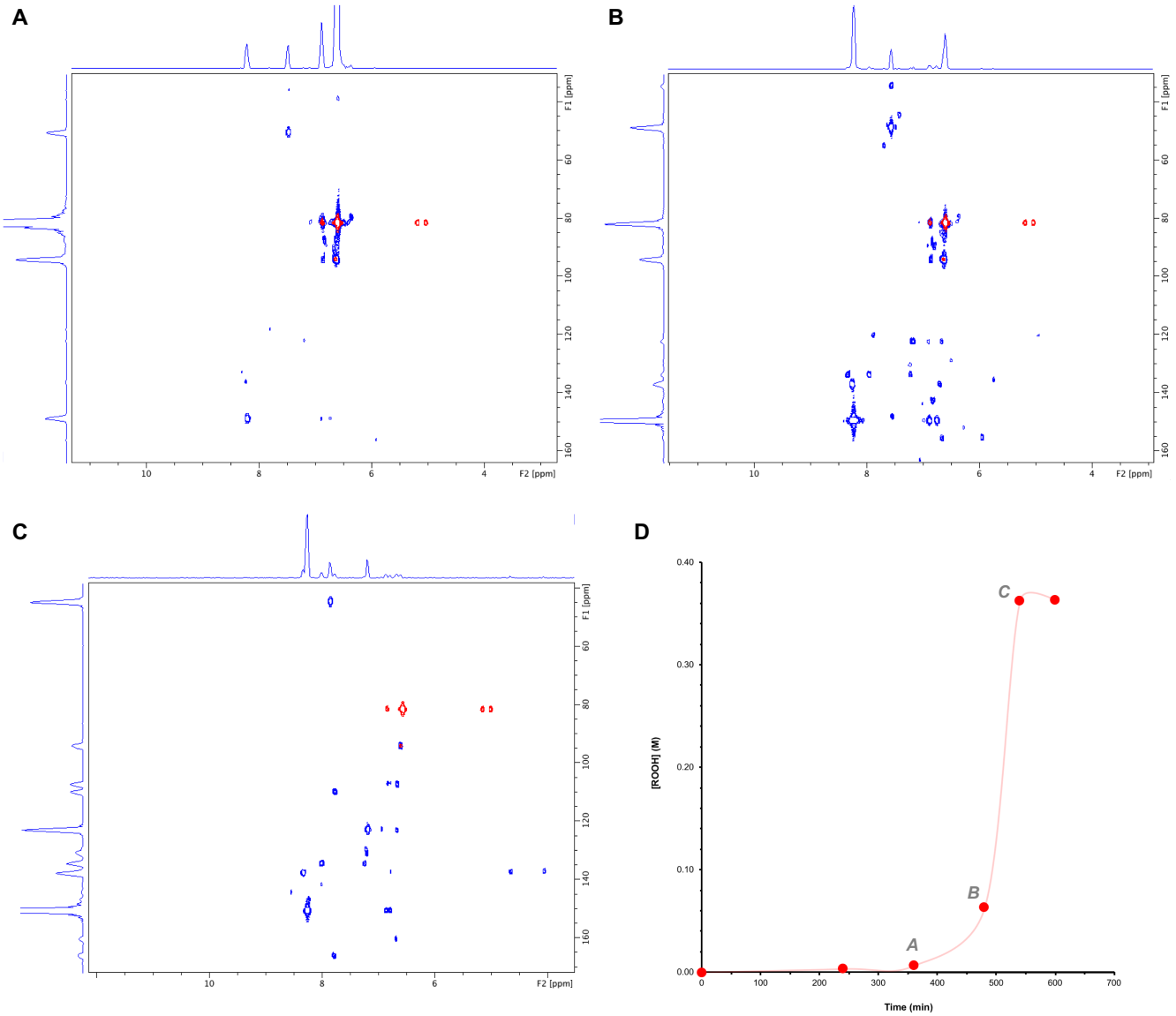

Figure 2.14 Representative HMBC spectra of **2.1** speciation (blue) overlaid with parent compound, **2.1** (red) at: (**A**) 6 hours, (**B**) 8 hours, (**C**) 9 hours, during a high-temperature autoxidation using 10 mM **2.1**. (**D**) Accompanying hydroperoxide trace of **2.1**-inhibited autoxidation, with corresponding spectra labelled at each time point.

We found this result surprising; **2.5** appeared to be the major species in solution via HMBC at this point during the experiment. Unfortunately, we did not observe any distinct chromophores other than **2.1** and **2.5** via UPLC at 6 or 8 hours, despite multiple prominent signals observed via HMBC.

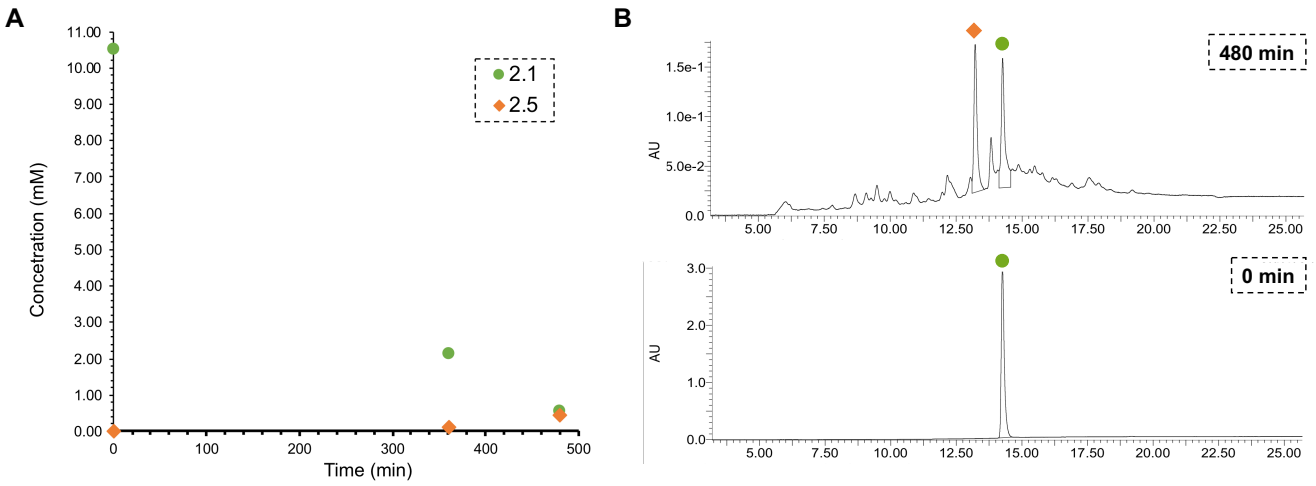

Figure 2.15 (**A**) Concentration of **2.1** and **2.5** during autoxidation, via UPLC-PDA. (**B**) UPLC chromatograms of autoxidation samples taken at 0 min and 480 min with **2.1** (green) and **2.5** (orange) at 285nm and 239 nm, respectively.

2.2.5 Monitoring the Speciation of 2.5

We posited that since **2.5** was formed early in the autoxidation, it may undergo further reactions to afford some of the other oxidation species observed later in the autoxidation. To test this assertion, we performed an autoxidation wherein **2.5** was added at the outset, but carried out otherwise under the typical conditions. Unsurprisingly, **2.5** failed to inhibit the autoxidation whatsoever, as indicated by the hydroperoxide trace (see Figure S2.6 in Appendix). Interestingly, corresponding HMBC spectra displayed the formation of a species with the same chemical shift as **2.1** (≈ 84 ppm), as well as the typical speciation 'fingerprint' observed upon consumption of **2.1** (Figure 2.16).

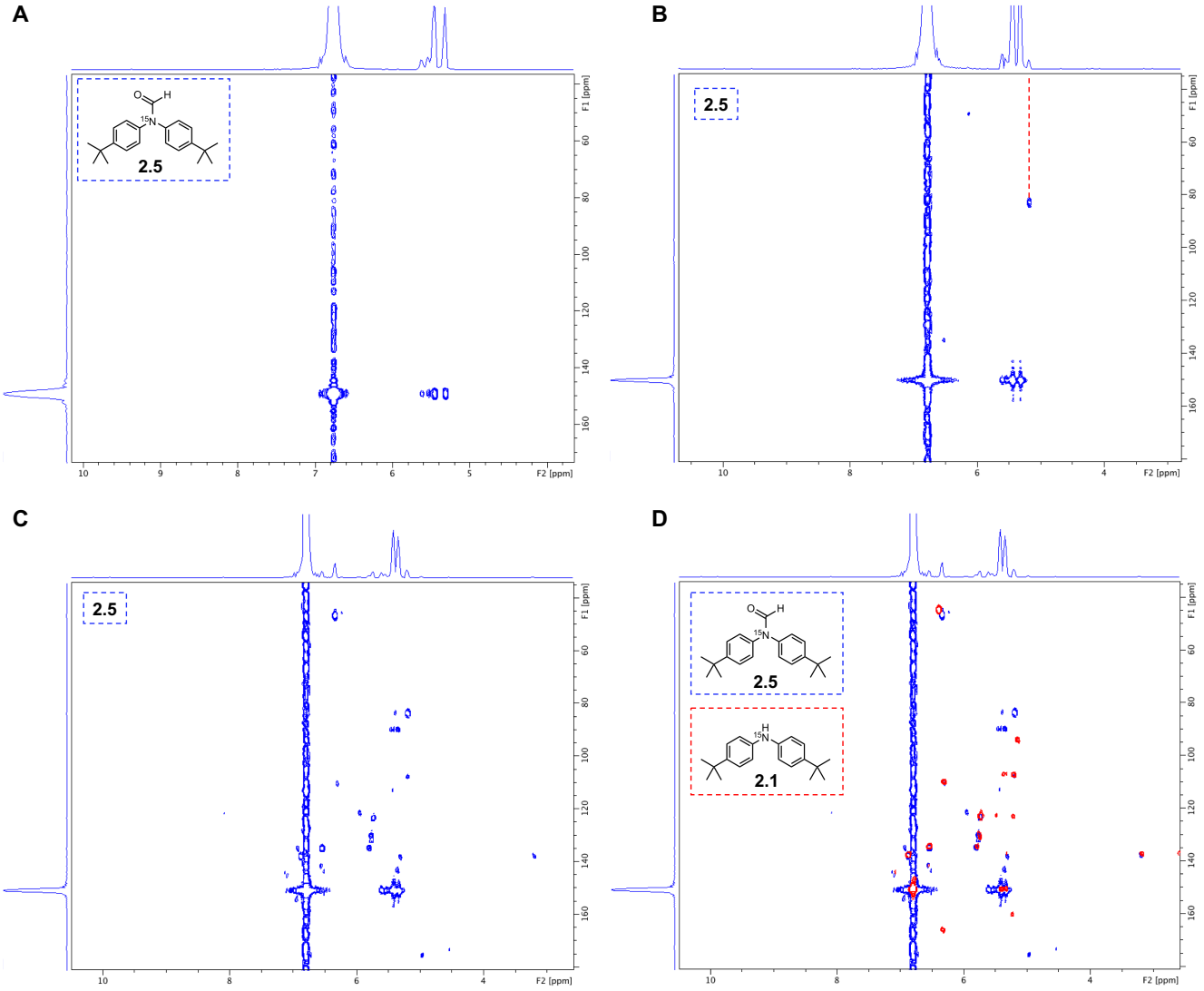

Figure 2.16 Representative HMBC spectra of **2.5** speciation upon autoxidation at: (**A**) 0 hours, (**B**) 40 minutes with new species indicated (red), (**C**) 2 hours, and (**D**) 2 hours with speciation of **2.1** overlaid (red).

The results suggest that **2.5** can be converted to **2.1** *in situ*, which is subsequently overwhelmed by the oxidizing environment resulting in the speciation typically observed at the end of **2.1**-inhibited autoxidations. As **2.5** provides no inhibition, the concentration of chain-carrying and initiating species increases rapidly as the beginning of the experiment; slow generation of **2.1** is not enough to inhibit the autoxidation. The formamide, **2.5**, is relatively stable under the conditions: HMBC indicated that it was still the major product seven hours into the experiment, indicating that conversion of **2.5** to **2.1** is sluggish, yet a quantitative method would be required

to properly evaluate conversion. Although the results were the opposite of what was anticipated, they suggest that the oxidation products could simply be latent forms of the original RTA, not irreversibly altered structures; a feature that could perhaps be harnessed advantageously (more on this later).

2.2.6 Examining Turnover and Oxidation of Purported Korcek Intermediates using ^{1}H ^{15}N HMBC

Concomitant to efforts of identifying diarylamine oxidation products, we were also interested in the prospect of using the ^{15}N-enriched diarylamines and HMBC method to complement previous work regarding diarylamine turnover and the purported Korcek cycle.[2,4] High performance liquid chromatography (HPLC) of aliquots of autoxidations carried out in the presence of diarylnitroxide (**2.1a)** or the diarylalkoxyamine (**2.1c)** as inhibitors yielded the parent diarylamine (**2.1**); a result that we anticipated could be corroborated by HMBC. Typical, high-temperature autoxidations using enriched **2.1a** as the RTA confirmed its conversion to **2.1** at detectable concentrations 40 minutes into the experiment, along with two other species with nitrogen shifts of 93.8 ppm and 147.9 ppm respectively; the latter of which overlaps with signals of **2.5** and the former being previously observed during autoxidations using **2.1** (Figure 2.17 A,B). This was surprising, as formation of **2.5** was never observed at such an early time when autoxidations were carried out using **2.1**. However, the species at 93.8 ppm was commonly present in autoxidations of **2.1** from the outset, which led us to believe it was simply a small impurity; perhaps the triarylamine, which formed as a by-product during the cross-coupling to yield **2.1**. Yet the *in situ* formation of the species from **2.1a** indicated that it was an off-cycle product that stemmed from turnover of **2.1a** into **2.1**, or vice versa. At the one-hour mark, a signal at 50.1 ppm began to accumulate in detectable concentrations, and appeared in close proximity to one of the prominent products of autoxidation using **2.1** (Figure 2.17 C). Although we could not confirm that the products were common due to the difference in chemical shift, the result indicated that the species formed via off-cycle reaction during conversion between **2.1** and **2.1a**. The signal intensity of **2.1** grew considerably during further progression of autoxidation, while the 'off-cycle' species remained relatively faint in comparison.

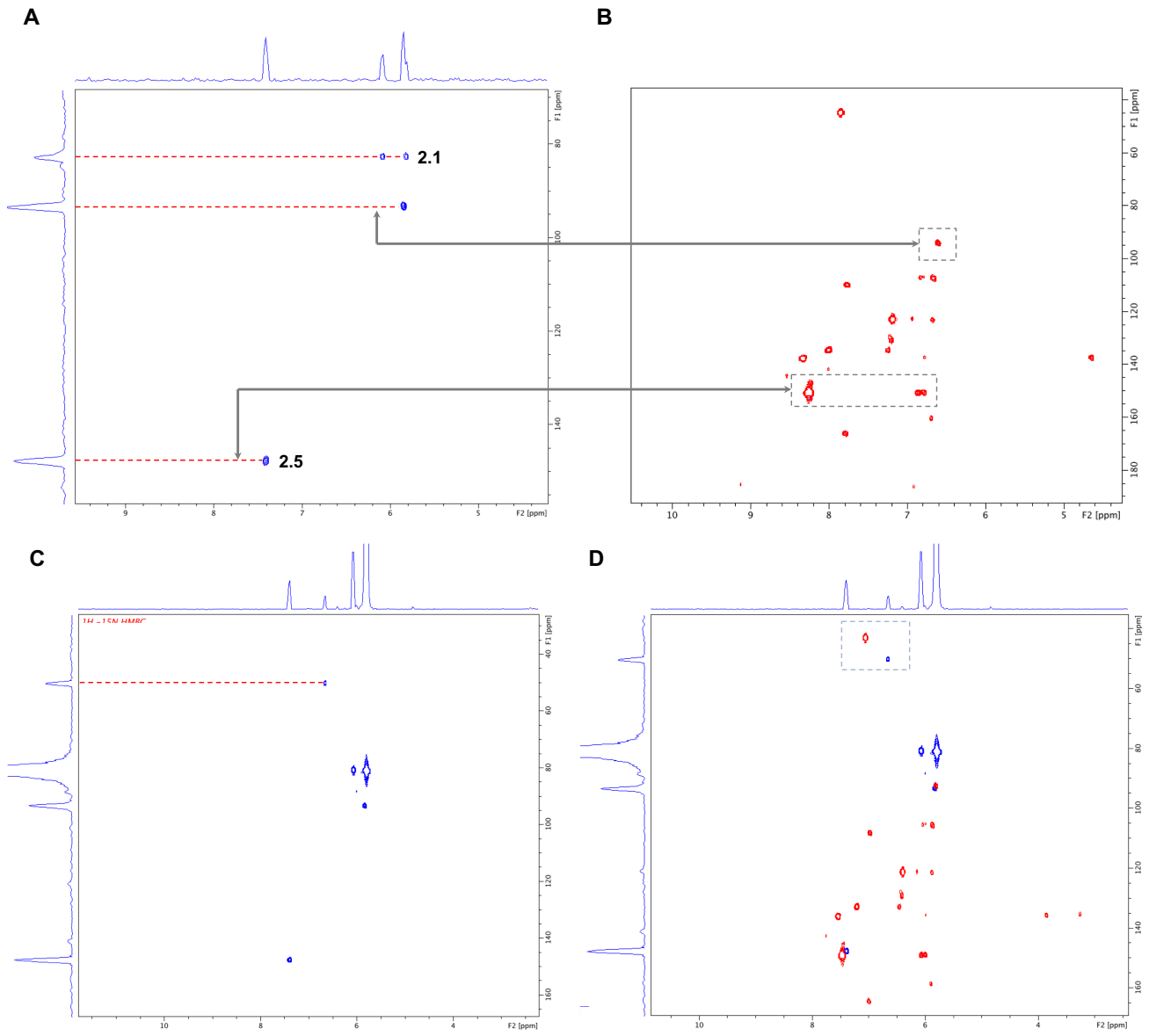

Figure 2.17 HMBC spectra of autoxidation inhibited by **2.1a**: (**A**) Formation of **2.1** and other species at 40 minutes (indicated), (**B)** Speciation of **2.1** autoxidation with common products indicated, (**C**) Product at 50 ppm at 1h, (**D**) Speciation of **2.1a** at two hours (blue) vs. oxidation products of **2.1** (red).

More oxidation species were observed at the ten-hour mark, and by twelve hours we observed a near-identical oxidation fingerprint to those observed starting with **2.1**. Additionally, a large signal corresponding to **2.1** remained (Figure 2.18 A,B). Primarily, this supports the assertion that diarylamine and diarylnitroxide are involved in a regenerative cycle that yield common autoxidation products. Surprisingly, the experiments also

indicate that inhibition of autoxidation is prolonged when using the corresponding nitroxide as the primary inhibitor (see Figure S2.7 in the Appendix for the hydroperoxide data). Our group has reported the increased inhibition afforded by nitroxides over corresponding amines in unsaturated substrates,[18] but not at high temperatures in (purportedly) saturated substrates.

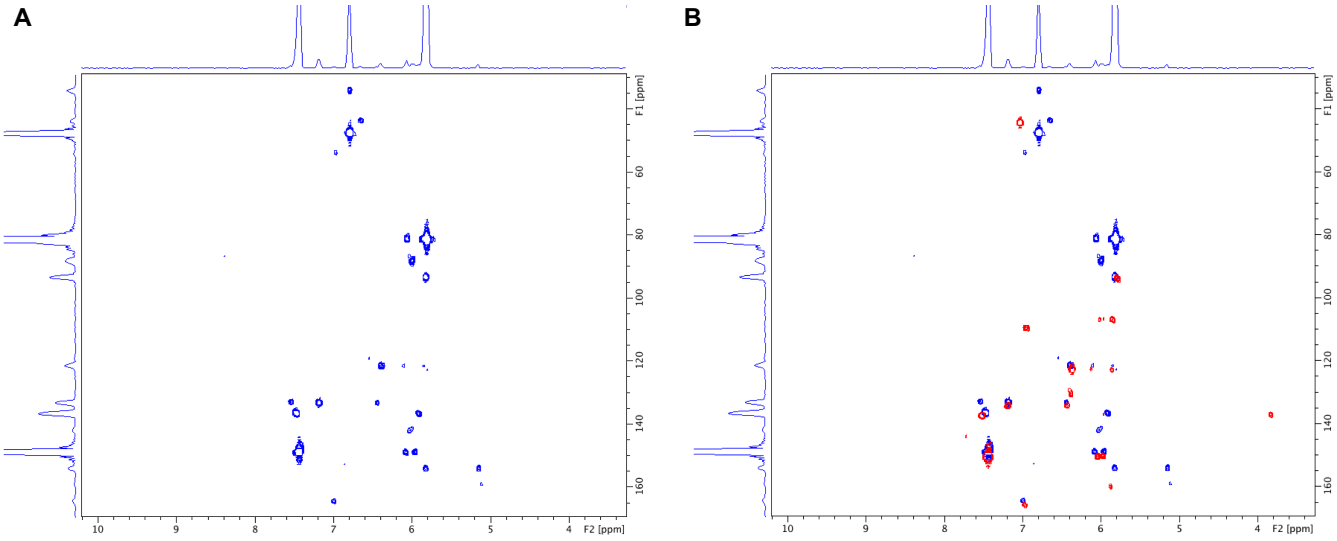

Figure 2.18 HMBC spectra of: (**A**) Speciation of **2.1a** at 12 hours, (**B**) Speciation of **2.1a** at 12 hours (blue) overlaid with speciation of parent diarylamine, **2.1** (red).

Analogous experiments starting with the diarylalkoxyamine (**2.1c**) also demonstrated regeneration of **2.1**, albeit more rapidly than with **2.1a**. Signals for **2.1** were observed within two minutes and **2.1c** appeared to have been completely converted within fifteen minutes (Figure 2.19A-C), in good agreement with previous studies on the thermal decomposition of diarylalkoxyamines.[4] We also observed a faint signal for species at 93.8 ppm, as well as a faint signal for a species at 73.2 ppm; yet the latter was not observed past this point in the autoxidation (Figure 2.19 C). No other significant speciation was observed until the ten-hour mark, but **2.1** had been fully consumed after twelve hours, yielding the full 'fingerprint' of oxidation products (see Figure S2.8 in the Appendix for hydroperoxide data). Again, the oxidation products matched up almost identically to those when autoxidations were performed with **2.1** (Figure 2.19 D); an expected result due to the rapid conversion of **2.1c** to **2.1** during the early stages of autoxidation.

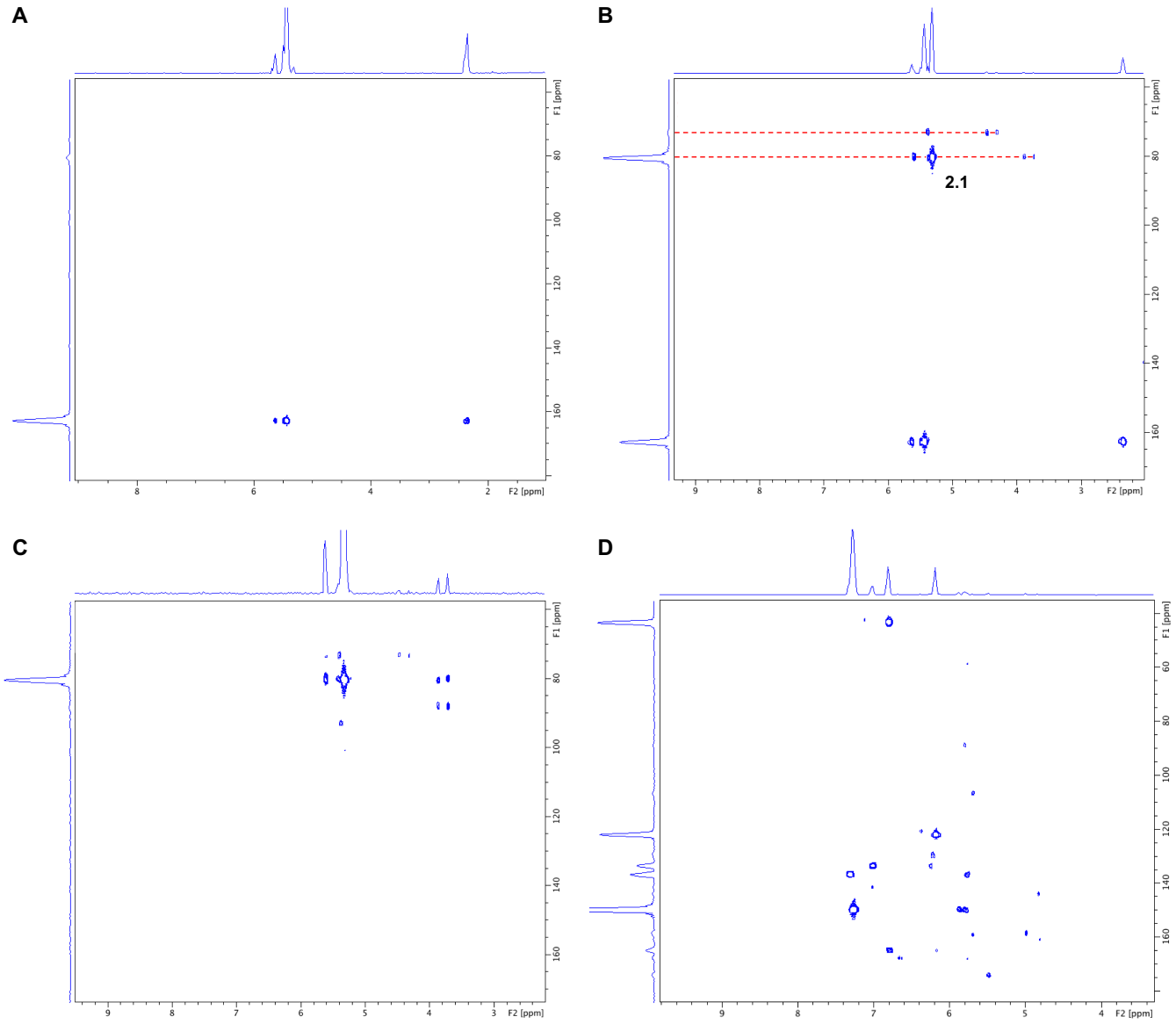

Figure 2.19 HMBC spectra of: (**A**) **2.1c** at beginning of experiment, (**B**) Formation of **2.1** from **2.1c**, along with other product, 2 minutes into autoxidation (both indicated), (**C**) Full conversion of **2.1c** into **2.1** by 15 minutes, with other minor species observed, (**D**) Full speciation upon full consumption of **2.1** (via **2.1**).

2.3 Discussion

In order to maximize the efficacy of diarylamine RTAs for high-temperature applications, we must further our understanding of the mechanisms by which they are degraded, a crucial part of which is determination of the products they form. As previous reports of diarylamine speciation during high-temperature autoxidations are limited, we were eager to explore this matter using our spectroscopic method in hopes that it would help elucidate the fates of these compounds.

Our synthetic efforts were tailored towards products that had been previously identified under similar conditions as well as others that had not yet been identified, but were implicated by computational work or our chemical intuition. Unexpectedly, our authentic standard of **2.2** did not correspond to any of the products; a confusing result considering that the diarylformamide **2.5** was one of the most prominent products observed by NMR. We were also surprised to find that **2.4** was not observed at any stage during the autoxidation, particularly during the early stages. As mention earlier, the hydrazine-type dimer **2.3** is not stable at higher temperatures, therefore a high steady-state concentration was not expected (or observed). However, isomerization to **2.4** generates a much more stable C-N bond upon re-aromatization, which is unlikely to homolyze readily. This transformation seems more likely at the early stages of autoxidation when peroxyl radical concentrations are relatively low; diarylaminyl radicals would have a higher probability of encountering another diarylaminyl as there are fewer free peroxyl radicals to combine with. Additionally, **2.4** had been identified as a major product of diarylamine autoxidation, although it is important to note that those studies performed experiments with RTA loadings of 20 weight-percent, which would undoubtedly promote dimerization to a greater extent. As mentioned, the concentrations of diarylamine used in real-world, high-temperature applications are 1.0 weight-percent; the same loading used in the large-scale experiments from which we attempted product isolations. Yet, the formation of **2.4** was not observed at this loading, nor at our typical loading of 10 mM (0.36 weight-percent). However, it is possible that **2.4** forms but reacts further to generate other (oxidation) products; rapid consumption of **2.4** following its formation would prevent it from accumulating in a concentration sufficient for

detection by HMBC. Our anticipation is that **2.4** cannot inhibit autoxidation due to the steric bulk of the *ortho*-substituent (a hypothesis that is under study), but as seen in Chapter 3, poorly-reactive diarylamine derivatives can still be further functionalized under the harsh experimental conditions. This appeared to be the case of **2.4** as well, which was found to form under the experimental conditions outlined in Chapter 3, yet was not observed past the early-stages of autoxidation. Under the experimental conditions used in this chapter, **2.4** may have formed at rates slower relative to its consumption. To support this hypothesis, the inhibition rate constant (k_{inh}) of **2.4** must be obtained in order to elucidate its reactivity towards chain-carrying radicals. In addition, bulk amounts of the compound could be synthesized and used in high-temperature autoxidations as the 'inhibitor' to identify its downstream products; similar to our experiments with the diarylformamide **2.5**.

Despite our interest in the iminoquinone **2.6** as a likely product of diarylamine oxidation, we were unable to obtain an authentic standard for the compound. Our primary effort based on the simple nucleophilic attack by aniline at the carbonyl of the quinone reagent resulted in a 'mess' of products due to the lack of regioselectivity offered by the quinone. Our subsequent strategy of oxidizing methoxy-bearing diarylamines to the corresponding iminoquinones using a reported method of DMP-mediated oxidation was also unsuccessful.[16] Although we anticipated that the reported reaction could be extended to *ortho*-methoxy substrates from the solely *para*-substituted scope, the failure was demonstrative of our lack of mechanistic understanding. While further investigation into the product distribution of the reaction is necessary, alternative routes to the compound need also be explored. As consultation of the literature demonstrates the obscurity of such scaffolds (and their synthesis), optimization of the DMP-mediated oxidation might be the most prudent approach. Large-scale isolation attempts of inhibited time points might also afford the desired compound (amongst others), and could be performed parallel to synthetic efforts. On this note, it is also important to consider the reactivity of iminoquinones; although they lack a labile hydrogen, they could further react during autoxidation to produce downstream products. It is not out of the question that they exist as intermediate-products, and do not accumulate to a significant degree, however this would make their isolation out of substrate difficult. Such could

also be the case during our synthetic attempts, yet the stability of the *para*-iminoquinones under the DMP-mediated conditions has been demonstrated.

An interesting finding was the identification of **2.5** as a prominent product that accumulated earlier than many other species. One might automatically assume that **2.5** results from a condensation reaction with formic acid, pushed forward due to removal of water from the system; similar to how we envisioned **2.2** would form. There are a couple issues with this explanation however, the first being that formic acid is too volatile to possess a significant lifetime under the experiment conditions. Secondly, formation of formic acid is difficult to rationalize based on the proposed mechanism of acid formation during autoxidation (Scheme 2.3).[4,10]

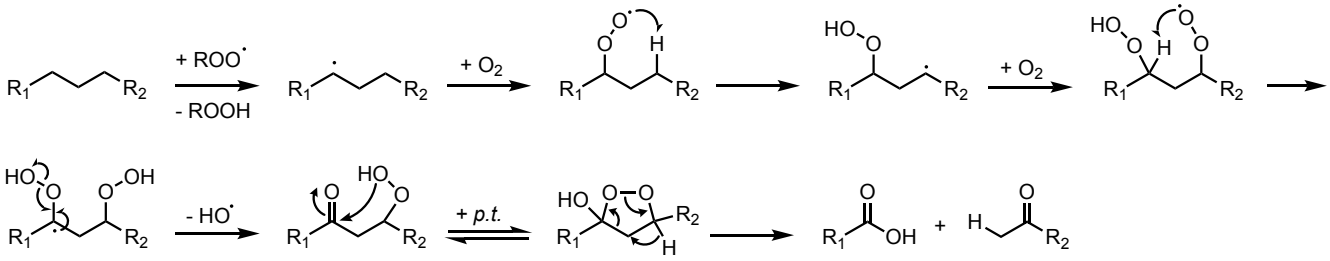

Scheme 2.3 Proposed mechanism of carboxylic acid formation during high-temperature autoxidation of linear alkanes.[4,10]

Based on this mechanism, generation of formic acid requires that R_1 = H, meaning the initial H-atom abstraction by peroxyl radical would need to occur at a 1˚ carbon. This is thermodynamically less favourable due to the BDE difference associated with forming a 1˚ carbon-centred radical versus a 2˚ carbon centred radical and statistically less likely due to the low probability of a peroxyl radical undergoing favourable collision with one of the two terminal positions over the fourteen secondary positions of the *n*-alkane. However, previous studies have demonstrated the formation of formate (formic acid) in reasonable quantity during autoxidation of oleic, linoleic, and linolenic acid at 110˚C.[19] Additionally, reports of the analysis of cyclohexane autoxidation samples highlighted formic acid and cyclohexylformate as major products.[20]

An alternative route to formamide (**2.5**) production could be explained by reaction of **2.1** with formate esters. Formate esters have not been previously identified as major products of alkane autoxidation, but there is

precedent to support their formation through reactions with peracids and aldehydes, which are known products of hydrocarbon autoxidation (Scheme 2.4). Experimental and computational studies have demonstrated the formation of formate esters through Baeyer-Villiger-type oxidation of saturated aldehydes with *meta*-chloroperoxybenzoic acid (mCPBA).[21,22] Migratory aptitudes tend to favour the formation of two acids via transfer of the alkyl substituent instead of the hydrogen, but such differences might be smaller at elevated temperatures, like 160˚C. To the best of our knowledge, there are no systematic studies of this nature from which we can gain insight.

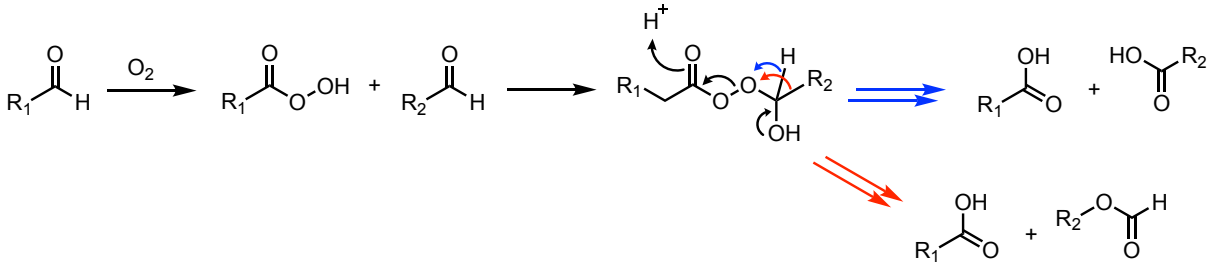

Scheme 2.4 Baeyer-Villiger-type oxidation of aldehydes to yield carboxylic acids (blue) and carboxylic acid and formate ester (red).[21,22]

Formate products were also found to form in greater ratios relative to acid in non-hydrogen-bonding solvents (i.e. decane, toluene) than in protic solvents such as methanol. Although acid formation is still favoured, this nevertheless provides a potential source of formamide production and should be explored further.

Our quantification of **2.5** with LC methods demonstrated that its accumulation before the end of inhibition is not significant, yet consumption of **2.1** over the same period is drastic. This was perplexing, as HMBC spectra did not indicate the formation of any products during this period. It is possible that **2.1** could fragment to generate volatile species that exit the system (e.g. 4-*tert*-butylaniline, which boils at approximately 90˚C). However, further experiments are necessary to properly assess this issue, as not enough data points were acquired at the beginning of the experiments to draw any strong conclusions. Experiments that quantify **2.1** throughout inhibition could reveal to what extent the post-inhibition speciation is relevant; our approach will need to be reconsidered if **2.1** concentration decreases drastically early into autoxidation with no visible species

by UPLC or HMBC. In addition, acquiring mass data alongside PDA quantification might provide useful information on speciation not easily observed by PDA: significant speciation was observed at the eight-hour mark during autoxidation with **2.1**, yet the resulting PDA chromatogram was difficult to assess due to a lack of distinct chromophores for many peaks. The lack of distinct products observed by UPLC could be due to poor extraction efficiency of the **2.1**-derived oxidation products; low concentrations of the products combined with a strong affinity to the non-polar substrate may limit identification via UPLC-PDA. In the future, the HMBC method could be utilized to identify species present in UPLC extracts to indicate the species present in each quantification experiment. It is also possible that multiple species with similar chemical shift, that appear as a single signal via HMBC, could possess fairly different elution times, i.e. diarylamine-derived products that possess alkyl-group isomers which resolve on the C18 column. Although preparatory efforts using flash chromatography have failed thus far, prep-HPLC techniques may be useful for extracting individual species that arise in earlier states of autoxidation.

Understanding how the 'diarylformamide' **2.5** forms is an important follow-up study, yet the reactivity of **2.5** during autoxidation experiments is intriguing in its own right. Autoxidation experiments using **2.5** as the 'inhibitor' were intended to determine if the species was an intermediate oxidation product that further reacted to yield other species, yet instead it demonstrated that **2.5** is the favoured product of an equilibrium with **2.1**. As **2.1** is at the lower end of RTA reactivity when compared with phenoxazines (PNX), phenothiazines (PTZ), or pyrimidinyl diarylamines, the slow production of it from the reverse reaction resulted in its immediate oxidation to non-RTA products. The slow release of compound could however, be a useful strategy to dose small amounts of RTA into a system if the reaction to yield 'free-RTA' was tailored to a specific rate and matched with RTA potency. This could be especially useful for the more reactive RTAs, such as phenothiazine and phenoxazine, which undergo HAT so rapidly that they accumulate high concentrations of aminyl radicals, leading to dimerization/oligomerization. Although the RTA activity of such dimers have not been studied, the oligomers form insoluble deposits that are counterproductive to lubrication, let alone inhibition. Phenothiazine for example,

is prone to self-reactions at high concentrations and temperatures, at which it forms insoluble polymers and deposits through radical-radical couplings due to the rate at which it forms aminyl radical.[23] This reduces its usefulness as an RTA in large quantities, as a portion of the material is sacrificed to such end in order to obtain inhibition. Phenoxazine is also vulnerable to such side-reactions, and is more sensitive to one-electron oxidation than phenothiazine. As such, the 'radical flux' is even greater due to formation of radical cation, which leads to formation of similar non-RTA products. Reducing the concentration of free-RTA could limit such reactions and perhaps provide a prolonged inhibition period.

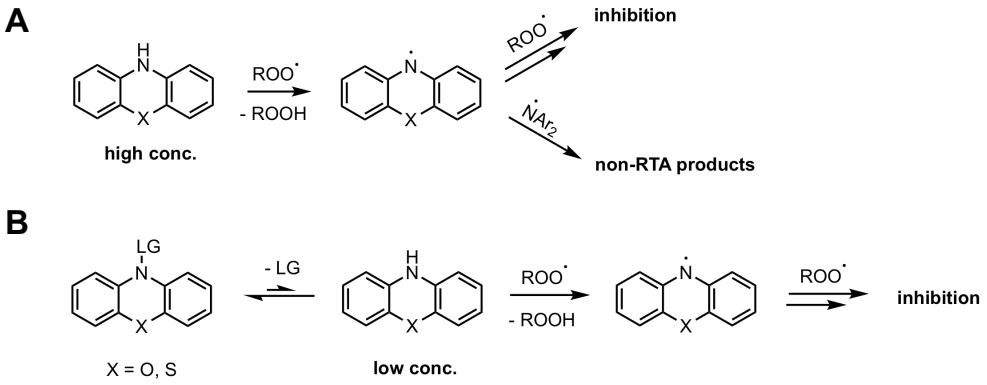

Figure 2.20 (**A**) Competing reactions of aminyl radicals of PNX, PTZ when used at high concentrations. (**B**) Potential latent-RTA strategy for limiting high concentrations of PNX, PTZ associated with non-productive pathways.

We were pleased that our HMBC method was able to corroborate previous findings of diarylamine regeneration from the diarylnitroxide radical and diarylalkoxyamine.[2,4] In the seminal work by Korcek, diarylnitroxides were used as the inhibitors of high-temperature autoxidation, in which their conversion to the corresponding diarylamine was monitored using HPLC. The investigators noted that diarylalkoxyamine was not detected during these experiments, therefore they examined its role further by generating it *in situ* at low temperatures under oxygen-free conditions, followed by high-temperature decay monitored by HPLC. The major decay product was the diarylamine, which was afforded in a 64% yield relative to the starting material. Later studies by Haidasz et al. demonstrated nearly quantitative conversion of diarylamine when authentic diaryl-alkoxyamine was used from the outset under similar conditions, rather than via *in situ* generation. Our

autoxidation experiments using nitroxide (**2.1a**) demonstrated that the diarylamine is regenerated to detectable levels within 40 min, but interestingly showed the formation of oxidation products early on into the experiment. Strangely, this finding came coupled with superior inhibition obtained when performing inhibited autoxidation with **2.1a** rather than **2.1**. The rate of initiation is relatively low at the beginning of high-temperature autoxidation, meaning fewer chain-carrying species are present. Diarylamine reacts readily with a peroxyl radical to yield the diarylaminyl radical, which also consumes a peroxyl radical to form the diarylnitroxide. Assuming the Korcek cycle is correct, the diarylnitroxide however, must compete with oxygen for alkyl radicals in order to form the diarylalkoxyamine and thus regenerate the diarylamine. It is possible that the increased concentration of diarylnitroxide allows it to be more competitive with oxygen (for reaction with alkyl radicals), which would slow the rate of peroxyl formation and potentially provide superior inhibition. However, this is difficult to reconcile with our understanding of diarylamine kinetics, which demonstrate that the primary HAT from diarylamine to peroxyls governs the rate of inhibition. As this was an auxiliary finding, we plan to investigate it further in a systematic manner; across a range of temperatures and concentrations, in order to confirm the increased activity of the diarylnitroxide.

Paradoxical to the results that suggest improved performance from **2.1a**, HMBC spectra indicted it is more prone to undergo 'non-Korcek' reactions to yield off-cycle products. One of these products was observed as the diarylformamide **2.5**, which would indicate that it forms at some point during conversion of **2.1a** to **2.1**. This suggests that the diarylnitroxide is a less efficient inhibitor, leading to the increased formation of hydrocarbon-derived oxidation products, including formate esters, which in turn react with **2.1** to yield the diarylformamide **2.5**. It is high unlikely that the **2.1a** itself is involved in the formation of **2.5**; our preliminary proposition is that diarylamine undergoes two-electron chemistry with formate esters to yield **2.5**, and there is no clear mechanistic pathway from **2.1a** to **2.5**. As the autoxidation is still under inhibition during the formation of **2.5** when starting with **2.1a**, UPLC studies could be used to quantify its formation over time in order to provide a rough rate estimation. It is also possible that the level of olefins in the 95% *n*-hexadecane used for experiments is

substantial enough to result in the **2.1a** providing superior inhibition through the added benefit of our recently reported mechanism of peroxyl cross-dismutation.[18] Further studies of the nitroxide's performance and speciation could be useful for the ultimate objective of improving performance of diarylamine additives.

Gratifyingly, the results of our autoxidation experiments using the diarylalkoxyamine (**2.1c**) also demonstrated its conversion to **2.1**, which unsurprisingly yielded the expected oxidation product distribution. Although **2.1c** is purported to play a prominent role in regeneration of **2.1**, it is not observed to accumulate within detection by HMBC. The aforementioned work by Korcek et al. also failed to demonstrate its formation during autoxidation.[2] As such, it can be said with confidence that **2.1** *can* be regenerated from **2.1c**, but not that **2.1c** is a key intermediate in its catalytic mechanism. The transformation of **2.1c** to **2.1** was quicker than from **2.1a** (as expected for an intramolecular reaction vs. an intermolecular reaction) and did not appear to generate any significant speciation, indicating that diarylalkoxyamine is not a source of oxidation species. The thermal decomposition rate constant (k_{dec}) of diarylalkoxyamines bearing saturated alkyl groups at 120˚C was measured to be $2.4 \times 10^4\ M^{-1}s^{-1}$;[4] a value that would increase at 160˚C. It is possible that the little turnover of **2.1** combined with a fast rate of decomposition prevent the accumulation of **2.1c** in sufficient quantities to be detected by HMBC techniques.

Although the HMBC technique is limited in the information it can provide regarding each species, especially when present at low concentrations, it has provided us with a small library of compounds of known ^{15}N chemical shifts. We are currently using such data to help develop accurate computational methods for calculating theoretical spectral data for compounds that have not yet been synthesized or tested. This approach will ideally enable us to streamline our endeavours by way of rapid assessment of the validity of synthetic targets or compounds of interest, such as the iminoquinone **2.6**. As mentioned, preparative HPLC experiments will likely be useful in determining the speciation of **2.1** during the inhibited period, and will complement synthetic and computational efforts. The *ortho* C-N dimer **2.4** was not observed to form during autoxidation, yet we posited that it may react further to prevent its accumulation; perhaps through peroxyl addition analogous to that

which forms **2.6**. Further oligomerized and oxygenated products have been implicated previously (see Figure 1.13), and would likely require isolation rather than *de novo* synthesis. We also hope that continued work into direct oxidation of the diarylamine using various initiators might elucidate the products that form during the early stages of autoxidation.

A benefit provided by the results is a spectroscopic baseline of the product distribution of diarylamines; our HMBC results depict a qualitative 'fingerprint' of the products formed during autoxidation in a simplified environment. From here, we hope to examine the changes that occur in different, or more complex, systems that are relevant to the speciation of diarylamines; beyond what is demonstrated and discussed in Chapter 3. This could involve tracking changes in the product distribution across temperature ranges, in the presence of other RTAs (i.e. phenols), additives used in lubricant formulations (i.e. viscosity modifiers, 'NO_x scrubbers', anti-wear agents, detergents, etc.), and/or under different experimental conditions. Primarily, these experiments could have useful application in the rapid-assessment of lubricant quality (i.e. state of the active inhibitor) to complement more time-consuming analyses by LC and GC. Additionally, such data can be used for mechanistic insight regarding the changes (if any) in the diarylamine product distribution in the presence of other additives or under different conditions. As certain additive combinations used in commercial lubricants have empirically been demonstrated as synergistic, the source of such reactivity could be elucidated through HMBC spectroscopic analysis.

2.4 Conclusions

Our foray into using NMR techniques to determine the speciation of diarylamine antioxidants during autoxidation was largely an exploratory effort, but yielded some interesting findings and demonstrated its utility to complement traditional methods. Our most prominent success was the identification of the diarylaminic oxidation species **2.5** using HMBC, which we corroborated with quantitative data using ultra-performance liquid chromatography. Our method also determined that previously-reported diarylaminic autoxidation products **2.3** and **2.4** did not appear to form under our conditions. Autoxidation and speciation of purported Korcek

intermediates also provided insights into speciation of the RTA, and inadvertently alerted us to the potential superiority of nitroxides as inhibitors at high temperatures. Perhaps most importantly, the HMBC method has proven its utility in confirming speciation of the diarylamine in 'real-time' and will be a valuable tool for our future work in this area.

2.5 References

[1] Bolsman, T.; Blok, A. P.; Frijns, J. *Recl. Trav. Chim. Pays-Bas.* **1978**, *97*, 310-312.

[2] Jensen, R. K.; Korcek, S.; Zinbo, M.; Gerlock, J. L. *J. Org. Chem.* **1995**, *60*, 5396-5400.

[3] Ingold, K. U. *Chem. Rev.* **1961**, *61*, 563-589.

[4] Haidasz, E. A.; Shah, R.; Pratt, D. A. *J. Am. Chem. Soc.* **2014**, *136*, 16643-16650.

[5] Zeman, A.; Römer, R.; Von Roenne, V. *Lubr. Sci.* **1986**, *3*, 4, 309-326.

[6] von Philipsborn, W.; Müller, R. *Angew. Chem. Int. Ed.* **1986**, *25*, 5, 383-486.

[7] Chhabra, S.; Fischera, P.; Takeuchic, K.; Dubeya, A.; Ziareka, J. J.; Boeszoermenyia, A.; Mathieue, D.; Bermele, W.; Daveyf, N. E.; Wagnera, G.; Arthanaria, H. *Proc. Natl. Acad. Sci. U.S.A.* **2018**, *115*, 8, E1710-1719.

[8] Köck, M.; Junker, J.; Lindel, T. *Org. Lett.* **1999**, *1*, 13, 2041-2044.

[9] Shah, R.; Pratt, D. A. *J. Org. Chem.* **2016**, *81,* 15*,* 6649-6656.

[10] Jensen, R. K.; Korcek, S.; Mahoney, L. R.; Zinbo, M. *J. Am. Chem. Soc.* **1981**, *103*, 7, 1742-1749.

[11] Jalan, A.; Alecu, I. M.; Meana-Pañeda, R.; Aguilera-Iparraguirre, J.; Yang, K. R.; Merchant, S. S.; Truhlar, D. G.; Green, W. H. *J. Am. Chem. Soc.* **2013**, *135*, 30, 11100-11114.

[12] Popochień, B. A. *Interactions of Antioxidants with NO_x at Elevated Temperatures.* Ph.D. Dissertation, University of York, York, UK. **2012**.

[13] Kerr, J. A.; Sekhar, R. C.; Trotman-Dickenson, A. F. *J. Chem. Soc.* **1963**, 3217-3225.

[14] Zheng, Y.; Zheng, W.; Wang, J.; Chang, H.; Zhu, D. *J. Phys. Chem. A.* **2018**, *122*, 2764-2780.

[15] Nakamura, M.; Takatani, H.; Hatakeyama, T.; Suzuki, T.; Imayoshi, R.; Aoki, Y.; Hagiwara, H.; Soga, S. Asymmetric Bis(1,2-diarylamino)benzene and Method for Producing the Same. JP2017165722 (A). **2017**.

[16] Ma, H.; Wu, S.; Sun, Q.; Li, H.; Chen, Y.; Zhao, W.; Ma, B.; Guo, Q.; Lei, Z.; Yan, J. *Synthesis.* **2010**, *19*, 3295-3300.

[17] Denisov, E. T.; Denisova, T. G.; Pokidova, T. S. *Handbook of Free Radical Initiators.* Hoboken, NJ. **2003**.

[18] Harrison, K. A.; Haidasz, E. A.; Griesser, M.; Pratt, D. A. *Chem. Sci.* **2018**, *9*, 6068-6079.

[19] Souza, P. T.; Ansolin, M.; Batista, E. A. C.; Meirelles, A. J. A.; Tubino, M. *Fuel.* **2017**, *199*, 239-247.

[20] Kotel'nikova, T. S.; Voronina, S. G.; Perkel, A. L. *Russ. J. Appl. Chem.* **2006**, *79*, 3, 424-428.

[21] Lehtinen, C.; Brunow, G. *Org. Process Res. Dev.* **2000**, *4,* 544-549.

[22] Lehtinen, C.; Nevalainen, V.; Brunow, G. *Tetrahedron*. **2001**, *57*, 4741-4751.

[23] Smalheer, C.V. Additives. In *Interdisciplinary Approach to Liquid Lubricant Technology;* Ku, P. M., Ed.; Scientific and Technical Information Office, National Aeronautics and Space Administration, **1973**; pp 463.

2.6 Experimental

Reagents were purchased from commercial suppliers and used without further purification, unless otherwise specified. Column chromatography was performed using flash silica gel (40-63 μm, 230-400 mesh). Product characterization via nuclear magnetic resonance spectroscopy (^{1}H, ^{13}C) was performed using Bruker Avance II 400 MHz, II 300 MHz, or 300 MHz instruments, unless otherwise specified. Chemical shifts for protons are reported in parts per million and are referenced to residual protium in solvent (i.e. ^{1}H NMR: Acetone-d_6 at 2.05 ppm). Chemical shifts for carbon signals are reported in parts per million and are referenced to the carbon resonances of the residual solvent peak (i.e. ^{13}C NMR: Acetone-d_6 at 29.84 ppm). Chemical shifts for nitrogen signals are reported in parts per million and referenced to neat nitromethane (CH_3NO_2) in liquid ammonia (i.e. $CH_3{}^{15}NO2$ at 379.5 ppm with respect to NH_3), and were obtained using a Bruker Avance III 600 MHz cryoprobe. High-resolution mass spectra were obtained using a Kratos Concept Tandem MS.

2.6.1 Uninitiated, high-temperature hydrocarbon autoxidations

A bulk amount of hydrocarbon substrate (*n*-hexadecane, 95%) is run through a silica-alumina column and collected. A 25 mL borosilicate test tube is then filled with 10 mL of purified *n*-hexadecane, placed in the 24-tube parallel, stir-flow reactor, and thoroughly degassed with nitrogen (approximately 15 minutes). Primene is then added to the tube while bubbling with nitrogen, and heated to 160˚C. Inhibitor is then added to the mixture, at which point the t = 0 aliquot is removed. The nitrogen flow is then replaced with a 2 L/min flow of 765 ppm NO_2 in air, commencing autoxidation. Aliquots of the mixture are removed from the test tubes via Pasteur pipette at pre-determined intervals, or 'time-points', placed in vials, and either allowed to cool to room temperature for immediate analysis or placed in a -20˚C freezer for storage. Aliquots used for hydroperoxide analysis are obtained in volumes of 50-100 μL. Aliquots used for NMR analysis are obtained in volumes of approx. 600 μL.

2.6.2 Quantifying hydroperoxide concentration of autoxidation samples

5 μL of samples (autoxidation aliquots) are loaded onto a 96-well microplate, incubated at 37˚C, and diluted with a mixture of 20% isopropanol in methanol by the automated reagent dispenser of a BioTek microplate reader. The automated reagent dispenser then adds 30 μL of an acetonitrile solution containing 100 mM fluorogenic phosphine dye to each well. Next, the plate undergoes automated stirring for 30 seconds, pauses for 5 seconds, and then measures the fluorescence of each well for 1 minute (coumarin phosphine dye: absorption 340 nm, emission 425 nm). Hydroperoxide concentration in each well is then determined from the rate of phosphine oxidation using the rate constant corresponding to reaction of the dye with secondary hydroperoxides (k = 5.1 M^{-1} s^{-1}); assuming pseudo-first order kinetics.

2.6.3 Composition of Base-Oil Blend

Base-oil blend (BOB) obtained by thoroughly mixing 1 : 3.8 : 2.9 of Durasyn 164 : Yubase 6 : Yubase 4.

2.6.4 General Procedure for Buchwald-Hartwig Cross-Couplings of (^{15}N) anilines to diarylamines

To a dry, round-bottom flask with a magnetic stir bar that has been evacuated and back-filled with nitrogen are added *tris*(dibenzylideneacetone)dipalladium(0) (0.01 equiv.), BippyPhos (0.03 equiv.), and 2-methyl-2-butanol (0.6 M). The mixture is flushed nitrogen for fifteen minutes while stirring. Potassium *tert*-butoxide (1.5 equiv.) is added. After stirring for another five to ten minutes, aryl bromide (1 equiv.) and 4-*tert*-butylaniline (**1.3**) (1.5 equiv.) are added. The reaction is then heated to 80˚C and allowed to stir for approximately six hours under nitrogen or until verified complete by TLC. Once complete, the solution is diluted with 10% (v/v) ethyl acetate/hexanes and filtered through celite, after which it is extracted with distilled water and brine. The organic phase is dried with magnesium sulfate, filtered, and concentrated via rotary evaporation. The crude product is purified via flash chromatography and then recrystallized from hexanes at -20˚C.

***bis*(4-*tert*-butylphenyl)amine (2.1)**

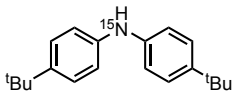

Yield: 94%. White needles, mp = 106-107˚C; ^{1}H NMR (400MHz, DMSO-d_6) δ 7.89 (d, J = 89.5 Hz, 1H), 7.22 (m, 4H), 6.97 (m, 4H), 1.25 (s, 18H). ^{13}C NMR (400MHz, DMSO-d_6) δ 141.51, 141.25, 141.09, 125.66, 125.65, 116.24, 116.22, 33.71, 31.33. HRMS (EI): *m/z* Calc: $C_{20}H_{27}{}^{15}N$: 282.2114 Found: 282.2098.

4-(*tert*-butyl)-*N*-(4-(*tert*-butyl)phenyl)-2-methoxyaniline (1.6)

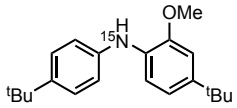

Yield: 99%. Pale red oil. ^{1}H NMR (400MHz, acetone-d_6) δ 7.28 (m, 2H). 7.18 (m, 1H), 7.08 (2H, m), 7.02 (d, J = 1.8 Hz, 1H), 6.88 (dd, J = 8.3, 1.8 Hz, 1H), 6.52 (d, J = 89.5 Hz, 1H), 3.87 (s, 3H), 1.30 (s, 9H), 1.29 (s, 9H). ^{13}C NMR (400MHz, $CDCl_3$) δ 147.95, 143.81, 142.99, 140.63, 140.53, 131.05, 130.94, 126.14, 118.28, 117.37, 114.31, 108.29, 55.77, 34.55, 34.27, 31.70, 31.63 HRMS (ESI): *m/z* Calc $C_{21}H_{30}{}^{15}NO^{+}$ (from addition of H^{+}): 313.2298 Found: 313.2292.

4-(*tert*-butyl)-*N*-(4-methoxyphenyl)aniline (1.7)

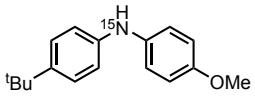

Yield: 91%. Beige solid. ^{1}H NMR (400MHz, acetone-d_6) δ 7.23 (m, 2H), 7.07 (m, 2H), 6.92 (m, 2H), 6.85 (m, 2H), 3.75 (s, 3H), 1.27 (s, 9H). ^{13}C NMR (400MHz, $CDCl_3$) δ 155.02, 142.85, 142.56, 142.47, 136.50, 136.40, 126.22, 121.55, 115.96, 114.77, 55.74, 34.18, 31.63. HRMS (EI): *m/z* Calc $C_{17}H_{21}{}^{15}NO$: 256.1593 Found: 256.1611.

2.6.5 General Procedure for Synthesis of Iminoquinones (2.6) & (2.7)

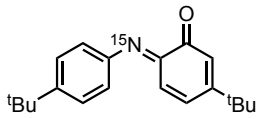

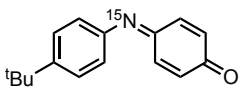

To a dry, round-bottom flask with a magnetic stir bar is added dichloromethane (0.2 M) and Dess-Martin Periodinane (DMP) (1.8 equiv.), as well as a drop of distilled water. Diarylamine (1.0 equiv.) is dissolved in a small amount of dichloromethane and added to the DMP-solution dropwise while stirring at room temperature. The reaction is monitored by TLC until complete, and then purified by flash chromatography to afford the product.

Synthesis of (^{15}N) 4-*tert*-butylbenzamide (1.1)

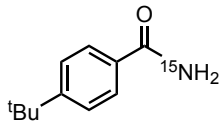

To a dry, round-bottom flask with a magnetic stir bar is added 4-*tert*-butylbenzoic acid (1 equiv.) and dichloromethane (0.5 M). Oxalyl chloride (1.2 equiv.) is added to the mixture while stirring, after which a few drops of dimethylformamide are added slowly. The reaction is allowed to stir at room temperature while open to air for approximately two hours (monitored by TLC). The solvent is then removed via rotary evaporation, and the resulting crude mixture is dissolved in diethyl ether while stirring at 0˚C. ^{15}N-ammonium chloride (0.5 equiv.), dissolved in distilled water (5 M) is added. Following this, sodium hydroxide (2 equiv.) in distilled water (10 M) is added dropwise to the mixture. The resulting precipitate is filtered, washed with distilled water and cold 25% (v/v) ether/hexanes, and dried via reduced pressure. Yield: 99%. White solid. ^{1}H NMR (400MHz, DMSO-d_6) δ 7.91 (d, J = 86.5 Hz, 1H), 7.81 (m, 2H), 7.45 (m, 2H), 7.26 (d, J = 86.4 Hz, 1H), 1.29 (s, 9H). ^{13}C NMR (400MHz, DMSO-d_6) δ 167.85, 167.69, 153.91, 131.58, 131.50, 127.31, 124.91, 34.56, 30.94. HRMS (EI): *m/z* Calc $C_{11}H_{15}{}^{15}NO$: 178.1124 Found: 178.1117.

Synthesis of (^{15}N) methyl (4-*tert*-butylphenyl)carbamate (1.2)

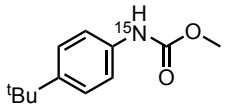

Sodium methoxide (13 equiv.) and methanol (0.066 M) are added to a dry round-bottom flask with a magnetic stir bar. To this mixture is added 4-*tert*-butylbenzamide (**1.1**) (1 equiv.) and N-bromosuccinimide (NBS) (1 equiv.), after which the flask is attached with a condenser and heated to reflux while stirring. After three minutes, an additional portion of NBS is added (0.5 equiv.) slowly to avoid excessive bubbling. This is repeated after another three minutes. Ten minutes after the second addition, check the reaction by TLC. Once complete, remove the majority of solvent by rotary evaporation. Dilute with 50% (v/v) ethyl acetate/hexanes, and extract with distilled water and brine, making sure to neutralize the aqueous phases. Combine and dry the organic phase with magnesium sulfate. Filter the mixture and remove the solvent by rotary evaporation. Purify the crude mixture via flash chromatography. Yield: 94%. White solid. ^{1}H NMR (400MHz, DMSO-d_6) δ 9.51 (d, J = 91.0 Hz, 1H), 7.36 (dd, J = 8.8, 2.0 Hz, 2H), 7.28 (m, 2H), 3.65 (s, 3H), 1.24 (s, 9H). ^{13}C NMR (400MHz, DMSO-d_6) δ 154.14, 153.87, 144.6, 136.56, 136.4, 125.32, 125.30, 118.01, 51.47, 33.87, 31.20. HRMS (EI): *m/z* Calc $C_{12}H_{17}{}^{15}NO_2$: 208.1230 Found: 208.1242.

Synthesis of (^{15}N) 4-*tert*-butylaniline (1.3)

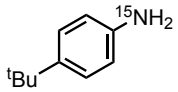

Methyl (4-*tert*-butyphenyl)carbamate (**1.2**) (1 equiv.) and potassium hydroxide (2 equiv.) are added to a round-bottom flask with a magnetic stir bar and dissolved in 99% ethanol (0.2 M). A condenser is added to the flask and the reaction is refluxed for approximately four hours while stirring. Once completion confirmed by TLC, the reaction mixture is diluted with 50% (v/v) ethyl acetate/hexanes and extracted twice with distilled water and once with brine. The organic phase is dried with magnesium sulfate, filtered, and concentrated via rotary

evaporation. The crude mixture is purified by flash chromatography to afford the product. Yield: 99%. Red-brown oil. ^{1}H NMR (400MHz, DMSO-d_6) δ 7.02 (m, 2H), 6.49 (m, 2H), 4.79 (d, J = 81.0 Hz, 2H), 1.19 (s, 9H). ^{13}C NMR (400MHz, DMSO-d_6) δ 146.01, 145.89, 137.82, 125.32, 125.31, 113.63, 113.61, 33.39, 31.49. HRMS (ESI): *m/z* Calc $C_{10}H_{16}{}^{15}N^{+}$ (from addition of H^{+}): 151.1253 Found: 151.1240.

Synthesis of (^{15}N) *bis*(4-*tert*-butylphenyl)aminoxyl (2.1a)

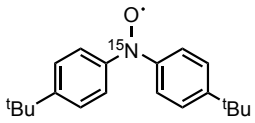

To a dry round-bottom flask under nitrogen with a magnetic stir bar is added *bis*(4-*tert*-butylphenyl)amine (**2.1**) (1 equiv.) and methanol (0.16 M). A condenser column is added to the flask and the solution is heated to reflux. Sodium tungstate dihydrate (0.1 equiv.) is dissolved in a minimum amount of distilled water and is added to the solution. Hydrogen peroxide diluted in methanol is added to the solution slowly. Check progress by TLC after one hour; if incomplete, add additional hydrogen peroxide in methanol and let react for an additional hour. Repeat until complete by TLC. Evaporate methanol by rotary evaporation. Dissolve crude in 25% (v/v) ethyl acetate in hexanes and extract with water and brine. Dry organic phase(s) with magnesium sulfate, filter through silica plug, and concentrate under reduced pressure. Product is recrystallized from hexanes or methanol at room temperature or -20˚C.

Yield: 83%. Vibrant red crystals, mp = 129-130˚C. *g*-value = 2.0059. HRMS (EI) *m/z* Calc $C_{20}H_{26}{}^{15}NO^{\bullet}$: 297.0200 Found: 297.1984.

Synthesis of (^{15}N) *bis*(4-*tert*-butylphenyl)hydroxylamine (2.1b)

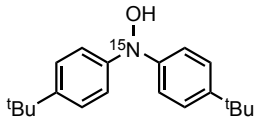

To a round-bottom flask with a magnetic stir bar is added *bis*(4-*tert*-butylphenyl)aminoxyl (**2.1a**) (1 equiv.) and tetrahydrofuran (0.11 M). Hydrazine hydrate [50%] (1 equiv.) is added slowly. The reaction is allowed to stir until red colour has completely disappeared leaving a pale beige or clear solution. Excess solvent is removed via rotary evaporation and placed on high vacuum overnight to yield the product.

Yield: 95%. Light beige solid. ^{1}H NMR (400MHz, DMSO-d_6) δ 9.72 (d, J = 1.1 Hz, 1H), 7.31 (d, J = 8.6 Hz, 4H), 7.04 (dd, J = 8.6, 1.5 Hz. 4H), 1.26 (s, 18H). ^{13}C NMR (400MHz, DMSO-d_6) δ 147.73, 147.68, 145.18, 125.31, 119.29, 33.95, 31.26. HRMS (EI): *m/z* Calc $C_{20}H_{27}{}^{15}NO$: 298.2063 Found: 298.2056.

Synthesis of (^{15}N) N,N-*bis*(4-*tert*-butylphenyl)-2-octyl-alkoxyamine (2.1c)

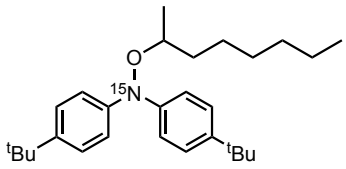

Bis(4-*tert*-butylphenyl)hydroxylamine (**2.1b**) (1 equiv.) is added to a round-bottom flask with a magnetic stir bar and dissolved in tetrahydrofuran (0.1 M). The solution is cooled to -78˚C while stirring, after which potassium *bis*(trimethylsilyl)amide (1 equiv.) is added dropwise. The reaction is allowed to stir for ten minutes, after which point 2-octyl-triflate is added dropwise. The solution is allowed to warm to room temperature over several hours while stirring. The mixture is diluted with ether and extracted twice with water and then brine. The organic phase(s) is dried magnesium sulfate, filtered, and concentrated via rotary evaporation, and then allowed to sit under reduced pressure overnight to yield the waxy product.

Yield: 23%. Pale oil. ^{1}H NMR (400MHz, benzene-d_6) δ 7.33 (dd, J = 8.6, 1.1 Hz, 4H), 7.25 (d, J = 8.6 Hz, 4H), 4.08 (m, 1H), 1.82 (m, 1H), 1.49 (m, 1H), 1.34-1.17 (m, 29H), 0.87 (t, J = 6.9 Hz, 3H). ^{13}C NMR (600MHz,

DMSO-d_6) δ 146.97, 146.93, 146.16, 141.39, 141.09, 140.99, 125.61, 125.47, 120.20, 116.15, 116.14, 77.17, 34.49, 33.89, 33.60, 31.32, 31.19, 31.17, 28.61, 24.60, 21.96, 19.06, 13.93, 1.77. HRMS (EI): *m/z* Calc $C_{20}H_{27}{}^{15}NO$: 410.3315 Found: 410.3299.

Synthesis of (^{15}N) N,N-*bis*(4-*tert*-butylphenyl)laurylamide (2.2)

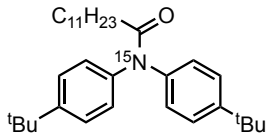

To a dry, round-bottom flask with a magnetic stir bar is added *bis*(4-*tert*-butylphenyl)amine (**2.1**) (1 equiv.) and dry dichloromethane (0.1 M). Pyridine (1.5 equiv.) and 4-dimethylaminopyridine (DMAP) (0.1 equiv.) are then added, followed by dropwise addition of lauroyl chloride (1.2 equiv.) dissolved in a small amount of dichloromethane. The mixture is allowed to stir under nitrogen for two hours or until verified complete by TLC. Dichloromethane is removed by rotary evaporation, and the crude is dissolved in 10% (v/v) ethyl acetate/hexanes. The mixture is extracted with distilled water, saturated sodium bicarbonate, and brine, and then dried with magnesium sulfate. The organic phase is then filtered and then concentrated via rotary evaporation. The crude product is purified by flash chromatography. Yield: 81%. Pale yellow oil. ^{1}H NMR (400MHz, acetone-d_6) δ 7.43 (s, 4H), 7.26 (s, 4H), 2.21 (t, J = 7.3 Hz, 2H), 1.59 (q, J = 7.4 Hz, 2H), 1.31 (s, 9H), 1.27 (m, 25H), 0.88 (t, J = 6.9 Hz, 3H). ^{13}C NMR (400MHz, $CDCl_3$) δ 173.72, 173.64, 140.58, 140.47, 128.23, 126.61, 125.94, 35.26, 35.21, 34.67, 32.06, 31.47, 29.76, 29.75, 29.63, 29.53, 29.49, 29.39, 25.79, 22.84, 14.27. HRMS (EI): *m/z* Calc $C_{32}H_{49}{}^{15}NO$: 464.3785 Found: 464.3813.

Synthesis of (^{15}N) *tetrakis*(4-*tert*-butylphenyl)hydrazine (2.3)

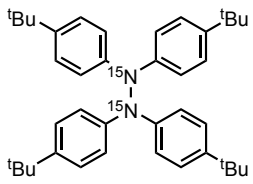

To a dry, round-bottom flask was added *bis*(4-*tert*-butylphenyl)amine (**2.1**) (1 equiv.) and acetone (0.22 M) with a magnetic stir bar. Potassium permanganate (0.3 equiv.) in acetone was added dropwise while stirring at room temperature. The solution was allowed to stir for five hours or until verified complete by TLC. The solution is then filtered through celite, concentrated, and purified via flash chromatography. Yield: 60%. White solid. ^{1}H NMR (400MHz, acetone-d_6) δ 7.29 (m, 8H), 7.23 (m, 8H), 1.26 (s, 36H). ^{13}C NMR (400MHz, acetone-d_6) δ 145.11, 142.39, 142.21, 126.75, 126.74, 118.28, 118.27, 34.68, 31.67. HRMS (ESI): *m/z* Calc $C_{40}H_{52}{}^{15}N_2$: 562.4071 Found: Mass not obtained.

Synthesis of (^{15}N) 4-*tert*-butylphenyl-N^1,N^1,N^2-tri-*tert*-butylbenzene-1,2-diamine (2.4)

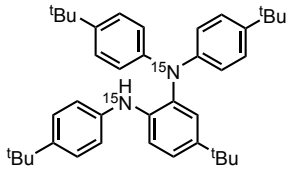

To a sealed tube without a cap was added a magnetic stir bar, *tetrakis*(4-*tert*-butylphenyl)hydrazine (**2.3**), and 99% *n*-hexadecane (0.20 M). The mixture was heated to 160˚C under constant bubbling of nitrogen while stirring. After four hours, the reaction was removed from heat while still bubbling gently. Once cooled, the mixture is allowed to sit at ambient temperature until product precipitates out of the substrate. The product is then removed from the hexadecane by filtration. Yield: 40%. White solid. ^{1}H NMR (400MHz, acetone-d_6) δ 7.25 (m, 9H), 6.96 (m, 4H), 6.87 (m, 2H), 6.30 (d, J = 88.0 Hz, 1H), 1.27 (s, 18H), 1.26 (s, 9H), 1.25 (s, 9H). ^{13}C NMR (400MHz, $CDCl_3$) δ 144.55, 144.45, 144.40, 144.12, 143.89, 140.53, 140.42, 138.78, 138.67, 134.20,

134.10, 127.61, 126.07, 125.96, 125.95, 123.65, 120.64, 120.63, 118.96, 118.95, 116.30, 34.29, 31.61, 31.58, 31.57. HRMS (EI): *m/z* Calc $C_{40}H_{52}{}^{15}N_2$: 562.4071 Found: 562.7058.

Synthesis of (^{15}N) *bis*(4-*tert*-butylphenyl)formamide ^{15}N (2.5)

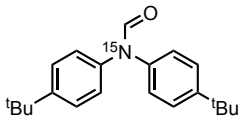

To a dry, round-bottom flask with a magnetic stir bar is added *bis*(4-*tert*-butylphenyl)amine (**2.1**) (1 equiv.), iodine crystals (0.05 equiv.), and 99% formic acid (2 equiv.). The reaction is heated to 70˚C while stirring and allowed to react for at least two hours. Once complete, the mixture is cooled and diluted with dichloromethane, and then carefully washed with saturated sodium bicarbonate, brine, and distilled water. The organic phase is dried with magnesium sulfate, filtered, and concentrated by rotary evaporation. The crude product is purified via flash chromatography. Yield: 64%. Off-white solid. ^{1}H NMR (400MHz, DMSO-d_6) δ 8.60 (d, J = 15.9 Hz, 1H), 7.44 (d, J = 8.3 Hz, 4H), 7.16 (ddd, J = 8.3 Hz, 3.4, 1.6 Hz, 4H), 1.28 (d, J = 3.8 Hz, 18H). ^{13}C NMR (400MHz, acetone-d_6) δ 162.04, 161.92, 150.48, 150.02, 140.63, 140.47, 138.83, 138.69, 127.35, 127.34, 126.63, 125.69, 125.67, 35.09, 35.07, 31.60, 31.58. HRMS (EI): *m/z* Calc: $C_{21}H_{27}{}^{15}NO$: 310.2063 Found: 310.2051.

Synthesis of 2-bromo-5-*tert*-butylphenol

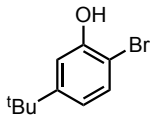

To a round-bottom flask with a magnetic stir bar is added 3-*tert*-butylphenol (1 equiv.) and dichloromethane (0.65 M). Bromine (1.1 equiv) is added dropwise. The mixture is allowed to react for one hour or upon completion verified by TLC. The mixture is then washed with distilled water and brine, and dried with magnesium sulfate. The organic phase is filtered and concentrated by rotary evaporation, and then further concentrated under high-vacuum reduced pressure. Flash chromatography can purify the product further, if

required. Yield: 93%. Pale yellow oil. ^{1}H NMR (400MHz, acetone-d_6) δ 8.49 (s, 1H), 7.38 (d, J = 8.5 Hz, 1H), 7.05 (d, J = 2.3 Hz, 1H), 6.83 (dd, J = 8.5, 2.3 Hz, 1H), 1.26 (s, 9H). ^{13}C NMR (400MHz, $CDCl_3$) δ 153.29, 151.90, 131.43, 119.32, 113.55, 106.97, 34.79, 31.30.

Synthesis of 1-bromo-2-methoxy-4-*tert*-butylbenzene (1.4)

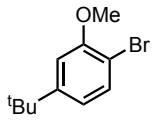

To a dry, round-bottom flask with a stir bar is added 2-bromo-5-*tert*-butylphenol (1 equiv.) and tetrahydrofuran (0.1 M). Potassium *tert*-butoxide (1.2 equiv.) is then added and the mixture is stirred for 30 minutes. Methyl iodide (1.0 equiv.) is then added dropwise, and the reaction is stirred at room temperature overnight or monitored by TLC. Once complete, the organic phase is diluted and washed with distilled water and brine, making sure to neutralize the aqueous phases. The organic phase is then dried with magnesium sulfate, filtered, and concentrated by rotary evaporation and high-vacuum reduced pressure to afford the product. Flash chromatography can be used to purify further, if necessary. Yield: 99%. Clear oil. ^{1}H NMR (400MHz, $CDCl_3$) δ 7.43 (d, J = 8.3 Hz, 1H), 6.92 (d, J = 2.1 Hz, 1H), 6.87 (d, J = 8.3, 2.1 Hz, 1H), 3.91 (s, 3H), 1.32 (s, 9H). ^{13}C NMR (400MHz, $CDCl_3$) δ 155.55, 152.44, 132.73, 119.16, 109.75, 108.60, 56.26, 35.03, 31.42.

2.7 Appendix

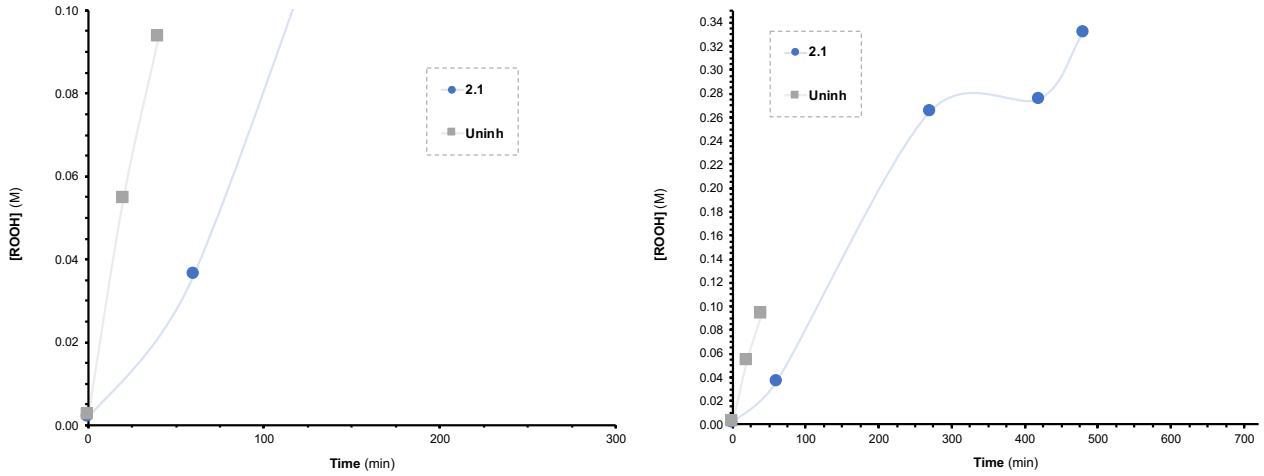

Figure S2.1 Hydroperoxide data corresponding to high-temperature autoxidation of PETX using 10 mM of **2.1** (blue) and no inhibitor (grey).

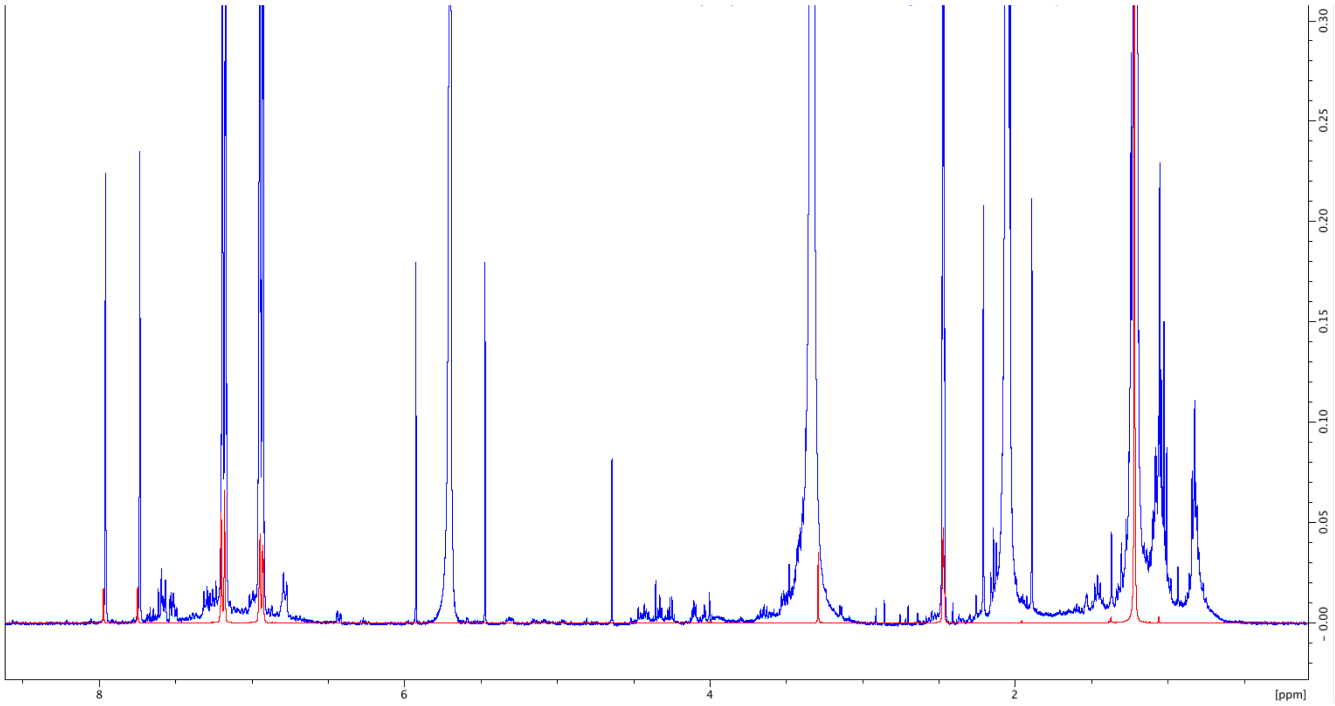

Figure S2.2 ^{1}H NMR spectrum of product(s) in organic phase of reactive base extraction of PETX autoxidation sample (blue) vs. ^{1}H NMR spectrum of **2.1**.

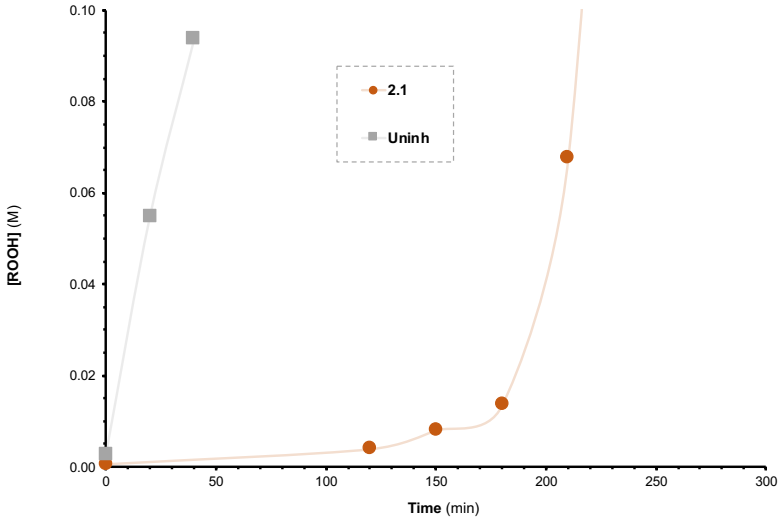

Figure S2.3 Hydroperoxide data corresponding to high-temperature autoxidation of YB4 using 10 mM of **2.1** (orange) and no inhibitor (grey).

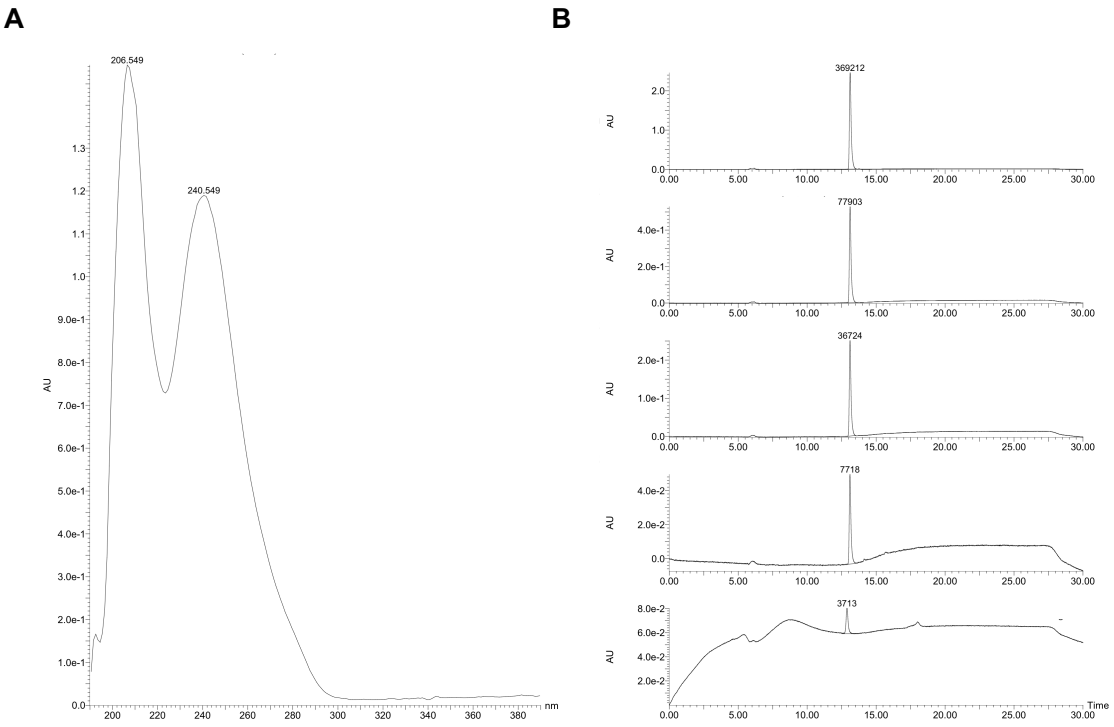

Figure S2.4 (**A**) Absorbance spectrum of **2.5**. (**B**) Chromatograms for calibration curve of **2.5** from top to bottom: 500, 100, 50, 10, 5 μM, via UPLC-PDA.

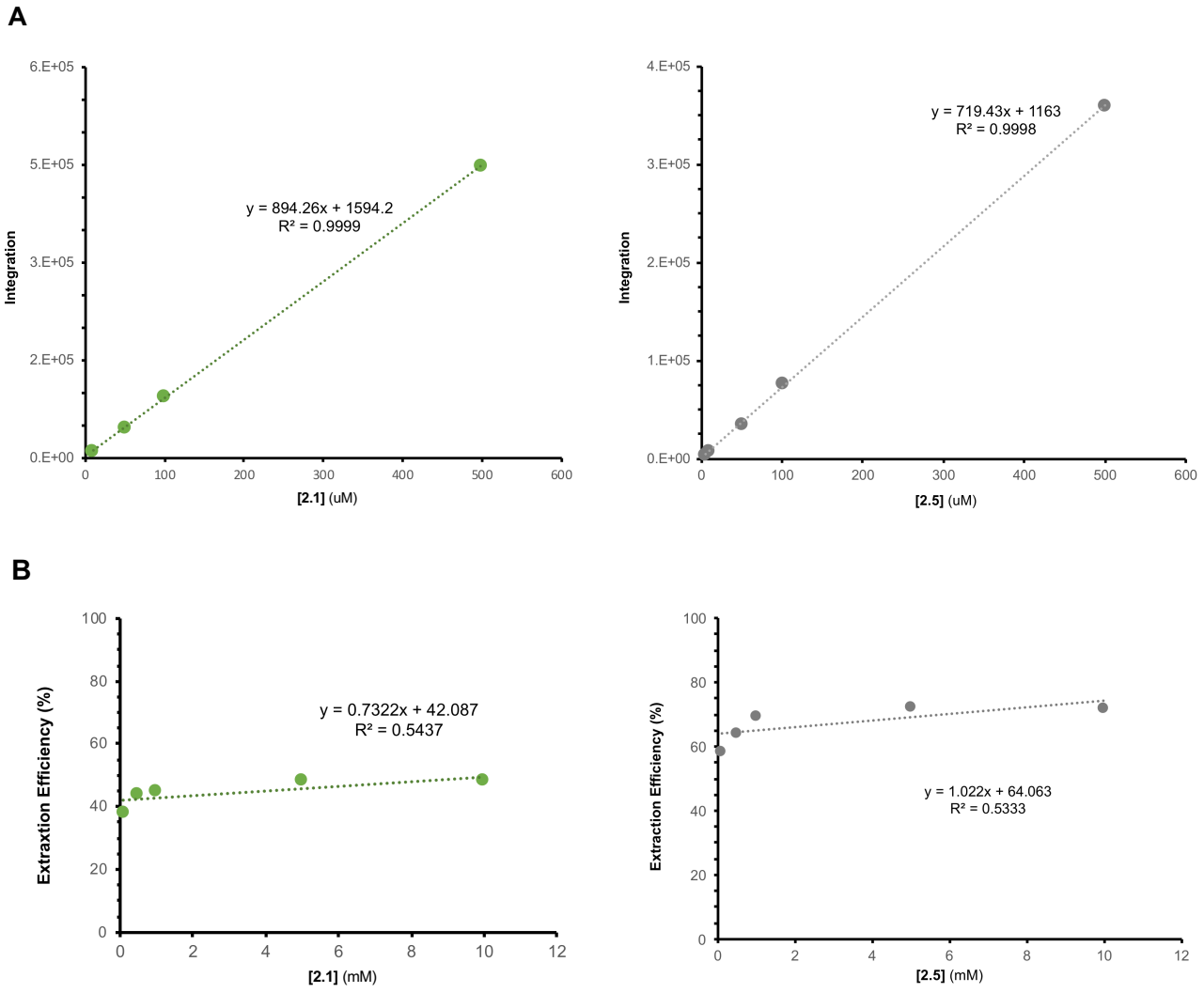

Figure S2.5 (**A**) Standard curves via UPLC-PDA for **2.1** (green) and **2.5** (grey). (**B**) Extraction efficiency curves via UPLC-PDA for **2.1** (green) and **2.5** (grey).

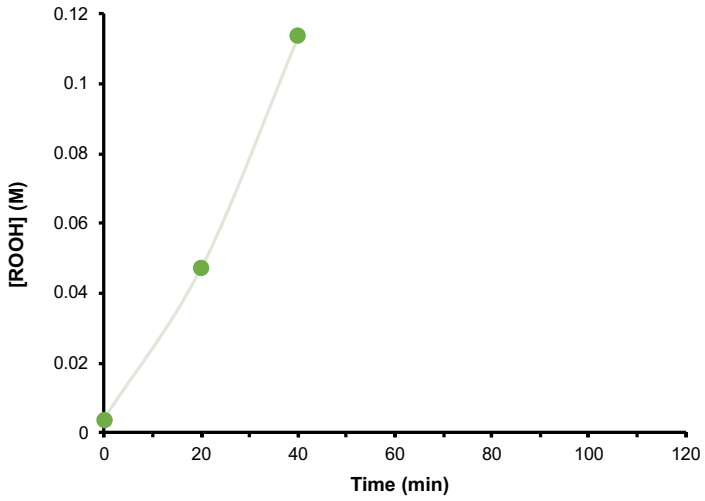

Figure S2.6 Hydroperoxide data of autoxidation of *n*-hexadecane at 160˚C using 10 mM of **2.5** as inhibitor (green).

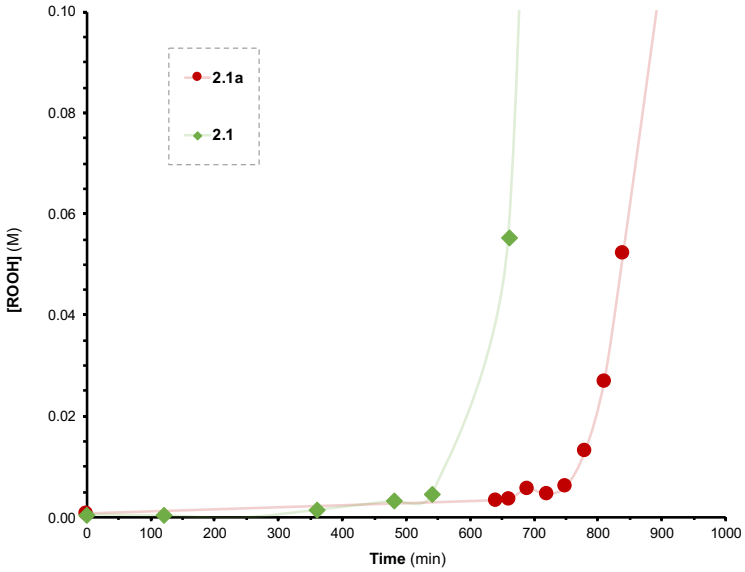

Figure S2.7 Hydroperoxide data of autoxidation of *n*-hexadecane at 160˚C using 10 mM of **2.1a** as inhibitor (red).

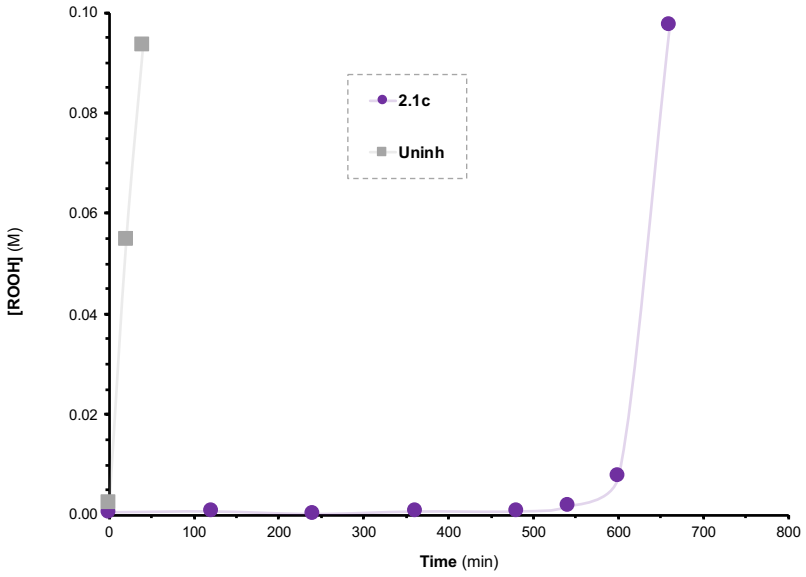

Figure S2.8 Hydroperoxide data of autoxidation of *n*-hexadecane at 160˚C using 10 mM of **2.1c** as inhibitor (purple).

^{1}H

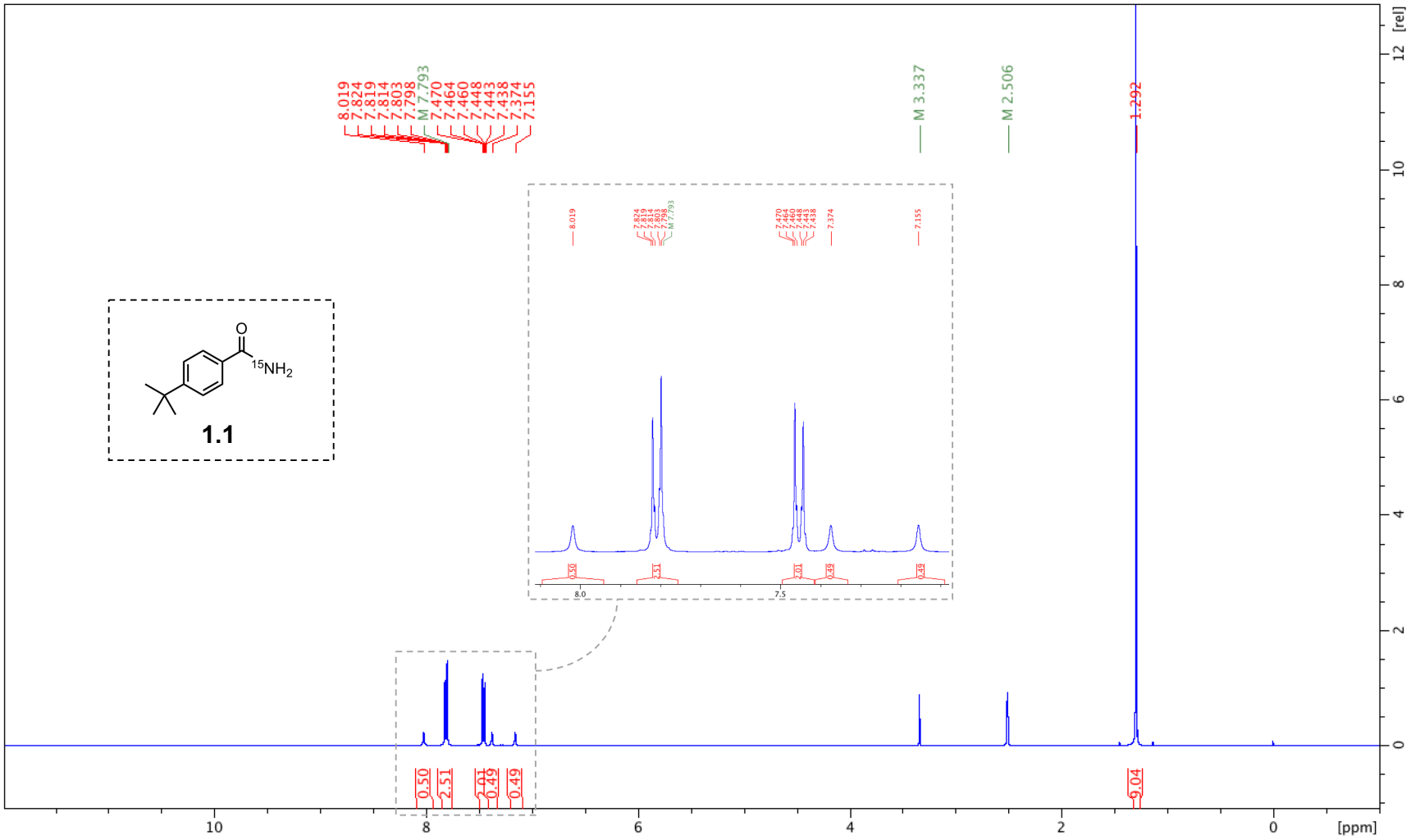
8.019
7.824
7.819
7.814
7.803
7.798
M 7.793
7.470
7.464
7.460
7.448
7.443
7.438
7.374
7.155
M 3.337
M 2.506
1.292
$^{15}NH_2$
1.1
0.50
2.51
2.01
0.49
0.49
9.04
10
8
6
4
2
0
[ppm]
12
10
8
6
4
2
0
[rel]

^{13}C

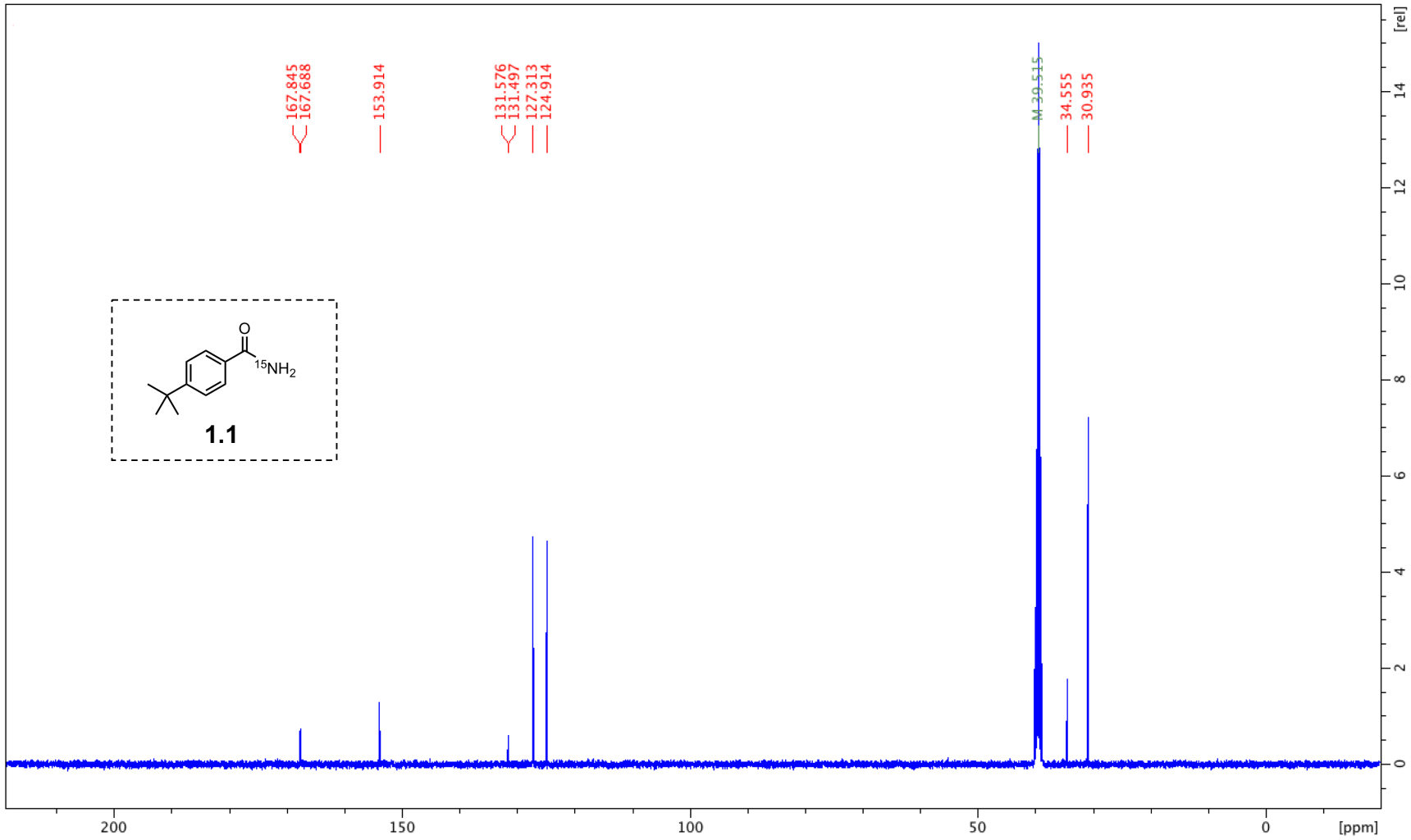
167.845
167.688
153.914
131.576
131.497
127.313
124.914
M 39.515
34.555
30.935
[rel]
0
2
4
6
8
10
12
14
200
150
100
50
0
[ppm]
O
15NH2
1.1

^{1}H

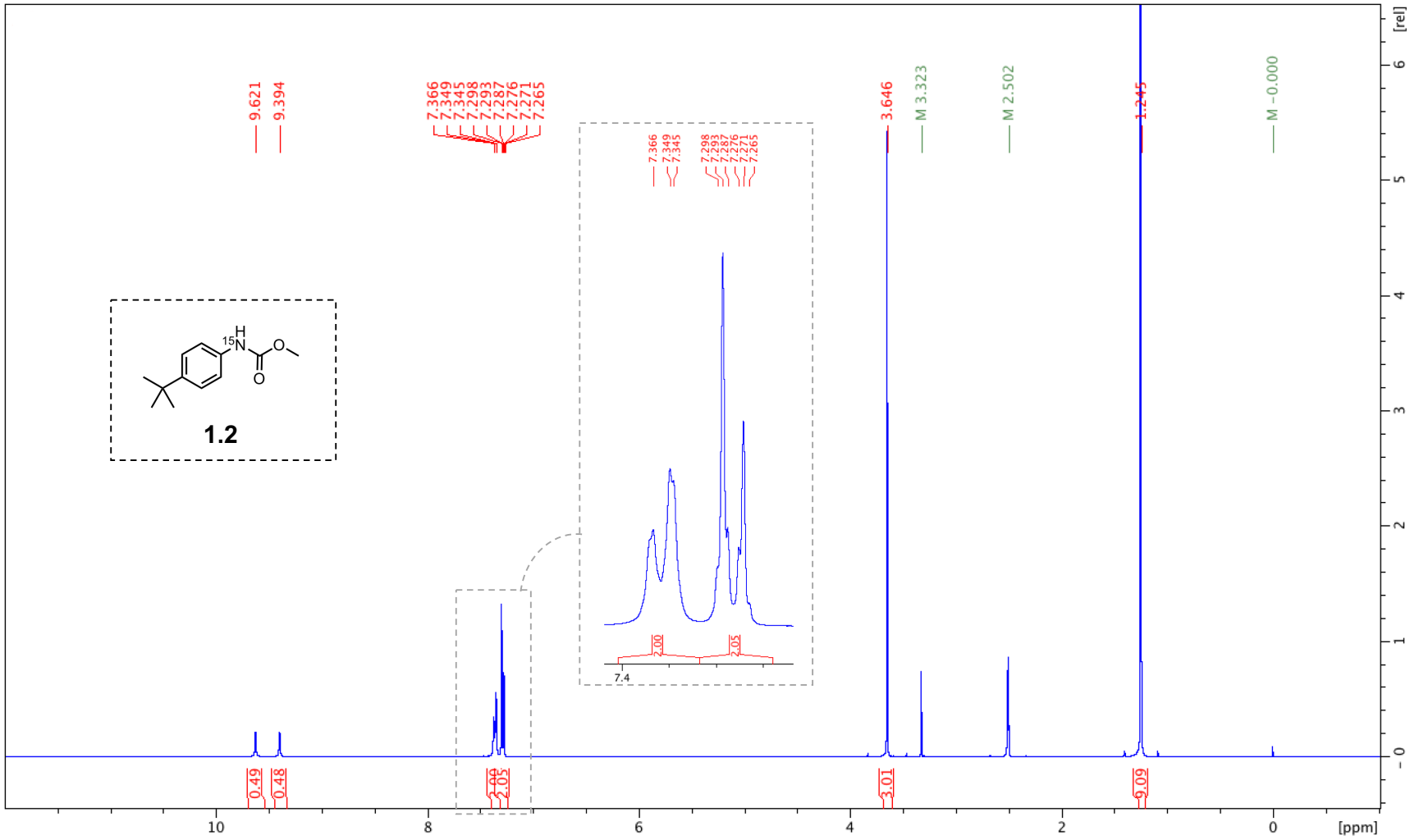
9.621
9.394
7.366
7.349
7.345
7.298
7.293
7.287
7.276
7.271
7.265
3.646
M 3.323
M 2.502
1.245
M -0.000
[rel]
[ppm]
0.49
0.48
2.00
2.05
3.01
9.09
1.2

^{13}C

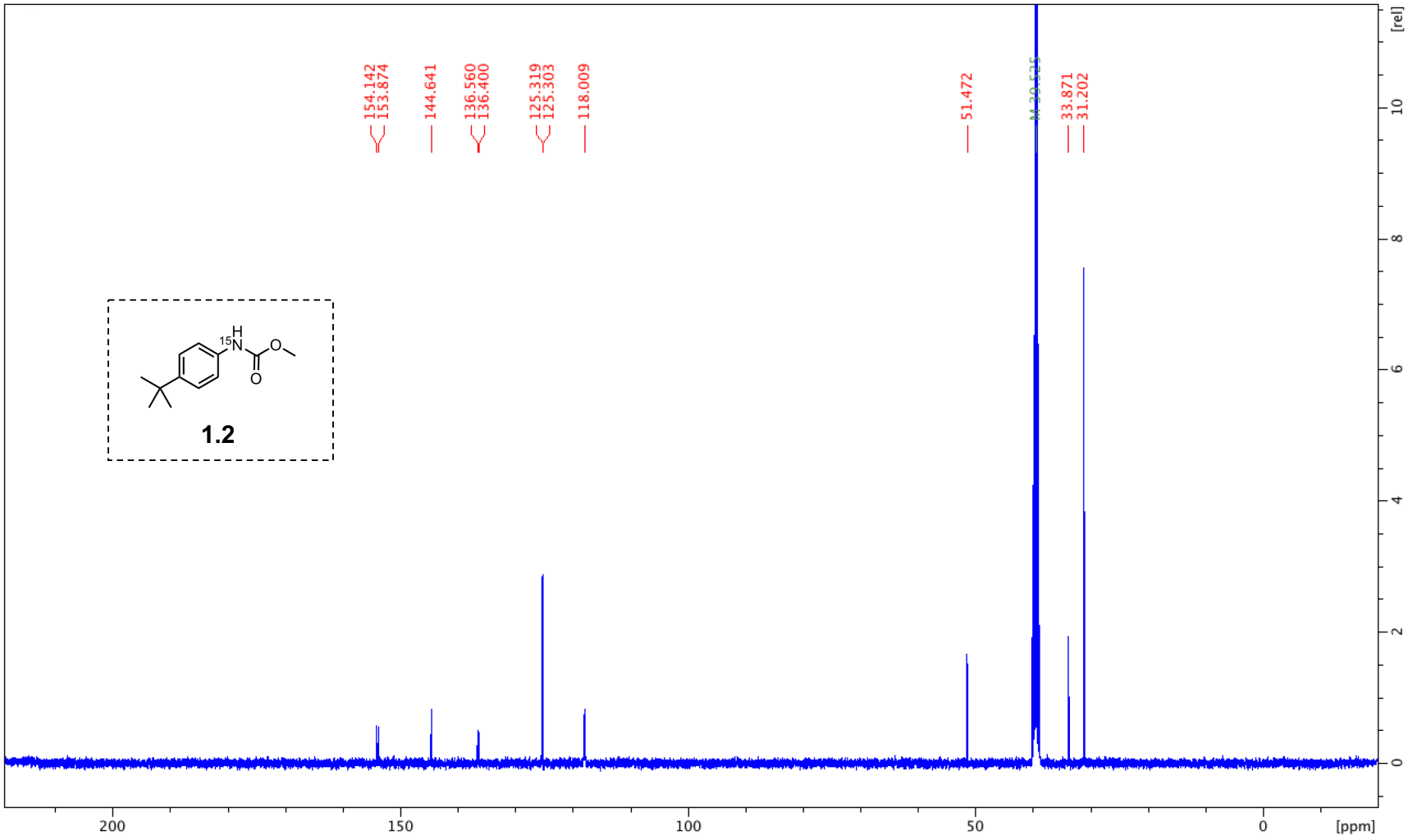
154.142
153.874
144.641
136.560
136.400
125.319
125.303
118.009
51.472
M 29.525
33.871
31.202
[rel]
10
8
6
4
2
0
200
150
100
50
0
[ppm]
15N
H
O
O
1.2

^{1}H

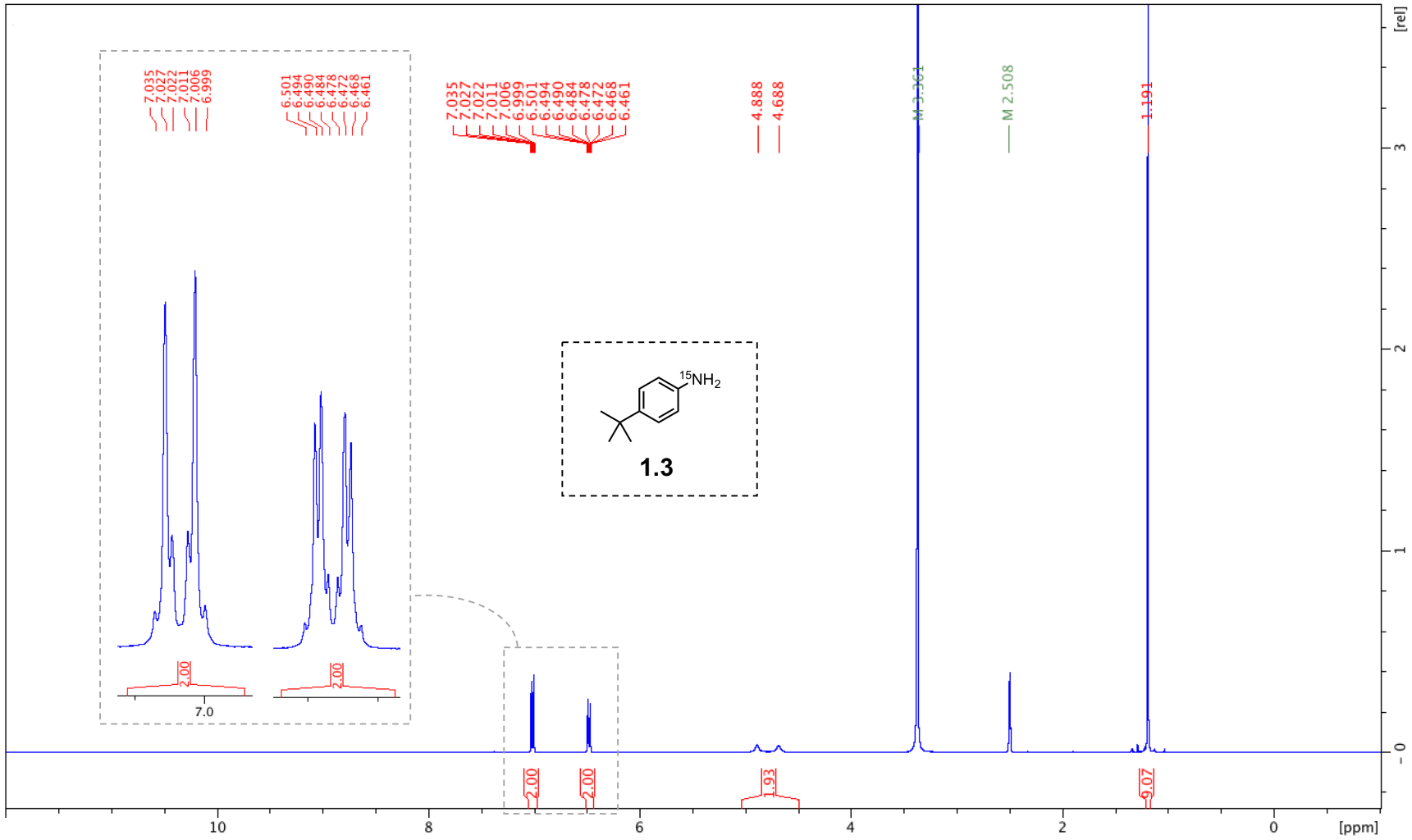
7.035
7.027
7.022
7.011
7.006
6.999
6.501
6.494
6.490
6.484
6.478
6.472
6.468
6.461
4.888
4.688
M 3.361
M 2.508
1.191
$^{15}NH_2$
1.3
2.00
2.00
1.93
9.07
7.0
10
8
6
4
2
0
[ppm]
[rel]

^{13}C

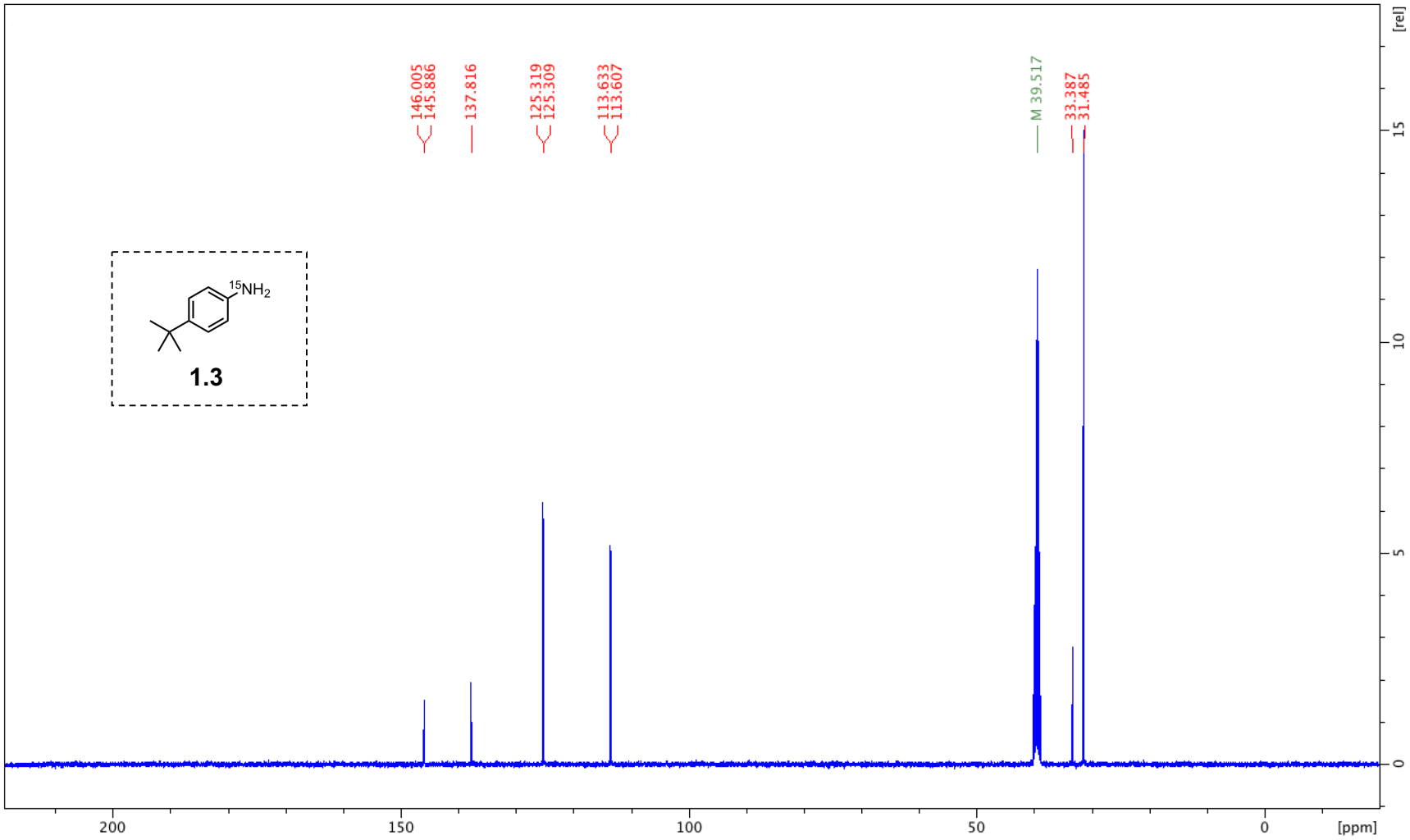
146.005
145.886
137.816
125.319
125.309
113.633
113.607
M 39.517
33.387
31.485
$^{15}NH_2$
1.3
[rel]
15
10
5
0
200
150
100
50
0
[ppm]

^{1}H

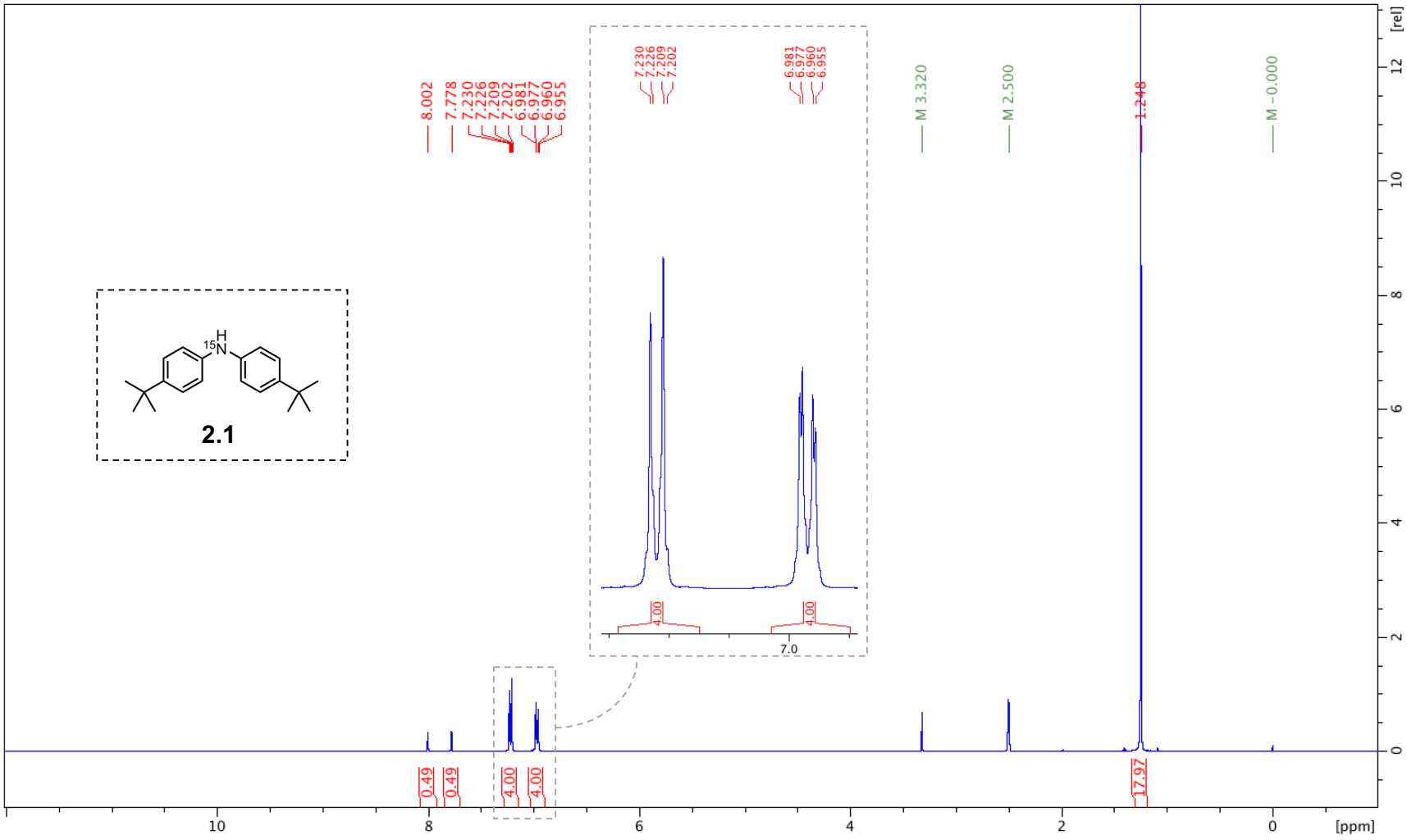
8.002
7.778
7.230
7.226
7.209
7.202
6.981
6.977
6.960
6.955
M 3.320
M 2.500
1.248
M -0.000
[rel]
[ppm]
0.49
0.49
4.00
4.00
17.97
4.00
4.00
7.0
2.1

^{13}C

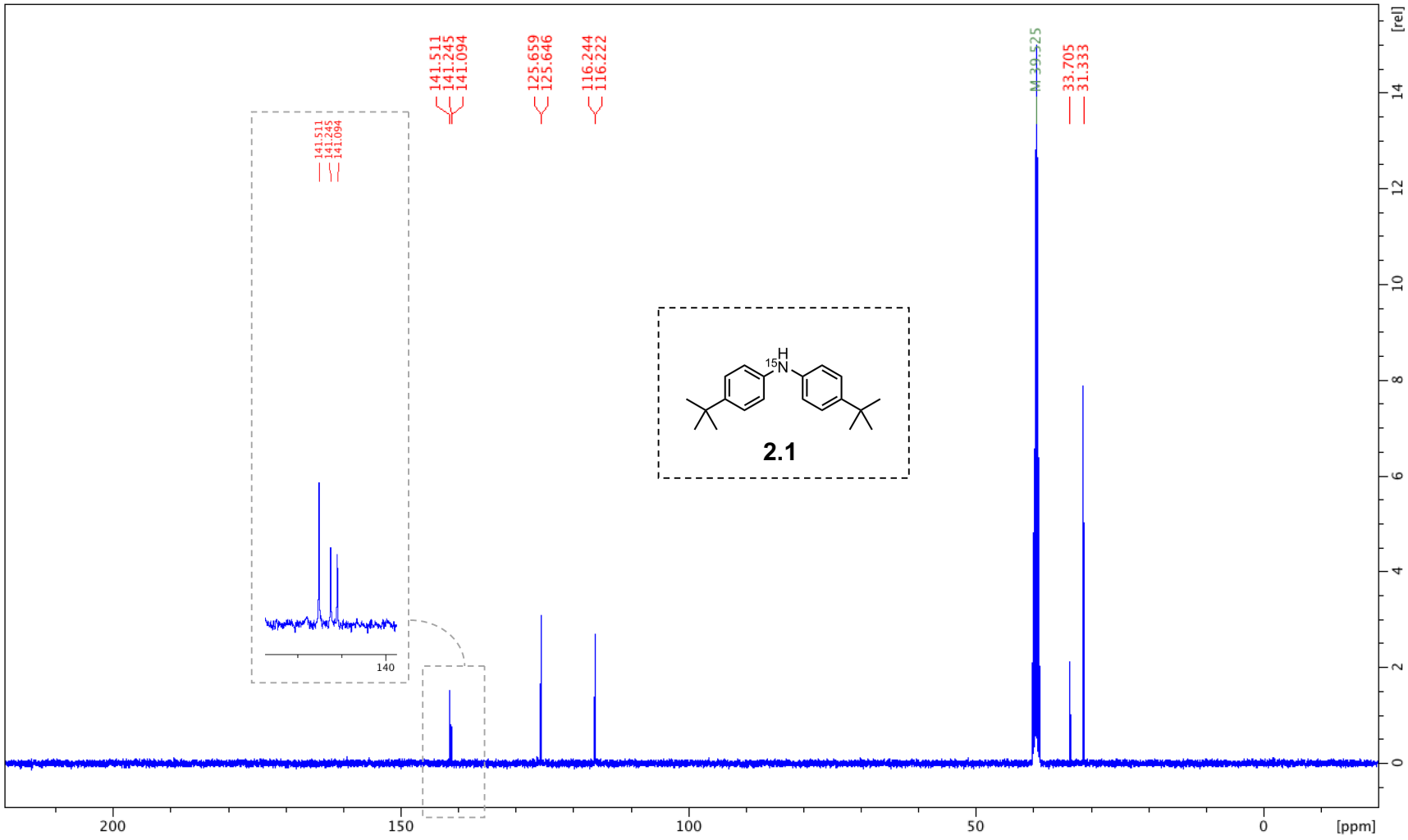
141.511
141.245
141.094
125.659
125.646
116.244
116.222
39.525
33.705
31.333
[rel]
14
12
10
8
6
4
2
0
200
150
100
50
0
[ppm]
140
2.1

^{1}H

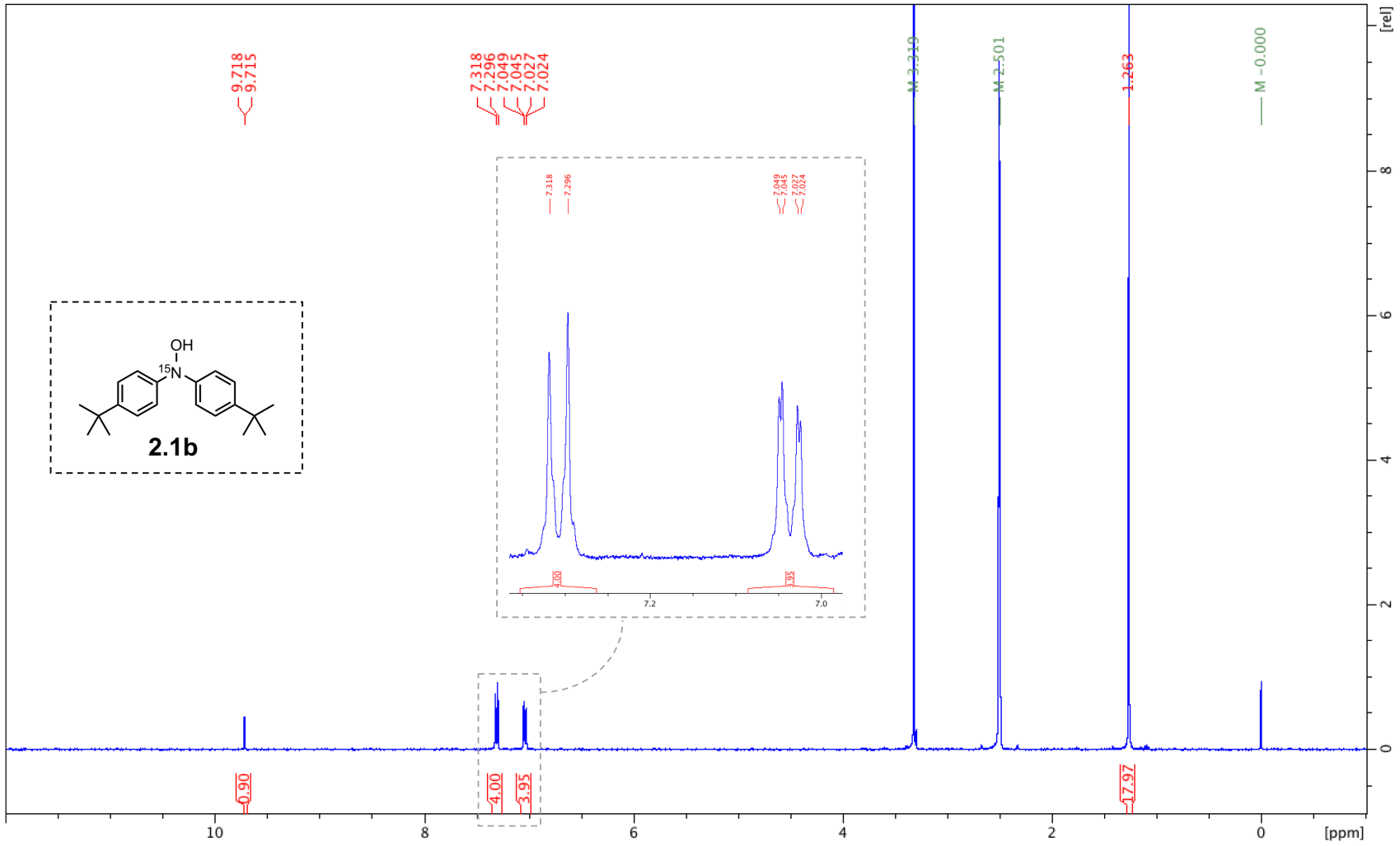
9.718
9.715
7.318
7.296
7.049
7.045
7.027
7.024
M 3.319
M 2.501
1.263
M -0.000
[rel]
OH
15N
2.1b
0.90
4.00
3.95
17.97
10
8
6
4
2
0
[ppm]

^{13}C

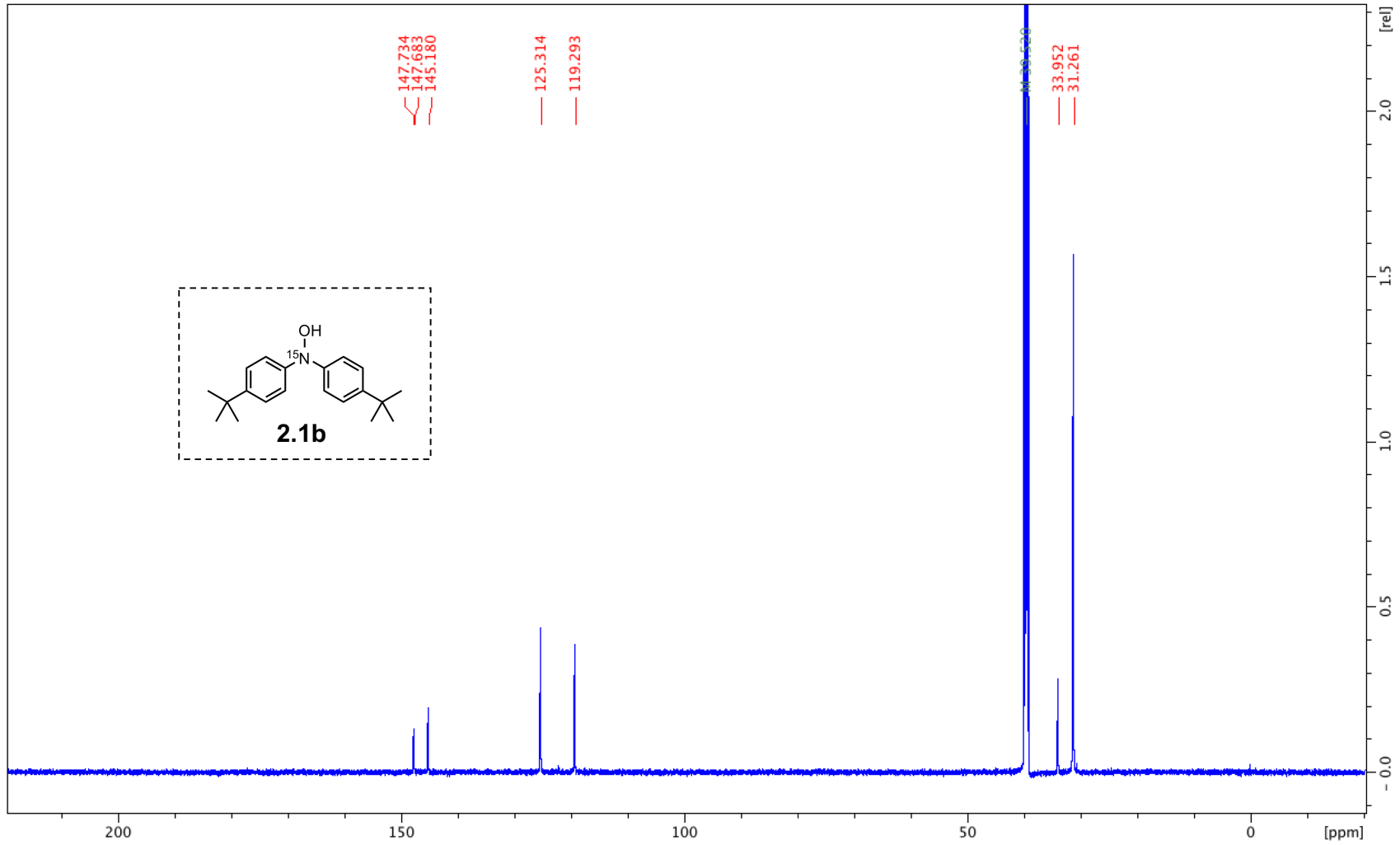
147.734
147.683
145.180
125.314
119.293
33.952
31.261
OH
15N
2.1b
200
150
100
50
0
[ppm]
[rel]
2.0
1.5
1.0
0.5
0.0

^{1}H

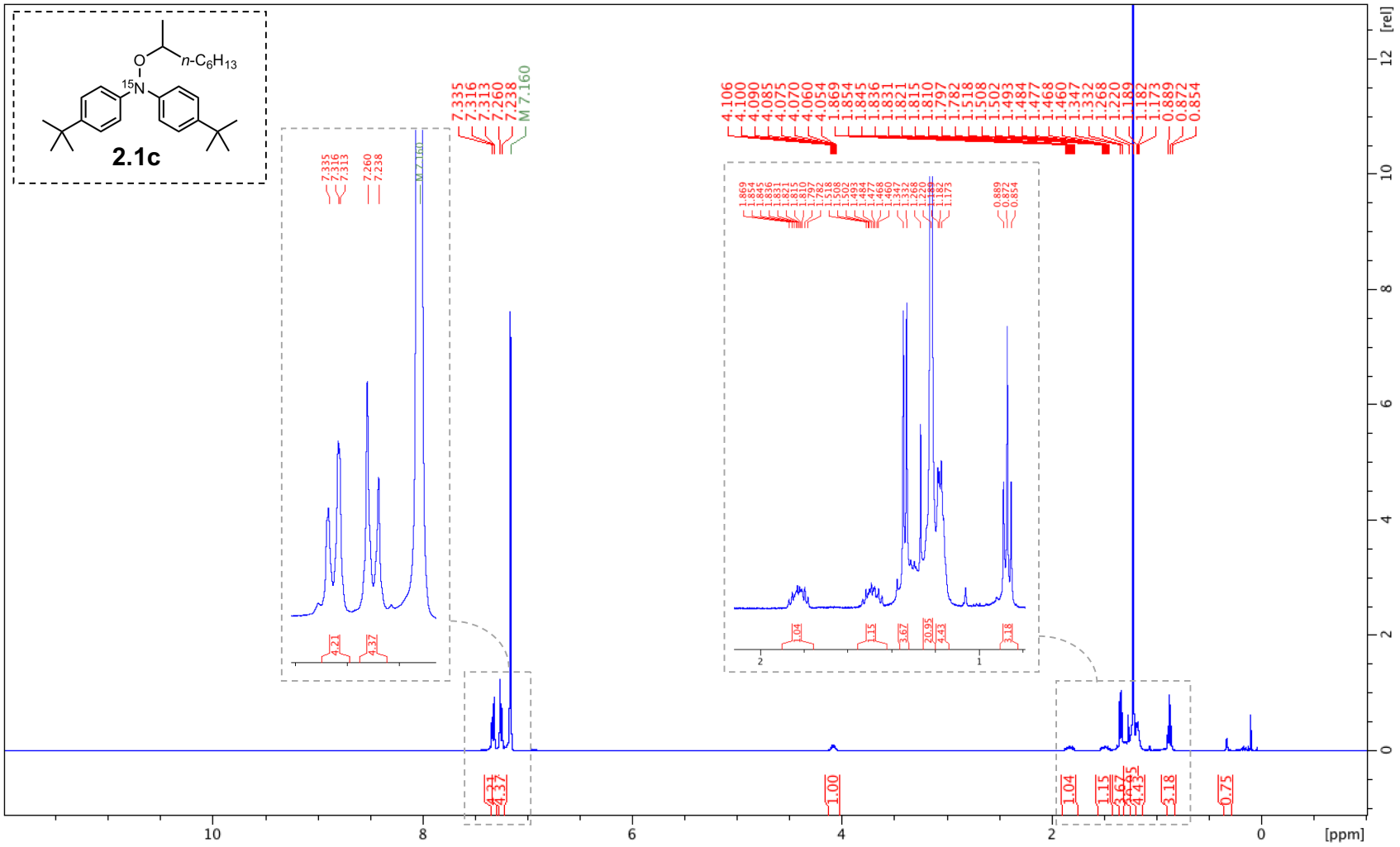
2.1c
n-C6H13
15N
7.335
7.316
7.313
7.260
7.238
M 7.160
4.106
4.100
4.090
4.085
4.075
4.070
4.060
4.054
1.869
1.854
1.845
1.836
1.831
1.821
1.815
1.810
1.797
1.782
1.518
1.508
1.502
1.493
1.484
1.477
1.468
1.460
1.347
1.332
1.268
1.220
1.189
1.182
1.173
0.889
0.872
0.854
4.21
4.37
1.00
1.04
1.15
3.67
20.95
4.43
3.18
0.75
[rel]
[ppm]

^{13}C

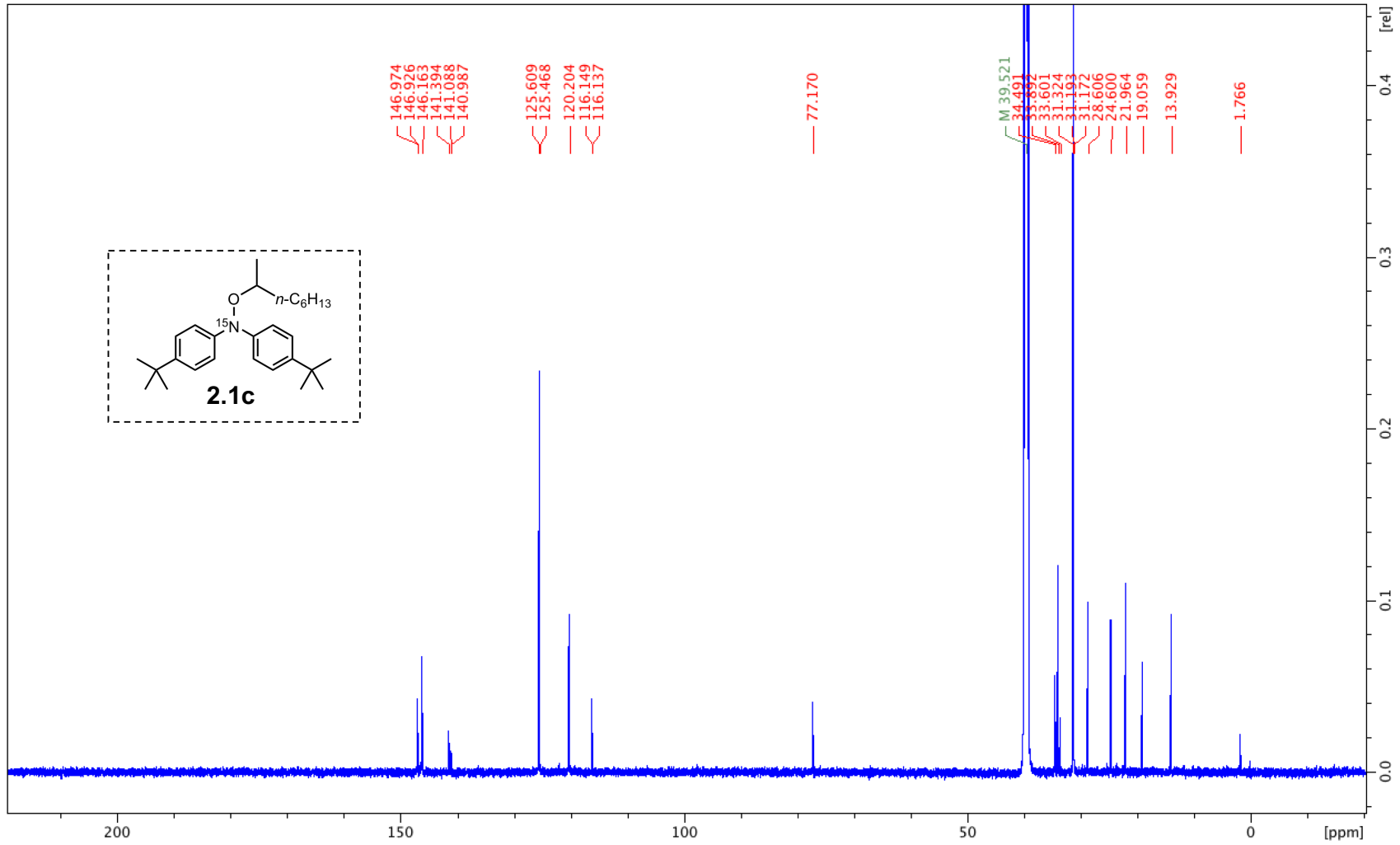
146.974
146.926
146.163
141.394
141.088
140.987
125.609
125.468
120.204
116.149
116.137
77.170
M 39.521
34.491
33.892
33.601
31.324
31.193
31.172
28.606
24.600
21.964
19.059
13.929
1.766
[rel]
0.4
0.3
0.2
0.1
0.0
200
150
100
50
0
[ppm]
O
n-C_6H_{13}
^{15}N
2.1c

^{1}H

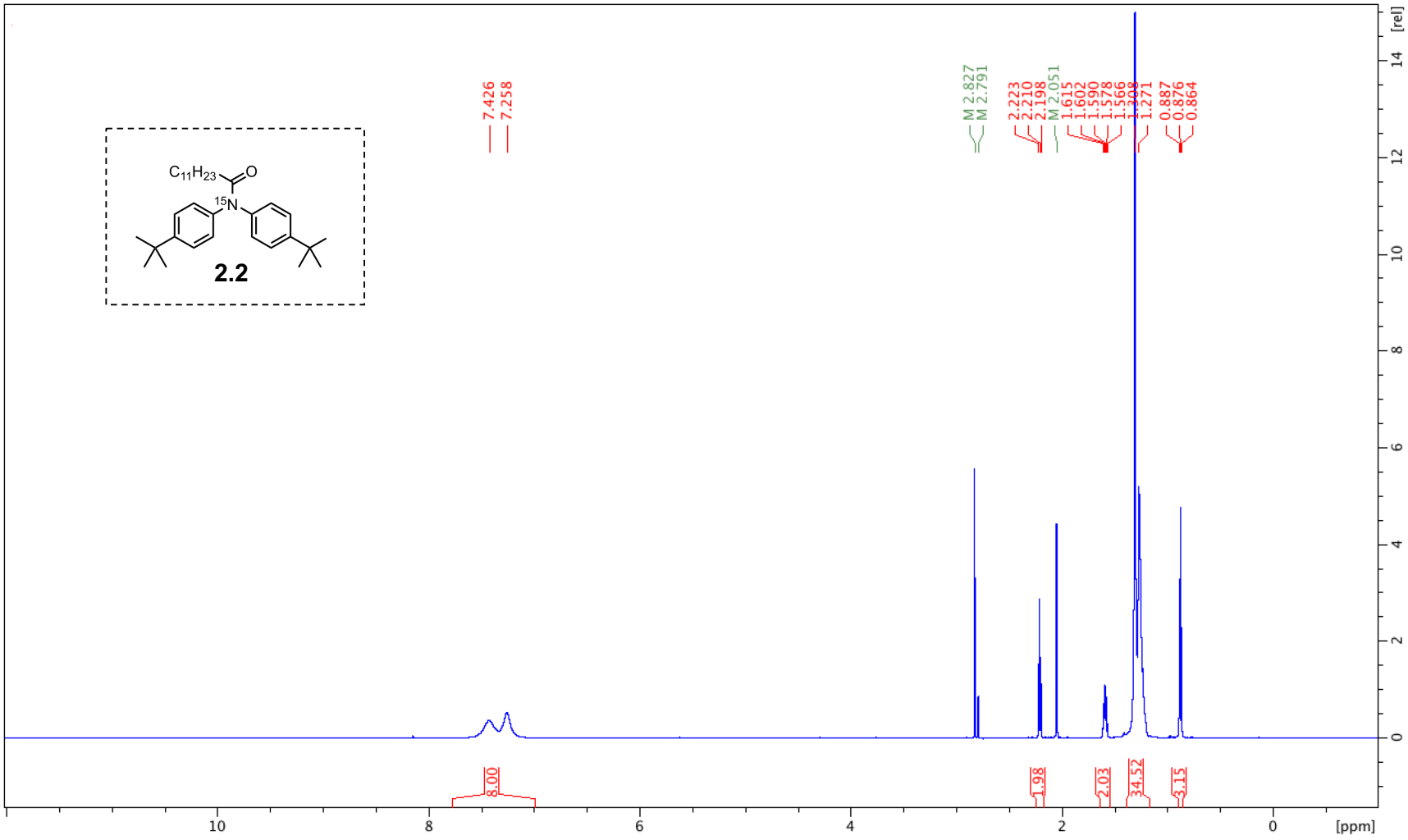
7.426
7.258
M 2.827
M 2.791
2.223
2.210
2.198
M 2.051
1.615
1.602
1.590
1.578
1.566
1.308
1.271
0.887
0.876
0.864
$C_{11}H_{23}$
O
^{15}N
2.2
8.00
1.98
2.03
34.52
3.15
10
8
6
4
2
0
[ppm]
[rel]

^{13}C

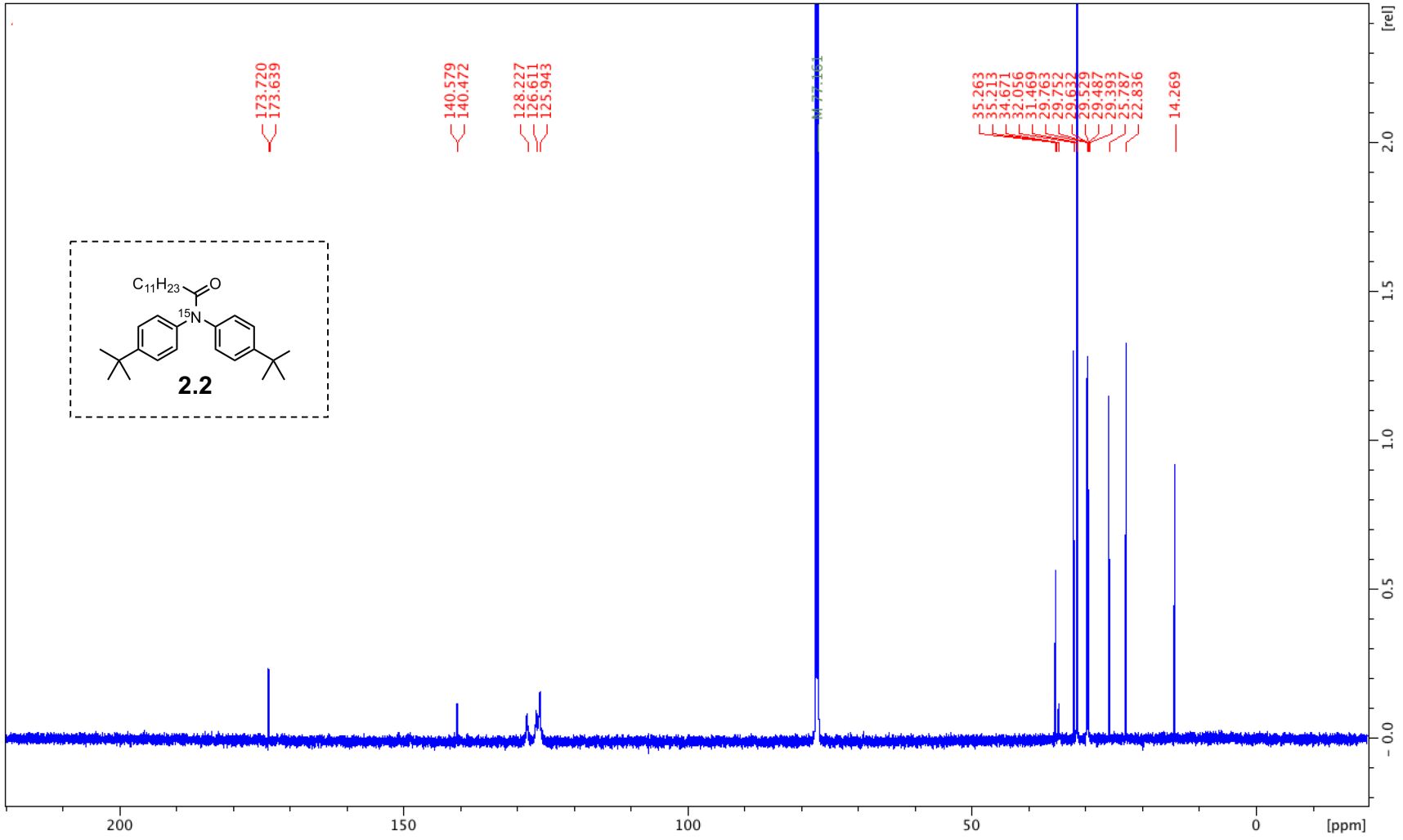
173.720
173.639
140.579
140.472
128.227
126.611
125.943
77.161
35.263
35.213
34.671
32.056
31.469
29.763
29.752
29.632
29.529
29.487
29.393
25.787
22.836
14.269
$C_{11}H_{23}$
O
^{15}N
2.2
[rel]
2.0
1.5
1.0
0.5
0.0
200
150
100
50
0
[ppm]

^{1}H ^{15}N HMBC

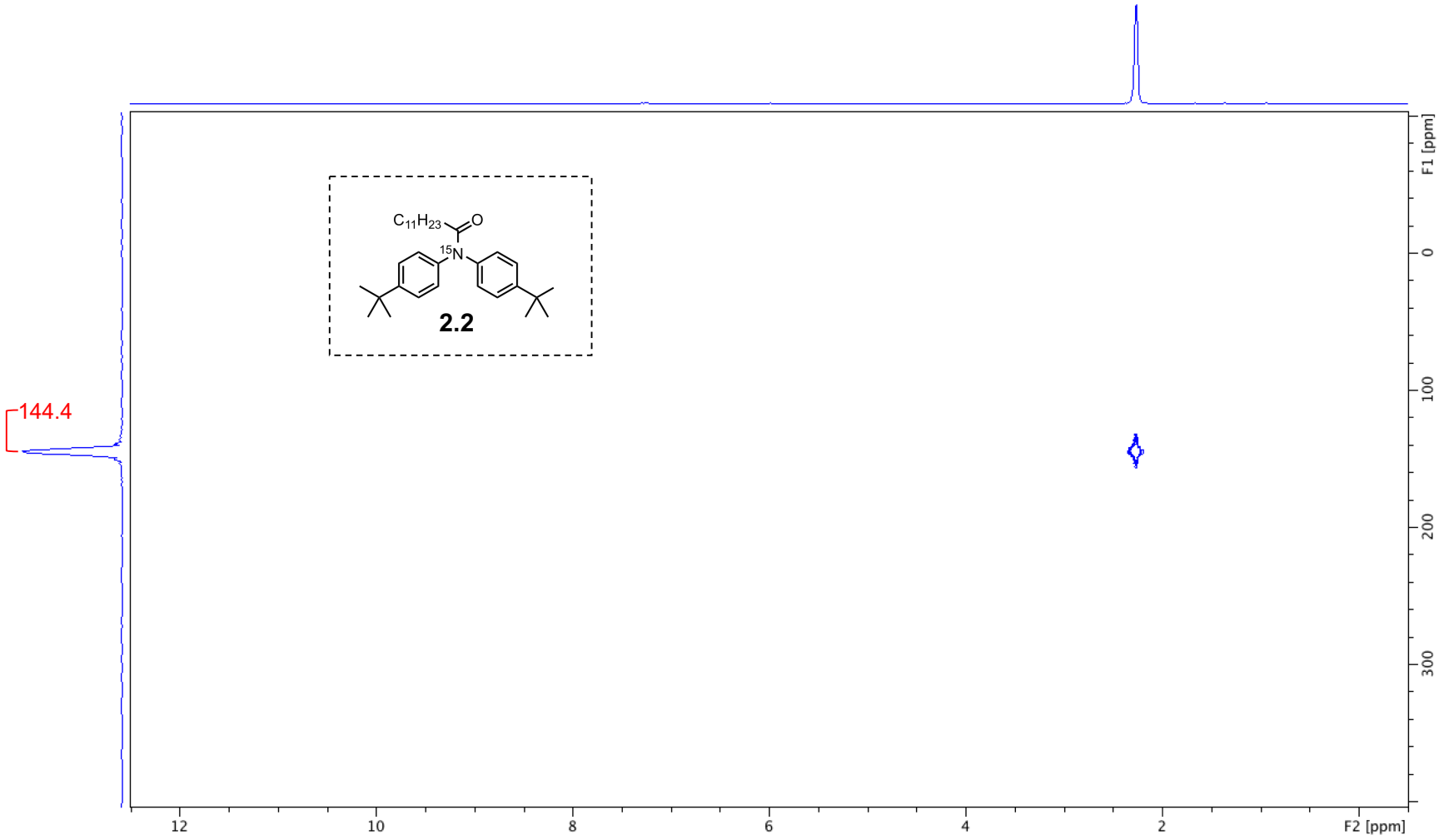

^{1}H

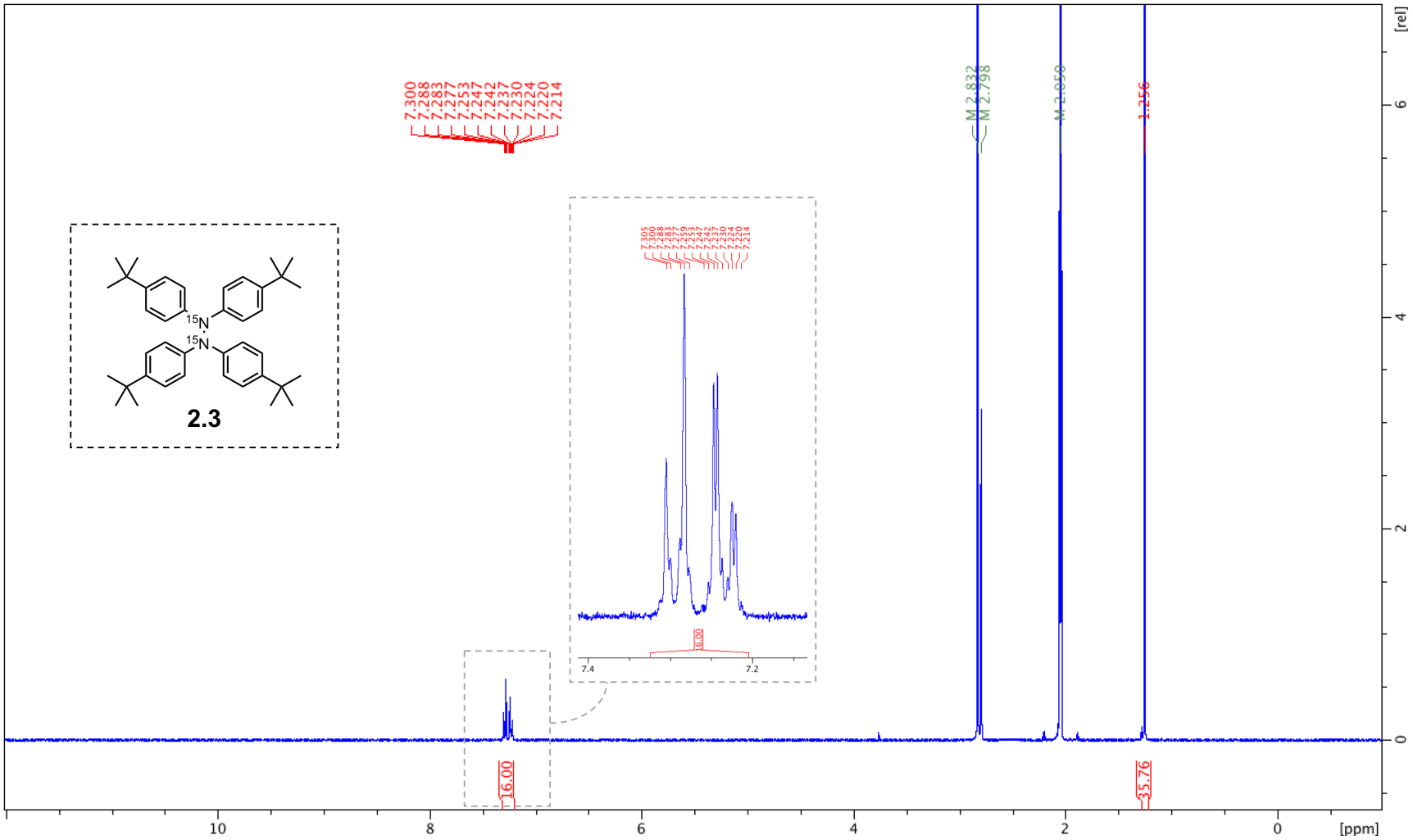
7.300
7.288
7.283
7.277
7.253
7.247
7.242
7.237
7.230
7.224
7.220
7.214
M 2.832
M 2.798
M 2.059
1.256
15N
15N
2.3
16.00
35.76
10
8
6
4
2
0
[ppm]
[rel]

^{13}C

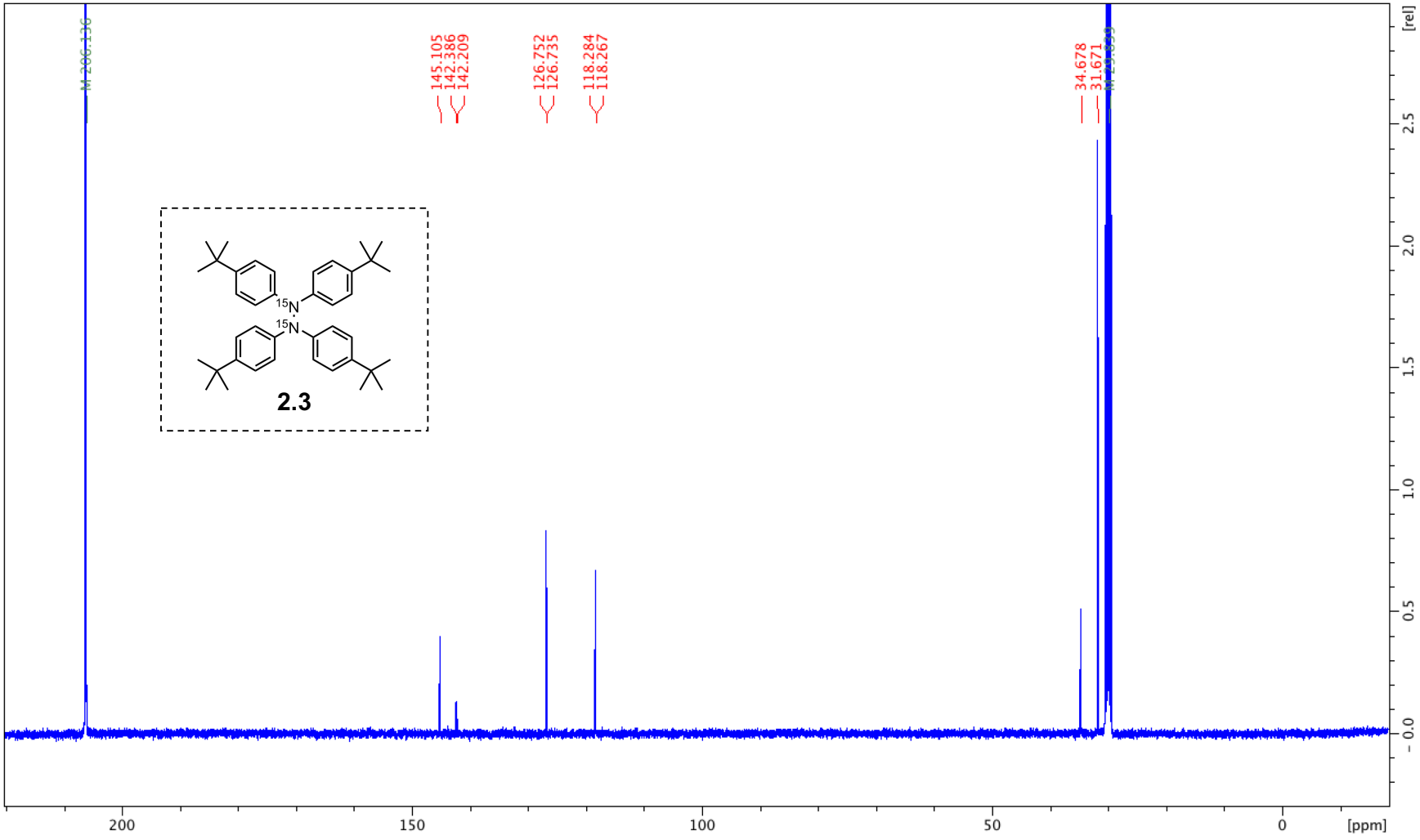
145.105
142.386
142.209
126.752
126.735
118.284
118.267
34.678
31.671
15N
15N
2.3
200
150
100
50
0
[ppm]
[rel]

^{1}H ^{15}N HMBC

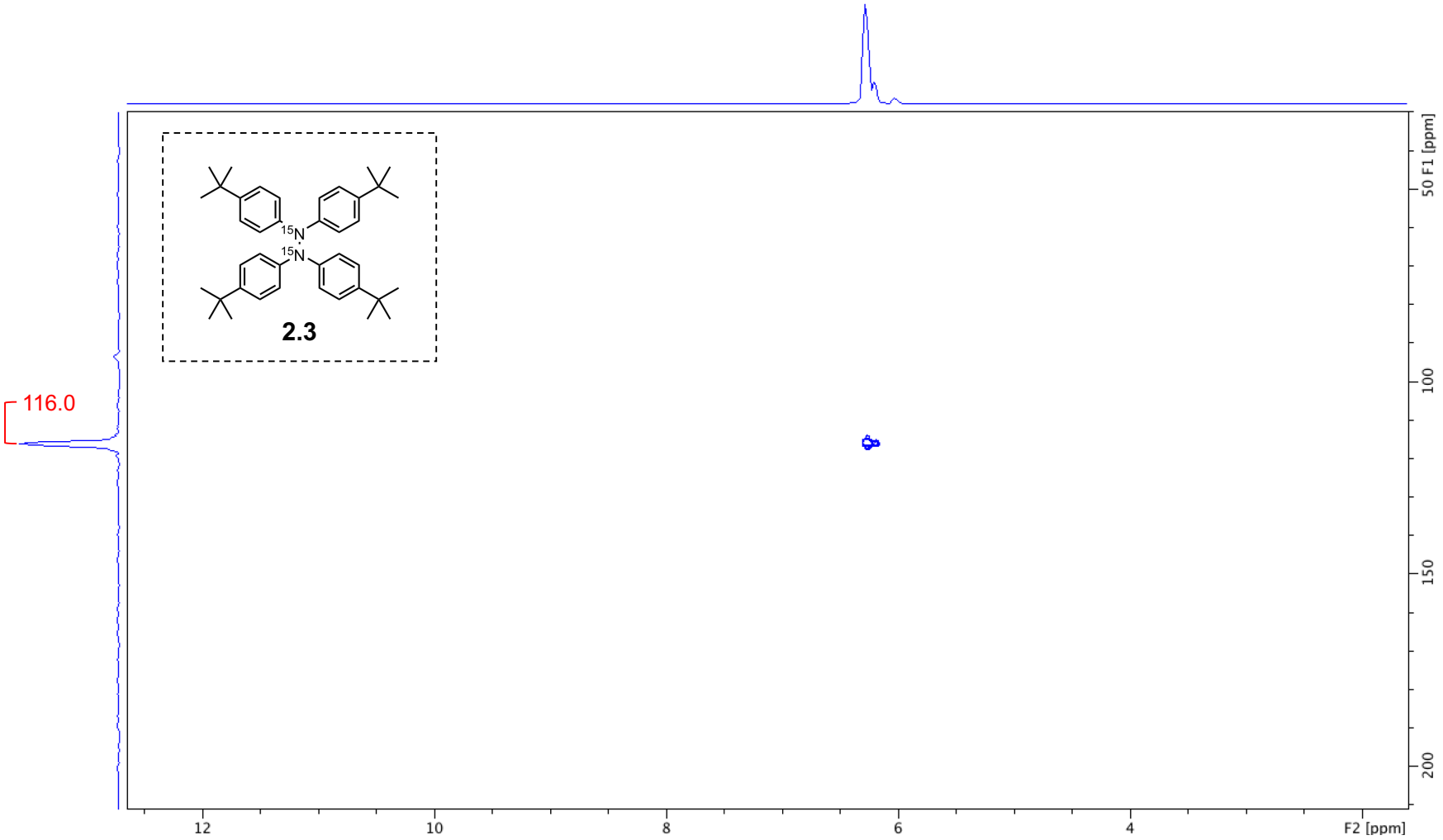

^{1}H

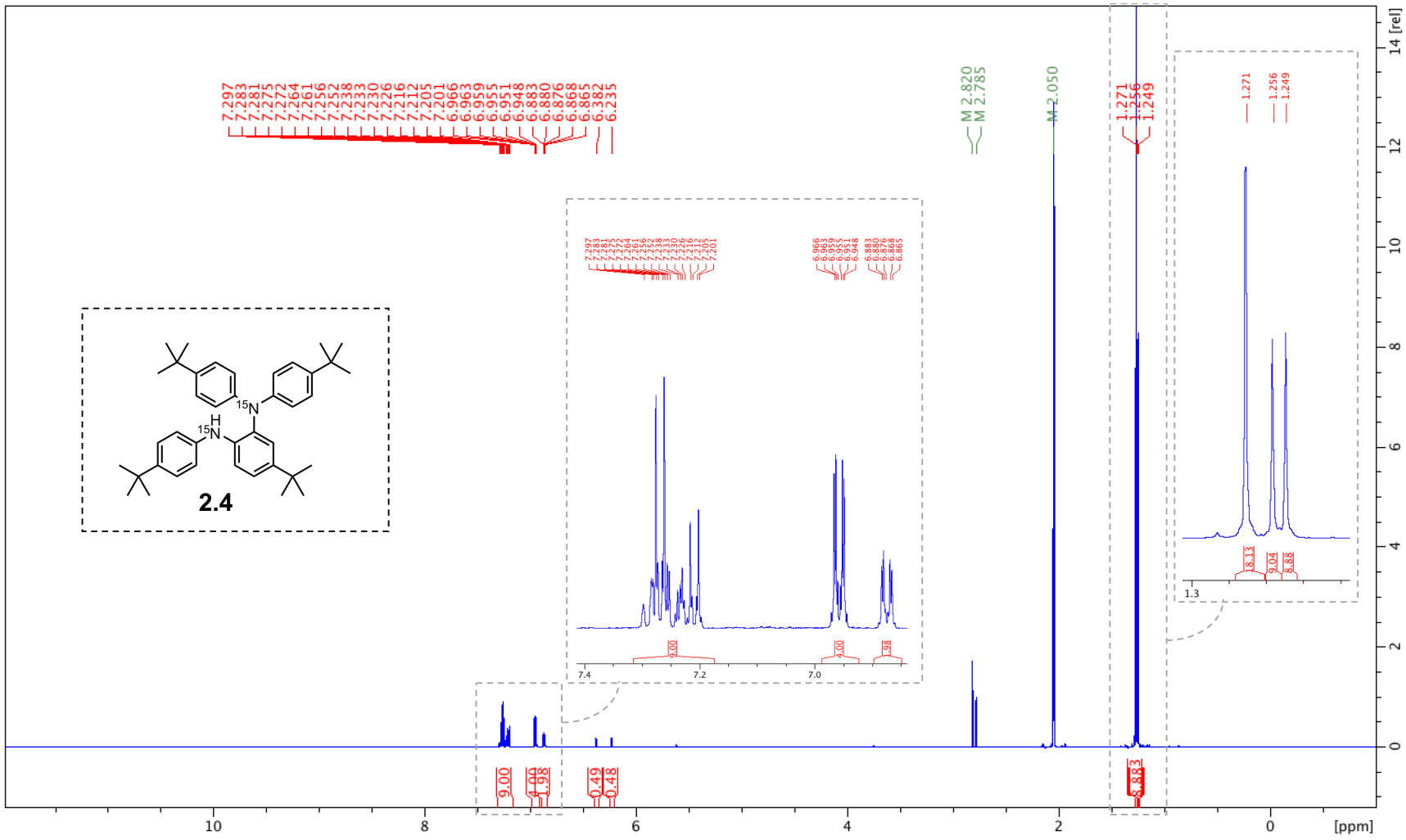
7.297
7.283
7.281
7.275
7.272
7.264
7.261
7.256
7.252
7.238
7.233
7.230
7.226
7.216
7.212
7.205
7.201
6.966
6.963
6.959
6.955
6.951
6.948
6.883
6.880
6.876
6.868
6.865
6.382
6.235
M 2.820
M 2.785
M 2.050
1.271
1.256
1.249
2.4
9.00
4.00
1.98
0.49
0.48
8.883
18.13
9.04
6.88
14 [rel]
[ppm]

^{13}C

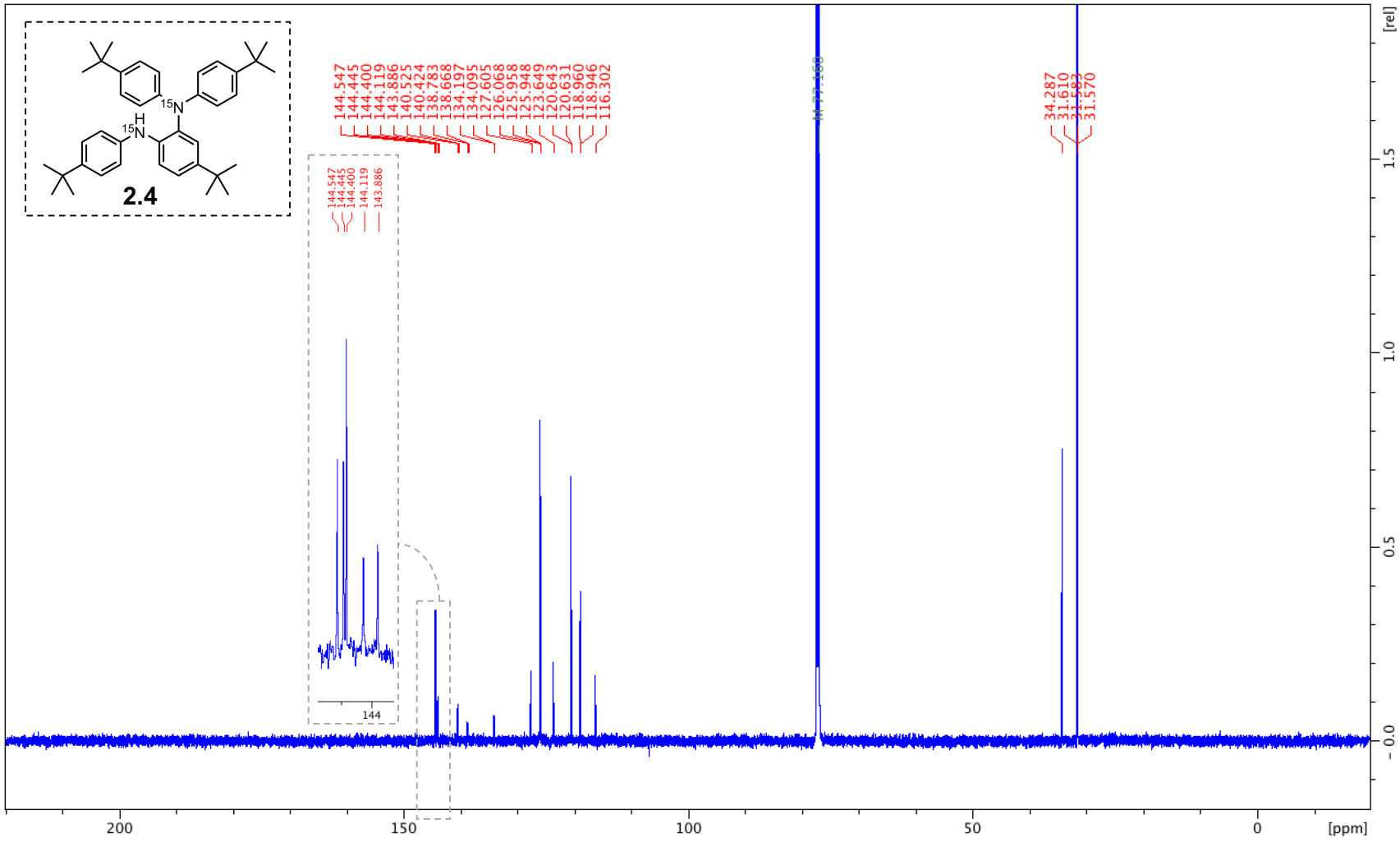
2.4
144.547
144.445
144.400
144.119
143.886
140.525
140.424
138.783
138.668
134.197
134.095
127.605
126.068
125.958
125.948
123.649
120.643
120.631
118.960
118.946
116.302
77.168
34.287
31.610
31.583
31.570
144
200
150
100
50
0
[ppm]
1.5
1.0
0.5
0.0
[rel]

^{1}H ^{15}N HMBC

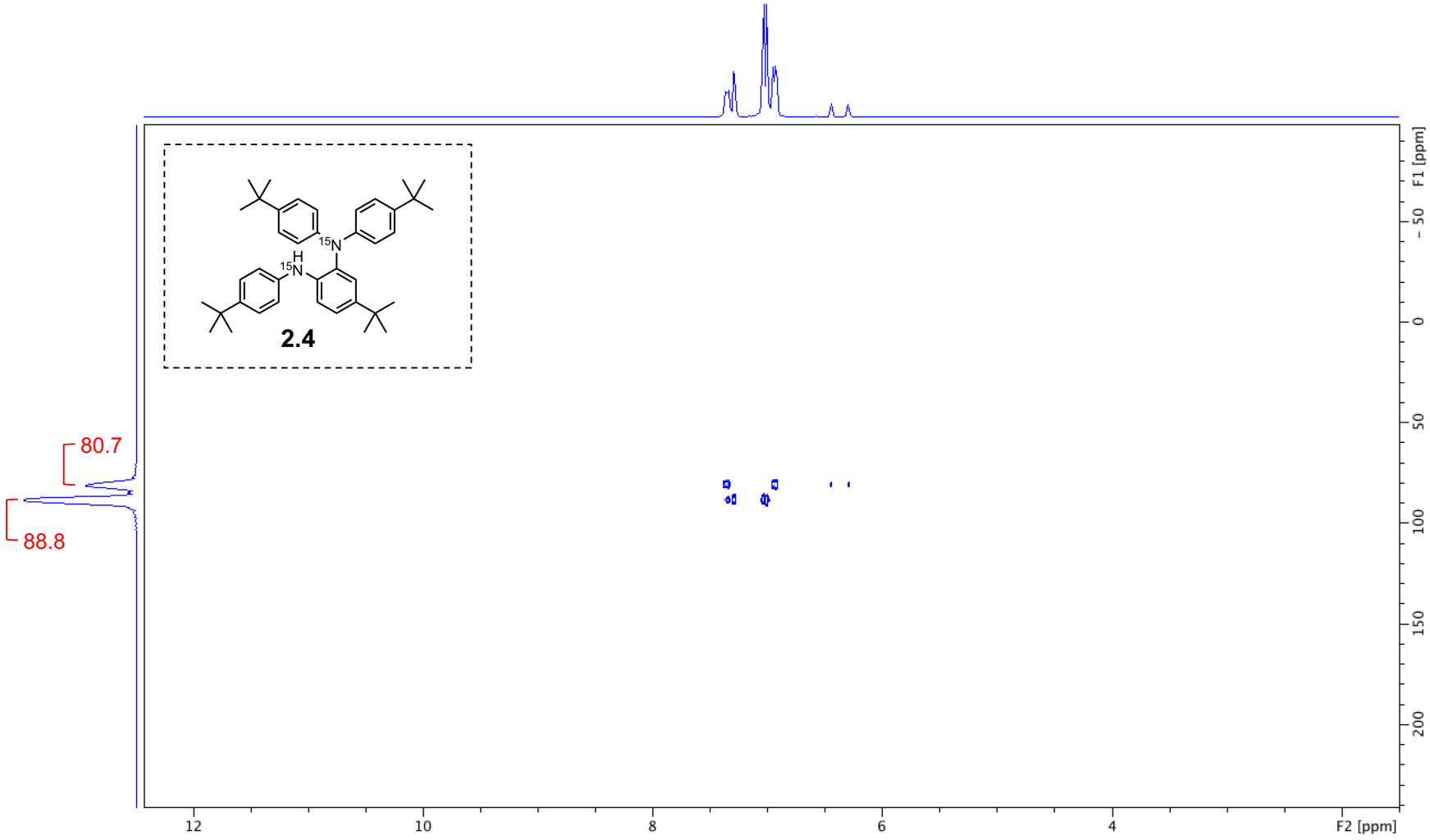

^{1}H

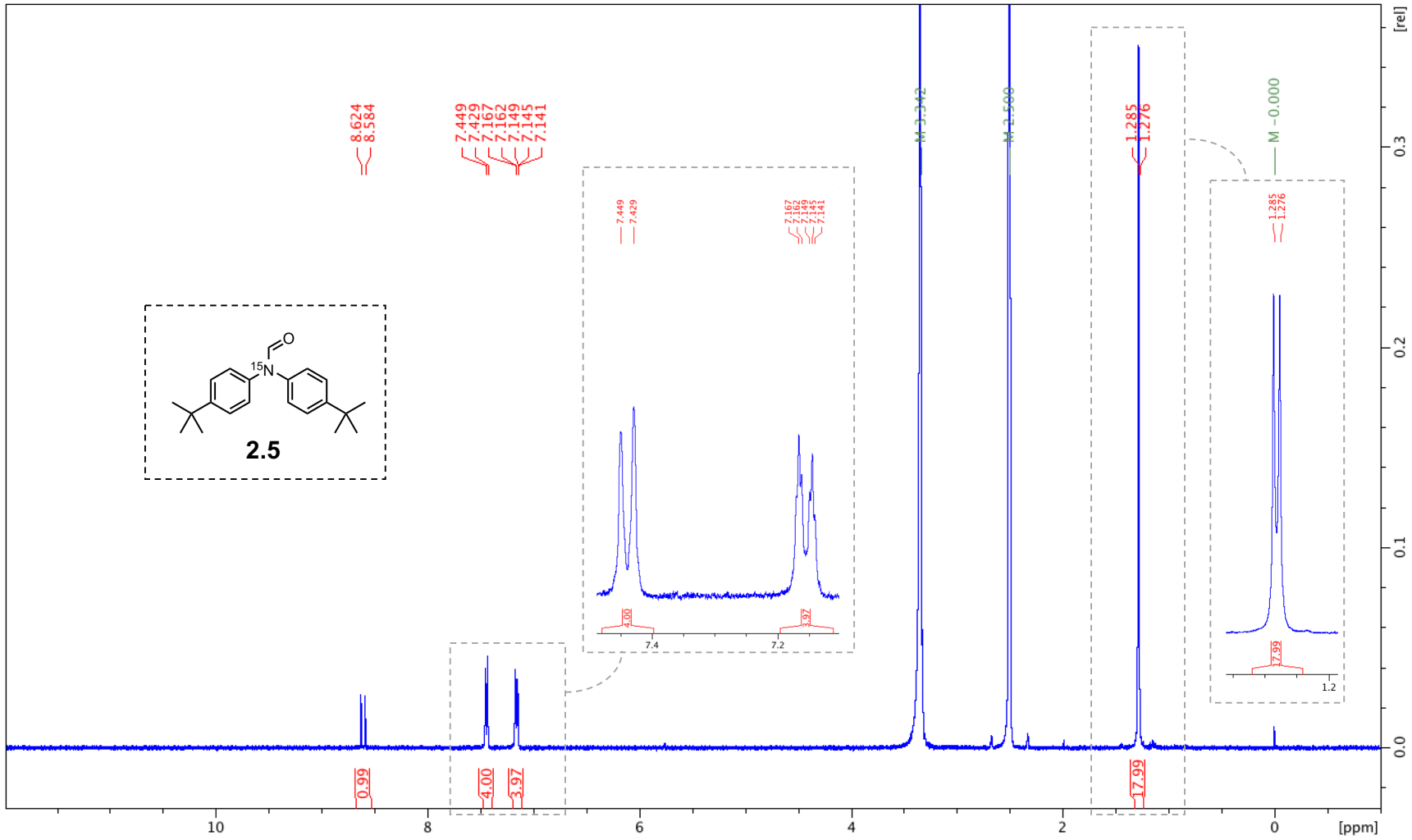
8.624
8.584
7.449
7.429
7.167
7.162
7.149
7.145
7.141
M 3.342
M 2.500
1.285
1.276
M -0.000
2.5
0.99
4.00
3.97
17.99
10
8
6
4
2
0
[ppm]
[rel]
0.0
0.1
0.2
0.3

^{13}C

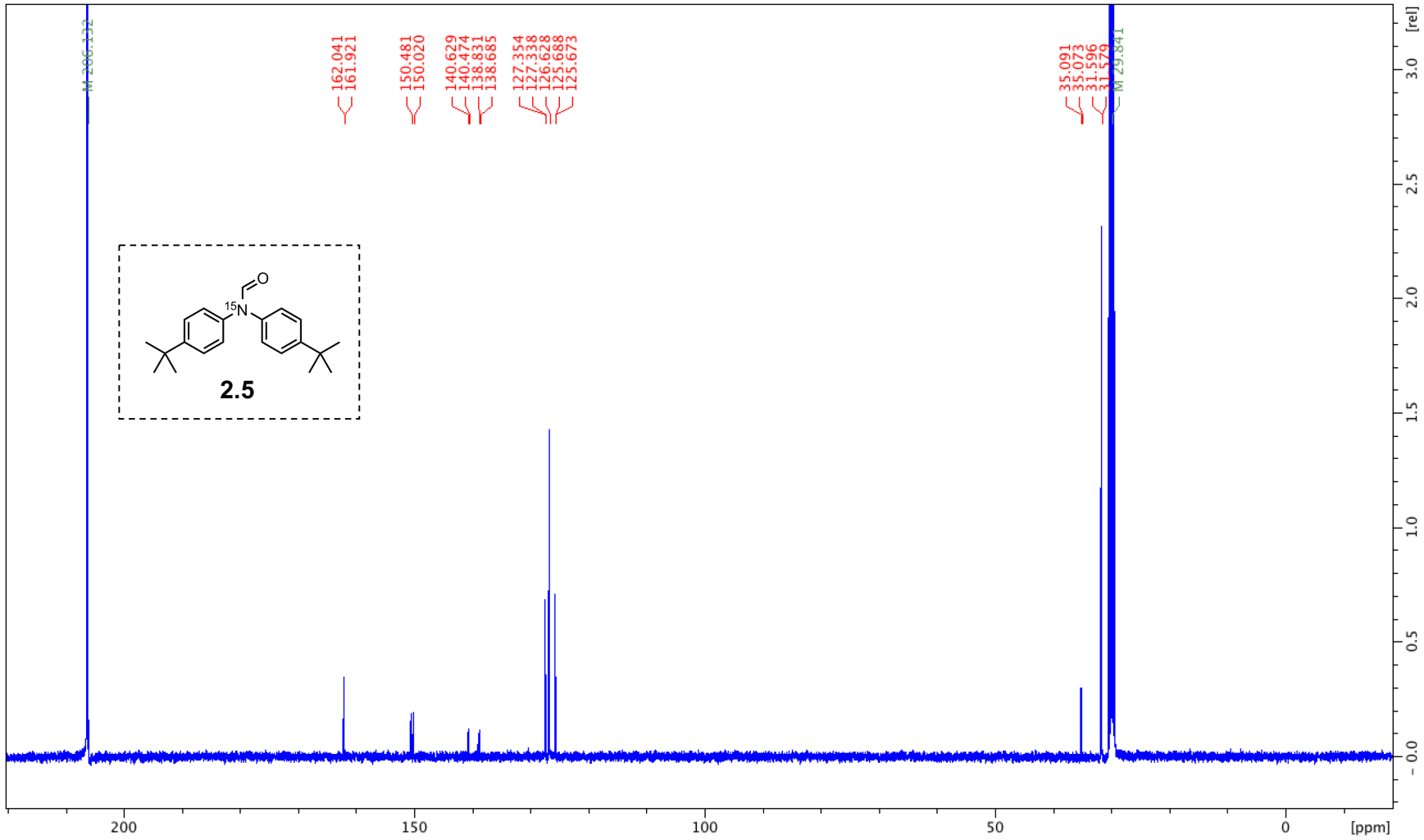
M 266.132
162.041
161.921
150.481
150.020
140.629
140.474
138.831
138.685
127.354
127.338
126.628
125.688
125.673
35.091
35.073
31.596
31.579
M 29.841
2.5
200
150
100
50
0
[ppm]
[rel]

^{1}H ^{15}N HMBC

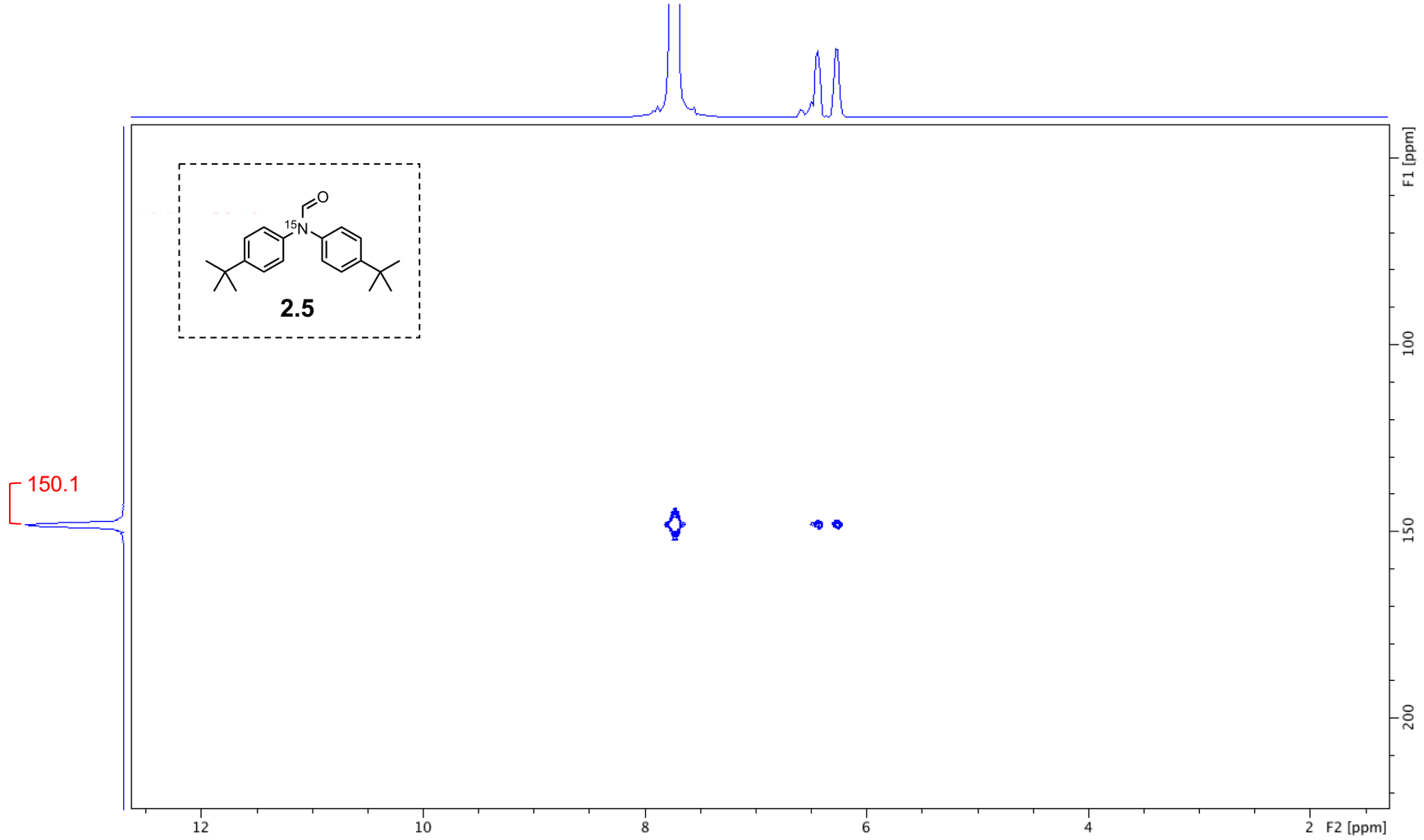

^{1}H (1.6)

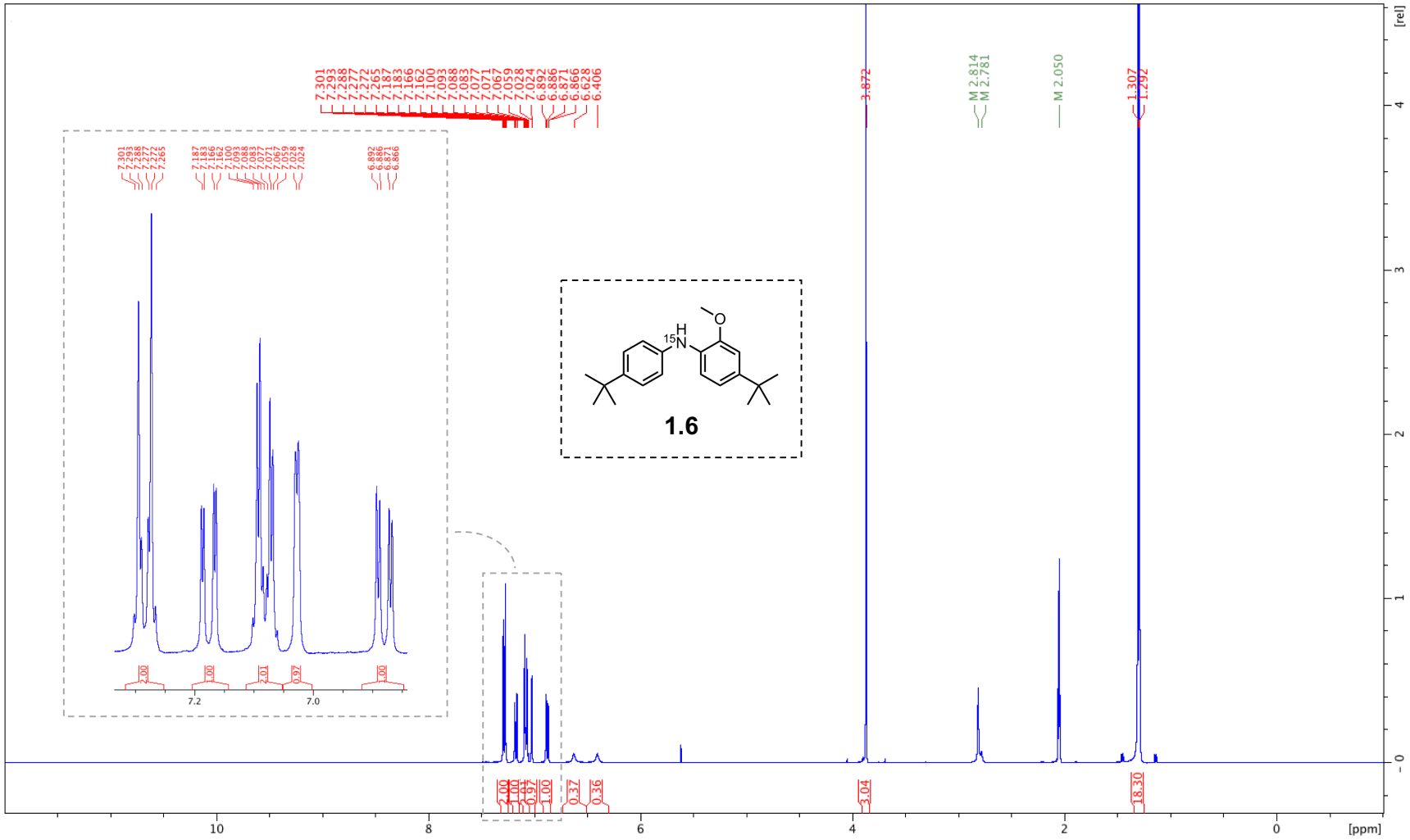
7.301
7.293
7.288
7.277
7.272
7.265
7.187
7.183
7.166
7.162
7.100
7.093
7.088
7.083
7.077
7.071
7.067
7.059
7.028
7.024
6.892
6.886
6.871
6.866
6.628
6.406
3.872
M 2.814
M 2.781
M 2.050
1.307
1.292
1.6
2.00
1.00
1.01
0.97
1.00
0.37
0.36
3.04
18.30
7.2
7.0
10
8
6
4
2
0
[ppm]
[rel]

^{13}C (1.6)

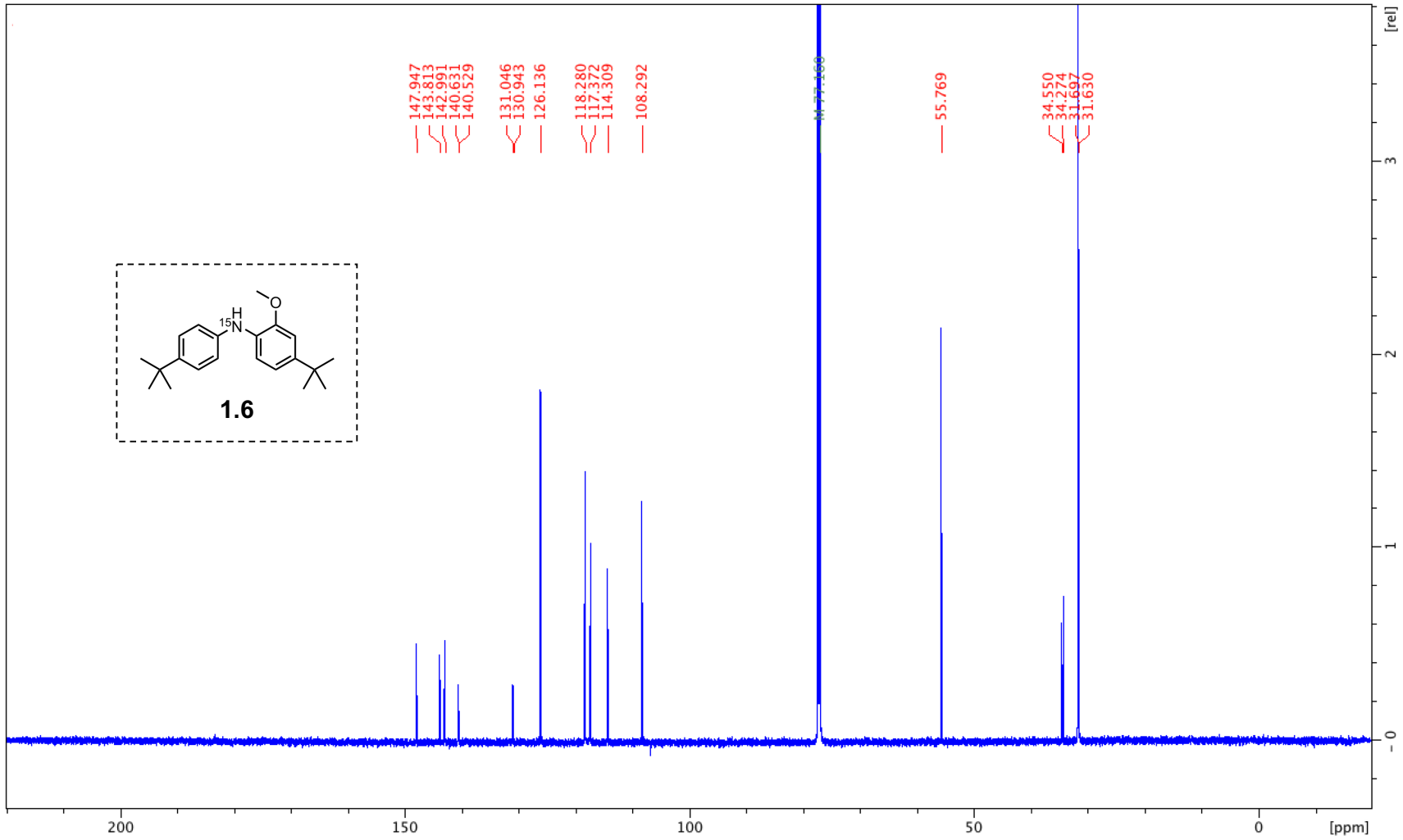
147.947
143.813
142.991
140.631
140.529
131.046
130.943
126.136
118.280
117.372
114.309
108.292
77.160
55.769
34.550
34.274
31.697
31.630
[rel]
3
2
1
0
200
150
100
50
0
[ppm]
15N
H
O
1.6

^{1}H (1.7)

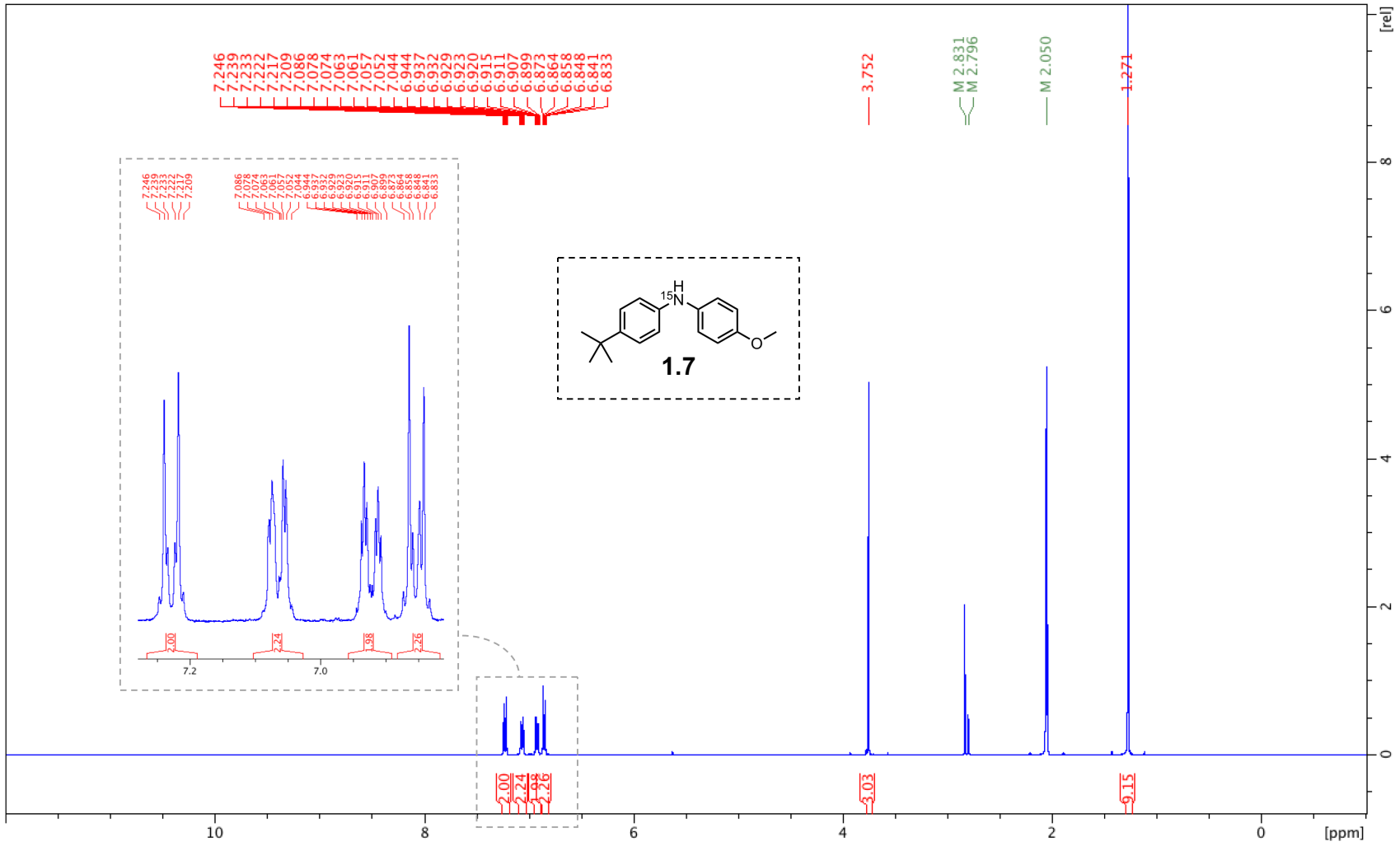
7.246
7.239
7.233
7.222
7.217
7.209
7.086
7.078
7.074
7.063
7.061
7.057
7.052
7.044
6.944
6.937
6.932
6.929
6.923
6.920
6.915
6.911
6.907
6.899
6.873
6.864
6.858
6.848
6.841
6.833
3.752
M 2.831
M 2.796
M 2.050
1.271
15N
H
O
1.7
2.00
2.24
1.98
2.26
7.2
7.0
2.00
2.24
1.98
2.26
3.03
9.15
10
8
6
4
2
0
[ppm]
[rel]

^{13}C (1.7)

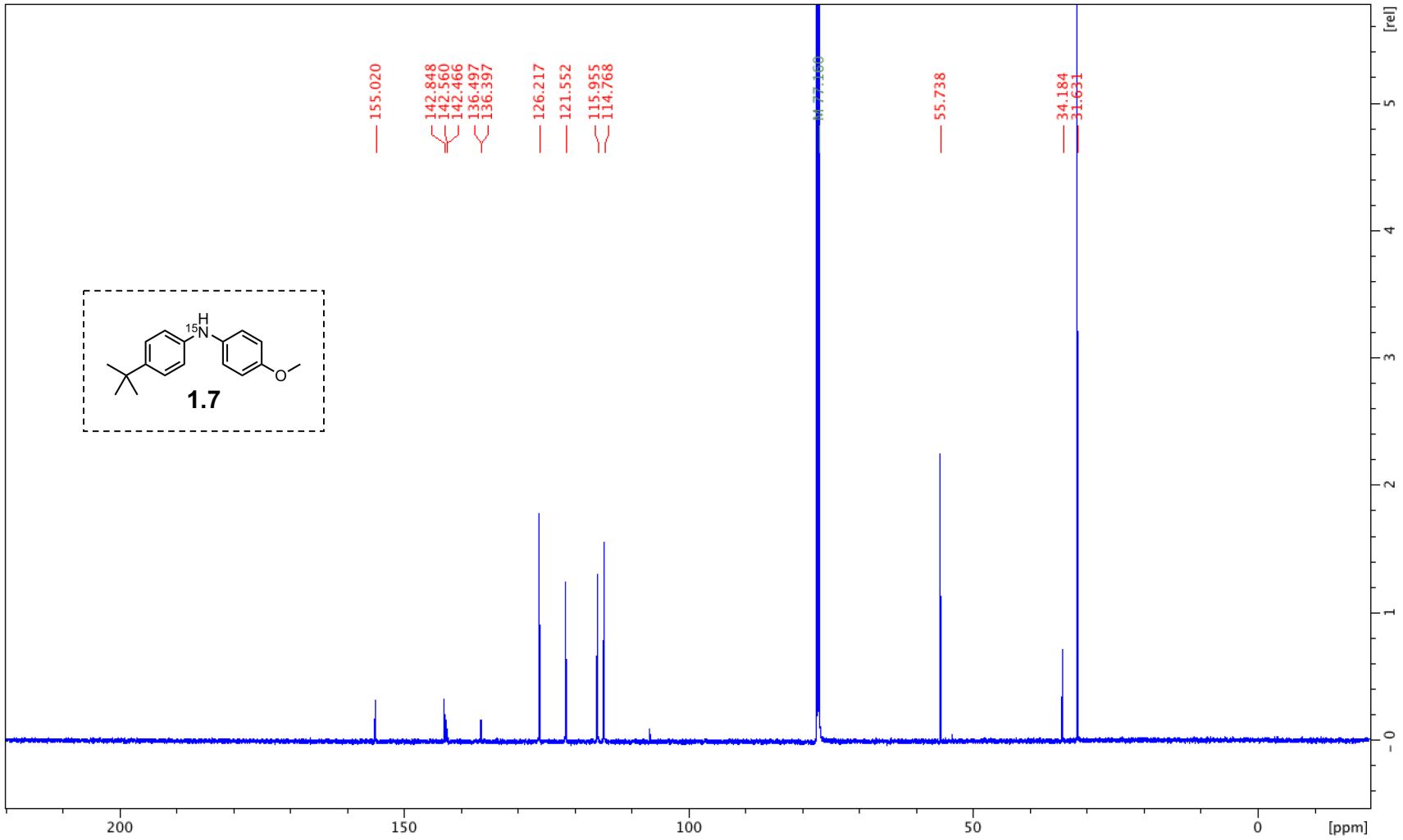
155.020
142.848
142.560
142.466
136.497
136.397
126.217
121.552
115.955
114.768
77.168
55.738
34.184
31.631
15NH
O
1.7
200
150
100
50
0
[ppm]
[rel]

Chapter 3: Effects of NO_x on Diarylaminic RTAs During Hydrocarbon Autoxidation at Elevated Temperatures

3.1 Introduction

Nitrogen oxides (NO_x) is a term used to describe the duo of nitric oxide (NO) and nitrogen dioxide (NO_2); the most prevalent nitrogen oxide air pollutants produced by hydrocarbon combustion. During combustion, NO is primarily produced through reactions between atmospheric oxygen and nitrogen at extremely high temperatures, at which O_2 and N_2 dissociate (Figure 3.1 A, Eq. 3.1-3.3).[1-4] Known as the "thermal", or Zeldovich, mechanism, NO formation occurs at the flame front in significant amounts when temperatures reach or exceed 1700˚C.[1-3] NO is also produced through a combustion mechanism between hydrocarbon-derived radicals and atmospheric nitrogen present in the combustion zone known as the "prompt", or Fenimore, mechanism (Figure 3.1 B, Eq. 3.4-3.6).[1,5-7] The vast majority NO is generated by the thermal mechanism, and is rapidly converted to NO_2 via reaction with hydroperoxyl radicals at high temperatures immediately after combustion (Figure 3.1 C, Eq. 3.7).[8-10]

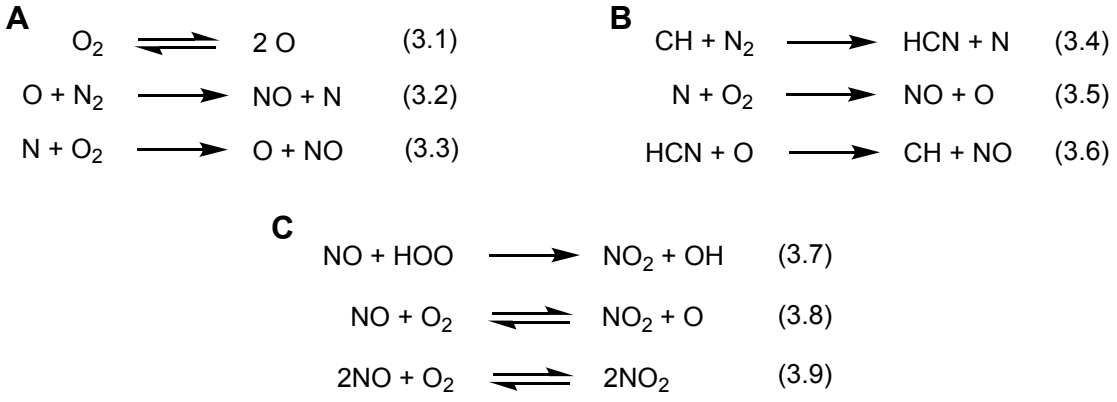

Figure 3.1 Mechanisms for NO_x formation during combustion. (**A**) Zeldovich (thermal) mechanism. (**B**) Fenimore (prompt) mechanism. (**C**) Formation of NO_2 from NO.[1-10]

As temperatures drop, NO is also converted to NO_2 by reaction with atmospheric oxygen in a temperature-dependent equilibrium (Figure 3.1 C, Eq. 3.8-3.9).[9-12] Although NO dominates under high temperatures adjacent

to or inside the flame zone, NO_2 can be found in concentration of 1000 ppm in gas samples from the piston regions of combustion engines, with our industry collaborators using 766 ppm NO_2 as a standard concentration in engine lubricant oxidation studies.[12-13]

NO_x present in "blow-by gas" interact with the lubricating oil that coats components of the piston region such as the piston and cylinder wall. Blow-by gas encounters small volumes of lubricating oil at high temperatures, contributing to a harshly oxidative environment that is largely responsible for lubricant degradation.[14-15] In addition, NO_x have been causally linked to the formation of sludge and insoluble particulates that disrupt engine function and hinder performance.[12, 16-18]

Studies of the effects of NO_x on hydrocarbon autoxidation under conditions that emulate those in an engine have demonstrated that NO_2 is a potent initiator due to its radical character, capable of abstracting hydrogen directly from the substrate to form alkyl radicals and nitrous acid (Scheme. 3.1, Eq. 3.10).[12,19] Nitrous acid homolyzes to produce initiating hydroxyl radicals and nitric oxide, which regenerates nitrogen dioxide in the presence of peroxyls or oxygen (Scheme 3.1, Eq. 3.11-3.12).[19,20] Therefore, each equivalent of NO_2 is capable of initiating two chain reactions in a mode that does not require the presence of trace peroxide, exacerbating the initiation process, and shortening the useful lifetime of the substrate.

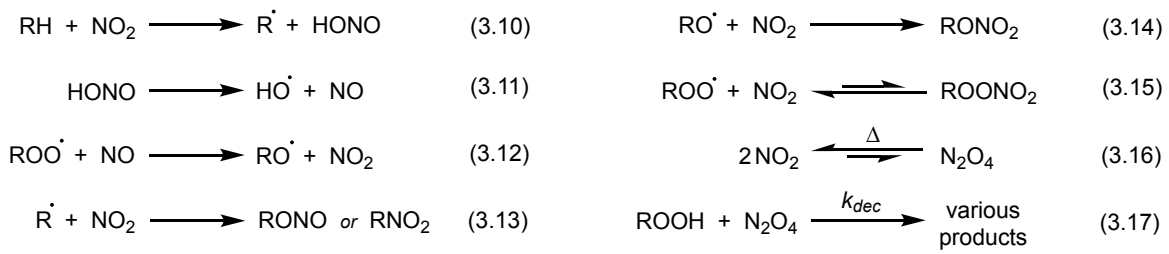

Scheme 3.1 Reactions of NO_x purported to increase the rate of initiation at the beginning of autoxidation and to decrease the rate of initiation in middle to later stages.[12,19-23]

Although previous studies demonstrated that NO_x drastically increase the initial rate of hydroperoxide formation (a common marker of autoxidation progress), the rate eventually decreases back to that of a system with no NO_x present.[12] Such results are explained partially by the reactions that NO and NO_2 undergo with substrate-derived oxidation products, which quell further contribution to the rate of initiation by NO_x (Scheme

3.1, Eq. 3.13-3.17).[12,21-23] However, it is also likely that homolysis of peroxide and hydroperoxide products eventually constitute the majority of initiation events as their concentrations increase.

Studies of hydrocarbon autoxidation under NO_x inhibited by phenolic RTAs demonstrate that NO_2 preferentially reacts with RTA, leading to faster consumption of the phenol and consequently, shorter inhibition times.[12] Although diarylamines are well-studied additives in the context of hydrocarbon autoxidation, research into the effects of NO_x on diarylamine-inhibited hydrocarbon autoxidations at elevated temperatures are rare in academic literature, industry collaboration with academic research groups notwithstanding. However, the intermediates and end-products of phenolic and diarylaminic RTAs stemming from high-temperature autoxidations using strictly NO_x have been examined.[24]

Popochień monitored the formation of intermediates and products for both a phenolic RTA and a diarylaminic RTA during high-temperature autoxidations via NO_x in N_2 through GC-FID and a solvent-suppressed GC-MS method.[24] The authors found that the product distribution for phenolic RTAs was relatively simple compare to diarylamines, which formed seven intermediates/products during experiments; all of which were designated based on m/z values and reported, or plausible, fragmentation patterns (Figure 3.2). Most of the amine-derived products were dimeric, purportedly forming through radical-radical combination.

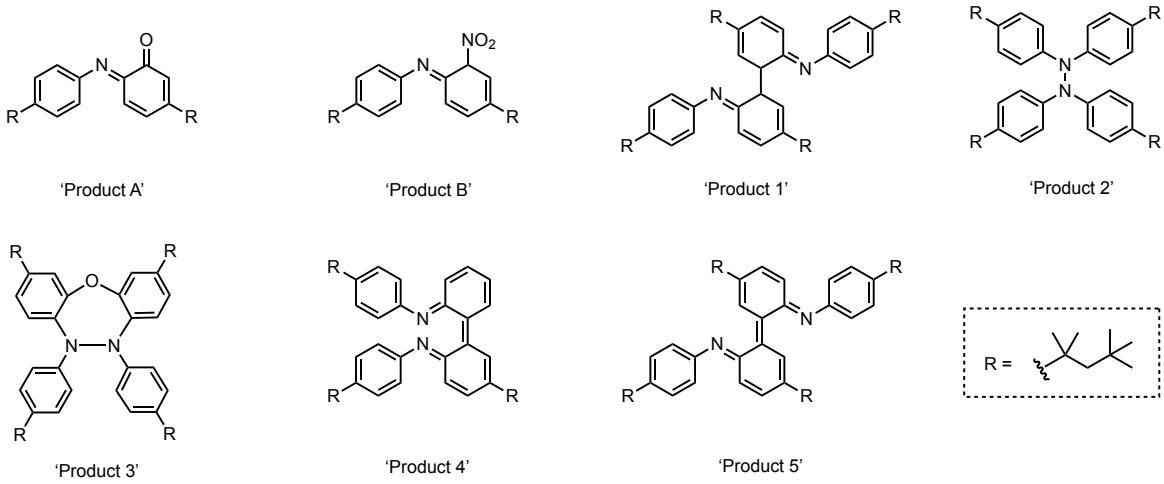

Figure 3.2 Reported products of diarylamine autoxidation at high-temperatures under NO_x conditions, observed with GC-FID and GC-MS.[24]

Unfortunately, none of the products were compared to authentic standards, isolated and characterized, nor were their suggested mechanisms probed in any way. The work also relies on the assumption that all of the products were separable from substrate-derived oxidation products and that the observed products were the only ones to form. Concomitantly, the product distribution appeared suspiciously homogeneous; four of the products are dimers derived from diarylaminyl radical couplings. Our recent studies using ^{15}N NMR techniques indicated that 'Product 2' is not stable at higher temperatures and was not observed to form in any significant concentration during autoxidation experiments; in clear disagreement with the reported results (see Chapter 2 for more details).

Beyond the end-products, the degree to which NO_x impacts the ability of diarylamines to inhibit high-temperature hydrocarbon autoxidation has not been well reported. Investigations by Popochień were performed at 180˚C in squalane (a branched, saturated alkane) under 1000 ppm NO_2 (with the balance in nitrogen), and were monitored using discontinuous methods. This work indicated that diarylamine was consumed within the first hour of the experiment, but the results were not contrasted to experiments performed solely in oxygen, or even in the presence of oxygen, making meaningful comparison to previous experiments (such as those described in Chapter 2) difficult.[25-27] We sought to monitor high-temperature NO_x autoxidations with both our novel ^{1}H ^{15}N HMBC technique and recently reported hydroperoxide quantification assay in order to observe the effects of NO_x on diarylamine RTA activity; correlating reaction progress with diarylamine speciation.[28] Our objectives were not only to compare to our previously-obtained results with diarylamines as inhibitors of autoxidations under oxygen, but also to determine how the results compare to the aforementioned efforts under NO_x conditions. We anticipated that NO_x would likely decrease the efficacy of diarylamine in an analogous fashion to what was reported for hindered phenol: reaction between NO_2 and diarylamine might be expected to reduce inhibition time. We also expected that such reactions would give rise to the products observed by Popochień, which we hoped would be observed throughout experiments via HMBC NMR.

3.2 Results

3.2.1 Efficacy of Diarylaminic RTA in the Presence of NO_x

To determine if NO_x had any effect on the ability of diarylamines to retard autoxidation, 95% n-hexadecane was autoxidized at 160˚C using a mixture of 765 ppm NO_2 in air in the presence of varying amounts of *bis*(4-*tert*-butylphenyl)amine, **3.1** (Figure 3.3 A). The experiments were monitored by the formation of substrate-derived hydroperoxides (ROOH) using our reported fluorogenic, coumarin-conjugated phosphine.[28] Uninitiated autoxidations with 1 mM and 10 mM of **3.1** were run in triplicate, in addition to triplicate autoxidations in the absence of RTA. Uninhibited autoxidations were run in parallel to provide a baseline rate of autoxidation under otherwise identical conditions. Throughout the experiment, small aliquots (<100 μL) were removed from the reaction vessels at 20 minute intervals for hydroperoxide quantification.

Shortly after subjecting the test tubes to the flow of NO_2 (approximately 5-10 minutes), the autoxidation mixture began to take on a vibrant, orange-red colour. The colour change became increasingly prominent over the first hour of the experiment, after which point it ceased to visibly change further. Although colour changes are expected during autoxidations with higher concentrations of diarylaminic RTAs due to the distinct red colour of diarylnitroxide radical intermediates, such changes occur more gradually and do not produce such bright hues. As a result, the end of the inhibition period was not as easily judged based on colour as with autoxidations performed with pure O_2; the 'normal' change from a reddish-brown to pale yellow-green was not observed due to the seemingly permanent orange colour of the mixture.

Uninhibited autoxidations show rapid accumulation of substrate-derived hydroperoxides; an expected result for both autoxidations carried out under either O_2 or NO_x in air (Figure 3.3 B). In the presence of 1 mM **3.1**, a short inhibition period was observed before oxidation overwhelmed the RTA and hydroperoxide concentrations increase rapidly. A more pronounced inhibition period was clear in autoxidations with 10 mM **3.1**

present; hydroperoxide concentrations were suppressed for over 90 minutes before onset of the rapid increase in oxidation products.

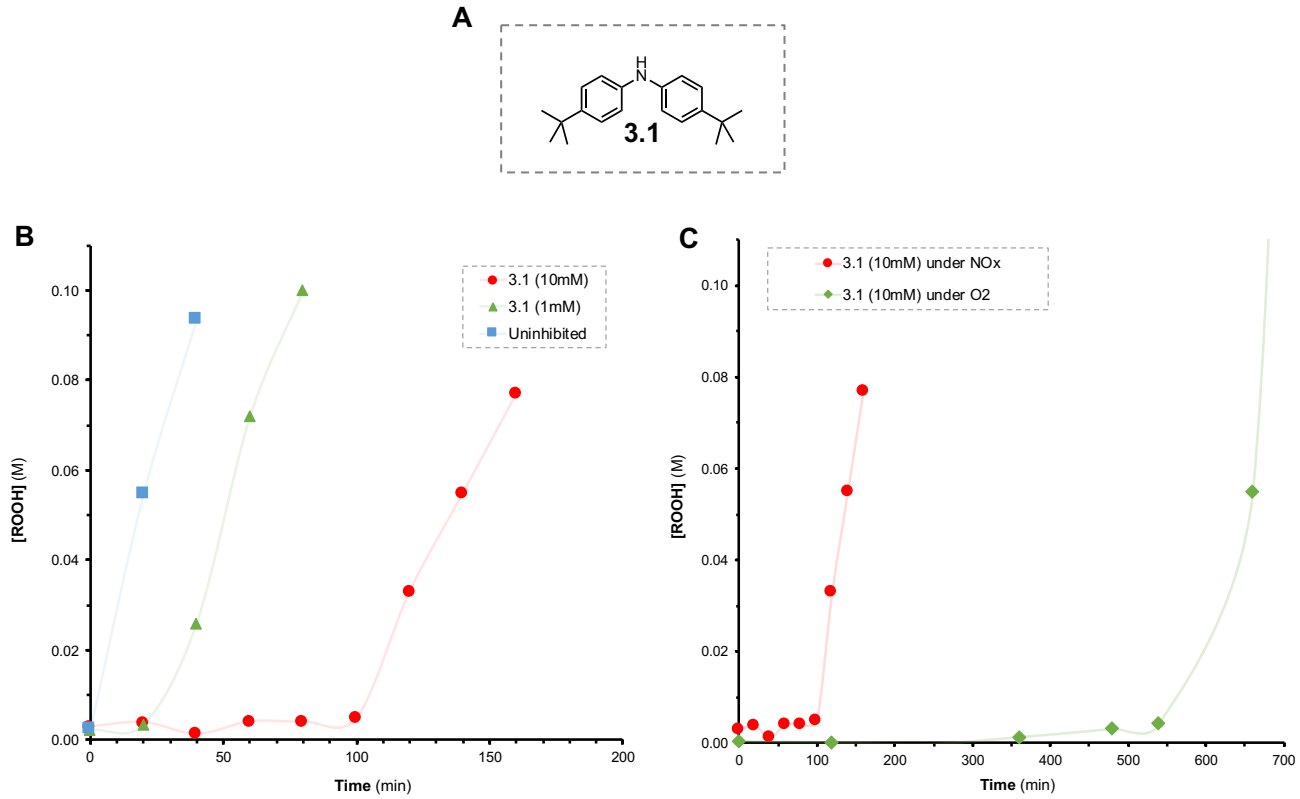

Figure 3.3 (**A**) Chemical structure of **3.1**. (**B**) Autoxidation of n-hexadecane at 160˚C via parallel reactor under constant flow (2 L/min) of 765 ppm NO_2 in air. Uninhibited (blue), 1 mM (green), and 10 mM (red) of **3.1**. (**C**) Autoxidation of n-hexadecane at 160˚C via parallel reactor inhibited by 10 mM of **3.1** under constant flow (2 L/min) of: 765 ppm NO_2 in air (red) and pure O_2 (green).

In accordance with previous reports using a hindered phenol,[12] autoxidations under the NO_x conditions in the presence of **3.1** appeared more deleterious to substrate; the inhibition period of **3.1** was observed to be considerably shorter than analogous experiments performed with pure O_2 (Figure 3.3 C). The root cause of the vastly different inhibition times was not immediately clear. Considering that the next objective was to observe the speciation of **3.1** under NO_x conditions, this finding was earmarked in hopes that spectroscopic studies might provide additional information regarding the fate of **3.1** during the experiment.

3.2.2 Diarylamine Speciation During Autoxidations Carried Out in the Presence of NO_x

To elucidate the fate of the diarylamine under NO_x-autoxidative conditions, we utilized our HMBC ^{1}H – ^{15}N spectroscopic method and ^{15}N-labelled diarylamine **3.1**. Under analogous, high-temperature NO_x conditions, *n*-hexadecane was autoxidized in the presence of 10 mM of isotopically labelled **3.1**. However, aliquots of larger volumes (≈ 500 μL) were withdrawn during the experiment in order to directly analyze by NMR. Representative data are shown in Figure 3.4.

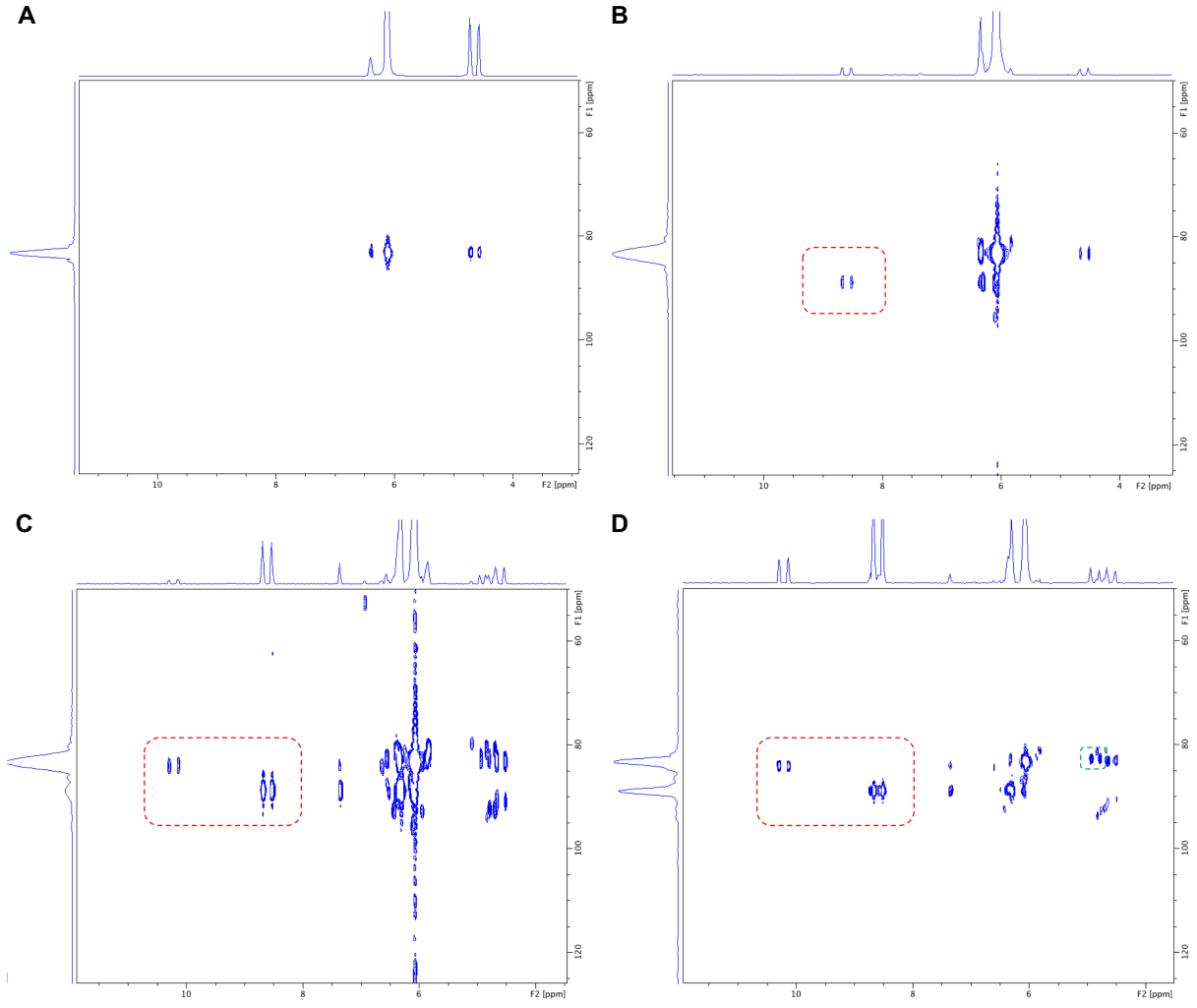

Figure 3.4 ^{1}H–^{15}N HMBC spectra of NO_x autoxidation of n-hexadecane at 160˚C inhibited by 10 mM of ^{15}N (**1**). (**A**) 0 h, (**B**) 10 min, (**C**) 30 min, (**D**) 1 h. Downfield doublets outlined in red, doublets near **3.1** outlined in green.

At the outset, only diarylamine (≈ 83 ppm) is observed in the autoxidation mixture (Figure 3.4 A). However, contrary to O_2 autoxidations, in which no obvious transformation of the diarylamine is observed in aliquots withdrawn at early time-points, we observed proton doublets corresponding to two species with nitrogen chemical shifts similar to **3.1** after ten minutes that continued to intensify thereafter (Figure 3.4 B-D, outlined in red). The doublets, which appear downfield of the proton correlation signals of **3.1** (84 and 89 ppm), are split by approximately 90 Hz; the coupling constant of protons directly bonded to a ^{15}N nucleus. Other species with similar chemical shifts to diarylamine were also observed, one of which also possessed a doublet just upfield that of **3.1** (Figure 3.4 D, outlined in green).

After one hour, the assumed N-H doublet peak of the primary intermediate (**3.2**) was similar in intensity to that of the starting material, suggesting it had accumulated in significant concentration; assuming similar relaxation times (Figure 3.5, outlined in red). The doublet of the secondary intermediate (**3.3**) (Fig. 3.5 B, outlined in orange) also grew during the first hour, but did not appear to accumulate to the same extent.

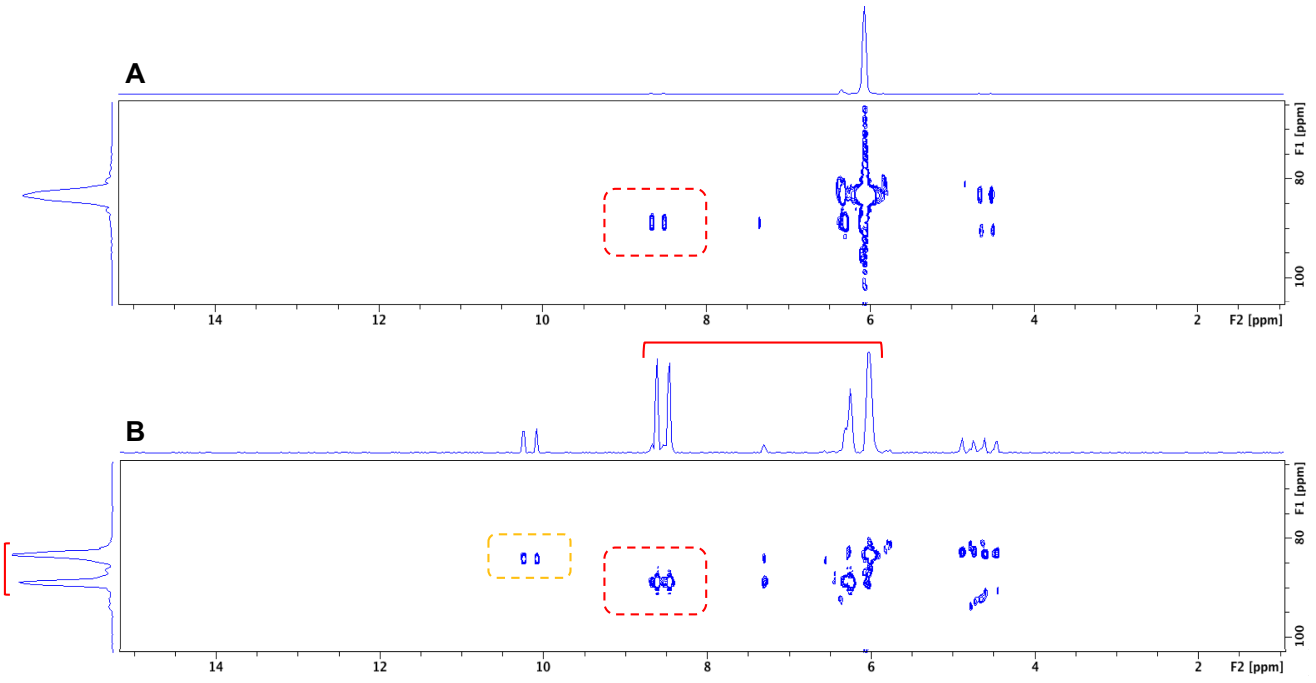

Figure 3.5 $^{1}H–^{15}N$ HMBC spectra of NO_x autoxidation of n-hexadecane at 160˚C inhibited by 10 mM of ^{15}N-**3.1**. (A) 10 min, (B) 60 min. Intermediates **3.2** and **3.3** outlined in red and orange, respectively.

No **3.1** was visible 160 minutes into the autoxidation, with the two intermediate species comprising a significant amount of the ^{15}N material observed, along with other minor products. Concurrently, hydroperoxide concentrations began to increase rapidly. After this point, ^{15}N diarylamine-derived oxidation products began to form in the same chemical shift region as previously observed under O_2 autoxidations (Figure 3.6 B). The most prominent nitrogen peaks corresponded to chemical shifts of approximately 48 ppm and 120 ppm, both coupling to protons in the aromatic region: 7.1 ppm and 7.3 ppm respectively.

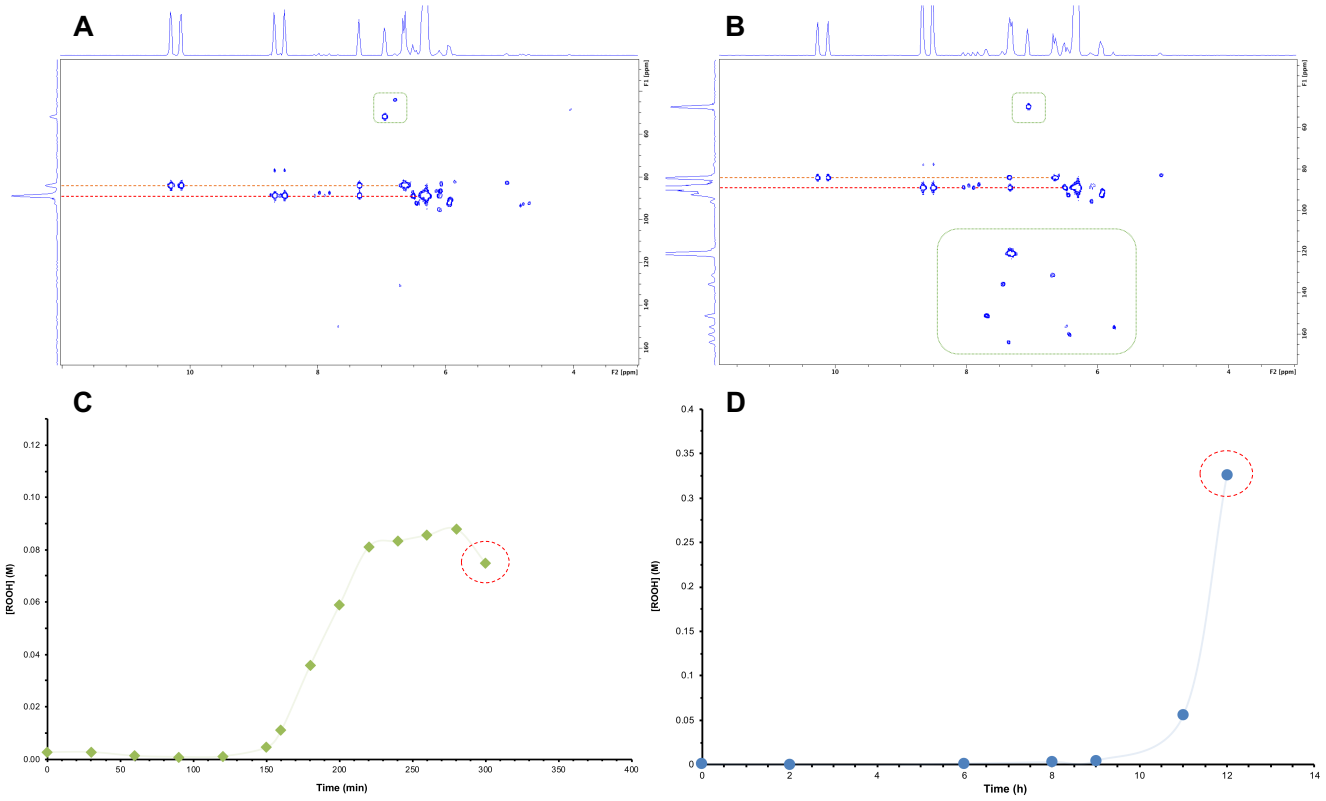

Figure 3.6 $^{1}H-^{15}N$ HMBC spectra of NO_x autoxidation of n-hexadecane at 160˚C inhibited by 10 mM of ^{15}N **3.1** at: (**A**) 160 minutes, (**B**) 200 minutes, with **3.2** and **3.3** indicated (red and orange, respectively) and other products outlined (green). Point on hydroperoxide trace which formation of diarylamine-derived oxidation species is observed under: (**C**) NO_x conditions, and (**D**) O_2 conditions.

Interestingly, however, reaction progress curves and the formation of the diarylamine-derived oxidation products under NO_x following the end of the inhibited period was not as rapid as under only O_2; hydroperoxide concentrations increased rapidly and then were sustained at a roughly steady-state concentration before full

decomposition of **3.1** was observed. This result is in contrast to experiments with O_2, in which the diarylamine was consumed once hydroperoxide concentrations increased rapidly to a maximal concentration (Figure 3.6 C-D). Between 200 minutes and the time at which **3.1** was completely consumed (300 minutes), minor product formation was observed as the concentration of intermediates began to decrease (Figure 3.7).

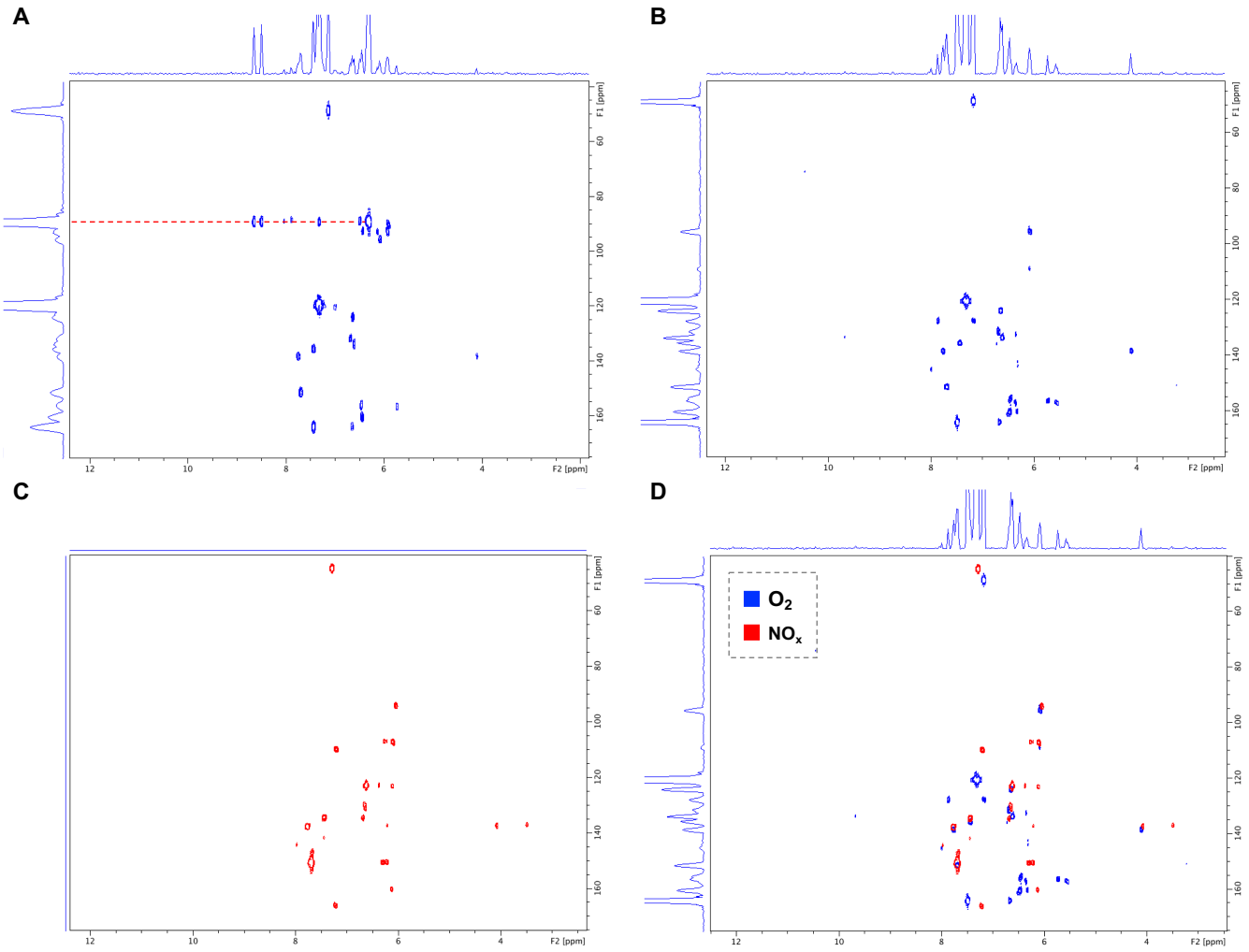

Figure 3.7 $^{1}H–^{15}N$ HMBC spectra of NO_x autoxidation of n-hexadecane at 160˚C inhibited by 10 mM of ^{15}N **3.1** at: (**A**) 250 minutes and (**B**) 300 minutes with (**3.2**) indicated in red. (**C**) Speciation of **3.1** observed via autoxidation in the absence of NO_x. (**D**) Overlay of HMBC spectra corresponding to autoxidation of **3.1** under O_2 conditions (red) and NO_x conditions (blue).

The concentration of **3.3** decreased before that of **3.2**, and appeared to be consumed completely by 250 minutes (Figure 3.7 A). During this time, additional products were observed in the range of 120 to 165 ppm range of the

nitrogen spectrum. In contrast, **3.2** remained one of the prominent species in solution through 250 minutes, being fully consumed by 300 minutes (Figure 3.7 B). Some commonalities were observed when comparing this speciation of **3.1** to analogous spectra acquired from an autoxidation carried out in the absence of NO_x. In addition to the general chemical shift ranges at which the oxidation products appear, an overlay of the two spectra indicated that some of the products may be identical (Figure 3.7 C,D). Perhaps this result should have been expected as the NO_x conditions still operated under a substantial flow of molecular oxygen into the reactions (oxygen is approximately 2.1×10^5 ppm in air). Regardless, it demonstrates that the NO_x conditions do not completely change the speciation of the diarylamine during the autoxidation; there are common products that result from both NO_x and O_2 interactions with **3.1**, or alternatively, the presence of NO_x at such concentrations does not make the role of O_2 completely irrelevant in the oxidation of diarylaminic RTAs.

Monitoring diarylamine speciation via chromatography becomes increasingly difficult as autoxidation progresses beyond the inhibited period due to the substrate-derived products that arise (as discussed in Chapter 2). However, we were able to utilize TLC-MS to analyze the accumulation of intermediates **3.2** and **3.3** during the early stages of autoxidation, at which point separation from substrate remained possible. Performing small-scale extractions with the autoxidation mixture and relatively immiscible acetonitrile allowed for separation of the less greasy components of the experiment into an organic solvent suitable for chromatography. Aluminum-backed TLC plates spotted with the acetonitrile extracts and developed with a slightly polar mobile-phase provided ample separation for TLC-MS analysis.

Expectedly, time points (0, 30, 60, and 120 minutes) demonstrated the gradual disappearance of **3.1**, concomitant with the appearance of two major spots with R_f values similar to **3.1**, likely corresponding to the species observed via NMR (Figure 3.8 A). Although they could be visualized by UV irradiation, the spots were easily distinguishable on the plate even without the use of a lamp; they possessed a bright, orange colour distinct against the off-white silica. We reasoned that these coloured intermediates could be the source of, or at least play a role in, the drastic colour change observed in the initial stages of the autoxidation. Spot 2 ($R_f = 0.80$) appeared

more rapidly than spot 3 (R_f = 0.60), and appeared higher in concentration based on the UV absorbance and the intensity of the colour.

Subsequent MS analysis of the spots using atmospheric-pressure chemical ionization (APCI +/-) provided intense peaks in positive ion mode with *m/z* values of 283.2. 328.2, and 373.2 for spots 1, 2, and 3 respectively. As expected, the mass of the spot for the starting diarylamine **3.1** corresponded to the exact mass (282.2) plus a proton. The mass acquired for spot 2 corresponded to the exact mass of **3.1** plus a proton and NO_2, while the mass for spot 3 corresponded to the exact mass of **3.1** plus a proton and 2 equivalents of NO_2. Previous work reported that the analogous, *mono*-ortho-NO_2 dearomatized imino-tautomer was formed under similar conditions, supporting the notion that such functionalization occurred *ortho* when *para* sites were inaccessible.[24]

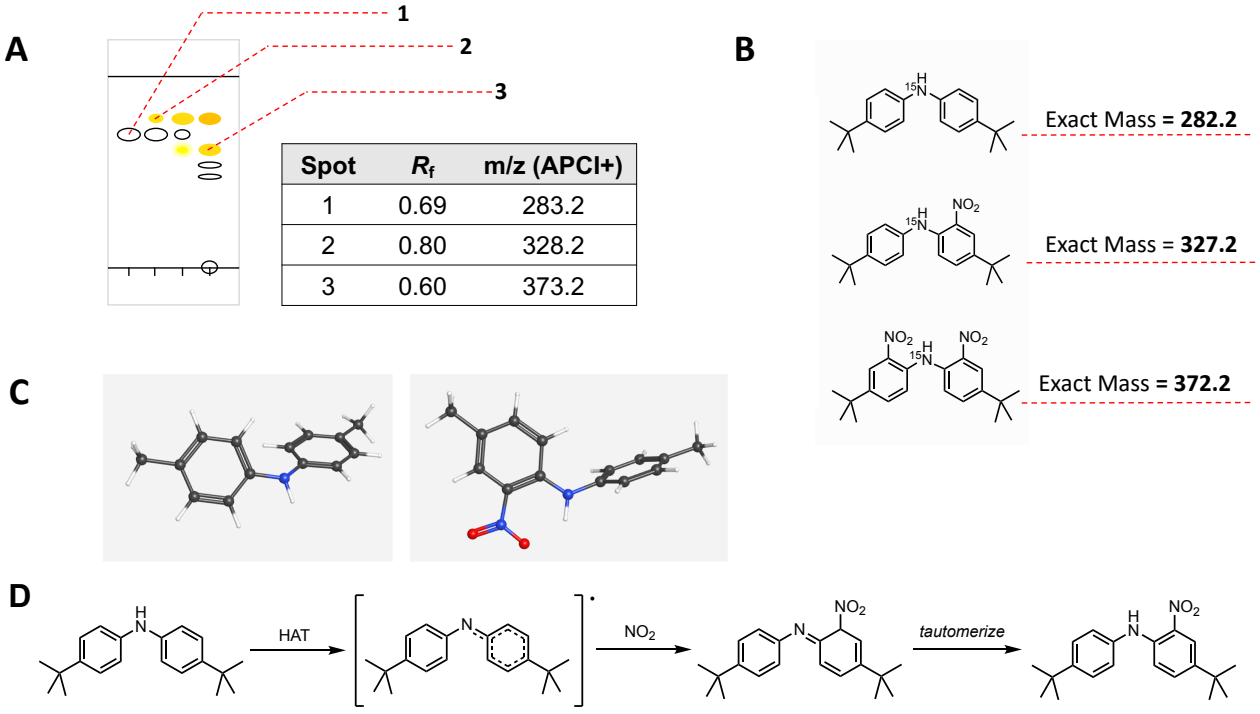

Figure 3.8 (**A**) TLC-MS results of extracted autoxidation aliquots. (**B**) **3.1** and related compounds presumed to correspond to results of TLC-MS. (**C**) Optimized geometry structures of **3.1** (left) and **3.2** (right) using B3LYP-631G* level of theory. (**D**) Presumed pathway for radical *ortho* nitration of **3.1** during autoxidation.

Our immediate assumption based on the results was **3.1** could be nitrated once or twice by NO_2 dissolved in solution during the initial stages of autoxidation, forming *mono*- and *di*-nitro diarylaminic

derivatives. Although the substitution pattern could not be gleaned from the HMBC spectra or MS results, it was assumed that such substitutions likely occurred *ortho* to the amine; either through direct C-N radical-radical combination or via N-nitro/so intermediates (Figure 3.8 D)

We hypothesized that in addition to the initiating capability of NO_x, which was previously shown to exacerbate the early stages of autoxidations,[12] NO_x could hinder the diarylamine's ability to undergo productive reactions by 'deactivating' it through direct reaction, as reported for hindered phenol.[12] As previous studies of RTAs have indicated, electron-rich (donating) aryl substituents increase the efficacy of the RTA through a weakened N-H bond, whereas electron-poor (withdrawing) aryl substituents generally hinder turnover.[29-32] In addition to the electronic effect, we reasoned that nitration *ortho* to the nitrogen could further deactivate the diarylamine via intramolecular H-bonding and steric bulk. Optimized geometry structures of *para*-methyl diarylamine and an *ortho*-nitrated derivative illustrated this effect: the aromatic rings of *para*-methyl diarylamine are twisted out-of-plane relative to the N-H bond and each other, whereas a strong intramolecular interaction between the N-H and *ortho*-nitro group of the derivative restricts such rotation (Figure 3.8 C).

3.2.3 Synthesis of the Observed Intermediates of Diarylamine Speciation During NO_x Autoxidation

To confirm the identities of the nitrated diarylamine derivatives and subsequently determine their activity as RTAs, we synthesized authentic standards of both compounds, ^{14}N and ^{15}N alike. We reasoned that ^{14}N derivatives could be used to quantify their inherent RTA activity and used directly in high-temperature autoxidations to assess whether they contribute any inhibition activity. Enriched ^{15}N-compounds could be used as authentic standards to confirm the identity of the observed intermediates in NO_x autoxidations as well as primary 'inhibitors' of autoxidations to observe their resulting oxidation products.

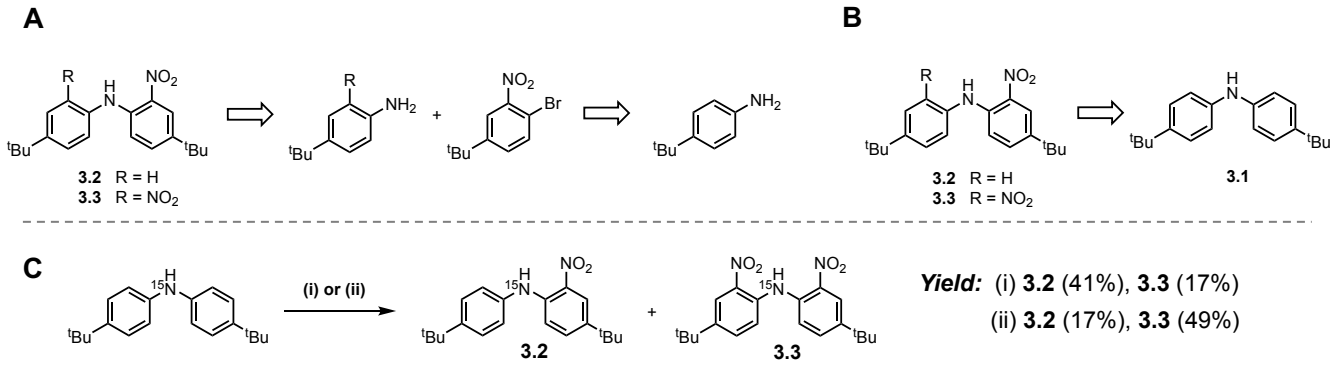

Figure 3.9 Synthetic disconnections for **3.2** and **3.3** from (**A**) *4-tert*-butylaniline, and (**B**) **3.1**. (**C**) Synthesis of **3.2** and **3.3** under conditions: (*i*) 1:1 HNO_3:H_2SO_4 in $CHCl_3$, 25˚C, approx. 5-10 minutes, or (*ii*) 1 eq. $Cu(NO_3)_2$ in acetic anhydride, 25˚C, overnight.

We envisioned a number of potential routes to (2-nitro-4-*tert*-butylphenyl)-4-*tert*-butylphenylamine (**3.2**) and *bis*(2-nitro-4-*tert*-butylphenyl)amine (**3.3**). Direct nitration offered the most straightforward method, but more sophisticated pathways could also afford to the desired compounds in expectedly high yields (Figure 3.9 A,B). Having a considerable quantity of both ^{14}N and ^{15}N **3.1**, we elected to take the simplest route to acquire the compounds, synthesizing both **3.2** and **3.3** via acid or Menke nitration (Figure 3.9 C). Although relatively poor yielding, we reasoned that performing the reaction and work-up in a single day with the ample quantity of **3.1** on-hand was the most efficient route. Conveniently, **3.2** and **3.3** were also both obtained from a single reaction and easily separated by flash chromatography.

After obtaining pure samples of **3.2** and **3.3**, we analyzed the isotopically labelled versions with our ^1H ^{15}N HMBC technique and were pleased to find that the signals observed from each compound corresponded identically to the observed intermediates during NO_x autoxidation. Compounds **3.2** and **3.3** were found to have nitrogen chemical shifts of approximately 91.0 and 85.0 ppm respectively in acetone-d_6, which was in close agreement with the presumed products under NO_x conditions (Figure 3.10 A). Overlaying spectra of the authentic standards on top of spectra obtained during autoxidation of **3.1** under NO_x conditions illustrated near perfect overlap between the corresponding 2D signals (Figure 3.10 B).

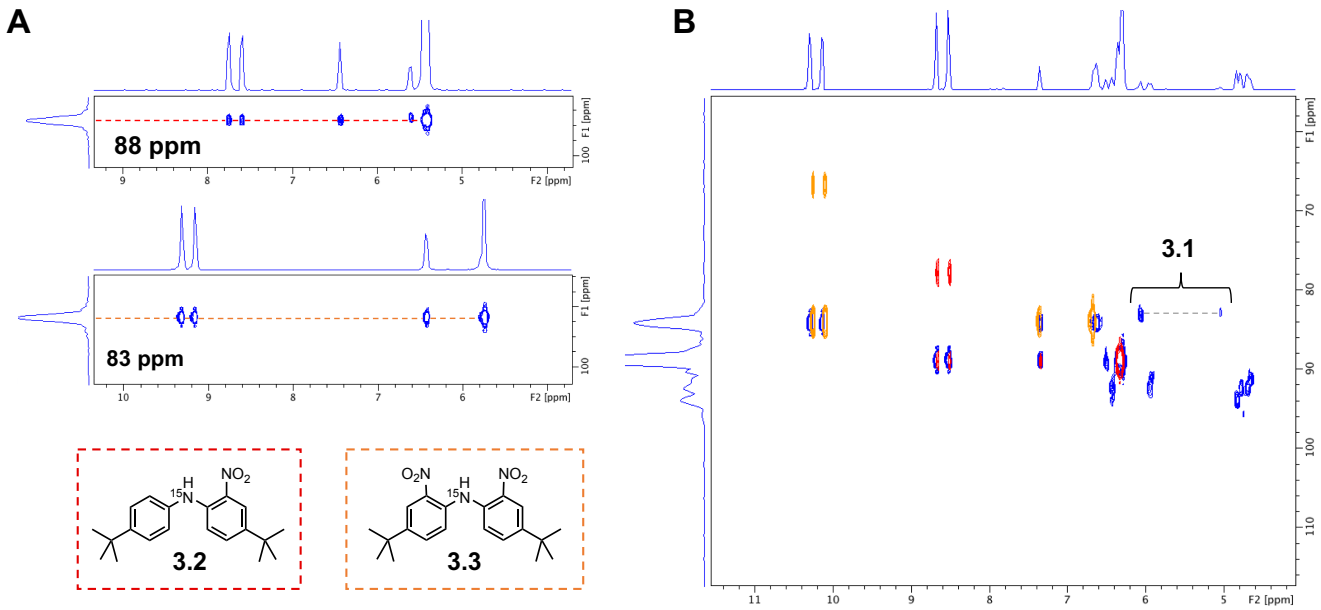

Figure 3.10 (**A**) HMBC spectra of **3.2** (red) and **3.3** (orange) in *n*-hexadecane at beginning of experiment. (**B**) HMBC overlay of **3.2** (red), **3.3** (orange), and 80-minute time-point aliquot of autoxidation of **3.1** under NO_x conditions (blue), with **3.1** indicated.

Confusingly, the 2D spectra for **3.2** and **3.3** both displayed a set of doublets with the exact same proton chemical shifts, but upfield nitrogen chemical shifts, that did not possess any other $^{1}H - {}^{15}N$ coupling. As ^{1}H NMR, ^{13}C NMR, and HRMS had indicated that the compounds were pure, it was odd to observe other nitrogen species in solution. To determine if there were multiple ^{15}N species with N-H coupling in the samples of **3.2** and **3.3**, we analyzed them with ^{15}N 90Hz INEPT experiments in deuterated solvent rather than *n*-hexadecane, tuned for the N-H coupling we observed (Figure 3.11). Both compounds displayed lone nitrogen peaks at the expected chemical shifts (90.8 and 84.6, respectively), indicating that only the starting materials were present in solution.

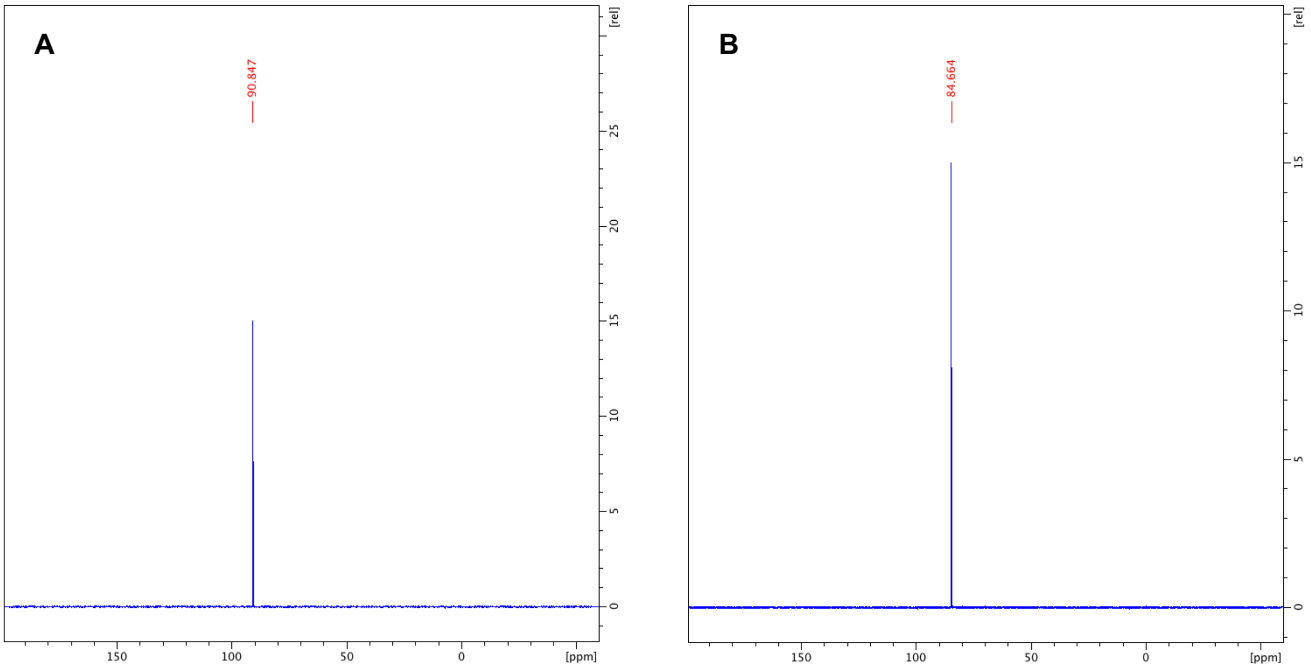

Figure 3.11 ^{15}N INEPT spectra tuned for 90Hz (N-H) coupling of: (**A**) **3.2**, and (**B**) **3.3**. Both spectra were obtained in acetone-d_6. Nitrogen chemical shifts were referenced to neat nitromethane in liquid ammonia.

As we observed the peaks even before heating the material, we discounted the notion that **3.2** and **3.3** were unstable at higher temperatures. We pondered whether or not the 'phantom' peaks were caused by restricted rotation of the aryl rings or nitro group due to the relatively viscous medium of *n*-hexadecane (3.45 cP at 20˚C)[33] compared to acetone-d_6 (0.32 cP at 20˚C) at low temperatures. Unfortunately, we were unable to test this hypothesis due to practical limitations; none of the NMR instruments capable of heating samples were equipped with the solvent-suppression program, and sensitivity would likely be impeded by the lack of cryoprobe.

We also considered the possibility that the polarity of the solvent might be a contributing factor. Acetone-d_6 would provide much better solvation of the compounds and their polar functional groups than *n*-hexadecane, which would promote intermolecular and intramolecular interaction. Due to the insolubility of **3.2** and **3.3** in linear alkanes, such as hexanes, at room temperature, coupled with the remaining issue of instrument limitations, no efforts were made to investigate further.

As previously mentioned, the downfield doublets that alerted us to formation of **3.2** and **3.3** early into the autoxidation experiments in the presence of NO_x were accompanied by many signals in close proximity to **3.1** (Figure 3.4 C). We noted that the *ortho*-substituted diarylamine-dimer **2.4** in the same region (see Chapter 2 for details), and overlaying the corresponding spectra indicated that **2.4** was formed (Figure 3.12).

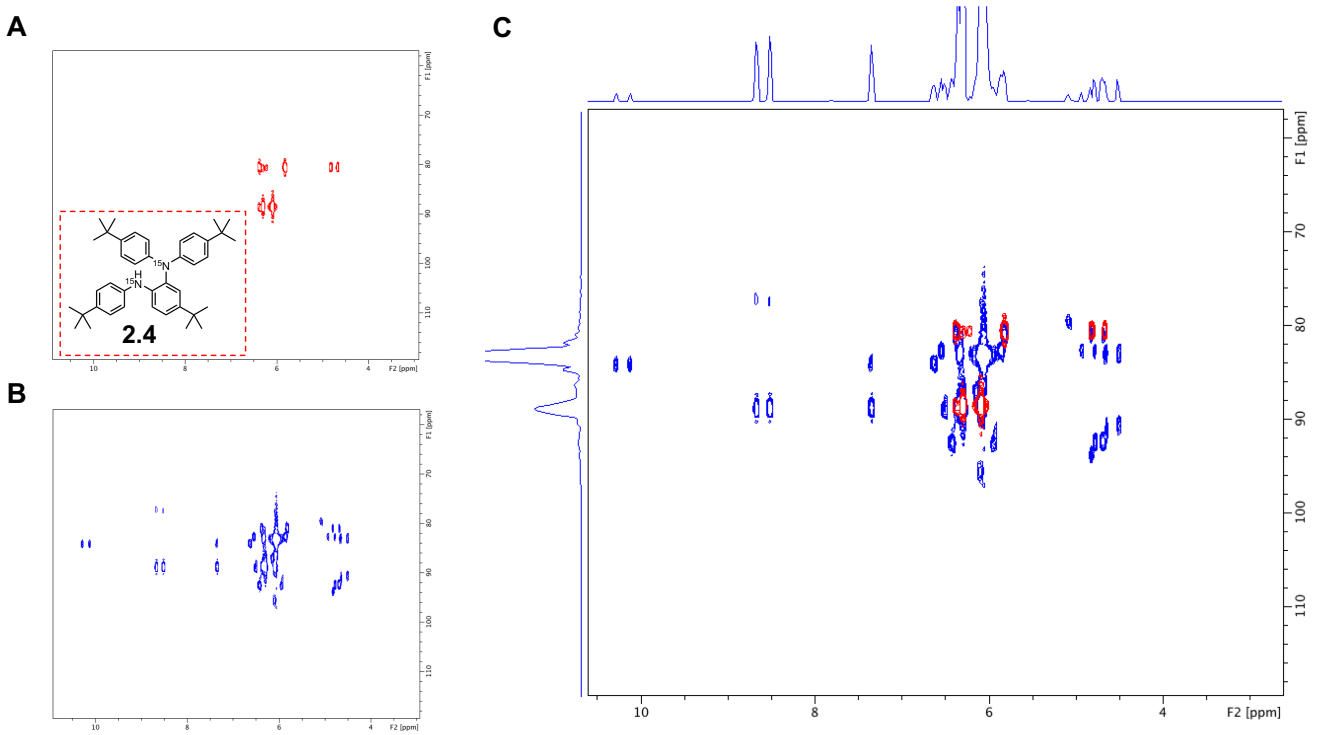

Figure 3.12 HMBC spectra of: (**A**) *ortho*-diarylamine dimer **2.4**, and (**B**) Autoxidation of **3.1** in the presence of NO_x at 50 minutes. (**C**) Overlay of spectra from (**A**) and (**B**) displays nearly identical overlap.

Unlike **3.2** and **3.3** however, **2.4** was consumed relatively rapidly; signals corresponding to the species were not observed past the one-hour mark of autoxidation, indicating it had reacted further.

3.2.4 RTA Activity of Nitrated Diarylamines During Autoxidation in the Presence of NO_x

To assess the RTA activity of the newly-synthesized nitrated-diarylamines **3.2** and **3.3**, we first used them as inhibitors for autoxidations at lower temperatures (37˚C) in hopes that we could obtain their respective inhibition rate constants (k_{inh}) and radical-trapping stoichiometries (n) and compare them with an abundance of kinetic data for other RTAs. Autoxidation reaction progress was monitored using a continuous, visible-light

spectrophotometric method developed by our group.[34] Using a colourimetric substrate that undergoes co-autoxidation in the presence of an autoxidizable hydrocarbon at known rates, kinetic parameters of RTAs can be calculated based on the rate of dye consumption, which is derived directly from changes in absorbance, provided the propagation rate constant of the dye is known. Using this method, inhibition rate constants can be derived from the initial rates of inhibited autoxidations (Eq. 3.1), and reaction stoichiometries can be calculated from the inhibition times (Eq. 3.2). As we anticipated the nitrated diarylamines to be poor RTAs, we elected to perform the co-autoxidations of STY-BODIPY (k_p = 141 M^{-1} s^{-1})[34] in cumene (k_p = 0.34 M^{-1} s^{-1})[35] to provide a greater likelihood that they may compete with propagation (highly-efficient RTAs are assessed using the more-reactive PBD-BODIPY combined with a more reactive substrate such as styrene).

As anticipated, **3.2** and **3.3** performed considerably worse than their parent diarylamine, evident by the fact that reaction progress curves were almost indistinguishable from that of the uninhibited autoxidation. However, some retardation in the rate of autoxidation was observed for the *mono*-nitrated derivative at elevated loadings (Figure 3.13 A for **3.2**, see Appendix Figure S3.11 for **3.3**). The parent compound, **3.1** (k_{inh} = 7.3 ± 2.5 × 10^4 $M^{-1}s^{-1}$) performed comparably with earlier reports using similar compounds,[34,36] outstripping the relatively sluggish **3.2** and **3.3** by at least two orders of magnitude; both were estimated to possess k_{inh} << 10^3 $M^{-1}s^{-1}$ since concentrations of **3.2** had to be increased 100-fold in order to observe a reproducible retardation of autoxidation. No retardation of the autoxidation by **3.3** could be observed. A summary of the calculated and estimated rate constants is compiled in Table 3.1.

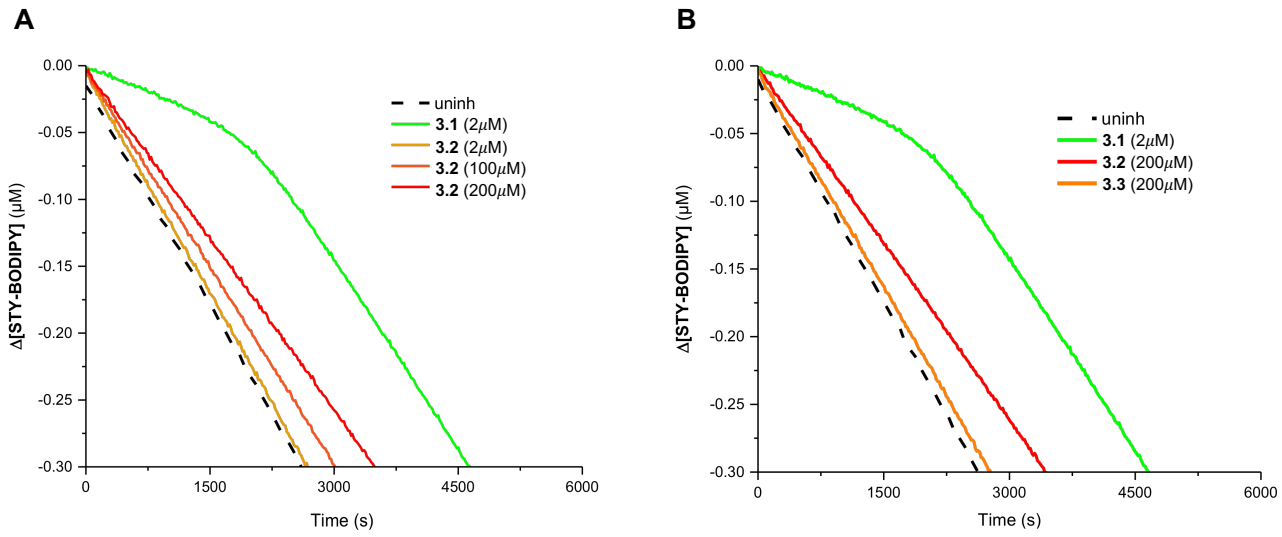

$$k_{inh} = \frac{k_{\text{STY-BODIPY}}[\text{STY-BODIPY}]R_i}{nR_{inh}[\text{RTA}]} \quad [3.1] \qquad n = \frac{t_{inh}R_i}{[\text{RTA}]} \quad [3.2]$$

Figure 3.13 Co-autoxidations of cumene (3.6 M) and STY-BODIPY (10 μM) initiated by AIBN (6 mM) in PhCl at 37˚C (**A**) Comparison between uninhibited (black), 2 μM **3.1** (green), and 2 μM (yellow), 100 μM (orange), and 200 μM (red) **3.2**. Uninhibited trace offset on *y*-axis by -0.015 μM. (**B**) Comparison between uninhibited (black), 2 μM **3.1** (green), 200 μM **3.2** (red), and 200 μM **3.3** (orange). Uninhibited trace offset on *y*-axis by -0.015 μM.

Although the nitro-derivatives showed little to no RTA activity at ambient temperatures, we pondered whether or not they would demonstrate increased activity at higher temperatures in unsaturated substrates via the recently reported mechanism of nitroxide-catalyzed cross-dismutation of (hydro)peroxyl species,[37] RTAs that readily react to produce nitroxides under autoxidative conditions in olefinic substrates inhibit autoxidation more efficiently than RTAs that cannot do so. Due to our results at 37˚C, we anticipated that the electron-poor aryl substituents of **3.2** and **3.3** would continue to hinder them from reacting quickly with peroxyls at 100˚C, limiting their ability to form nitroxides. The compounds were tested at 100˚C using the same co-autoxidation method but with 1-hexadecene (k_p = 1.0 M^{-1} s^{-1})[35] and PBD-BODIPY (k_p = 8283 M^{-1} s^{-1})[34] in lieu of cumene and STY-BODIPY.

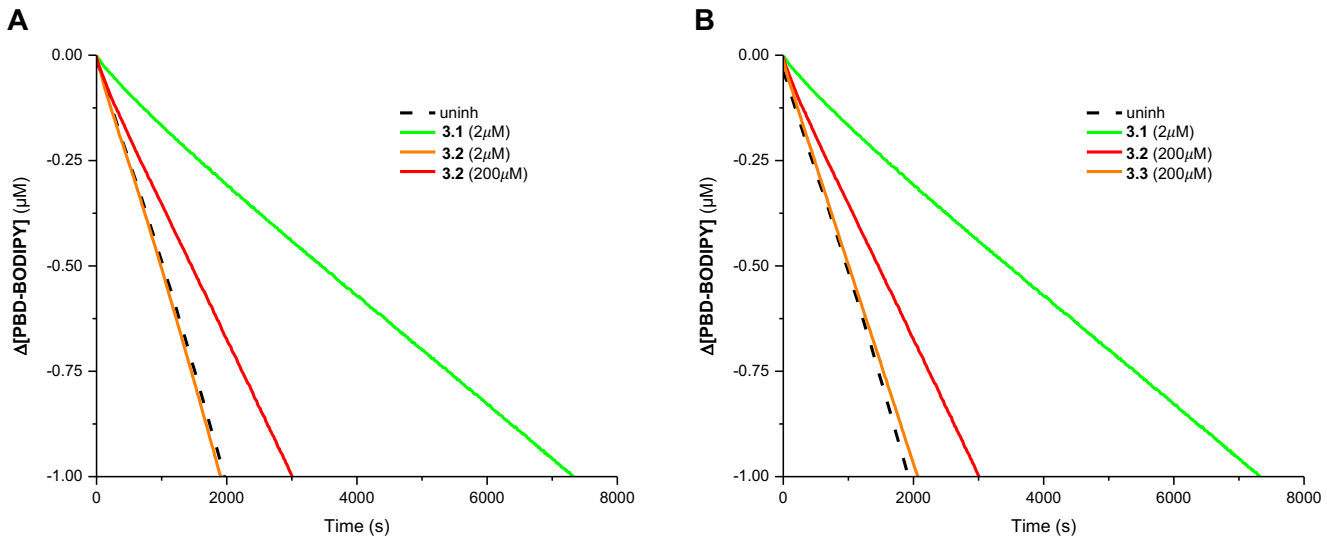

Figure 3.14 Co-autoxidations of 1-hexadecene (2.68 M) and PBD-BODIPY (10 μM) initiated by dicumyl peroxide (1 mM) in PhCl at 100˚C (**A**) Comparison between uninhibited (black), 2 μM **3.1** (green), and 2 μM (orange), 200 μM (red) **3.2**. (**B**) Comparison between uninhibited (black), 2 μM **3.1** (green), 200 μM **3.2** (red), and 200 μM **3.3** (orange). Uninhibited trace offset on y-axis by -0.025 μM.

Consistent with results at 37˚C in cumene, neither compound demonstrated significant inhibitory effects, only slightly decreasing the rate of PBD-BODIPY consumption compared to uninhibited traces (Figure 3.14). Again, diarylamine **3.2** was clearly more effective than **3.3** (Figure 3.14 A,B). The parent compound **3.1** performed similarly to previous experiments (k_{inh} = 7.4 ± 0.3 × 10^5 $M^{-1}s^{-1}$) and provided a stark contrast of inhibition alongside the nitrated derivatives. Similar to experiments performed in cumene at 37˚C, rate constants for **3.2** and **3.3** were estimated (k_{inh} << 10^4 $M^{-1}s^{-1}$) given that they could not match the effect of **3.1** even when present at 100-fold greater concentration. Results are summarized in Table 3.1.

cumene, 37˚C		1-hexadecene, 100˚C	
Compound	k_{inh} (M^{-1} s^{-1})	Compound	k_{inh} (M^{-1} s^{-1})
3.1	(7.3 ± 2.5) × 10^4	**3.1**	(7.4 ± 0.3) × 10^5
3.2	<< 10^3	**3.2**	<< 10^4
3.3	<< 10^3	**3.3**	<< 10^4

Table 3.1 Experimental and estimated rate constants for compounds **3.1**-**3.3** obtained during co-autoxidations of cumene and 1-hexadecene at 37˚C and 100˚C, respectively. Diarylamine **3.1** proved over two orders of magnitude faster than **3.2**, **3.3** under both sets of conditions.

Next, the nitrated compounds were tested in *n*-hexadecane at 160˚C under constant flow of O_2; the conditions of most interest and our standard for high-temperature autoxidations. As **3.2** and **3.3** had performed poorly at 37˚C and 100˚C, coupled with the fact that **3.1** performed considerably worse during NO_x experiments, we expected the compounds to show minimal inhibition. Experiments were performed with **3.2** and **3.3** in parallel with an uninhibited autoxidation and one inhibited by the proven parent compound, **3.1** (Figure 3.15 A). At 2 mM loadings of RTA, **3.2** and **3.3** exhibited no significant inhibitory effect, with **3.3** almost overlapping perfectly with the uninhibited autoxidation. Diarylamine **3.2** appeared to provide a miniscule benefit, more so just retarding the rate of autoxidation rather than inhibiting the process. Both **3.2** and **3.3** paled in comparison to **3.1**, which was found to inhibit the autoxidation for over two hours.

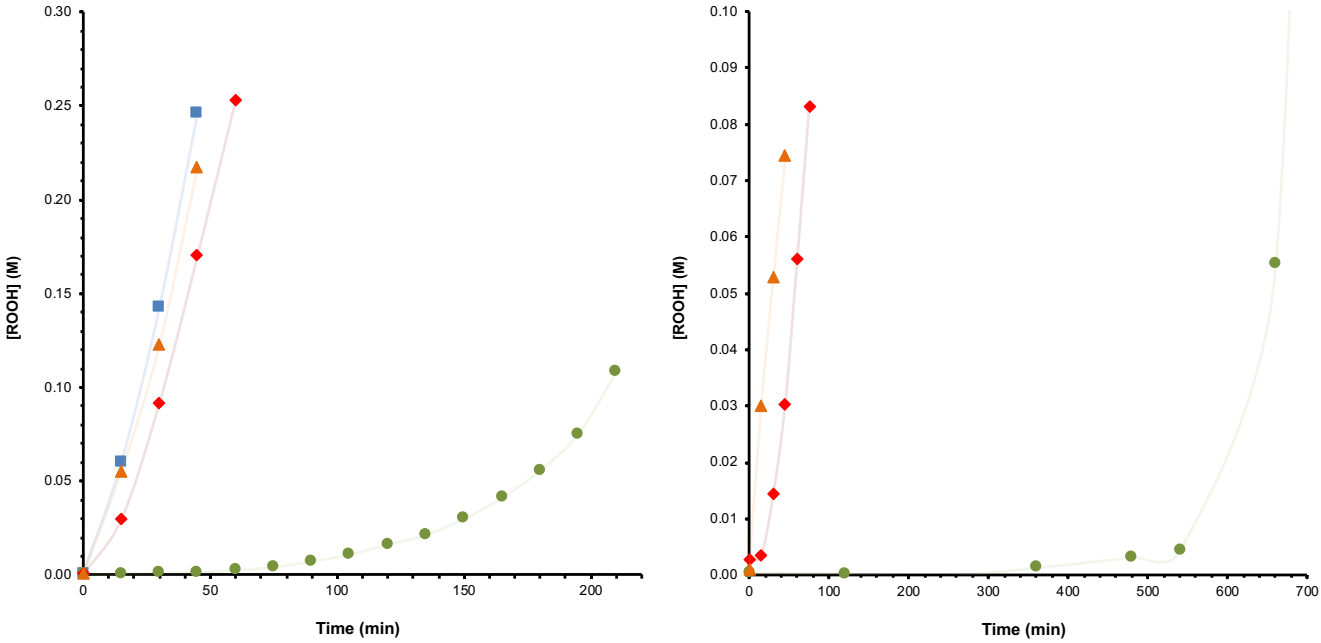

Figure 3.15 Autoxidation of n-hexadecane at 160˚C via parallel reactor under constant flow (2 L/min) of pure O_2 with: (**A**) no inhibitor (blue) and 2 mM: **3.1** (green), **3.2** (red), **3.3** (orange), and (**B**) 10 mM **3.1** (green), **3.2** (red), **3.3** (orange).

Increasing the concentration of diarylamines 5-fold (to the typical RTA loading used for HMBC-monitored experiments) only exacerbated the difference of inhibition provided by the nitrated compounds and the parent amine. Diarylamines **3.2** and **3.3** still failed to demonstrate any significant RTA activity at this higher loading,

while **3.1** provides a time of inhibition (t_{inh}) of approximately 9 hours (Figure 3.15 B). While we did not anticipate to see a large increase in activity at 10 mM loadings, the experiment provided the inhibition parameters for future experiments using isotopically labelled compounds. However, we had noted that full speciation of **3.1** under NO_x conditions was prolonged past the end of the inhibited period, and anticipated a similar result when monitoring the speciation of **3.2** and **3.3**.

3.2.5 Monitoring the Speciation of Nitrated Diarylamines During High-Temperature Autoxidations

With a sufficient amount of the ^{15}N-enriched nitrated diarylamines in hand, we sought to determine the fate of **3.2** and **3.3** under both O_2 and NO_x conditions. Ideally, such experiments would inform us on the products derived solely from oxygenated conditions and those derived from autoxidation in the presence of NO_x.

Autoxidations carried out in the presence of **3.2** under O_2 demonstrated that hydroperoxides rapidly accumulate long before consumption of **3.2** is observed; in agreement with prior observations of autoxidation inhibited by **3.1** under NO_x. This suggests that the reduced activity of **3.2** as an RTA translates similarly to its reactivity towards deleterious pathways. Detected consumption of **3.2** commenced 2-3 hours into the autoxidation, with 4 peaks appearing downfield of **3.2** in the nitrogen spectrum (Figure 3.16 A).

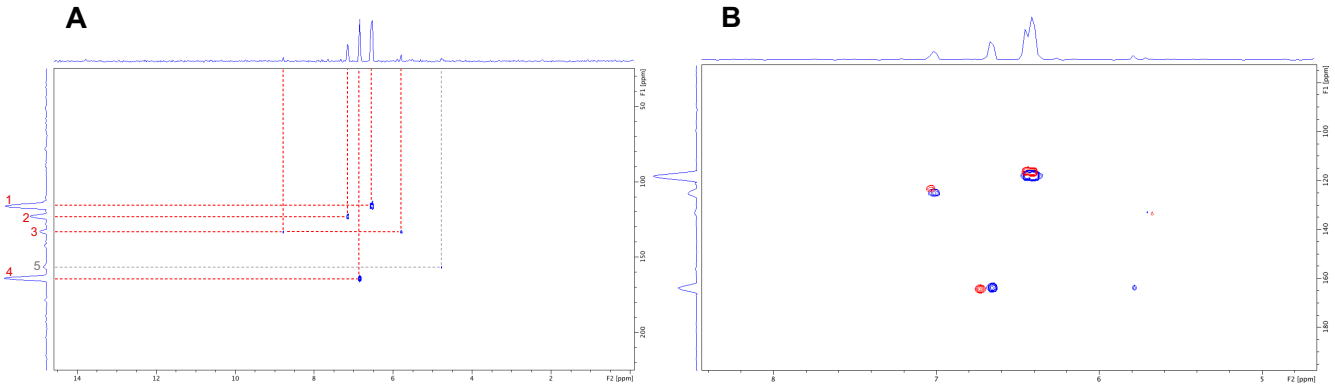

Figure 3.16 (**A**) O_2 autoxidation speciation of **3.2** observed by HMBC. (**B**) Overlap/correlation of speciation of **3.2** under O_2 (red) and NOx (blue).

No other significant species are observed upon further disappearance of **3.2**, indicating that the starting material is further funneled into the three existing major products, forms the minor products observed, or is functionalized

into products not observable or detected by HMBC. When autoxidations were carried out in the presence of NO_X, **3.2** formed the same three major products observed under O_2 conditions, indicating that NO_x do not play a direct role in diarylamine oxidation beyond forming the nitrated-derivative (Figure 3.16 B).

Autoxidations under both O_2 and NO_x when using **3.3** as the inhibitor yielded similar results to that of **3.2**: speciation was observed downfield of the initial inhibitor **3.3**, of which only 3 signals were prominent (Figure 3.17 A). In a similar fashion to **3.2**, speciation of **3.3** appeared independent of NO_x, corroborating the previous observation that NO_x only contributes to diarylamine oxidation insofar as forming the nitrated intermediates. The most prominent of the observed species (found at ≈ 116 ppm in the nitrogen spectrum) appeared to be a doublet or two overlapping species. We noted that the most downfield species observed generally disappeared upon full consumption of **3.3**.

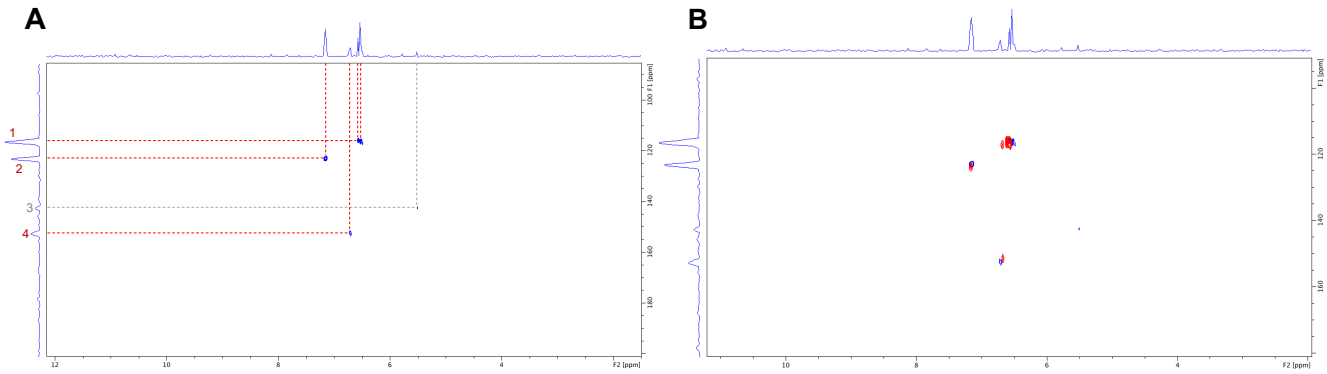

Figure 3.17 (**A**) O_2 autoxidation speciation of **3.3** observed by HMBC. (**B**) Overlap/correlation of speciation of **3.3** under O_2 (red) and NOx (blue).

3.3 formed the same three products whether autoxidized under NO_x or O_2 conditions, corroborating the previous observation that NO_x is irrelevant in the speciation of diarylamines or its nitrated derivatives beyond forming **3.2** and **3.3** (Figure 3.17 B).

Another interesting result was the similarity in speciation between **3.2** and **3.3** when oxidized by either O_2 or NO_x: some of the peaks overlap almost perfectly, indicating that the resulting species are similar enough to have near identical nitrogen chemical shifts to each other, or are in fact, the same species (Figure 3.18 A). Two

of the species differ between autoxidation of **3.2** and **3.3**, but it should be noted that the major products appear to be the same.

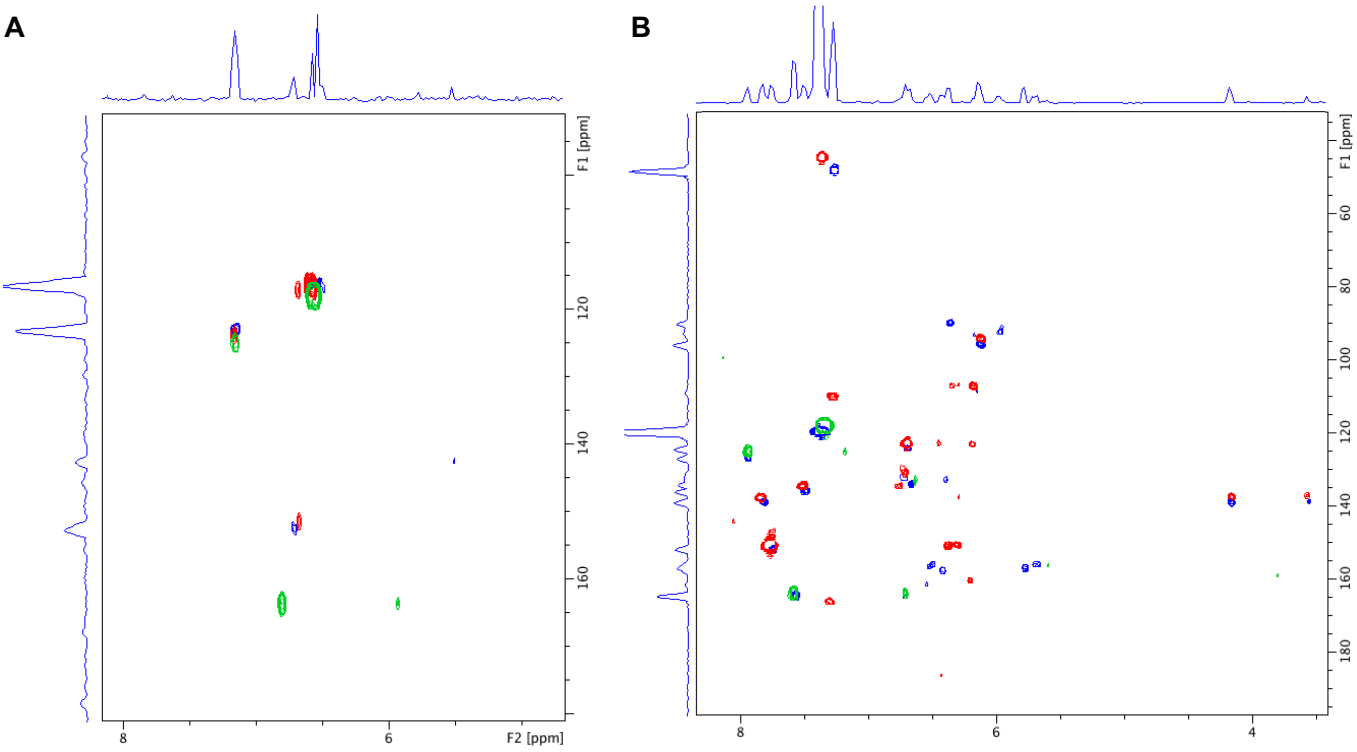

Figure 3.18 (**A**) HMBC spectra overlay of speciation of **3.3** under O_2 (red) and NOx (blue), and speciation of **3.2** under NO_x (green). (**B**) HMBC spectra overlay of: **3.1** when autoxidized with O_2 (red), **3.1** when autoxidized with NO_x (blue), and **3.2** when autoxidized with either O_2 or NO_x (green).

Overlaying this data with that of autoxidations inhibited by **3.1** in the presence of either O_2 or NO_x highlights the marginal differences between speciation of **3.1** under O_2 versus speciation under NO_x (Figure 3.18 B). Most of the species derived from **3.1** under NO_x conditions are 'normal'; they identical to oxidation products formed under O_2. The remaining, prominent species result from further functionalization of the intermediates **3.2** and **3.3** that accumulate through aryl nitration during the early stages of the process. Only a handful of the observed signals do not appear to correspond to either case. Having only observed these species under NO_x conditions in the presence of **3.1** suggests that alternative, NO_x–specific oxidation pathways can be taken that avoid *ortho*-nitration, yet HMBC experiments, although only quasi-quantitative, suggest they are minor.

3.2.6 Quantifying the Accumulation of Nitrated Diarylamines Formed During Autoxidations in the Presence of NO_x

After monitoring inhibition of autoxidation by **3.2** and **3.3** at a range of temperatures, and subsequently determining their inability to provide significant protective effects, we sought to quantify the formation of each species over the course of a high temperature autoxidation under NO_x conditions in which **3.1** was used as the inhibitor. Although evident that formation of **3.2** and **3.3** is counterproductive to inhibition, quantification of their respective concentrations over time would indicate the degree to which such transformations are responsible for the reduced inhibition times observed.

Unfortunately, quantitative, direct ^{15}N methods are prohibitively insensitive and HMBC experiments could not be used for this purpose. Such experiments are useful in providing a semi-quantitative picture of the speciation, but are unable to provide accurate relative, or absolute, concentration values because the intensity of signals are dependent on a variety of factors (coupling constants, T2 relaxation times, pulse excitation profiles, etc.). Although extractions of autoxidation samples have proved impractical (if not impossible) once inhibition has ended, **3.2** and **3.3** accumulate from the beginning of experiments up to and beyond the point at which hydroperoxide concentrations spike, allowing for facile extractions of early time points with methanol. The methanol samples were then analyzed on reverse-phase UPLC, monitoring the excellent chromophores **3.1**-**3.3** by UV-Vis using the photo-diode array detector. The corresponding diarylnitroxide (**3.4**) of the parent amine was also monitored to properly assess the mass balance and prevent any peaks from being assigned incorrectly (Figure 3.19). Concentrations were calculated using calibration curves prepared with authentic standards, and corrected for extraction efficiency (see Appendix Figures S3.1-S3.3 for standard curves), providing a clear picture of the accumulation of **3.2** and **3.3** during autoxidation (Figure 3.19).

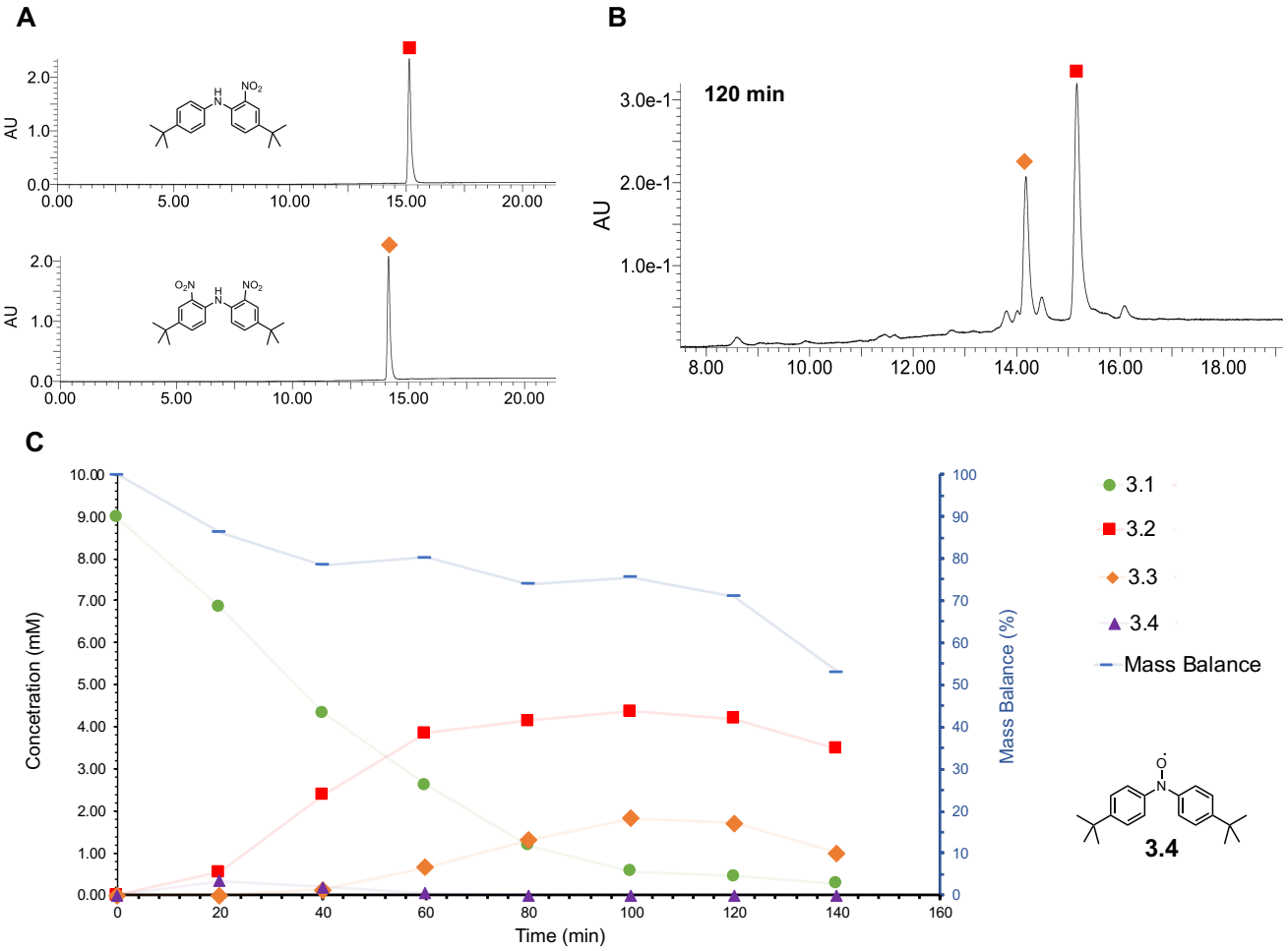

Figure 3.19 (**A**) Chromatograms of authentic standards of **3.2** and **3.3** via UPLC-PDA, at 260 nm and 285 nm, respectively. (**B**) Representative chromatogram of high-temperature hydrocarbon autoxidation in the presence of NO_x. (**C**) Accumulation of known species during high-temperature hydrocarbon autoxidation in the presence of NO_x: **3.1** (green), **3.2** (red), **3.3** (orange), **3.4** (purple). Total mass balance (blue) shown as percentage.

Diarylamine **3.1** was consumed fairly rapidly during the first 80 minutes, after which point its concentration slowly tapers off towards zero. After 20 minutes, a small amount of **3.2** has accumulated; in agreement with the observed colour change, TLC-MS results, and observation of its formation via HMBC. Its concentration continues to climb rapidly for 60 minutes, after which point its accumulation slows, peaking at 100 minutes before gradually decreasing. The *mono*-nitrated diarylamine **3.2** reaches over 4 mM at this peak, comprising almost 50% of the original concentration of **3.1** and representing the majority of the quantifiable mass balance. Not surprisingly, there is a lag period in the accumulation of **3.3**, which does not begin to increase

significantly until the 60-minute mark; when the *mono*-nitrated intermediate **3.2** is present in high concentration. Diarylamine **3.3** also reaches its concentration peak at 100 minutes (of just under 2 mM), after which point it decreases similarly to **3.2**. The diarylnitroxide **3.4** did not accumulate to any significant degree, peaking at less than 0.5 mM after 20 minutes.

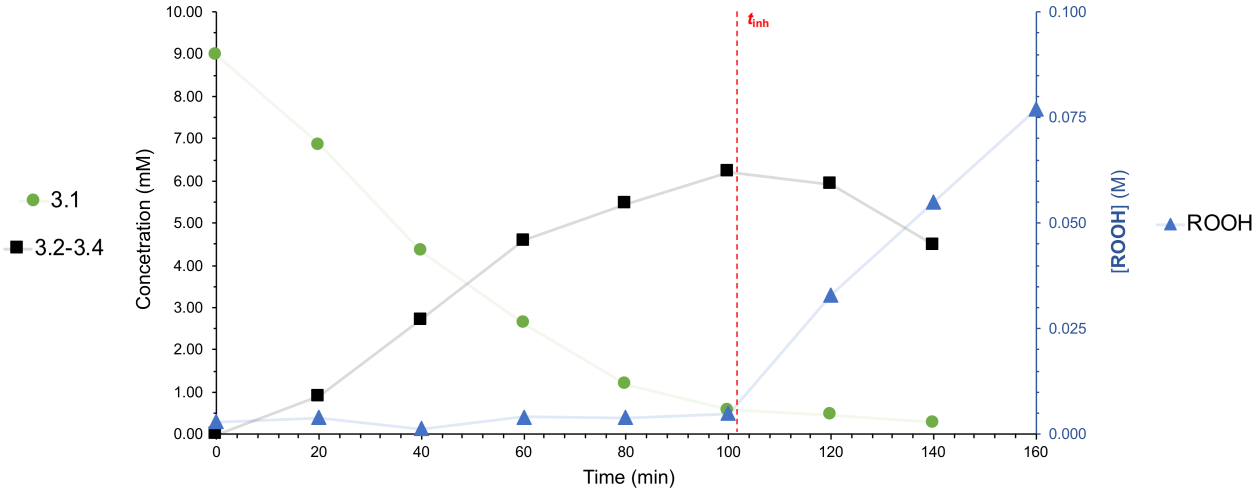

Figure 3.20 Consumption of **3.1** (green) and formation of **3.2-3.4** (black) during autoxidation compared with hydroperoxide trace (blue). Approximate time of inhibition (t_{inh}) indicated in red.

Comparing the consumption of **3.1**, formation of its nitrated products, and hydroperoxide formation illustrates that the majority of material is accounted for prior to the end of the inhibited period (Figure 3.20). The total mass balance accounted for by **3.1**-**3.4** during the experiment decreased approximately 20% during the first hour, but then decreased by only about 10% for the next hour. During the inhibition period (0-100 minutes), **3.1** is consumed while 'intermediate' products accumulate. After inhibition, concentrations of the products begin to decrease as hydroperoxide concentration increases rapidly. These results are consistent with observations made via HMBC NMR; the intensity of accumulated intermediates decreases once the inhibited period has ended, while yet-unidentified oxidation products of the starting materials and intermediates species form (Figure 3.21). During the inhibition period, formation of other products in minor quantities is observed; likely the species that comprise the 'missing' mass balance. Most of these species possess chemical shifts similar to that of the starting

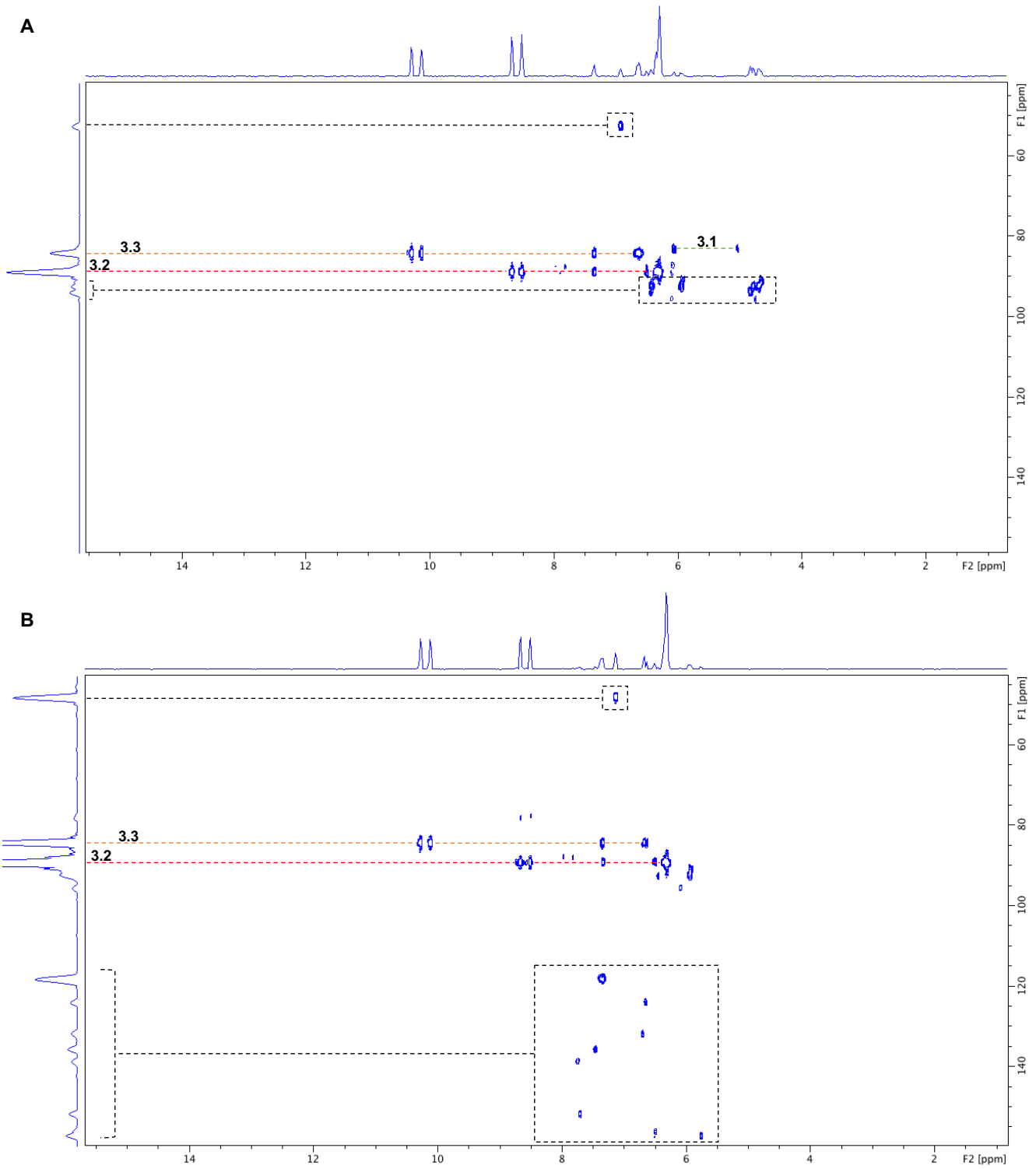

Figure 3.21 ^{1}H ^{15}N HMBC spectra of NO_x autoxidation using **3.1** at (A) 100 minutes, and (B) 140 minutes. Known compounds indicated: **3.1** (green), **3.2** (red), **3.3** (orange). Unknown species indicated with black.

material and nitrated intermediates, however an upfield outlier with a nitrogen shift close to 50 ppm is quite prominent. Although extractions became more difficult post-inhibition, samples up to the 5-hour mark were analyzed using the aforementioned method, after which both phases became miscible. Among a variety of minor peaks observed via PDA, one species (λ_{max} = 256 nm) was observed to accumulate in relatively large quantity from 100 minutes to 180 minutes, subsequently decreasing in integration values afterwards (Figure 3.22). The unknown species, **3.5** could not be accurately quantified due to lack of authentic standard and extraction efficiency data, but appeared quite significant based on peak integration. In order to provide insight on the identity of **3.5** as well as other species, the 180-minute UPLC sample was analyzed using a mass scan (150 to 650 *m/z*) via ESI positive ion mode.

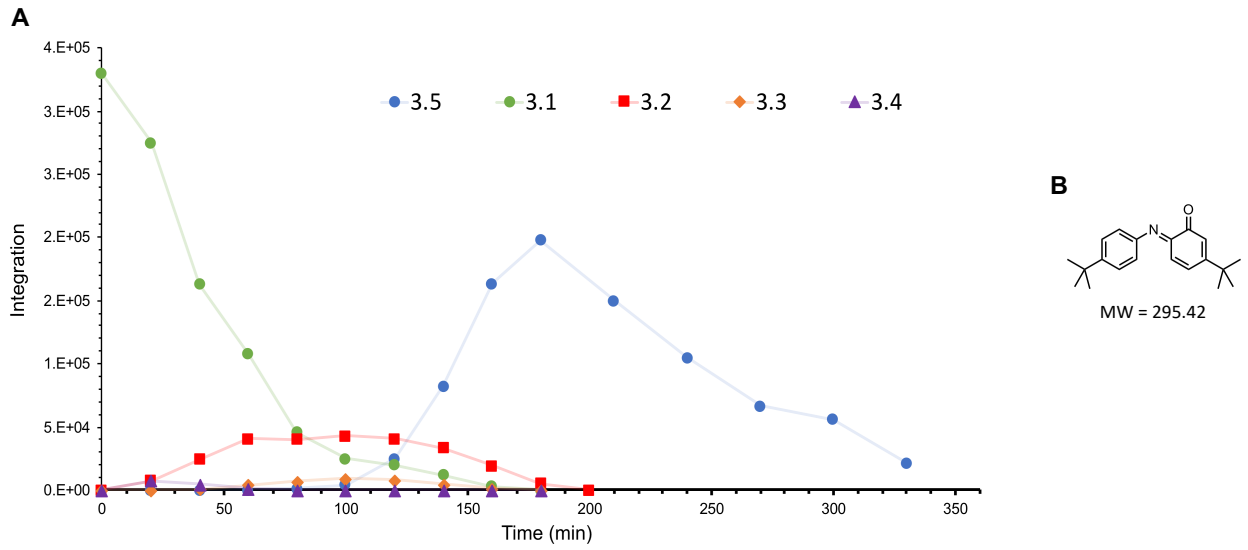

Figure 3.22 (**A**) Formation of unknown species, **3.5** (blue), during autoxidation during and beyond inhibition period. Other species indicated: **3.1** (green), **3.2** (red), **3.3** (orange), **3.4** (purple). (**B**) Proposed chemical structure of **3.1**.

The unknown **3.5** correlated to a strong *m/z* signal at 293.4; close to the molecular weight of the N-aryl iminoquinone (Figure 3.22 B, also highlighted in Chapter 2 as **2.6)**, which has been a product of interest for our group and implicated by Popochień in similar studies.[24] Mass scans of the other prominent chromophores present in the sample did not yield other immediately obvious products (see Appendix Figures S3.4-S3.10 for chromatograms). Efforts to prepare this compound are underway.

3.3 Discussion

Diarylamines are a key component in additive formulations found in commercial lubricants due to their ability to efficiently inhibit high-temperature autoxidation, and by extension, prolong the useful lifetime of lubricants and engine components. Previous reports have implicated NO_x, a major constituent of blow-by gas present in combustion engine conditions, as particularly damaging to substrate and RTA alike.[12,24] As NO_2 has previously been shown to react directly with butylated hydroxytoluene (BHT), we were eager to assess the effect of NO_2 on the efficacy of diarylamine as an RTA and its speciation during an inhibited autoxidation.

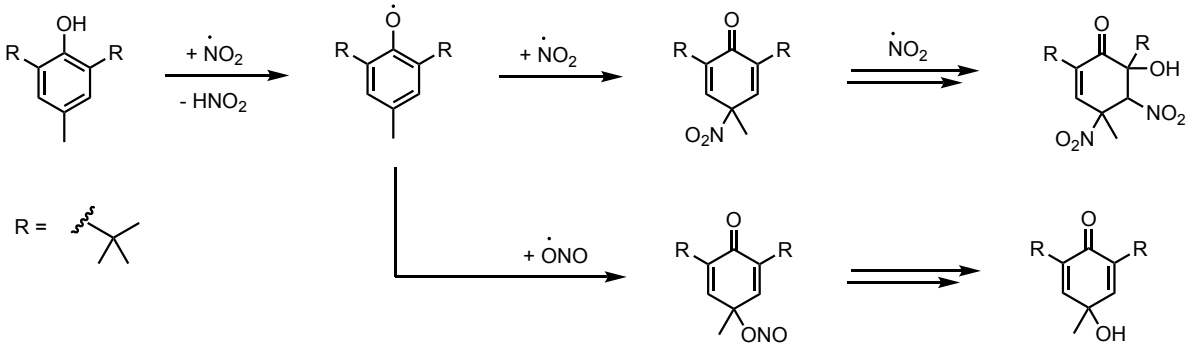

Scheme 3.2 Previously observed products and purported reaction pathways for reaction of butylated hydroxytoluene and nitrogen dioxide under ambient conditions.[39,40]

As expected, the diarylamine performed relatively poorly in the presence of industrially-relevant levels of NO_x in air, however, the degree to which inhibition was reduced was surprisingly drastic. This was the first indicator that NO_x were reacting directly with diarylamine and not simply acting as an initiator. We were gratified that our HMBC protocol used in tandem with isotopically-enriched diarylamine **3.1** enabled the observation of the rapid emergence of intermediates **3.2** and **3.3**, indicating a chemical change to the parent compound. After obtaining mass data for the intermediates, we speculated that radical nitration of the aryl rings was forming *mono*- and *di*-nitro diarylaminic derivatives. The more prominent of the two, **3.2**, had been previously identified in GC-MS studies by Popochień, but **3.3** had not. Popochień had also depicted **3.2** in its tautomeric form, having not undergone re-aromatization (Figure 3.2). This is an important distinction as restoring aromaticity is not only energetically favourable, but regenerates the amine from the imine; a species

much more likely to possess RTA activity. Although one might not expect tautomerization to be particularly facile in hexadecane or similar substrates, previous studies have unequivocally demonstrated that they do occur.[41] However, we anticipated that **3.2** and **3.3** would possess little to no RTA activity due to the 'deactivation' of the aryl substituents. Previous studies on structure-activity relationships of diarylamines demonstrate that equipping them with electron-donating substituents greatly improves performance.[25,36,38] Diarylamines with such features possess lower N-H BDEs, resulting in increased k_{inh} values, and therefore, the ability to more quickly react with propagating peroxyls. Conversely, electron-withdrawing substituents, such as nitro substituents, have the opposite effect: the N-H bond is strengthened, decreasing the rate at which formal H-atom transfer to a peroxyl radical occurs. Although the kinetics of HAT are governed by other factors (as previously discussed), BDE values can provide insight as to why the rate decreases: nitration of *di*-tolylamine (DTA) at the *ortho* position results in a N-H BDE increase of 6.3 kcal/mol. Once formed, the drastic decrease in lability of the N-H bond leaves it closer to general BDEs of secondary or tertiary C-H bonds at 94.5 kcal/mol and 91.0 kcal/mol, respectively;[43] much higher than that of a diarylamine of reasonable performance (i.e. 80-85 kcal/mol). Unsurprisingly, neither **3.2** or **3.3** showed significant RTA activity at ambient or elevated temperatures, only retarding autoxidation of cumene at 37˚C or 1-hexadecene and *n*-hexadecane at 100˚C and 160˚C, respectively, when used in much higher concentration than the parent diarylamine.

In terms of formation, *ortho*-nitration is thermodynamically less favourable than combination between aminyl and peroxyl radicals (Scheme 3.3).[42] Yet, our experimental results demonstrate that the **3.2** accumulated to a significant degree.

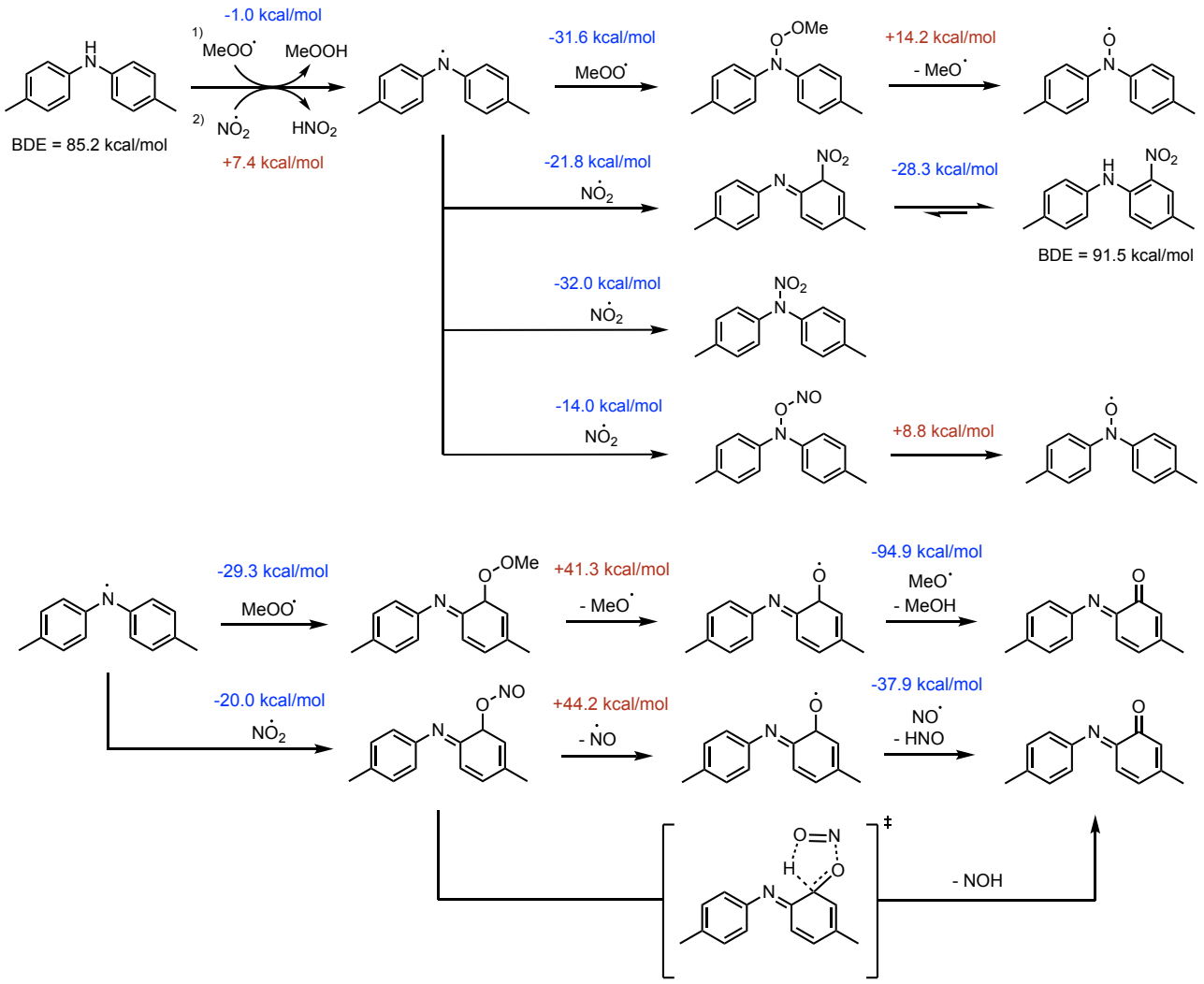

Scheme 3.3 Relevant free energies and bond dissociation enthalpies for reactions between *di*-tolylamine and either (methyl)peroxyl radicals or NO_2 at the CBS-QB3 level of theory.[42]

It is difficult to draw any concrete, mechanistic conclusions about the formation of **3.2** and **3.3** without kinetic data but computations can provide insight into the thermodynamically favoured pathways. Initial H-atom of abstraction of DTA is predicted to be much more favourable for peroxyl radicals than NO_2, owing to the fact that the O-H bond of a hydroperoxide is ca. 8 kcal/mol stronger than the N-H bond in HNO_2 (experimental values have been reported as 87.8 kcal/mol vs. 79.0 kcal/mol, respectively).[43,44] However, subsequent reactions between the resultant diarylaminyl radical and either methylperoxyl or NO_2 are similarly downhill. Peroxyl radical combination with the diarylaminyl radical is still favoured over *ortho*-nitration by almost 10 kcal/mol, but

formation of the nitroxide via O-O homolysis is a steep uphill climb compared to restoring aromaticity of the *ortho*-nitro imine. Although NO_2 acts as an initiator to generate alkyl radicals which rapidly form peroxyls, we cannot disregard the possibility that the immediate input of NO_2 into the system could be responsible for the rapid formation of **3.2**. Per our calculations, HAT from diarylamine to NO_2 is less favourable than to peroxyls, yet the steady-state concentration of peroxyls in the early stages of autoxidation are likely to be much lower than that of NO_2. If this is the case, perhaps competition for diarylaminyl radicals between NO_2 and peroxyl radicals is skewed in favour of NO_2, as one would expect the rates of radical-radical combination to be similar. Reports on the kinetics of HAT between NO_2 and hydrocarbons are scarce, and work that has been carried out has only examined such reactions at ambient temperatures.[9,19] Reactions between NO_2 and saturated hydrocarbons are immeasurably slow under such conditions, yet rates likely increase significantly at 160˚C. Investigations into the rates of HAT between NO_2 and **3.1**, as well as *n*-hexadecane (or similar) at high temperatures would be required to solidify our understanding of how **3.2** forms.

Another important observation is the appearance of **3.3**, which was not previously identified in similar studies.[24] Our immediate assumption is that formation of **3.3** relies upon a radical mechanism similar to that of **3.2** (Scheme 3.4). We noted that the BDE of **3.2** likely precluded it from reacting effectively with peroxyl radicals to inhibit autoxidation, as demonstrated by its abysmal rate constants at 37˚C and 100˚C, yet that it is still reactive enough to be consumed alongside substrate. Our UPLC quantification experiments demonstrated the concentration decrease of **3.2** over time, and HMBC experiments unequivocally showed its full conversion to other products. This is unsurprising, as the N-H BDE of **3.2** is still much lower than that of a 2˚ C-H, and hydrogen-atom abstraction from **3.2** by a peroxyl or NO_2 is kinetically more favourable due to polar effects, triplet repulsion, and secondary orbital effects (see Chapter 1 for details). Furthermore, formation of **3.3** in the absence of diarylaminyl radical would in turn require the HNO_3 to generate the nitronium ions; assuming the reaction would proceed via electrophilic aromatic substitution. However, there is little precedent to suggest HNO_3, let alone NO_2^+, forms under the experimental conditions.

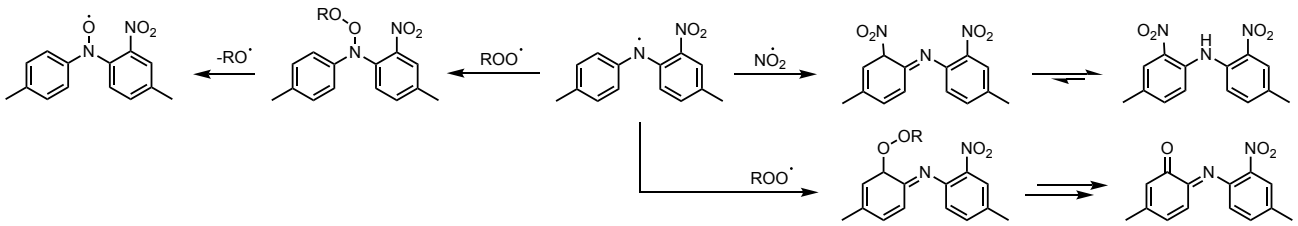

Scheme 3.4 Putative competing fates of the nitrated diarylaminyl radical in autoxidations carried out in the presence of NO_x.

The inability of **3.2** to effectively inhibit autoxidation of 1-hexadecene at 100˚C perhaps indicates that combination of diarylaminyl and peroxyl radicals (or NO_2) to form the **3.2**-derived nitroxide is either kinetically slow due to steric encumbrance, thermodynamically unfavourable, or both. Inhibitory activity, albeit meagre, is observed by both **3.2** and **3.3** in cumene and 1-hexadecene, suggesting that H-atom abstraction still occurs. However, the activity in 1-hexadecene could be solely due to initial H-atom abstraction; it is difficult to invoke the formation of reasonable amounts of nitroxide *in situ* with such poor activity demonstrated. Assuming the aminyl radical of **3.2** forms via H-atom abstraction, it demonstrates little ability to form nitroxide from its aminyl radical, likely due to steric bulk of the neighbouring NO_2. Thus, the only productive pathway forward would be *ortho*-nitration or peroxyl addition via the corresponding imine; far removed from steric interactions of the other aryl substituent (Scheme 3.4). In order to support the plausibility of this hypothesis, attempts could be made to synthesize **3.2**-derived nitroxide in a system void of NO_2 to determine the feasibility of its formation and stability. Computations could also complement the experiments by providing relative energies of the species of interest.

In addition to the mechanism of formation of **3.2** and **3.3**, the degree to which they accumulate during autoxidation is important for diagnosing the severity of the problem and addressing potential solutions. The shocking decrease of inhibition times when autoxidizing substrate with NO_x (in the presence of **3.1**), accompanied by the semi-quantitative data provided by HMBC results, indicated that a significant portion of **3.1** was converted to **3.2** and **3.3**; a suspicion confirmed by quantitative UPLC experiments. The most obvious solution to mitigate nitration of **3.1** would be to block off the vulnerable sites, such as addition of *ortho*-alkyl

groups to aryl substituents. Although past results obtained by our group and others indicate that *ortho*-functionalization reduces RTA efficacy for diarylamines and similar RTA scaffolds like phenothiazines (Figure 3.23 A),[25,32,45-47] a reduction in activity could be tolerated if it were to completely or significantly prevent nitration. Additionally, the use of more potent diarylamines or alternative RTA compounds such as phenoxazine or phenothiazine should be explored (Figure 3.23 B).

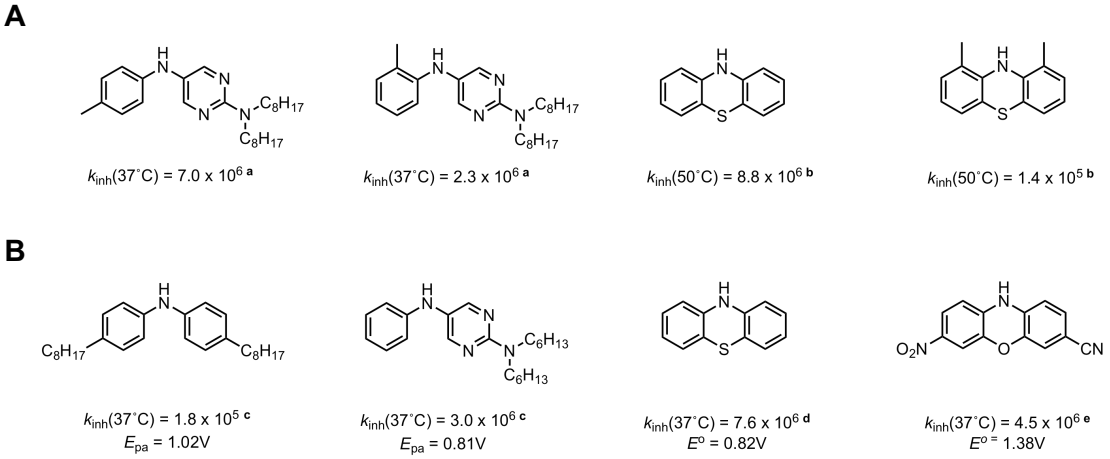

Figure 3.23 (**A**) Comparison of k_{inh} differences between *ortho*-substituted heterocyclic diarylamines and phenothiazines. (**B**) Comparison of relevant properties between *para*-alkylated diphenylamine and other RTA scaffolds.[25,32,45-47] All k_{inh} values in $M^{-1}s^{-1}$. ***a*** Values determined via AIBN-initiated co-autoxidation of PBD-BODIPY and 1,4-dioxane/styrene in PhCl. ***b*** Values determined via AIBN-initiated autoxidation of styrene in benzene. ***c*** Values determined in PhCl using peroxyl radical clock methodology. ***d*** Value determined in PhCl. ***e*** Value determined via AIBN-initiated co-autoxidation of PBD-BODIPY and 1,4-dioxane in PhCl.

Nitration is shown to completely shut down the activity of **3.1**, likely due to a significant drop in k_{inh}. However, it is possible that compounds with far superior k_{inh} values can withstand nitration and still provide acceptable reactivity to retard autoxidation: phenoxazines substituted with strongly electron-withdrawing groups still demonstrate rate constants far-and-above those of 'standard' diarylamines. Such lines of inquest would be informative next steps towards developing robust additive formulations and should be included in future work.

The HMBC procedure provides a picture of 'real-time' speciation that other experiments cannot, and unambiguously differentiates speciation of diarylamine from substrate speciation given the lack of nitrogen in the latter. Interestingly, **3.3** was not identified in reports by Popochień, in which a total of seven compounds were identified, yet was a major product observed by HMBC spectra and chromatographic analysis. Perhaps the absence of **3.3** in reports was due to the differences in conditions, and not other factors. Upon initial consideration, one might anticipate that the primary difference in Popochień's conditions (using NO_2 in N_2, not air) would lead to *more* nitration of starting material.[24] This is assuming though, that NO_2 is sufficiently reactive to abstract a hydrogen atom from the nitrated diarylamine **3.2** and that peroxyl radicals are not necessary for this reaction; NO_2 is approximately 8 kcal/mol more stable than peroxyl, which might preclude formation of the **3.2**-derived aminyl radical in the absence of the latter. Again, little is known about the rates of such reactions and only so much can be surmised on the basis of thermodynamic alone. That said, hydrogen-atom abstraction from **3.2** by NO_2 is more favourable than from a linear, saturated hydrocarbon. Yet the concentration mismatch of said species may have resulted in negligible nitration of **3.2**.

We were also pleased to observe HMBC signal overlap of the *ortho*-diarylamine-dimer (**2.4** in Chapter 2) with speciation of **3.1** early into our autoxidation experiments in the presence of NO_x. Although we lacked the necessary amount of material on-hand to further analyze its formation by UPLC, such work is currently underway. The dimer species **2.4** would have appeared particularly similar to the hydrazine-type dimer 'Product 2' (Figure 3.2) when observed by mass spectrometry. As we demonstrated in our synthesis of **2.4**, such a species is not stable at elevated temperatures and isomerizes to the *ortho*-adduct. Formation of **2.4** in the presence of 765 ppm NO_x, but not under an atmosphere of O_2, is not difficult to rationalize when considering the effect of NO_2 in the initial stages of autoxidation. With the constant flow of NO_2 into the system, high-temperatures likely allow for facile hydrogen-atom abstraction from both substrate and **3.1**, resulting in the formation of diarylaminyl radical at concentrations higher than those when only O_2 is bubbled through the mixture. As a result, diarylaminyl radical couplings occur at increased rates, giving rise to **2.4** at detectable levels. Interestingly, **2.4** is

also an intermediate oxidation product; it still possesses a relatively labile, although sterically encumbered, N-H bond and HMBC spectra indicated its consumption over time. Further studies to quantify its reactivity and accumulation, as well as speciation when autoxidized, will be useful to determine its overall effect on autoxidation and allow for further identification of **3.1**-derived products.

It is not overly surprising that fewer products in total were identified by Popochień: in addition to a lack of oxygen present in the system, the autoxidations were only monitored for 120 minutes and they did not analyze later time points, during which we observed further speciation of intermediates. A significant portion of the ^{15}N species are accounted for by oxidation of **3.1** through O_2-mediated pathways, as signals overlap in a virtually identical manner to analogous experiments outlined in Chapter 2. Yet, a smaller number of products, including the most prominent species based on signal intensity, were demonstrated to be oxidation products of **3.2** and **3.3**. These products were shown to form independent of NO_x, indicating that NO_2 was not incorporated into the structures further. Of these products could be the analogous N-formylated derivative(s), which was observed as one of the more prominent products in O_2 autoxidations (Figure 3.24). Though we anticipate that this is unlikely: formamide production likely results from acyl substitution of the diarylamine on a formate ester, therefore reducing nucleophilicity may preclude this reaction, and would also fail to explain why **3.2** and **3.3** appear to form identical oxidation products, save minor differences. In addition, none of the oxidation products of **3.2** or **3.3** appear to have doublets corresponding to N-H splitting observed for the N-formyl derivative of **3.1**.

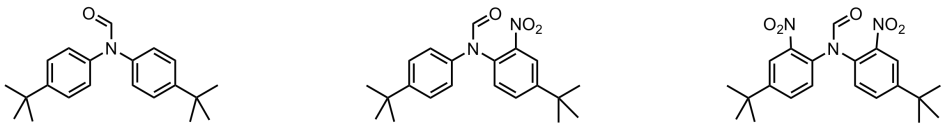

Figure 3.24 N-formylated derivatives of (from left to right): **3.1**, **3.2**, and **3.3**.

Further oxidation of **3.2** and **3.3** might include peroxyl addition to *ortho* or *para* sites on aryl substituents after H-atom abstraction by propagating radicals to generate iminoquinone products, which computations indicate could also be generated through the loss of nitric oxide from nitrosooxy groups at *ortho* positions, should they form (Scheme 3.2, Scheme 3.5).[42]

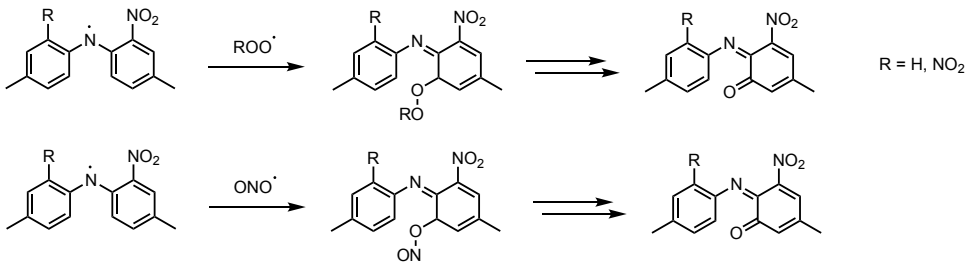

Scheme 3.5 Potential pathway of formation of iminoquinone products bearing nitro groups.

Such a result may explain the observed overlap between oxidation products of **3.2** and **3.3**. As mass values obtained from scans of UPLC samples provide no clearer insight into speciation, attempts to isolate products via prep-scale experiments may be necessary. Performing decompositions of **3.2** and **3.3** individually at high loadings would provide a simplified product distribution for analysis and isolation.

The remainder of products formed under NO_x did not derive from **3.2** or **3.3** but were also not correlated to any products observed under O_2, suggesting alternative nitrations occurred or that substrate-derived products unique to NO_x conditions interact with **3.1** to generate unique speciation. Other likely, alternative nitration modes are N-nitration to generate nitramines or *para*-nitration, the latter of which requires NO_2 to combine with diarylaminyl radical at a position hindered by the bulky *tert*-butyl substituent (Scheme 3.6 A).

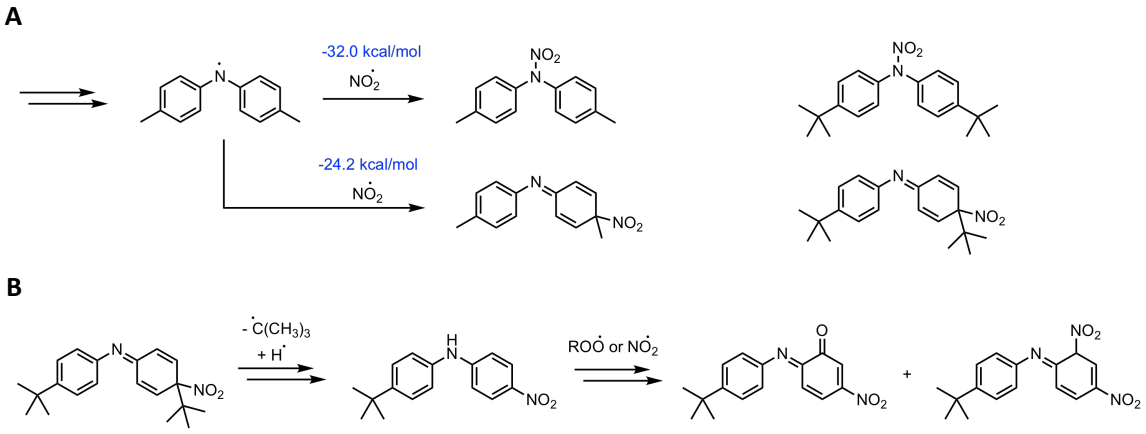

Scheme 3.6 (**A**) Alternative nitration modes to *ortho*: N-nitration and *para*-nitration of DTA, alongside analogous products for **3.1**. Free-energy structure calculated at CBS-QB3 level of theory.[42] (**B**) Re-aromatization and further nitration/oxidation of *para*-nitrated compound.

Calculations show that the resulting structure is thermodynamically downhill when bearing a methyl substituent, but steric hinderance of the *tert*-butyl group might prevent such an outcome.[42] Loss of the *tert*-butyl group would allow for re-aromatization and subsequent nitration or oxidation of the *para*-nitro aryl substituent, but we have no computational basis to support these outcomes (Scheme 3.6 B). As we have already identified the formation of the dimer product **2.4** in the presence of NO_x, perhaps similar dimer products arise due to such increases in diarylaminyl radical; this outcome was highlighted by the work of Popochień. In addition, the consumption of **2.4** indicates that such species may remain reactive to further oxidation or nitration, therefore a myriad of potential products could be envisioned. Computational predictions and prep-scale isolations would likely be the most useful tools to explore such avenues. The effect of NO_x on substrate was not a point of focus in this work, but may be partially responsible for the differences in speciation of **3.1** observed. Thus far, however, we have no evidence of substrate incorporation into diarylaminic oxidation products, under either O_2 or NO_x, and similar reports are void of such species.[24] In addition, the products of *n*-hexadecane autoxidation under NO_x at elevated temperatures have not been reported in the literature. Identifying products of such nature would likely require isolation via preparative chromatography as predicting the outcome of the numerous potential reactions becomes exceedingly difficult.

Results from autoxidations under NO_x differ from those in O_2 as they provide a clear strategy for improving diarylamine, or RTA, performance: prevent the formation of nitrated species or design RTAs that can withstand nitration. However, the unexplained drop in mass balance at the beginning of the experiment and the formation of later oxidation products require further examination to improve our understanding of diarylamine-oxidation pathways. The speciation differences observed were largely attributed to the formation of the intermediates **3.2** and **3.3**, but HMBC spectra indicated that some of the oxidation products unique to NO_x autoxidation were not derived from either compound (Figure 3.18). Determining the speciation will likely require similar efforts to those described in Chapter 2, of which computational work will play a large role. However, NO_x autoxidations differed in that time-point samples were immiscible with extraction solvent long

past the end of inhibition, enabling the use of chromatographic techniques much further into speciation periods. Coupling this with large-scale experiments (higher loadings of RTA) might allow for oxidation products to be isolated through prep-HPLC methods rather than obtained via targeted synthetic and computational efforts. The chemical structures of products that have been previously identified make for difficult syntheses, therefore HPLC isolation would prove valuable to complement computations. HMBC would also be a key factor in such experiments, as it could be used to confirm the species present in post-extracted HPLC samples and then back-compared to the observed species during autoxidation experiments; a measure that previous studies have not possessed. Future computational work should also include calculations of energy barriers and transition states to complement the previous calculations of free energy structures.

3.4 Conclusions

Our examination of diarylamine-inhibited hydrocarbon autoxidation at elevated temperatures using levels of NO_x relevant in engine lubricants in air demonstrated a decrease in RTA performance by over 75% compared to analogous experiments under O_2. Through use of our recently developed ^{1}H ^{15}N HMBC technique we observed two significant transformations of a diarylamine RTA in the early stages of the autoxidations. The first transformation, nitration of the diarylamine, had been previously reported in similar experiments, but the second transformation, further nitration of the diarylamine, has only now been uncovered. Subsequently, we were able to synthesize authentic standards of each product and demonstrate their inability to effectively suppress hydrocarbon autoxidation in various substrates across a range of temperatures. Realizing the importance of such a finding regarding the use of diarylamine additives in such systems, we quantified the accumulation of these non-RTA products during autoxidation and found that over 50% of the parent diarylamine was nitrated to such end. The lack of RTA activity of the aforementioned products, in addition to the large concentrations of their accumulation, highlight that standard, *para*-alkylated diarylamines are not optimized for use under such conditions. Our results exhibit that in absence of alternative NO_x scavengers, more reactive or robust RTAs are likely necessary to provide sustained periods of inhibition, and should be the subject of further

study. In addition, continued efforts are required to determine the fate(s) of diarylamine that have eluded us so far. Determining the products that account for the remainder of the mass balance at the beginning of experiments, as well as the multitude of species observed towards the end, should remain a priority.

3.5 References

[1] Studzinski, W. M.; Liiva, P. M.; Choate, P. J.; Acker, W. P.; Litzinger, T.; Bower, S.; Smooke, M.; Brezinsky, K. *SAE Technical Paper No. 932815*, **1993**.

[2] Turns, S. R. *Prog. Energy. Combust. Sci.,* **1995**, *21*, 361-365.

[3] Raine, R. R.; Stone, C. R.; Gould, J. *Combust. Flame.* **1995**, *102*, 241-255.

[4] Rakopolous, C. D.; Michos, C. N. *Eng. Conv. Manag.* **2008**, *29,* 2924-2938.

[5] Fenimore, C. P. *Thirteenth International Symposium on Combustion. The Combustion Institute.* **1970**, 313.

[6] Hartung, J. *Chem. Rev.* **2009**, *109*, 4500-4517.

[7] Miller, J. A.; Bowman, C. T. *Prog. Energy. Combust. Sci.,* **1989**, *15*, 287-338.

[8] Kones, J. *Int. Combust. Eng.* **2003**, *10*, 1-2.

[9] Huie, R. E. *Toxicology*. **1994**, *89*, 193-216.

[10] Baulch, D. L.; Bowman, C. T.; Cobos, C. J.; Cox, R. A.; Just, Th.; Kerr, J. A.; Pilling, M. J.; Stocker, D.; Troe, J.; Tsang, W.; Walker, R. W.; Warnats, J. *J. Phys. Chem. Ref. Data.* **2005**, *34*, 757-1397.

[11] Spindt, R. S.; Wolfe, C. L.; Stevens, D. R. *SAE Trans.* **1957**. *64,* 797.

[12] Johnson, M. D.; Korcek, S. *Lubri. Sci.* **1991**, *3*, 95-118.

[13] Davydov, E. Y.; Korcek, S.; Jensen, R. K.; Zaikov, G. E. *Int. J. Polymeric Mater.* **1997**, *37*, 201-216.

[14] Stark, M. S.; Gamble, R. J.; Hammond, C. J.; Gillespie, H. M.; Lindsay Smith, J. R.; Nagatomi, E.; Priest, M.; Taylor, C. M.; Taylor, R. I.; Waddington, D. J. *Trib. Lett.* **2005**, *19*, 163-168.

[15] Gamble, R. J.; Priest, M.; Taylor, C. M. *Trib. Lett.* **2003**, *14*, 147-156.

[16] Kreuz, K. L. *Lubrication.* **1969**, *55*.

[17] Bardy, D. C.; Assef, P. A. *SAE Technical Paper No. 700508,* **1970.**

[18] Moritani, H.; Nozawa, Y. *R&D Rev. Toyota CRDL.* **2003**, *38*, 36-43.

[19] Titov, A. I. *Tetrahderon.* **1963**, *19*, 557-580.

[20] Adachi, H.; Basco, N. *Int. J. Chem. Kinet.* **1982**, *14*, 1243-1251.

[21] Albright, L. F. Nitration. In *Encyclopedia of Chemical Technology, 3rd ed.* Purdue University, **1981**, Vol. 15, 841-853.

[22] Atkinson, R.; Aschman, S. M.; Carter, P. L.; Winer, A. M.; Pitts, J. N. *J. Phys. Chem.* **1982**, *86*, 4563-4569.

[23] Ptyor, W. A.; Castle, L.; Church, D. F. *J. Am. Chem. Soc.* **1985**, *107*, 211-217.

[24] Popochień, B. A. *Interactions of Antioxidants with NO_x at Elevated Temperatures.* Ph.D. Dissertation, University of York, York, UK. **2012**.

[25] Shah, R.; Haidasz, E. A.; Valgimigli, L.; Pratt D,. A. *J. Am. Chem. Soc.* **2015**, *137,* 7*,* 2440-2443.

[26] Jensen, R. K.; Korcek, S.; Zinbo, M.; Gerlock, J. L. *J. Org. Chem.* **1995**, *60*, 5396-5400.

[27] Bolsman, T.; Blok, A. P.; Frijns, J. *Recl. Trav. Chim. Pays-Bas.* **1978**, *97*, 310-312.

[28] Shah, R.; Pratt, D. A. *J. Org. Chem.* **2016**, *81,* 15*,* 6649-6656.

[29] Ingold, K. U. *Can. J. Chem.* **1963**, *41*, 2816-2825.

[30] Ingold, K. U.; Pratt, D. A. *Chem. Rev.* **2014**, *114*, 18, 9022-9046.

[31] Poon, J-F.; Pratt, D. A. *Acc. Chem. Res.* **2018**, *51*, 9, 1996-2005.

[32] Farmer, L. A.; Haidasz, E. A.; Griesser, M.; Pratt, D. A. *J. Org. Chem.* **2017**, *82*, 19, 10523-10526.

[33] Hardy, R. C. *J. Res. Natl. Bur. Stand.* **1958**, *61*, 5, 433-436.

[34] Haidasz, E. A.; Van Kessel, A. T. M.; Pratt, D. A. *J. Org. Chem.* **2016**, *81*, 3, 737-744.

[35] Howard, J. A.; Ingold, K. U. *Can. J. Chem.* **1967**, *45*, 793-802.

[36] Hanthorn, J. J.; Amorati, R.; Valgimigli, L.; Pratt, D. A. *J. Org. Chem.* **2012**, *77*, 6895-6907.

[37] Harrison, K. A.; Haidasz, E. A.; Griesser, M.; Pratt, D. A. *Chem. Sci.* **2018**, *9*, 6068-6079.

[38] Valgimigli, L.; Pratt, D. A. *Acc. Chem. Res.* **2015**, *48*, 4, 966-975.

[39] Brunton, G.; Cruse, H. W.; Riches, K. M.; Whittle, A. *Tetrahedron Lett.* **1979**, *12*, 1093-1094.

[40] Astolfi, P.; Panagiotaki, M.; Greci, L. *Eur. J. Org. Chem.* **2005**, 3052-3059.

[41] Haidasz, E. A.; Shah, R.; Pratt, D. A. *J. Am. Chem. Soc.* **2014**, *136*, 47, 16643-16650.

[42] Haidasz, E. A. Unpublished work. University of Ottawa, Ottawa, CA. **2015-2017**.

[43] Kerr, J. A. *Chem. Rev.* **1966**, *66*, 5, 465-500.

[44] Benson, S. W. *J. Chem. Educ.* **1965**, *42*, 9, 502-818.

[45] Shah, R.; Poon, J-F.; Haidasz, E. A.; Pratt, D. A. Unpublished work. **2020**.

[46] Lucarini, M.; Pedrielli, P.; Pedulli, G. F.; Valgimigli, L.; Gigmes, D.; Tordo, P. *J. Am. Chem. Soc.* **1999**, *121*, 11546-11553.

[47] Farmer, L. A. *A Linear Free-Energy Approach to the Study of Substituted Phenoxazines as a Potent Family of Radical-Trapping Antioxidants.* M.Sc. Dissertation, University of Ottawa, Ottawa, CA. **2018**.

3.6 Experimental

Reagents were purchased from commercial suppliers and used without further purification, unless otherwise specified. Column chromatography was performed using flash silica gel (40-63 μm, 230-400 mesh). Products characterization via nuclear magnetic resonance spectroscopy (^{1}H, ^{13}C) was performed using Bruker Avance II 400 MHz, II 300 MHz, or 300 MHz instruments, unless otherwise specified. Chemical shifts for protons are reported in parts per million and are referenced to residual protium in solvent (i.e. ^{1}H NMR: Acetone-d_6 at 2.05 ppm). Chemical shifts for carbon signals are reported in parts per million and are referenced to the carbon resonances of the residual solvent peak (i.e. ^{13}C NMR: Acetone-d_6 at 29.84 ppm). Chemical shifts for nitrogen signals are reported in parts per million and referenced to neat nitromethane (CH_3NO_2) in liquid ammonia (i.e. $CH_3{}^{15}NO2$ at 379.5 ppm with respect to NH_3) and were obtained using a Bruker Avance III 600 MHz cryoprobe. High-resolution mass spectra were obtained using a Kratos Concept Tandem MS.

3.6.1 Uninitiated, high-temperature hydrocarbon autoxidations

A bulk amount of hydrocarbon substrate (*n*-hexadecane, 95%) is run through a silica-alumina column and collected. A 25mL borosilicate test tube is then filled with 10 mL of purified *n*-hexadecane, placed in the 24-tube parallel, stir-flow reactor, and thoroughly degassed with nitrogen (approximately 15 minutes). Primene is then added to the tube while bubbling with nitrogen, and heated to 160˚C. Inhibitor is then added to the mixture, at which point the t = 0 aliquot is removed. The nitrogen flow is then replaced with a 2 L/min flow of 765 ppm NO_2 in air, commencing autoxidation. Aliquots of the mixture are removed from the test tubes via Pasteur pipette at pre-determined intervals, or 'time-points', placed in vials, and either allowed to cool to room temperature for immediate analysis or placed in a -20˚C freezer for storage. Aliquots used for hydroperoxide analysis are obtained in volumes of 50-100 μL. Aliquots used for NMR analysis are obtained in volumes of approx. 600 μL.

3.6.2 Quantifying hydroperoxide concentration of autoxidation samples

5 μL of samples (autoxidation aliquots) are loaded onto a 96-well microplate, incubated at 37˚C, and diluted with a mixture of 20% isopropanol in methanol by the automated reagent dispenser of a BioTek microplate reader. The automated reagent dispenser then adds 30μL of an acetonitrile solution containing 100 mM fluorogenic phosphine dye to each well. Next, the plate undergoes automated stirring for 30 seconds, pauses for 5 seconds, and then measures the fluorescence of each well for 1 minute (coumarin phosphine dye: absorption 340 nm, emission 425 nm). Hydroperoxide concentration in each well is then determined from the rate of phosphine oxidation using the rate constant corresponding to reaction of the dye with secondary hydroperoxides (k = 5.1 $M^{-1}s^{-1}$); assuming pseudo-first order kinetics.

3.6.3 Extraction and TLC-MS analysis of autoxidation samples containing diarylamine & intermediates

500 μL of the autoxidation aliquots is added to a 3 mL vial, followed by 500 μL of acetonitrile. The vial is sealed with a screw-cap and shaken vigorously for thirty seconds. The vial is allowed to rest for a minute, and then the screw-cap is removed to allow for separation. Once the phases have reached maximum separation (approx. 5-10 minutes), with hexadecane residing on top of acetonitrile, the top layer is carefully removed with a pipette. A small portion of acetonitrile is then removed from the bottom of the vial by pipette. The removed portion of acetonitrile is then spotted on an aluminum-backed TLC plate, and air dried. Once all the desired aliquots have been prepared, spotted, dried, and labelled, the plate is developed with a 10-25% diethyl ether in hexanes. Once developed, the plate is air dried and visualized by a short-wave UV lamp, with spots being circled lightly with pencil and labelled numerically or otherwise. Photographs or drawings of the plate are recorded prior to MS analysis. The labelled spots on the plate are then analyzed using both positive and negative APCI via Advion Plate Express/Expression CMS (TLC-MS).

3.6.4 Extraction and UPLC Analysis of autoxidation samples

150 μL of autoxidation samples is added to a small vial, followed by 150 μL of HPLC-grade methanol. After securing the vial with a screw cap, the mixture is vortexed at full power for 2-3 seconds. The vial is allowed to rest for approximately 2 minutes, at which point the *n*-hexadecane separates from the methanol. 50 μL of methanol is removed using an Eppendorf pipette or gas-tight glass syringe, and added to an HPLC vial containing 450 μL of HPLC-grade methanol. After placing an HPLC screw-cap on the vial, it is vortexed, labelled, and analyzed via reverse-phase UPLC using 1 mM NH_4OAc buffer (pH 5.5) with an 80% methanol in water (v/v) mobile phase through a ThermoScientific (250 × 4.6 mm) Hypersil GOLD (5 μ particle size).

3.6.5 Inhibited autoxidation of cumene

Cumene was washed three times with 1M sodium hydroxide, followed by water, and then brine. The organic phase was dried with $MgSO_4$ and filtered. The organic filtrate was then run through a column of silica/basic alumina (1:2) and stored at -20˚C for up to 5 days. The substrate was also purified through a column of silica/basic alumina (1:2) immediately before use. To a quartz cuvette was added 1140 μL HPLC-grade chlorobenzene and 1250 μL cumene. A Teflon screw cap was secured on the cuvette and it was shaken gently to mix the substrates, followed by incubation to the desired temperature. Cuvettes were blanked, after which was added 12.5 μL of STY-BODIPY in trichlorobenzene and 50 μL of 300 mM AIBN in chlorobenzene. The cuvettes were mixed thoroughly and autoxidized for approximately 1-1.5 hours. At this point, RTA stock solutions in chlorobenzene were added and loss of absorbance was monitored for several hours. Inhibition rate constants (k_{inh}) were determined by using the slope of the initial rate of dye consumption.

3.6.6 Inhibited autoxidation of 1-hexadecene

1-hexadecene was run through a column of silica/basic alumina (1:2) twice, and then stored at -20˚C for up to 7 days. To a quartz cuvette was added 440 μL HPLC-grade chlorobenzene and 2000 μL 1-hexadecene. A Teflon screw cap was secured on the cuvette and it was shaken gently to mix the substrates, followed by incubation to

the desired temperature. Cuvettes were blanked, after which was added 12.5 μL of PBD-BODIPY in trichlorobenzene and 50 μL of 50 mM dicumyl peroxide in chlorobenzene. The cuvettes were mixed thoroughly and autoxidized for approximately 5-10 minutes. At this point, RTA stock solutions in chlorobenzene were added and loss of absorbance was monitored for several hours. Inhibition rate constants (k_{inh}) were determined by using the slope of the initial rate of dye consumption.

3.6.7 Menke nitration of ^{14}N and ^{15}N *bis*(4-*tert*-butylphenyl)amine

A dry, round-bottom flask containing a magnetic stir bar is charged with *bis*(4-*tert*-butylphenyl)amine (1.8 mmol, 1 equiv.) and acetic anhydride (3.6 mL, 0.5 M). The mixture is cooled and equilibrated to 0˚C while stirring, at which point copper(II) nitrate (0.9 mmol, 0.5 equiv.) is added portion-wise. The reaction is allowed to stir overnight or for several hours, while warming to room temperature. The reaction progress is monitored by thin-layer chromatography. Once complete, the reaction is placed back on ice while stirring, and neutralized to pH 7 using ammonium hydroxide. The reaction is then extracted 2-3 times using ethyl acetate and water, after which point the organic phases are combined, dried with magnesium sulfate, filtered using vacuum or suction filtration, and concentrated using rotary evaporation. *Mono*- and *di*-nitrated diarylamine products are separated via flash chromatography using a gradient mobile phase (hexanes to 2% ethyl acetate in hexanes), and then purified further by recrystallization out of hexanes at room temperature or -20˚C.

3.6.8 Acid nitration of ^{14}N and ^{15}N *bis*(4-*tert*-butylphenyl)amine

A dry, round-bottom flask containing a magnetic stir bar was charged with *bis*(4-*tert*-butylphenyl)amine (7.1 mmol, 1 equiv.) and chloroform (16 mL, 0.44 M). The mixture is stirred at room temperature, during which time a 1:1 mixture of concentrated nitric acid (1 mL) and concentrated sulfuric acid (1 mL) is prepared on ice. The acid mixture is then slowly added dropwise to the reaction mixture over approx. 2-3 minutes while stirring, changing the reaction colour from clear-beige to a combination of red and black/brown. The reaction progress is monitored by TLC, and is typically complete within 10-15 minutes. Once complete, the reaction is diluted with

water and carefully neutralized to pH 7 with a 10% solution of sodium bicarbonate. The mixture is then extracted with dichloromethane and water twice, and once with brine. The organic phase then dried with magnesium sulfate, filtered using vacuum or suction filtration, and concentrated with rotary evaporation. *Mono*- and *di*-nitrated diarylamine products are separated via flash chromatography using a gradient mobile phase (hexanes to 2% ethyl acetate in hexanes), and then purified further by recrystallization out of hexanes at room temperature or -20˚C.

(2-nitro-4-*tert*-butylphenyl)-4-*tert*-butylphenylamine ^{14}N (3.2)

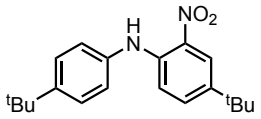

Yield (via 3.6.7): 41%. Vibrant, red crystals, mp = 109˚C; ^{1}H NMR (600 MHz, Acetone-d_6) δ 9.34 (s, 1H), 8.12 (d, J = 2.6 Hz, 1H), 7.63 (dd, J = 8.9, 2.4 Hz, 1H), 7.49 (ddd, J = 9.4, 4.9, 2.8 Hz), 7.30 (ddd, J = 9.4, 4.9, 2.8 Hz, 2H), 7.21 (d, J = 9.3 Hz, 1H), 1.35 (s, 9H), 1.32 (s, 9H). ^{13}C NMR (600 MHz, Acetone-d_6) δ 148.98, 141.99, 141.41, 137.58, 134.72, 133.61, 127.29, 124.76, 122.53, 117.20, 35.03, 34.62, 31.65, 31.20. HRMS (EI): *m/z* Calc $C_{20}H_{26}N_2O_2$: 326.1994 Found: 326.1996.

(2-nitro-4-*tert*-butylphenyl)-4-*tert*-butylphenylamine ^{15}N (3.2)

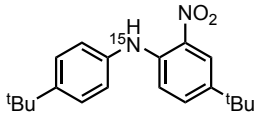

Yield (via 3.6.7): 40%. Vibrant, red crystals, mp = 109˚C; ^{1}H NMR (600 MHz, Acetone-d_6) δ 9.33 (d, J = 93.4 Hz, 1H), 7.63 (dd, J = 9.1, 2.5 Hz, 1H), 7.49 (m, 2H), 7.30 (m, 2H), 7.21 (dd, J = 9.1, 1.9 Hz, 1H), 1.35 (s, 9H), 1.32 (s, 9H). ^{13}C NMR (600 MHz, Acetone-d_6) δ 148.99, 142.05, 141.94, 141.42, 137.64, 137.53, 134.74, 133.61, 127.30, 127.29, 124.78. 124.76, 122.58, 117.21, 35.04, 34.62, 31.65, 31.20. ^{15}N NMR (600 MHz, Acetone-d_6) δ 91.0. HRMS (EI): *m/z* Calc $C_{20}H_{26}{}^{15}NNO_2$: 327.1965 Found: 327.1986.

***bis*(2-nitro-4-*tert*-butylphenyl)amine ^{14}N (3.3)**

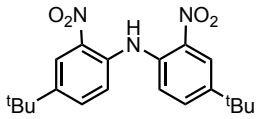

Yield (via 3.6.8): 49%. Vibrant, orange crystals, mp = 162˚C; ^{1}H NMR (400 MHz, Acetone-d_6) δ 10.72 (s, 1H), 8.17 (d, J = 2.3 Hz, 2H), 7.78 (dd, J = 8.8, 2.3 Hz, 2H), 7.65 (d, J = 8.8 Hz, 2H), 1.37 (s, 18H). ^{13}C NMR (600 MHz, Acetone-d_6) δ 146.13, 139.04, 135.92, 133.68, 123.19, 121.09, 35.08, 31.18. HRMS (EI): *m/z* Calc $C_{20}H_{25}N_3O_4$: 371.1845 Found: 371.1826.

***bis*(2-nitro-4-*tert*-butylphenyl)amine ^{15}N (3.3)**

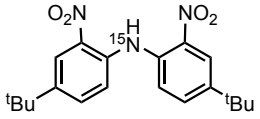

Yield (via 3.6.8): 47%. Vibrant, orange crystals, mp 162˚C; ^{1}H NMR (600 MHz, Acetone-d_6) δ 10.72 (d, J = 94.5 Hz), 8.16 (dd, J = 2.3, 0.7 Hz, 2H), 7.77 (dd, J = 8.8, 2.4 Hz, 2H), 7.65 (m, 2H), 1.37 (s, 18H). ^{13}C NMR (600 MHz, Acetone-d_6) δ 146.13, 139.03, 135.97, 135.85, 133.68, 123.18, 121.09, 35.08, 31.17. ^{15}N NMR (600 MHz, Acetone-d_6) δ 84.9. HRMS (EI): *m/z* Calc $C_{20}H_{25}{}^{15}NN_2O_4$: 327.1815 Found: 327.1855.

3.7 Appendix

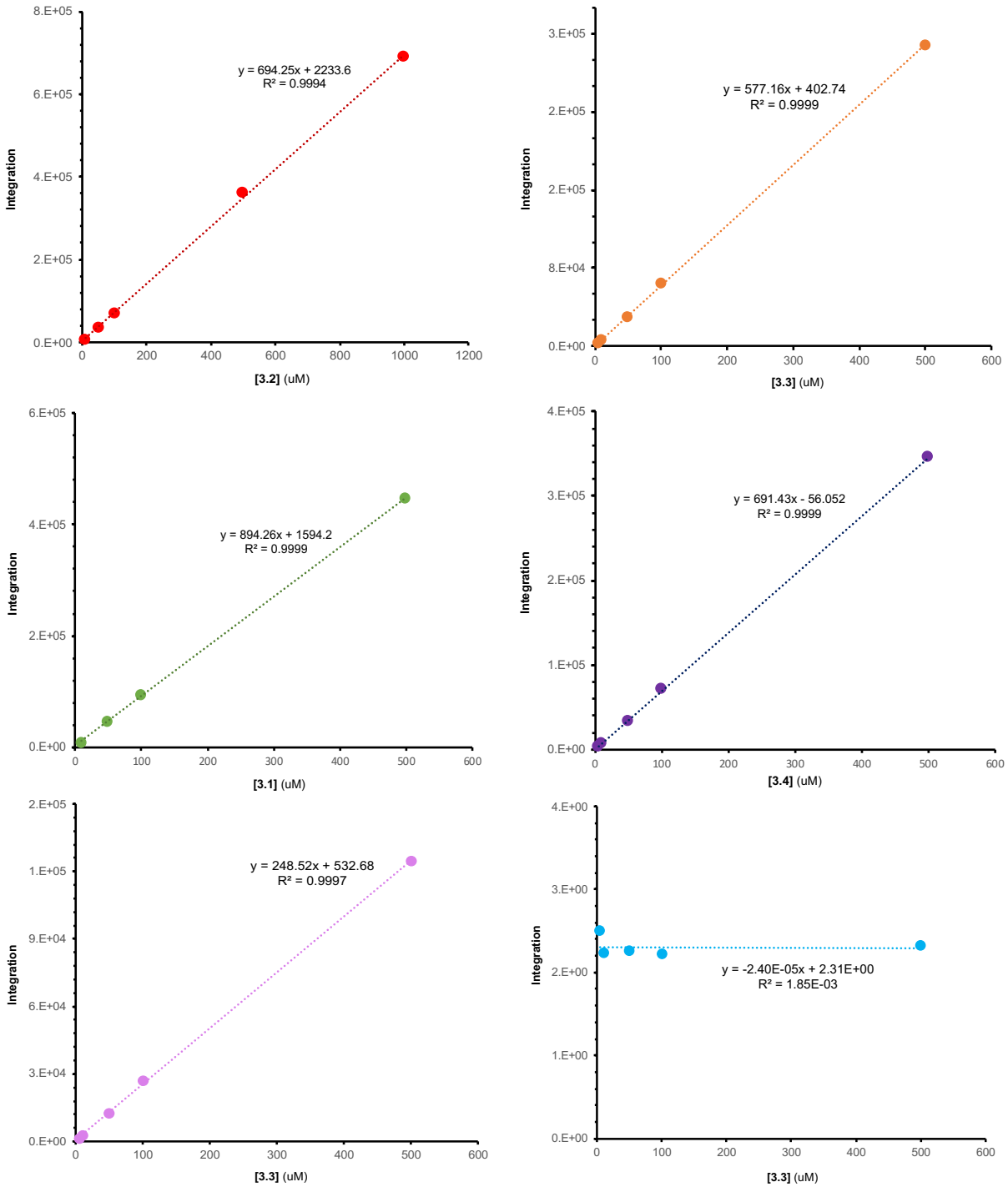

Figure S3.1 Calibration curves for: **3.1** at 285 nm (green), **3.2** at 262 nm (red), **3.3** at 285 nm (orange), **3.4** at 318 nm (purple), **3.3** at 389.5 nm (pink), **3.3** correction of 285/389.5 (blue). Obtained via (RP) UPLC-PDA.

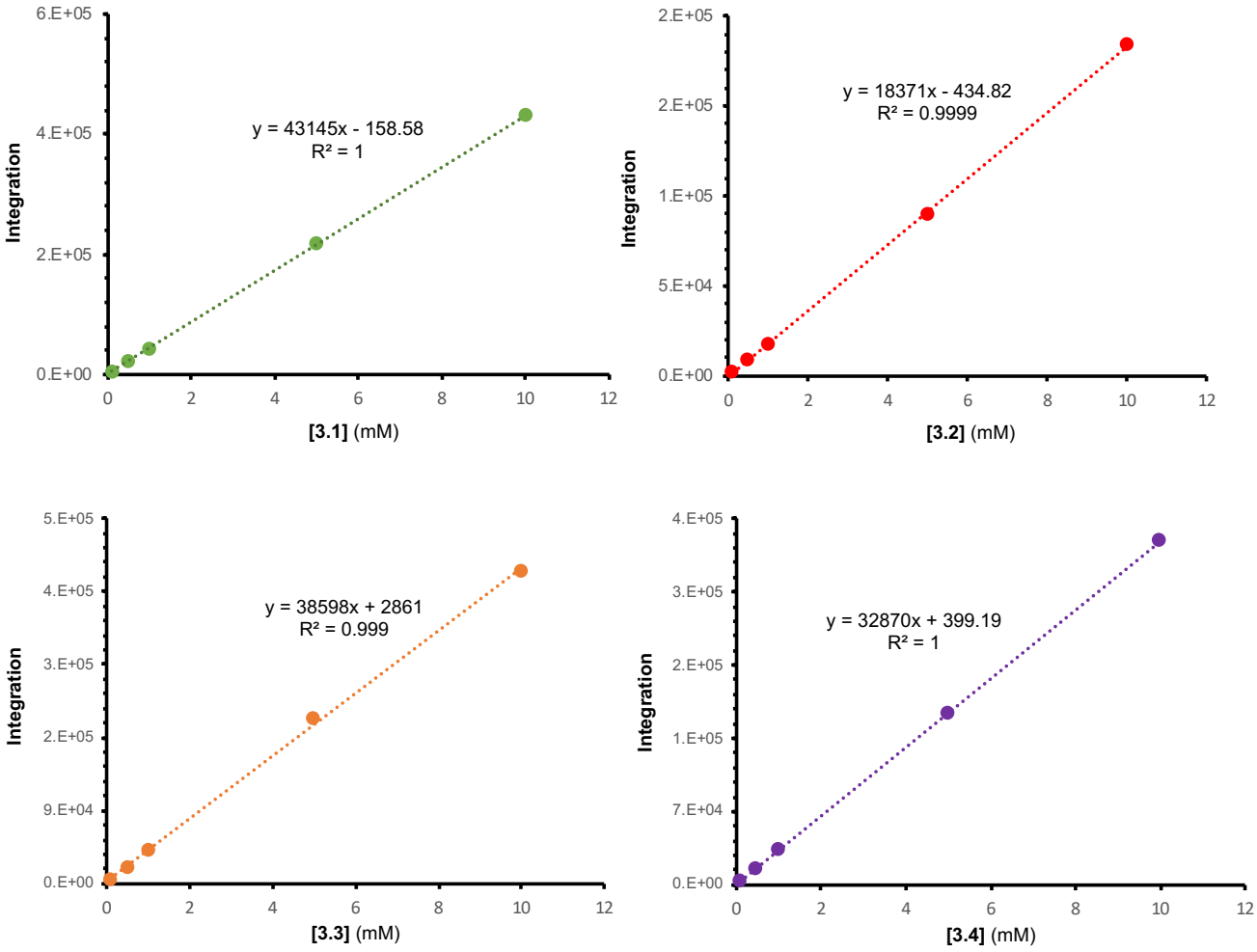

Figure S3.2 Extraction-efficiency calibration curves for: **3.1** at 285 nm (green), **3.2** at 262 nm (red), **3.3** at 285 nm (orange), **3.4** at 318 nm (purple). Obtained via (RP) UPLC-PDA.

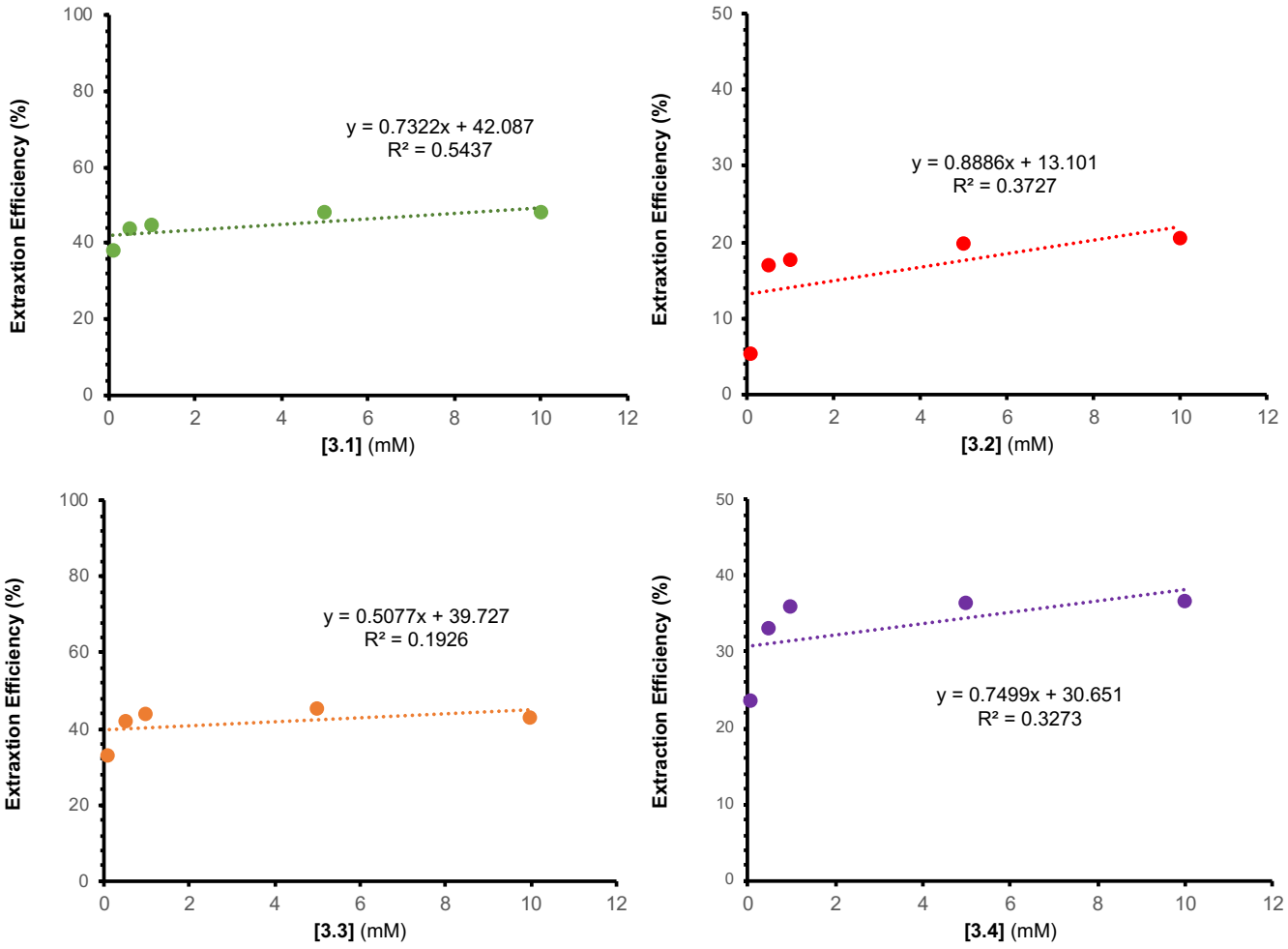

Figure S3.3 Extraction-efficiency calibration factors for: **3.1** at 285 nm (green), **3.2** at 262 nm (red), **3.3** at 285 nm (orange), **3.4** at 318 nm (purple). Obtained via (RP) UPLC-PDA.

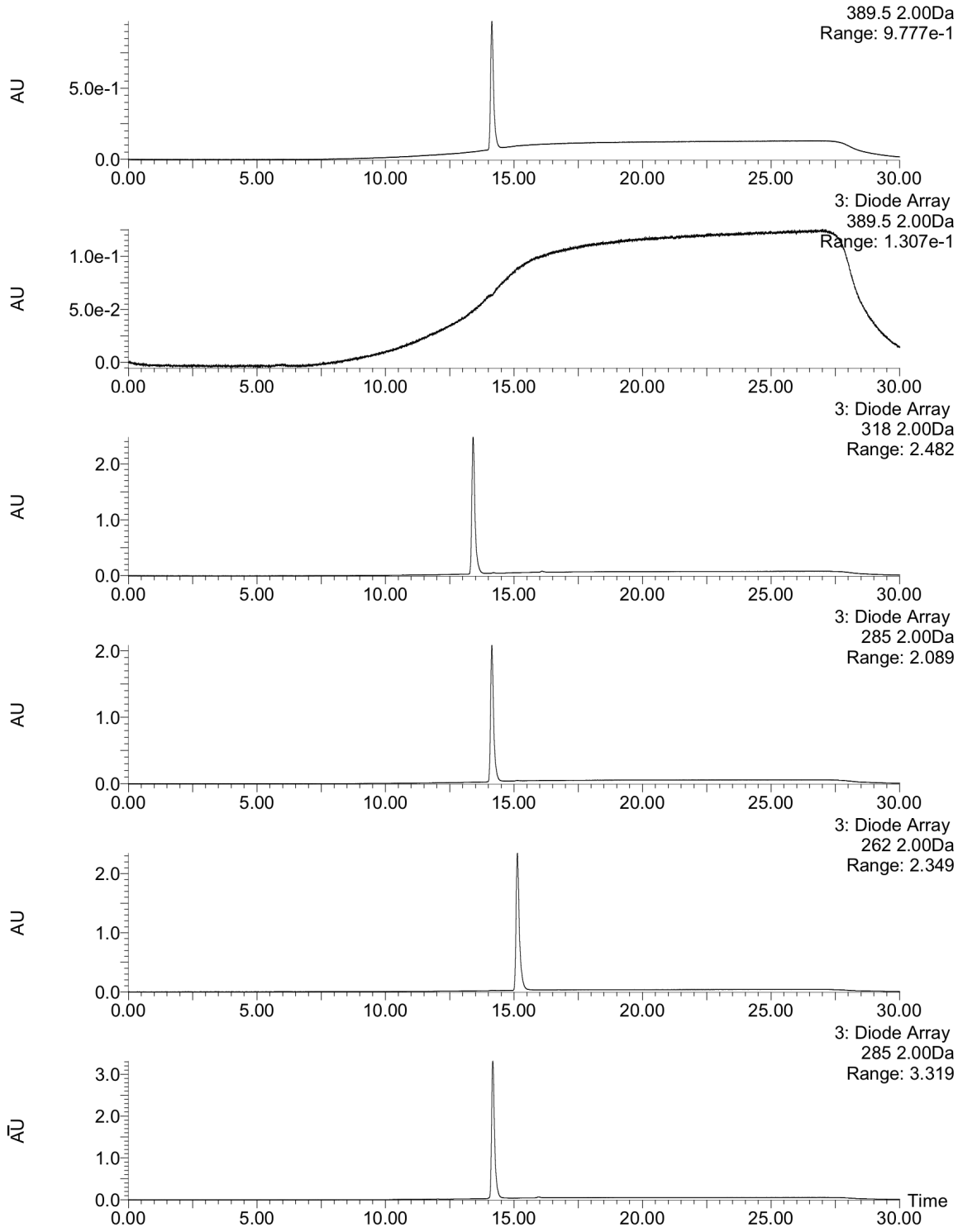

Figure S3.4 Chromatograms from bottom to top: **3.1** at 285 nm, **3.2** at 262 nm, **3.3** at 285 nm, **3.4** at 318 nm, **3.3** at 389.5 nm, **3.1** at 389.5 nm. Obtained via (RP) UPLC-PDA with 500 µM samples.

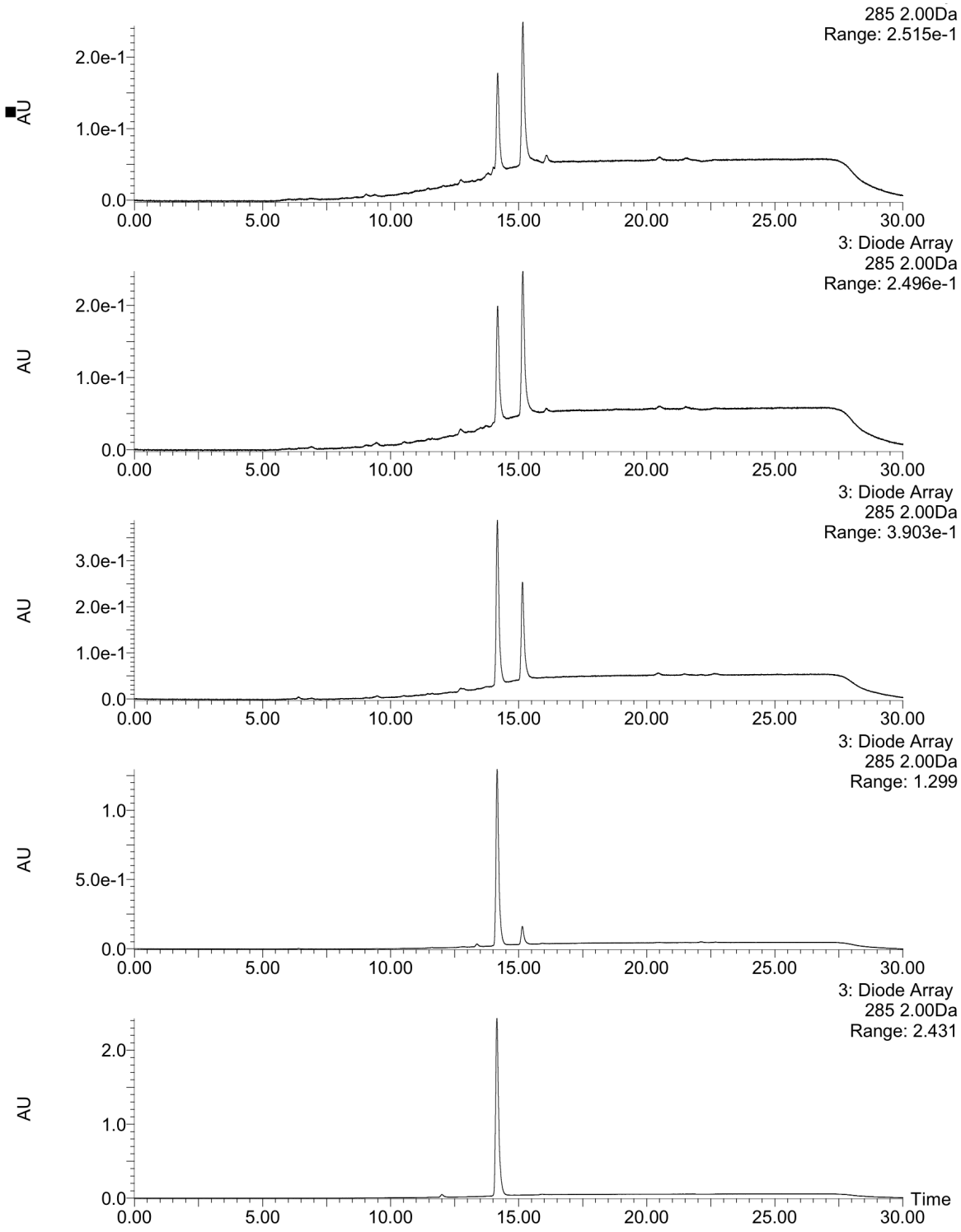

Figure S3.5 Chromatograms for high-temperature autoxidation of *n*-hexadecane inhibited by **3.1,** from bottom to top: 0 h, 40 min, 80 min, 100 min, 120 min. Chromatograms via PDA filtered at 285 nm.

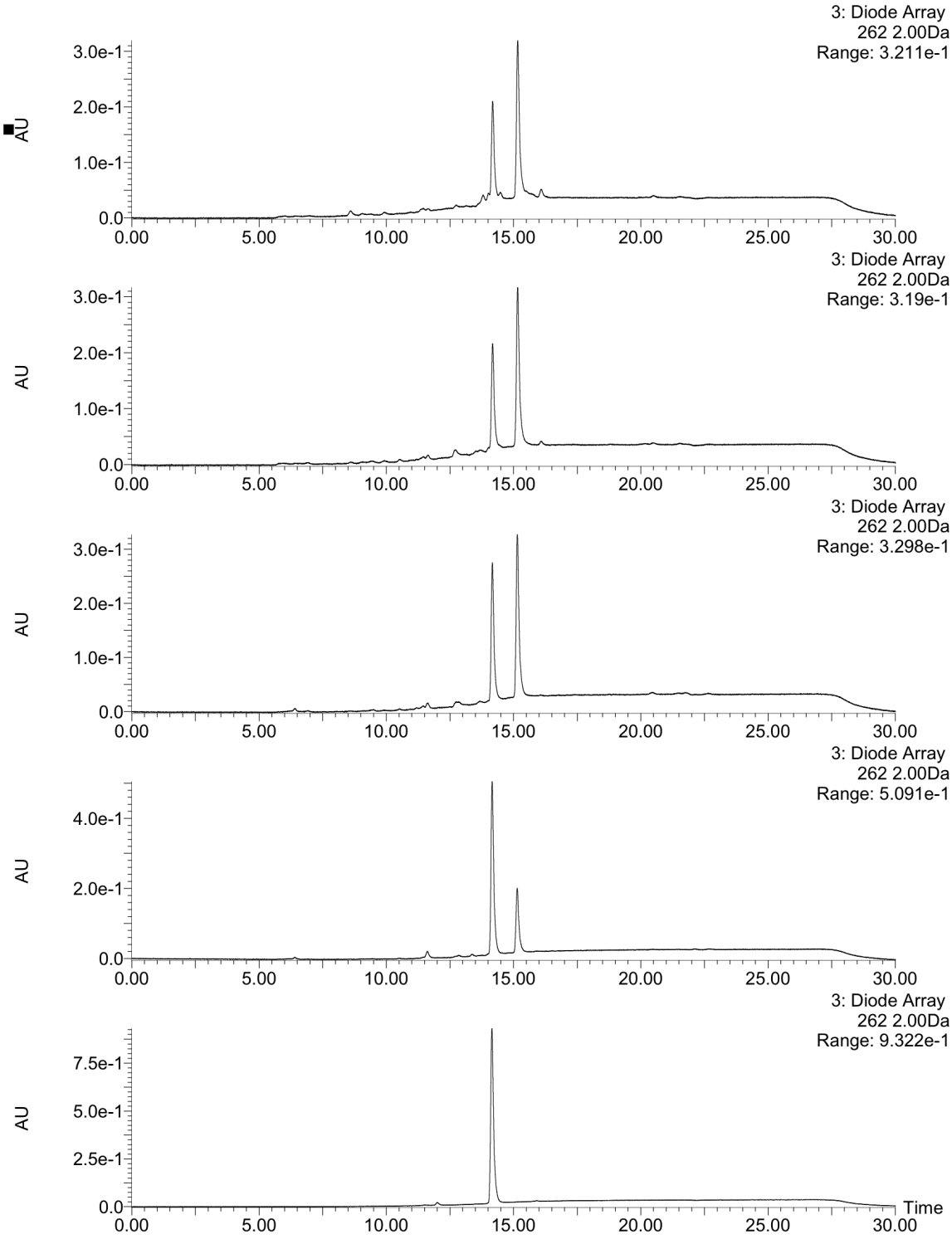

Figure S3.6 Chromatograms for high-temperature autoxidation of *n*-hexadecane inhibited by **3.1,** from bottom to top: 0 h, 40 min, 80 min, 100 min, 120 min. Chromatograms via PDA filtered at 262 nm.

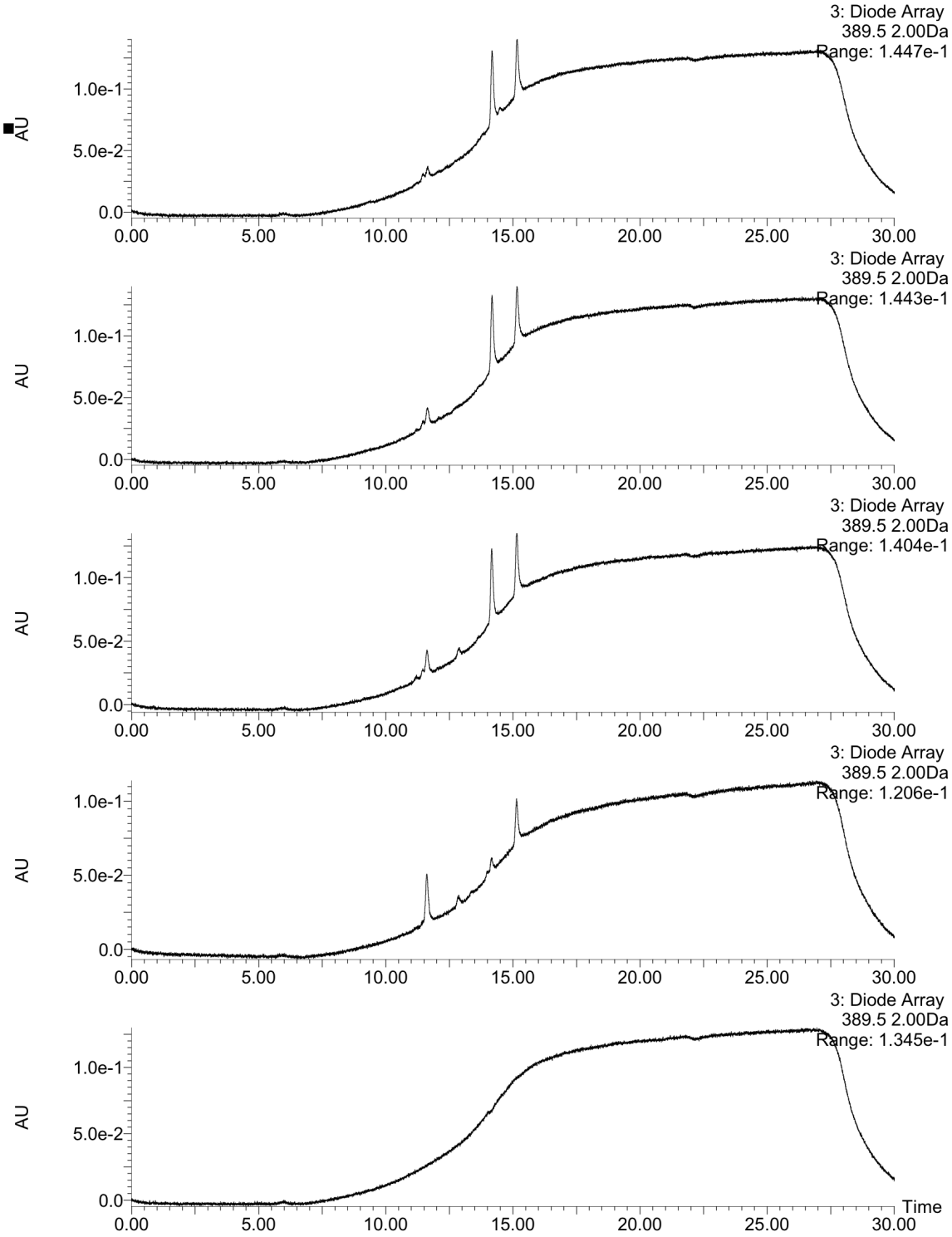

Figure S3.7 Chromatograms for high-temperature autoxidation of *n*-hexadecane inhibited by **3.1,** from bottom to top: 0 h, 40 min, 80 min, 100 min, 120 min. Chromatograms via PDA filtered at 389.5 nm.

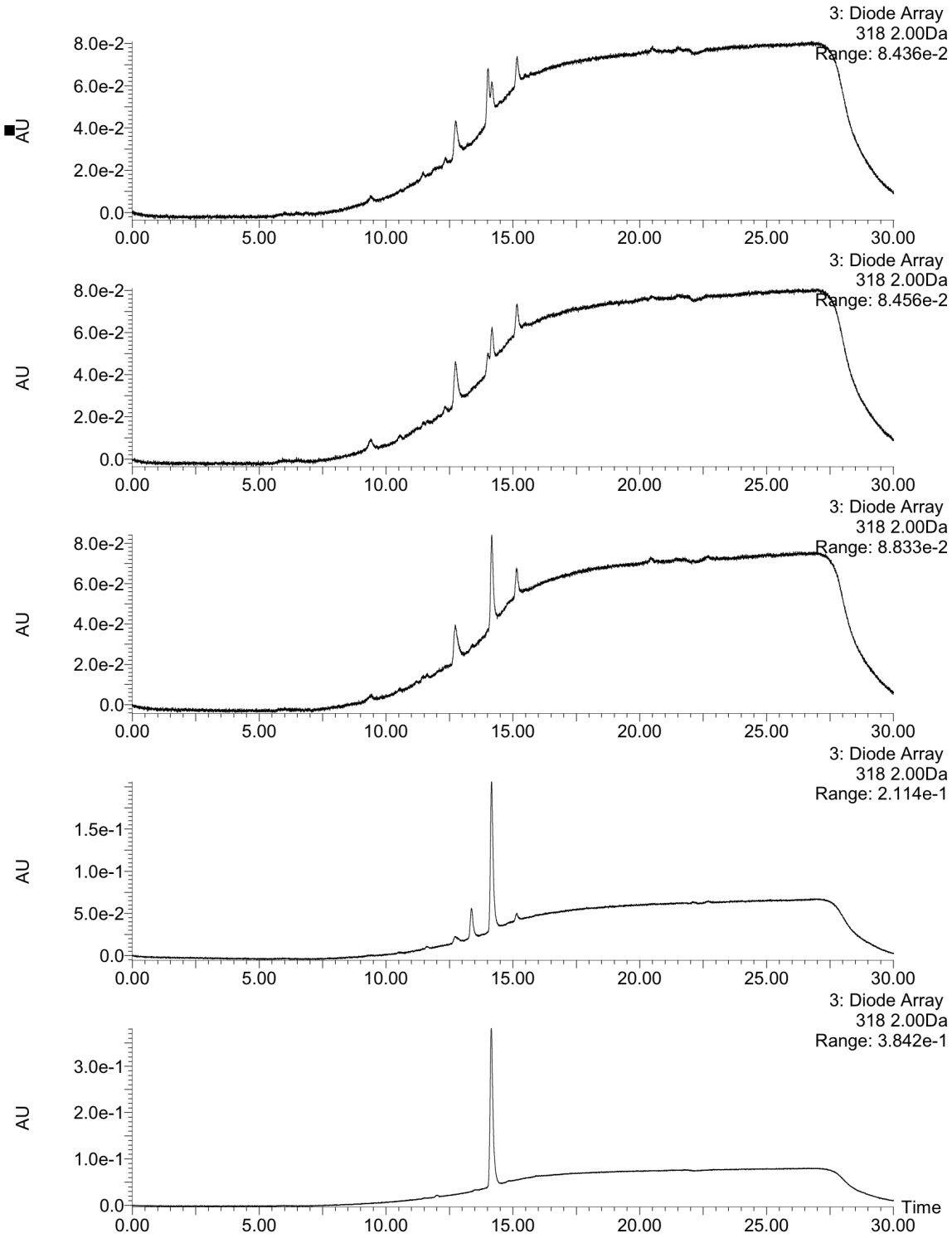

Figure S3.8 Chromatograms for high-temperature autoxidation of *n*-hexadecane inhibited by **3.1,** from bottom to top: 0 h, 40 min, 80 min, 100 min, 120 min. Chromatograms via PDA filtered at 318 nm.

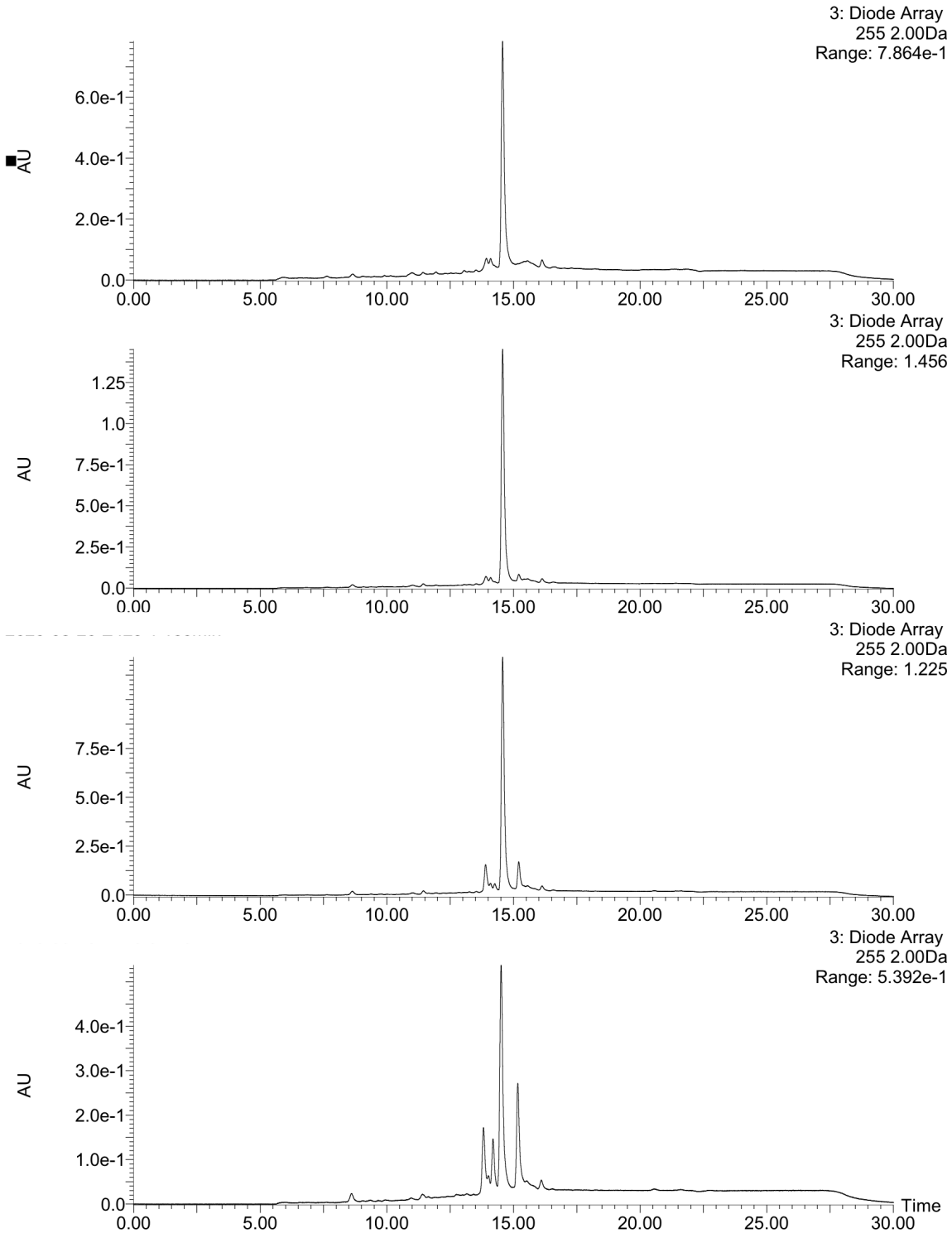

Figure S3.9 Chromatograms for high-temperature autoxidation of *n*-hexadecane inhibited by **3.1,** from top to bottom: 140 min, 160 min, 180 min, 240 min. Chromatograms via PDA filtered at 255 nm.

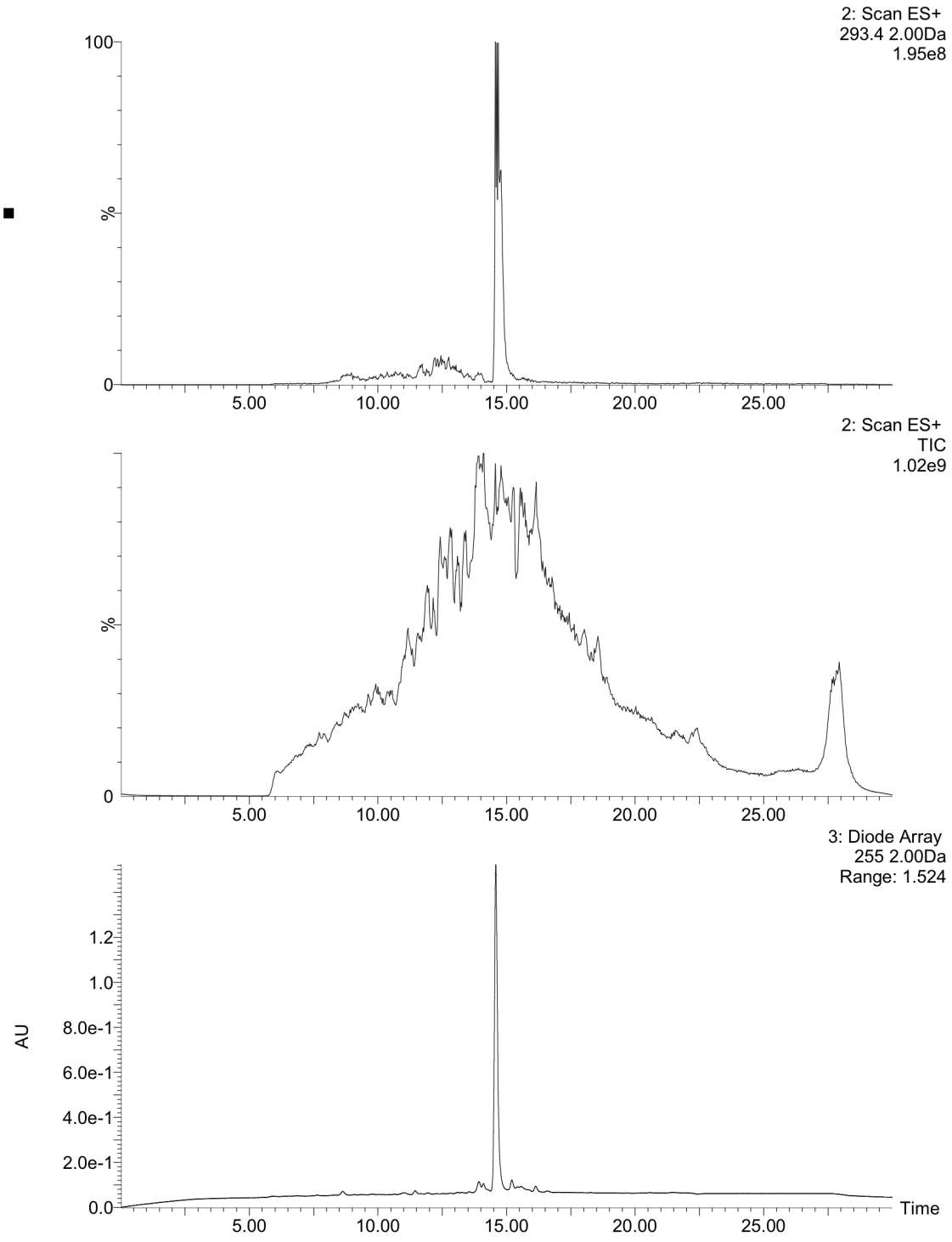

Figure S3.10 Chromatograms for high-temperature autoxidation of *n*-hexadecane inhibited by **3.1** at 180 min, from bottom to top: via PDA filtered at 255 nm, via MS (ESI+) scan 150 to 650, via MS (ESI+) scan filtered at 293.4. Chromatograms via UPLC-PDA or UPLC-MS (ESI+) scan 150 to 650 *m/z*.

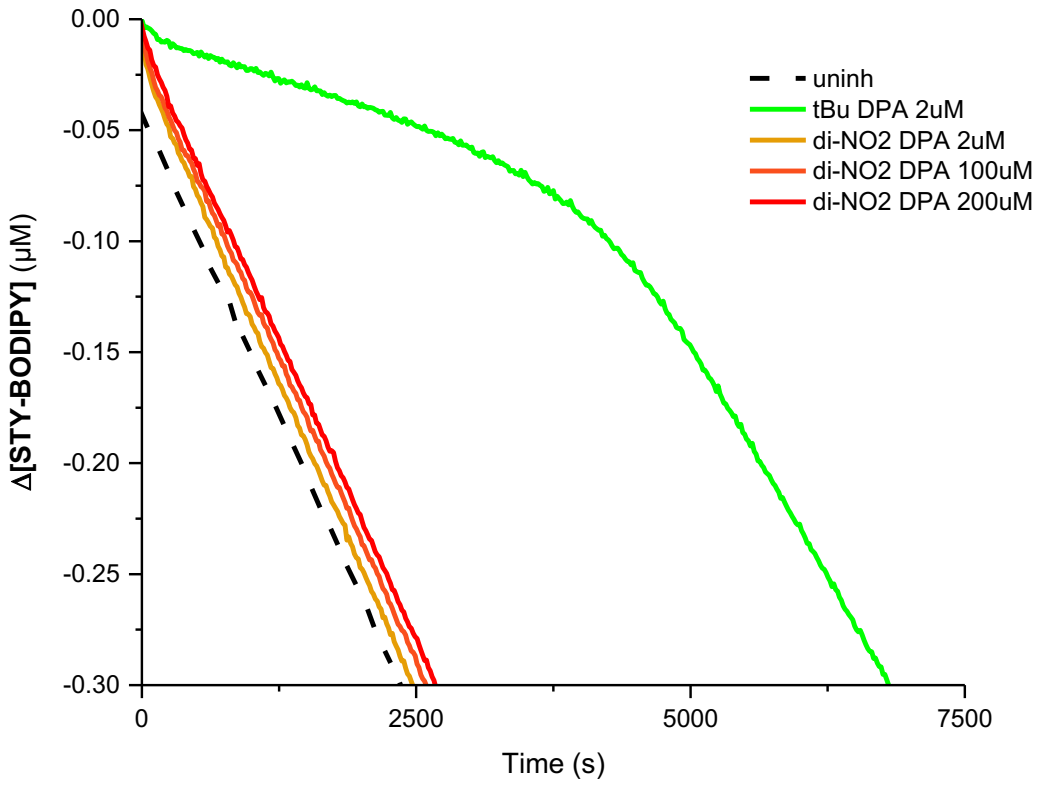

Figure S3.11 Co-autoxidations of cumene (3.6 M) and STY-BODIPY (10 μM) initiated by AIBN (6 mM) in PhCl at 37˚C, inhibited by **3.1** at 2 μM (green), and **3.3** at 2 μM (orange), 100 μM (pink), 200 μM (red).

^{1}H

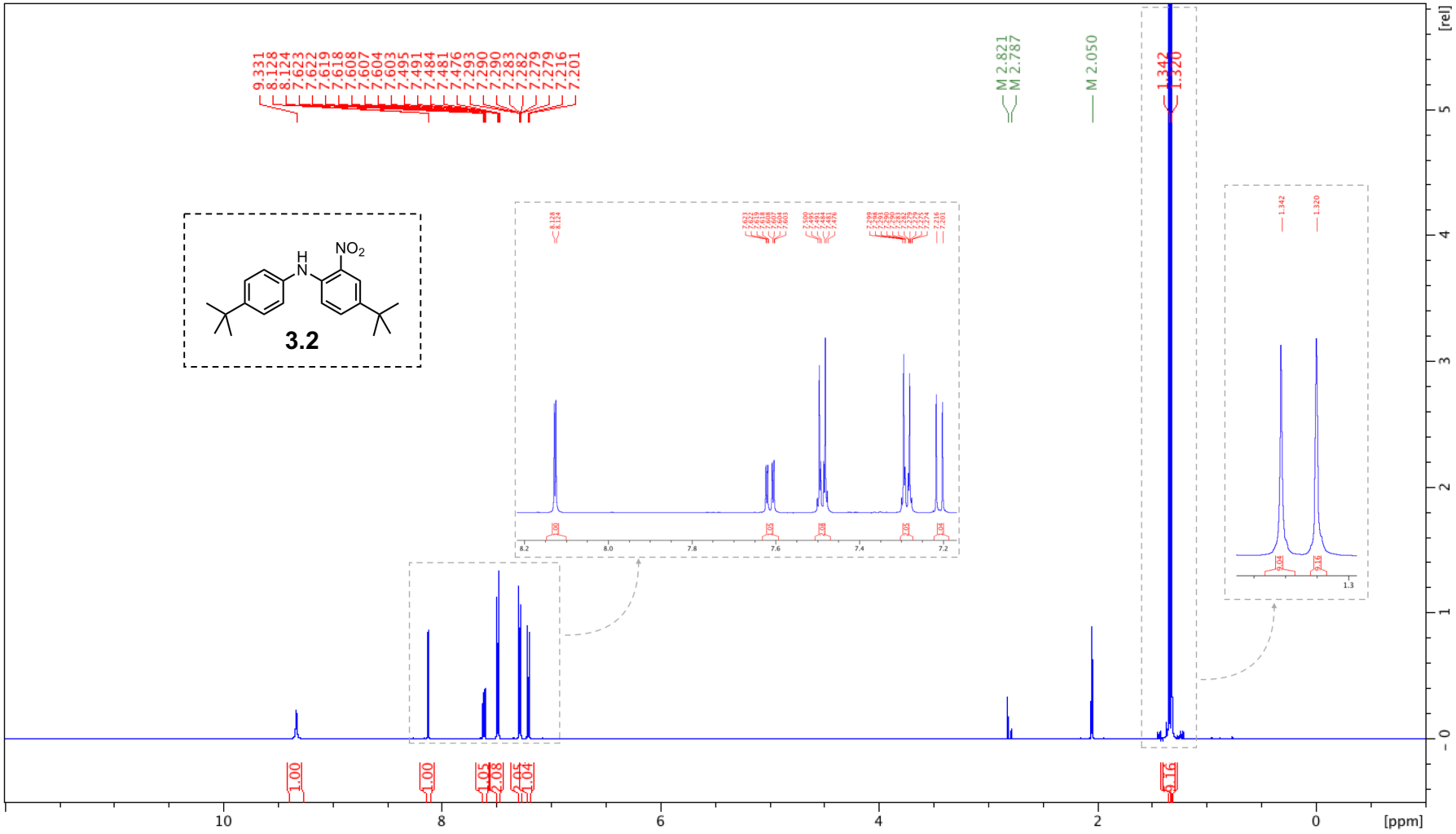
9.331
8.128
8.124
7.623
7.622
7.619
7.618
7.608
7.607
7.604
7.603
7.495
7.491
7.484
7.481
7.476
7.293
7.290
7.283
7.282
7.279
7.279
7.216
7.201
M 2.821
M 2.787
M 2.050
1.342
1.320
NO2
H
N
3.2
[rel]
[ppm]

^{13}C

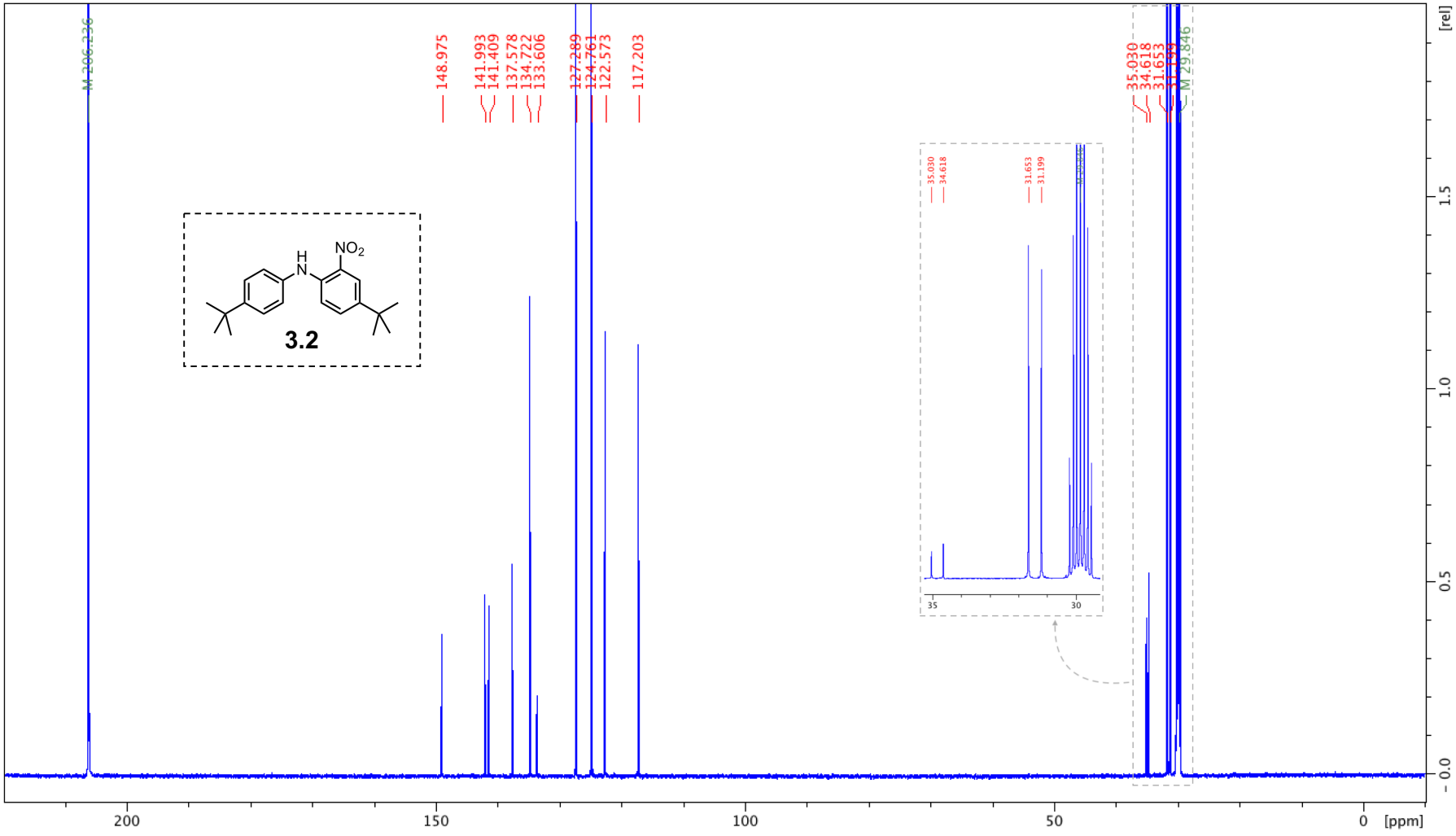
M 206.236
148.975
141.993
141.409
137.578
134.722
133.606
127.289
124.761
122.573
117.203
35.030
34.618
31.653
31.199
M 29.846
NO2
H
N
3.2
[rel]
1.5
1.0
0.5
- 0.0
200
150
100
50
0
[ppm]

^{1}H

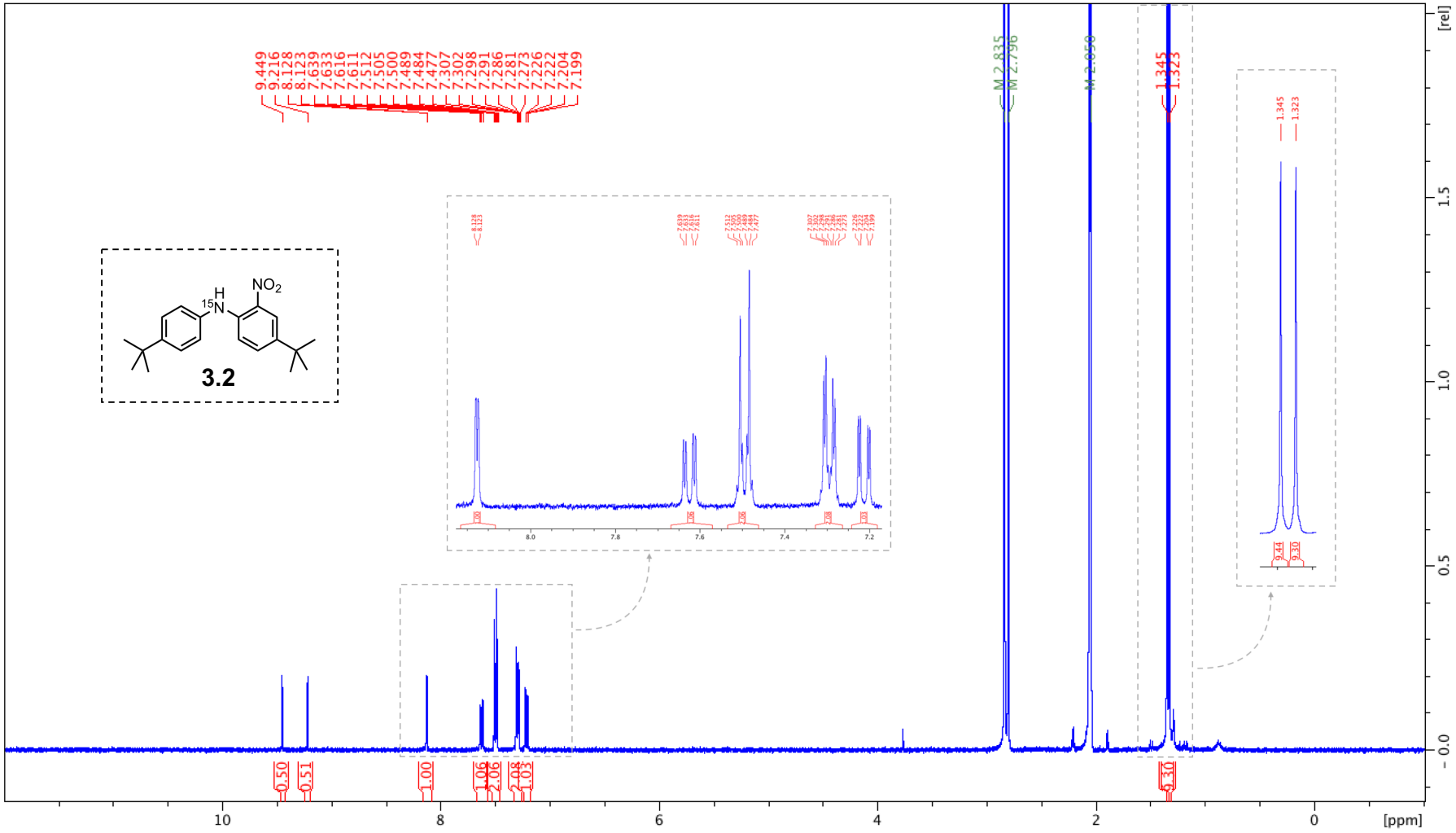
9.449
9.216
8.128
8.123
7.639
7.633
7.616
7.611
7.512
7.505
7.500
7.489
7.484
7.477
7.307
7.302
7.298
7.291
7.286
7.281
7.273
7.226
7.222
7.204
7.199
M 2.835
M 2.796
M 2.050
1.345
1.323
NO2
15N
H
3.2
[rel]
[ppm]

^{13}C

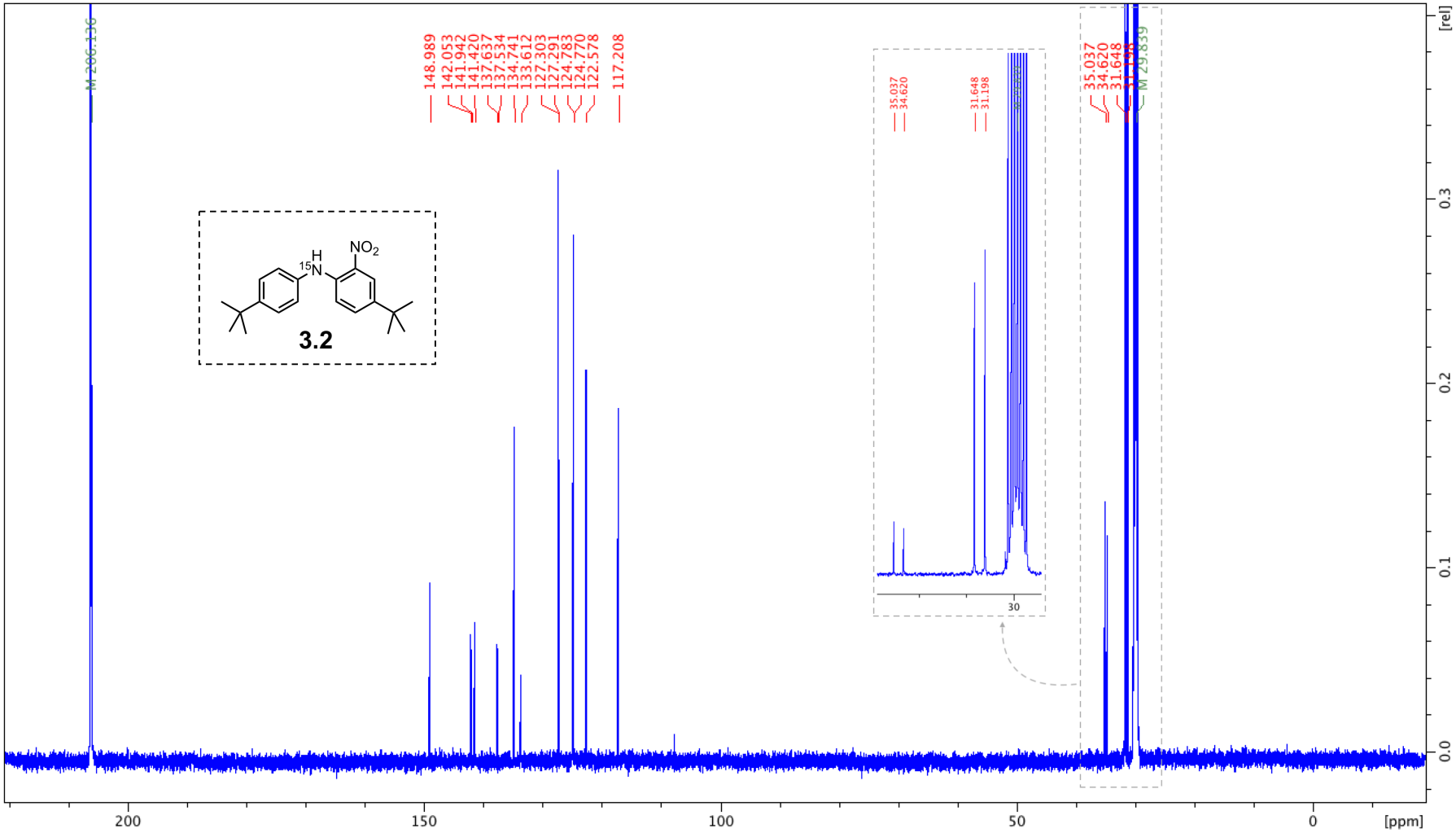
M 206.136
148.989
142.053
141.942
141.420
137.637
137.534
134.741
133.612
127.303
127.291
124.783
124.770
122.578
117.208
35.037
34.620
31.648
31.198
M 29.839
NO2
15N
H
3.2
[rel]
0.0
0.1
0.2
0.3
200
150
100
50
0
[ppm]

^{1}H ^{15}N HMBC

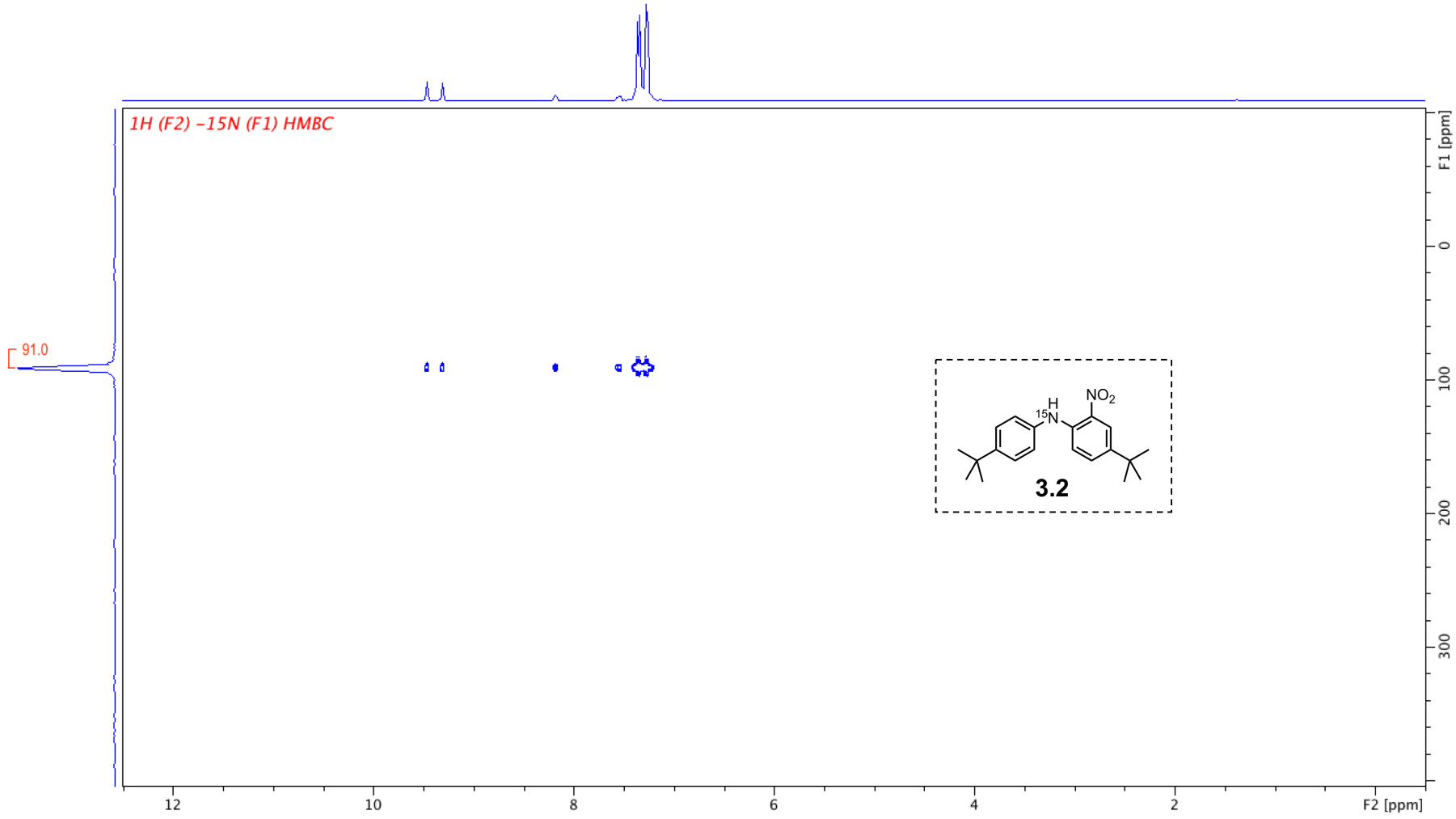
1H (F2) -15N (F1) HMBC
91.0
F1 [ppm]
0
100
200
300
12
10
8
6
4
2
F2 [ppm]
NO2
H
15N
3.2

^{1}H

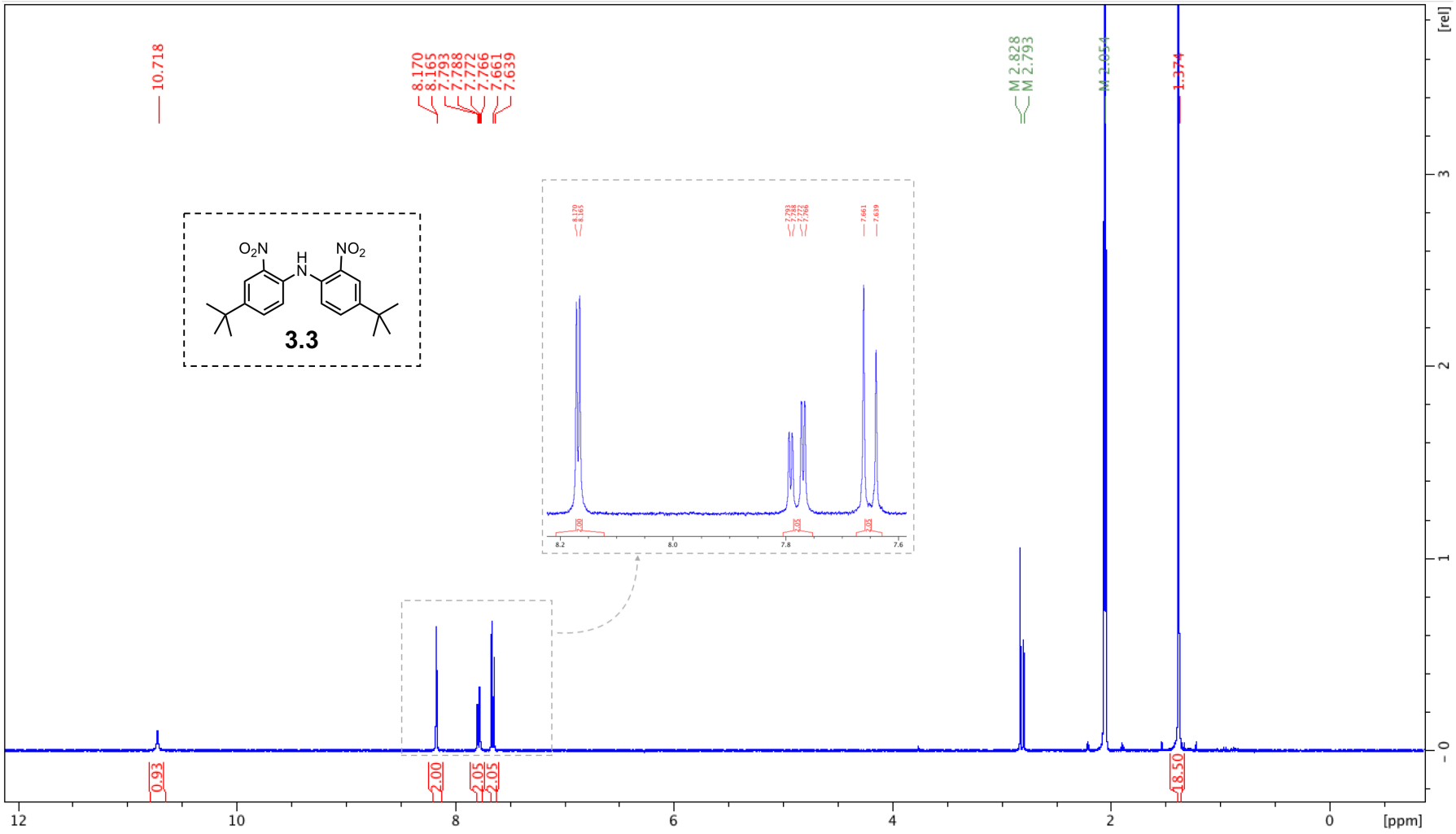
10.718
8.170
8.165
7.793
7.788
7.772
7.766
7.661
7.639
M 2.828
M 2.793
M 2.054
1.374
O2N
NO2
H
N
3.3
0.93
2.00
2.05
2.05
18.50
12
10
8
6
4
2
0
[ppm]
[rel]

^{13}C

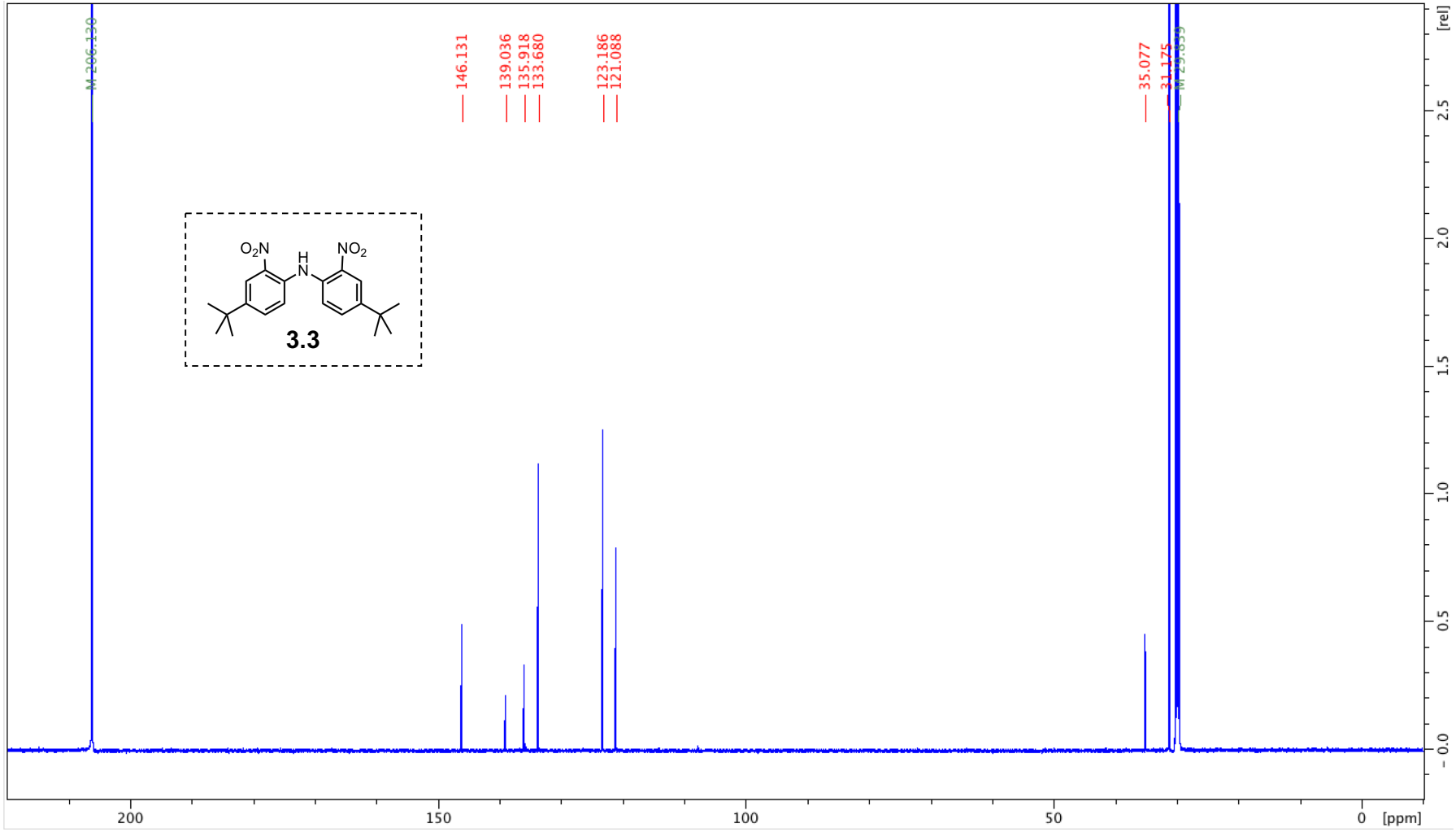
M 206.130
146.131
139.036
135.918
133.680
123.186
121.088
35.077
31.175
M 29.859
O2N
NO2
H
N
3.3
[rel]
2.5
2.0
1.5
1.0
0.5
- 0.0
200
150
100
50
0
[ppm]

^{1}H

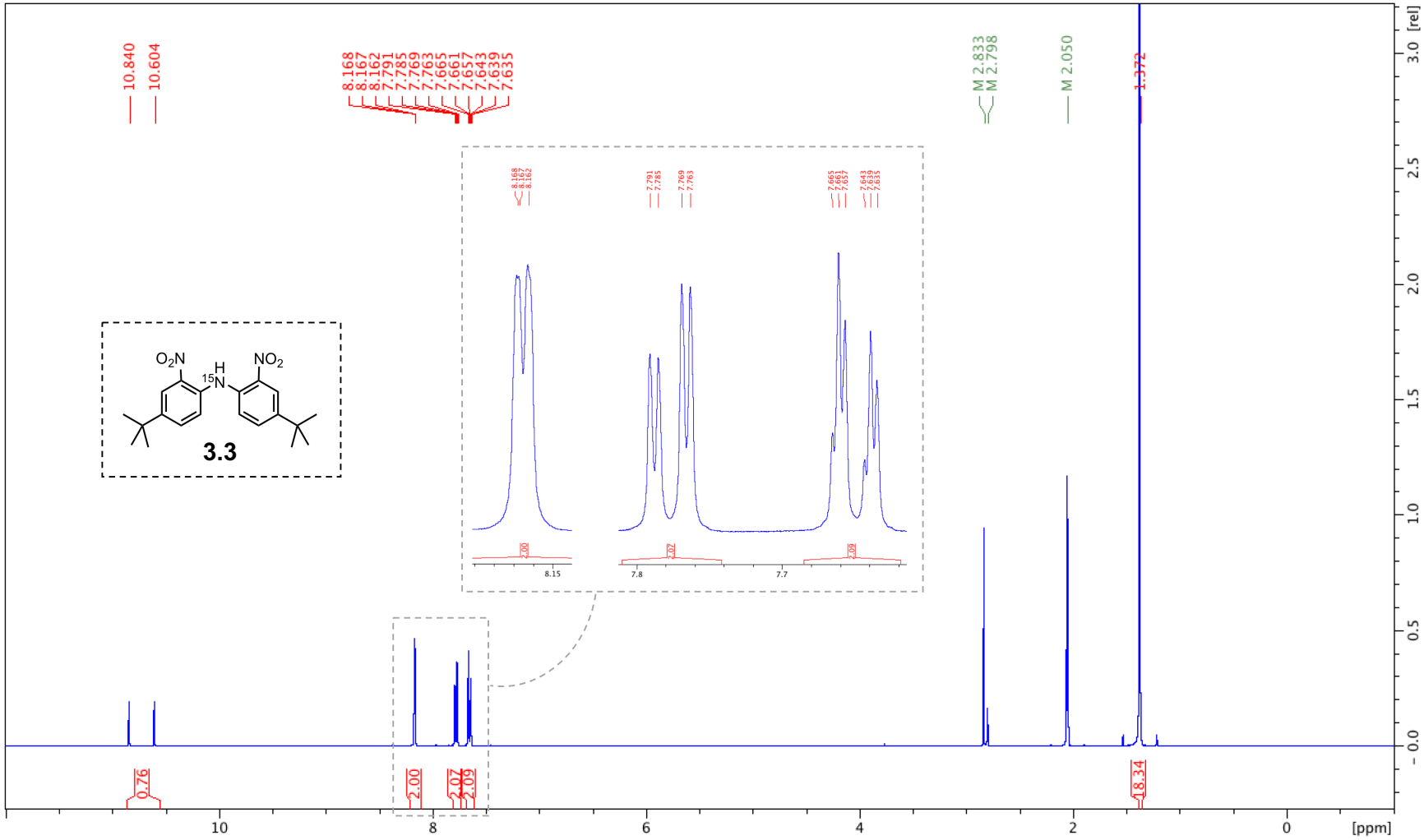
10.840
10.604
8.168
8.167
8.162
7.791
7.785
7.769
7.763
7.665
7.661
7.657
7.643
7.639
7.635
M 2.833
M 2.798
M 2.050
1.372
O2N
NO2
15N
H
3.3
0.76
2.00
2.07
2.09
18.34
10
8
6
4
2
0
[ppm]
3.0 [rel]
2.5
2.0
1.5
1.0
0.5
- 0.0

^{13}C

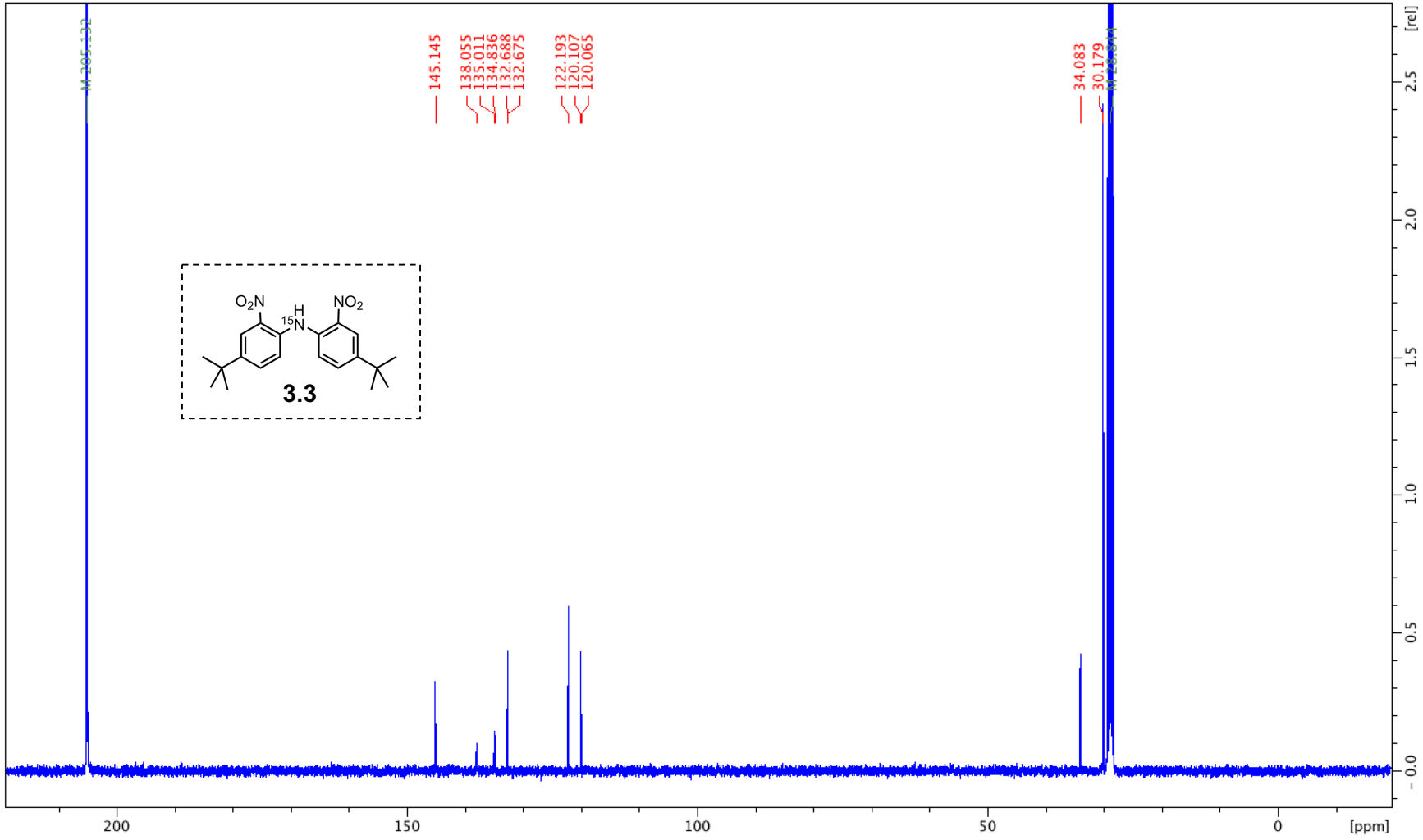
M 205.132
145.145
138.055
135.011
134.836
132.688
132.675
122.193
120.107
120.065
34.083
30.179
M 29.874
O2N
15N
H
NO2
3.3
[rel]
2.5
2.0
1.5
1.0
0.5
0.0
200
150
100
50
0
[ppm]

^{1}H ^{15}N HMBC

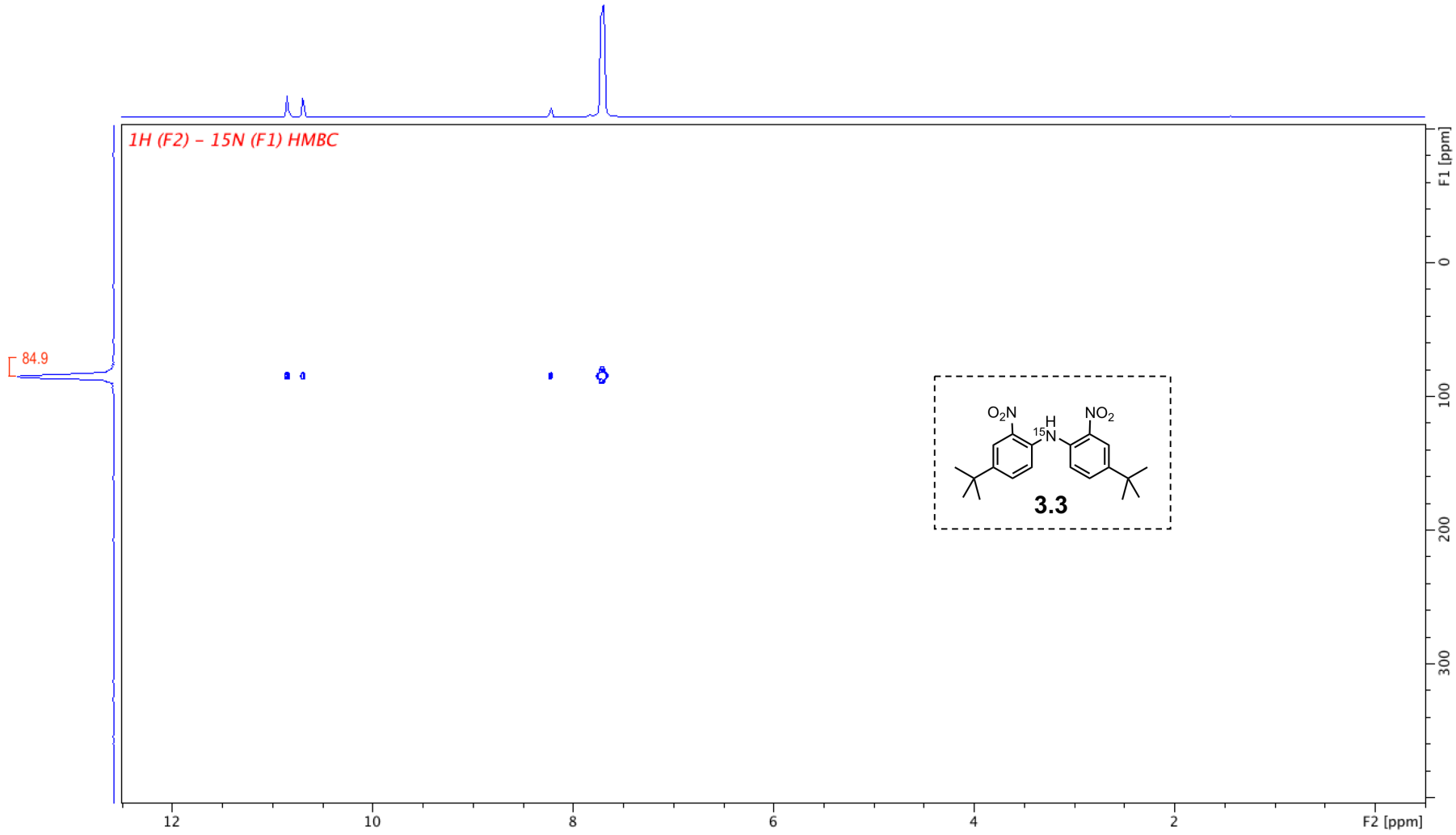
1H (F2) – 15N (F1) HMBC
84.9
12
10
8
6
4
2
F2 [ppm]
0
100
200
300
F1 [ppm]
O_2N
H
^{15}N
NO_2
3.3